DOCTOR OF SCIENCES

Phosphatriptycenes

from quantum chemical investigations to applications in main group and frustrated Lewis pair chemistry

Mahaut, Damien

Award date:
2023

Awarding institution:
University of Namur

Faculté des sciences

Phosphatriptycenes: from quantum chemical investigations to applications in main group and frustrated Lewis pair chemistry

---

Damien Mahaut

Jury members:

- Dr. Catherine Michaux (President, UNamur)
- Dr. Vincent Liégeois (UNamur)
- Prof. Olivier Baudoin (University of Basel, Switzerland)
- Prof. Lutz Greb (University of Heidelberg, Germany)
- Prof. Guillaume Berionni (Promotor, UNamur)
- Prof. Benoît Champagne (Promotor, UNamur)

A thesis submitted by Damien Mahaut in fulfillment of the requirements for the degree of Doctor of Sciences

June 22, 2023

Cover design: © Presses universitaires de Namur

Rue Grandgagnage 19
B – 5000 Namur (Belgium)
pun@unamur.be - www.pun.be

Registration of copyright: D/2023/1881/11
ISBN: 978-2-39029-173-2
Printed in Belgium.

Abstract

Frustrated Lewis pairs (FLPs) consisting of sterically hindered Lewis acids and bases constitute appealing alternatives to established transition metal catalysts. Expanding the scope of FLP and main group chemistry requires the development of Lewis bases or acids with new reactivities. To this end, constraining main group elements, such as phosphorus and boron, in a “non-classical” scaffold is a promising but little explored strategy. Due to their cage-shaped structure, 9-phosphatriptycene derivatives are weak Lewis bases with high potential in FLP chemistry. Similarly, boranes such as 9-boratriptycene derivatives exhibit an enhanced Lewis acidity due to their non-planar character.

This thesis describes the multi-step synthesis of 9-phosphatriptycene derivatives and their applications in FLP catalysis (hydrogenation of unactivated alkenes) and in main group chemistry (potential fluorinating agents). In addition, a density functional theory investigation was undertaken, focusing on their structure-property relationships as well as on the Lewis acidity of 9-boratriptycene derivatives and their applications in methane activation.

In essence, this work expands our understanding of the structure-property relationships affecting the reactivity of main group compounds. This fundamental advancement demonstrates that structural changes can constitute a new strategy for reactivity fine-tuning and brings solutions to long-lasting challenges in metal-free catalysis and main group chemistry.

Remerciements

Mener à son terme un projet de recherche, et *a fortiori* une thèse de doctorat, ne se fait pas seul. Je souhaiterais donc commencer ce manuscrit en exprimant ma gratitude envers tous ceux qui m'ont aidé.

Mes remerciements vont tout d'abord à mes deux promoteurs, Guillaume et Benoît, qui m'ont accueilli dans leur groupe, déjà dès le mémoire, m'ont donné l'expérience, le soutien et les moyens nécessaires pour réaliser cette thèse. Merci pour leur disponibilité, leur écoute et leurs conseils avisés tout au long de ces années de recherche, et pour leur énergie consacrée aux relectures et corrections de ce manuscrit.

La recherche n'est rien sans collaborations. Je tiens donc aussi à remercier Lei Hu qui a également participé au travail sur les phosphatriptycènes dans le cadre de sa propre thèse. Je remercie également les plateformes technologiques. Plus particulièrement, merci à Nikolay Tumanov pour son expertise en radiocristallographie, les nombreuses structures élucidées grâce à lui lorsque les autres techniques échouaient, et à Luca Fusaro pour ses compétences en RMN et son travail d'entretien des machines, un labeur permanent. Je n'oublie bien sûr pas Aurélien Chardon, qui a été un pilier pour le laboratoire RCO, et qui m'a beaucoup aidé et guidé pendant ma thèse, toujours à l'affût de nouvelles idées et disponible pour répondre à mes questions. Enfin, je remercie toutes les personnes qui contribuent à l'entretien des appareils de la plateforme technologique de calcul intensif (PTCI) de Namur, et plus globalement des ordinateurs du consortium des équipements de calcul intensif (CÉCI) pour la partie théorique de mon travail.

Merci également aux membres du jury et du comité d'accompagnement de thèse, qui ont accepté de relire mon travail et dont les commentaires et corrections ont permis de le mener à son terme.

Je remercie les organismes de financement, dont le F.R.S.-FNRS pour m'avoir accordé une bourse de doctorat, et l'UNamur et le NISM, qui m'ont permis de mener à bien mon projet dans un cadre professionnel de qualité et ont financé plusieurs déplacements scientifiques.

Je souhaite maintenant remercier tous les membres, anciens et présents, du laboratoire RCO. Merci particulièrement à Nicolas, Antoine, Sayandip, Kajetan et Marion pour l'ambiance chaleureuse que vous créez au sein du laboratoire. Merci

aussi à Esteban, resté un très bon ami après son séjour pour le mémoire, sa bienveillance et sa gentillesse. Merci à Xavier, collègue de bureau, pour son amitié et nos interminables discussions passionnantes. Ensuite je voudrais remercier les membres du laboratoire LCT, et particulièrement Charlotte, Pierre et François. Grâce à vous mes séjours au 2e étage ont toujours été agréables et marqués par la bonne humeur. Je suis très reconnaissant d'avoir eu la chance d'avoir deux groupes de recherche bienveillants et dans lesquels j'ai pu m'épanouir durant ces quatre années. Je pense aussi aux collègues et amis des autres laboratoires, ainsi qu'aux collègues de promos éparpillés à travers les différents labos et étages et du département. Merci aussi aux amis du 5e, pour ces belles rencontres et nouvelles amitiés créées ces dernières années.

Je ne voudrais pas manquer la chance de remercier ici Tom et Osi. Osi bien sûr, une belle complicité s'est développée grâce à ce chemin commun, du mémoire à la thèse en passant par ce fameux concours FRIA, et Tom dont l'amitié n'a pas diminué malgré la distance. J'ai de la chance d'avoir des amis comme vous.

Enfin, je souhaiterais finir ces remerciements par ceux dédiés à mes proches, ma famille et belle-famille, mes parents, mes sœurs, beaux-frères et neveux et nièces, qui m'ont soutenu, ont cru en moi tout au long de mon parcours et bien au-delà et dont la présence m'a fourni les bulles d'oxygènes nécessaires pour avancer dans mon projet. Pour terminer, merci à toi Amélie, ces quatre années de thèse auront vu grandir nos projets de vie communs. Merci d'être toujours là pour moi, même dans les moments difficiles. Merci à tous, je vous aime !

List of publications

A. Osi, N. Niessen, D. Mahaut, B. Champagne, A. Chardon, N. Tumanov, J. Wouters, G. Berionni, "Association of pyramidal boron Lewis superacids with pyridines: bending 2,4,6-collidine with the 10-sulfonium-9-boratriptycene", *Z. Anorg. Allg. Chem.* **2023**, e202300009.

D. Mahaut, B. Champagne, G. Berionni, "Frustrated Lewis pair-catalyzed hydrogenation of unactivated alkenes with sterically hindered 9-phosphatriptycenes", *ChemCatChem* **2022**, *14*, e202200294.

D. Mahaut, G. Berionni, B. Champagne, "9-phosphatriptycene derivatives: From their weak basicity to their application in frustrated Lewis pair chemistry", *J. Phys. Chem. A* **2022**, *126*, 2794-2801.

A. Osi, D. Mahaut, N. Tumanov, L. Fusaro, J. Wouters, B. Champagne, A. Chardon, G. Berionni, "Taming the Lewis superacidity of non-planar boranes: C-H bond activation and non-classical binding modes at boron", *Angew. Chem. Int. Ed.* **2022**, *61*, e202112342.

D. Mahaut, A. Chardon, L. Mineur, G. Berionni, B. Champagne, "Rational development of a metal-free bifunctional system for the C-H activation of methane: a density functional theory investigation", *ChemPhysChem* **2021**, *22*, 1958-1966.

L. Hu, D. Mahaut, N. Tumanov, J. Wouters, L. Collard, R. Robiette, G. Berionni, "Sterically hindered *ortho*-substituted phosphatriptycenes as configurationally stable P-chirogenic triarylphosphines", *Dalton Trans.* **2021**, *50*, 4772-4777.

T. H. Doan, A. Chardon, A. Osi, D. Mahaut, N. Tumanov, J. Wouters, B. Champagne and G. Berionni, "Making the bridge: methylene bridging effect on the structures, Lewis acidities and optical properties of semi-planar triarylboranes", *Chem. Eur. J.* **2021**, *27*, 1736-1743.

A. Chardon, A. Osi, D. Mahaut, A. B. Saida, G. Berionni, "Non-planar boron Lewis acids taking the next step: development of tunable Lewis acids, Lewis superacids and bifunctional catalysts", *Synlett* **2020**, *31*, 1639-1648.

A. Chardon, A. Osi, D. Mahaut, T. H. Doan, N. Tumanov, J. Wouters, L. Fusaro, B. Champagne, G. Berionni, "Controlled generation of 9-boratriptycene by Lewis adduct dissociation: accessing a non-planar triarylborane", *Angew. Chem. Int. Ed.* **2020**, *59*, 12402-12406.

F. Guibbal, S. L. Hopkins, A. Pacelli, P. G. Isenegger, M. Mosley, J. B. Torres, G. M. Dias, D. Mahaut, R. Hueting, V. Gouverneur, B. Cornelissen, "[^{18}F]AZD2461, an insight on difference in PARP binding profiles for DNA damage response PET imaging", *Mol. Imaging Biol.* **2020**, *22*, 1226-1234.

F. Guibbal, P. G. Isenegger, T. C. Wilson, A. Pacelli, D. Mahaut, J. B. I. Sap, N. J. Taylor, S. Verhoog, S. Preshlock, R. Hueting, B. Cornelissen, V. Gouverneur, "Manual and automated Cu-mediated radiosynthesis of the PARP inhibitor [^{18}F]olaparib", *Nat. Protoc.* **2020**, *15*, 1525–1541.

L. Hu, D. Mahaut, N. Tumanov, J. Wouters, R. Robiette, G. Berionni, "Complementary synthetic approaches toward 9-phosphatriptycene and structure-reactivity investigations of its association with sterically hindered Lewis acids", *J. Org. Chem.* **2019,** *84*, 11268-11274.

Table of contents

Introduction and objectives

1. Frustrated Lewis pair chemistry

1.1 From the Lewis theory to the definition of frustrated Lewis pairs

The pioneer work of Gilbert Lewis on acids and bases in 1923 led to the development of one of the most important and unifying theories of reactivity in modern chemistry.[1] Lewis defined acids and bases as, respectively, electron-pair acceptors and donors. According to him, both react to form covalently bonded adducts, effecting a mutual stabilization (*i.e.* quenching) of the two compounds, as shown with the example of the association of trimethylphosphine with boron trifluoride (Scheme 1). Both compounds are unstable to air, but the Lewis adduct they form is stable in air and water. The concept of donor-acceptor adduct formation is ubiquitous in all aspects of chemistry, spanning from the coordination chemistry of transition metals, the rationalization of reaction mechanisms, the adsorption at the surface of materials in solid state chemistry or polymer science, up to the development of new catalysts.

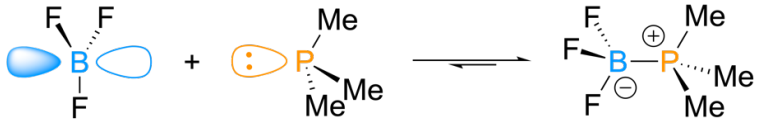

Scheme 1. Reaction of a Lewis acid (boron trifluoride) and a Lewis base (trimethylphosphine), to form a Lewis adduct. The lone pair of electrons of the phosphorus atom overlaps the empty 2p *orbital of the boron atom to form a covalent bond.*

The periodic table sorts elements according to their electronic configuration, which in turns defines their reactivity. Group 13 elements, starting with boron and aluminum display a vacant *p* orbital in neutral trivalent species, which are therefore prototypical Lewis acids. On the other hand, neutral trivalent derivatives of the group 15 elements, such as nitrogen and phosphorus, possess a lone pair of electrons and are thus Lewis bases. Organoaluminum and organoboron compounds were extensively used as catalysts in organic transformations.[2-5] Among the latter, arylboron species in particular are gaining increasing importance because they are easier to handle and more stable than their alkyl counterparts, and their reactivity can be tuned by the nature of the substituents on the aryl rings.[6-9] Amines and phosphines as Lewis bases are typical ligands in organometallic chemistry. Their electron-donation affects the reactivity of the metal center, itself acting as a Lewis acid, and can be tuned by

selecting ligands with specific steric and electronic properties.[10] Recently, they have also been used as organocatalysts (see Section 2), although less commonly than their Lewis acid counterparts.[11]

Frustrated Lewis pair chemistry provides new prospects in organocatalysis, where the reactivity of Lewis acids and bases are combined while preventing mutual quenching. This point will be detailed below. As mentioned previously, according to the Lewis theory,[1] a Lewis base (*e.g.* PR_3) will combine with a Lewis acid (*e.g.* BX_3) to form a covalent adduct ($R_3P{\rightarrow}BX_3$). However, the subtle effect of steric hindrance on their association was investigated later. In their 1942 report, Brown and coworkers studied the effect of steric strain on carbon-carbon bond rotation by comparing the stability of a series of amine-borane adducts (the B-N bond being isosteric to the C-C bond). They observed that the 2,6-lutidine does not coordinate with trimethylborane due to the excessive steric strain the B-N bond formation would generate (Scheme 2).[12]

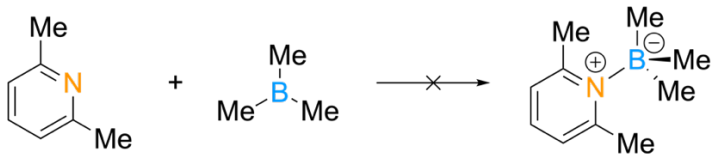

Scheme 2. Absence of reaction between 2,6-lutidine and trimethylborane.

In 2006, Stephan discovered that a phosphine-borane compound (**1**) was able to reversibly react with and release dihydrogen (H_2).[13] The reaction of **1** with H_2 is spontaneous at room temperature under 1 atm of dihydrogen while H_2 release is triggered by heating above 100°C (Scheme 3). Due to steric hindrance, dimesitylphosphine (Mes_2PH, Mes= 2,4,6-trimethylphenyl) and tris(pentafluorophenyl)borane **2** did not form the classical Lewis adduct but instead, under heating, generated the precursor to **1** *via* nucleophilic aromatic substitution at the *para* position of a C_6F_5 ring of **2**, leading to this seminal discovery. It constituted the first reported reversible metal-free hydrogen activation. While other phosphine-borane systems are capable of releasing H_2, the unique stability of **1** (*i.e.* the lack of polymerization or cyclization) is due to the steric hindrance around the P and B centers and allows its reversible reaction with H_2.

In his subsequent report, Stephan investigated the steric and electronic parameters influencing this reactivity.[14] More classical and simple frustrated pairs than **1** were shown to cleave dihydrogen, such as the $PtBu_3/B(C_6F_5)_3$ or $PMes_3/B(C_6F_5)_3$ combinations. Not all phosphine/borane pairs are suitable

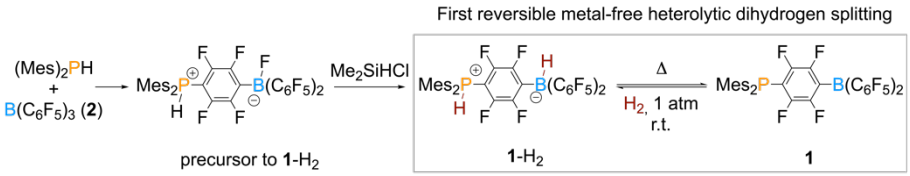

Scheme 3. First example of reversible heterolytic hydrogen splitting reported by Stephan.

however, as the steric hindrance in the acid or the base must be sufficient to prevent the formation of the Lewis adduct, while their acidity/basicity must remain high enough for reacting with dihydrogen. On the one hand, the combinations PMe_3 or $PPh_3/B(C_6F_5)_3$ for instance are lacking in steric repulsions and form a classical Lewis adduct. On the other hand, $PMes_3/BMes_3$ or $P(C_6F_5)_3/B(C_6F_5)_3$ do not react spontaneously with H_2 at room temperature because they are electronically deactivated (Scheme 4).[14]

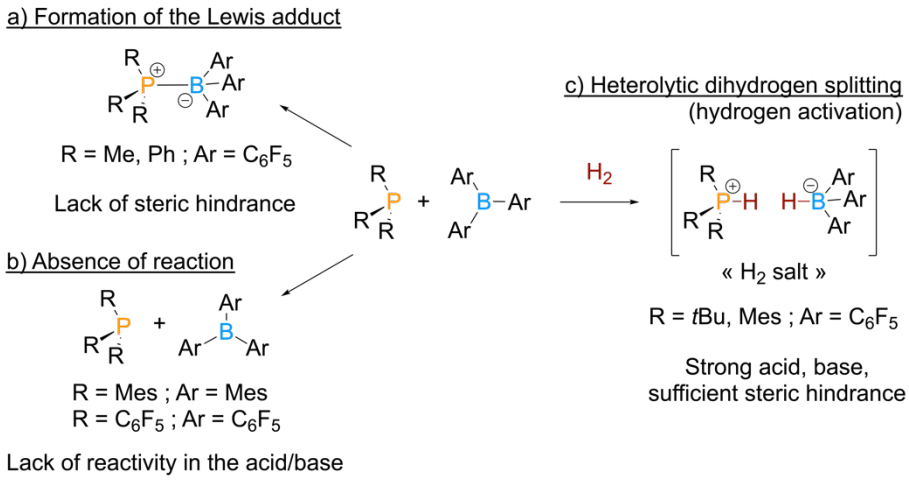

Scheme 4. Reactions of Lewis acid-base combinations in the presence of dihydrogen according to their substitution pattern.

These observations eventually led to the formal definition of "frustrated Lewis pairs" (FLPs) as sterically hindered Lewis acids and bases that cannot form the corresponding Lewis adduct because of steric repulsions (Scheme 5).[15-16] These bifunctional systems display completely new reactivity patterns and even some catalytic properties since both Lewis acid and base are now able to act synergistically on a reagent of small size in a "three-component" type reaction.

Stephan next demonstrated the ability of these systems to perform the metal-free hydrogenation of unsaturated substrates, namely imines, nitriles and aziridines.[17] The reaction was proposed to proceed as follows: first, the

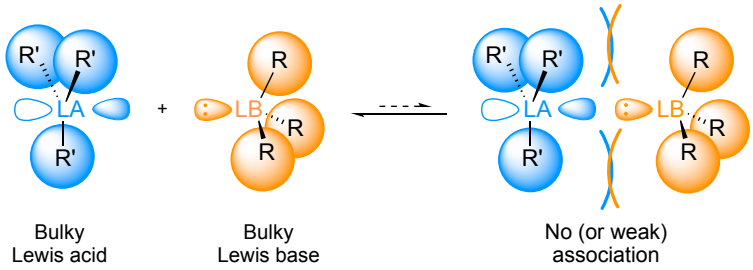

Scheme 5. Stephan's definition of a frustrated Lewis pair.

heterolytic splitting of H_2, generating formally a proton (phosphonium) at the Lewis base and an hydride (borohydride) at the Lewis acid, followed by proton transfer to the imine then hydride transfer to the imminium moiety, forming a new B-N bond, finally followed by the release of the corresponding amine and regeneration of the catalyst (Scheme 6). Hydrogenations with FLP systems is an important part of this PhD work, and a more detailed subsection on this reactivity is detailed hereafter.

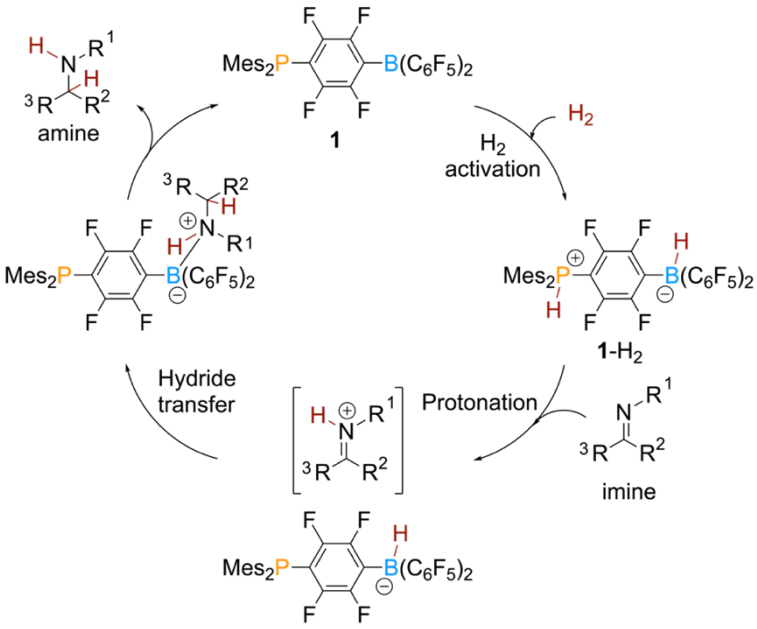

*Scheme 6. Proposed mechanism for an imine hydrogenation by FLP system **1**. Scheme reproduced from reference 18 with permission from the Royal Society of Chemistry.*

1.2 Reactivity of frustrated Lewis pairs

1.2.1 First hydrogenations and hydrogenation of alkenes and alkynes

Hydrogenation reactions are among the most widely used chemical transformations, especially in pharmacochemical industries and synthetic organic chemistry.[19-20] Ever since the founding work of Sabatier in the beginning of the 20th century, homogeneous or heterogeneous transition-metal-based catalysts were used for these transformations.[10, 21-22] However, the limited resources and toxicity of these elements incite chemists to develop alternatives.[23-26] As shown above, frustrated Lewis pairs are able to catalyze the hydrogenation of unsaturated substrates and thus constitute appealing surrogates to transition metal catalysts for this transformation. While other transition-metal-free systems are known to catalyze hydrogenations, they either require harsh conditions or use other sources of hydrogen, such as Hantzsch's ester (in hydride transfer reactions) or hydrogen transfer reagent surrogates.[27-34] FLPs offer the advantage of reacting directly with H_2. In addition, the reactivity of the Lewis acid and base can be finely tuned to target different types of substrates. Over the years, these systems were extensively used for transition-metal-free hydrogenations of unsaturated compounds, notably imines, alkenes, aromatics, and carbonyl compounds. Several comprehensive publications have reviewed these hydrogenation reactions, their scope and limitations.[18, 35-37]

As mentioned above, the first report of FLP-catalyzed hydrogenation described the transformation of imines, nitriles and aziridines to the corresponding amine. The phosphonium hydridoborate salt of **1** and another *t*Bu-substituted derivative were used as catalysts.[17] The reaction yields were dependent on the steric and electronic parameters of the substrates, for example bulky substituents were necessary for the reaction to proceed catalytically or electronically deactivated imines required longer reaction times. These observations shed light on some mechanistic aspects of the reaction, suggesting that proton transfer is indeed the initial step, and highlighting the possible coordination of the Lewis acid moiety to the substrate. Eventually, the hydrogenation of bulky imines and aziridines could be achieved with $B(C_6F_5)_3$ as lone catalyst, the substrate itself acting as Lewis base for hydrogen heterolytic cleavage.[38-39]

Notably, the group of Erker developed an intramolecular system capable of activating H_2, which was able to perform the hydrogenation of imines under milder conditions than the ones previously reported (25°C, 1.5 atm H_2 w.r.t. 80-120°C, 1-5 atm H_2). Allegedly, this difference in reactivity arises from the intramolecular character of the FLP system that reduces the entropy of activation, and from a lower Lewis acidity at the boron than in $B(C_6F_5)_3$. Other systems were developed afterwards, varying the linker, the Lewis base, or the Lewis acid (Figure 1).[40-41] Using weaker and bulkier Lewis acid was also investigated.[42-43] Interestingly, Ashley discovered that the solvent (THF) can act as Lewis base for FLP reactions with bulky, air-stable boranes [including $B(C_6Cl_5)(C_6F_5)_2$]. This is the first instance where FLP reactivity is achieved without significant steric hindrance in one of the reactive partners. Eventually, it was even observed that systems that form classical Lewis adducts can serve as FLP-type catalysts if the LA-LB bond can be dissociated at high temperatures. In addition to imines, this first generation of FLP catalysts (Figure 1) also allowed the hydrogenation of electron-rich polarized double-bonds: silyl-enol-ethers and enamines. These substrates display a more nucleophilic carbon-carbon double bond than that of regular olefins.

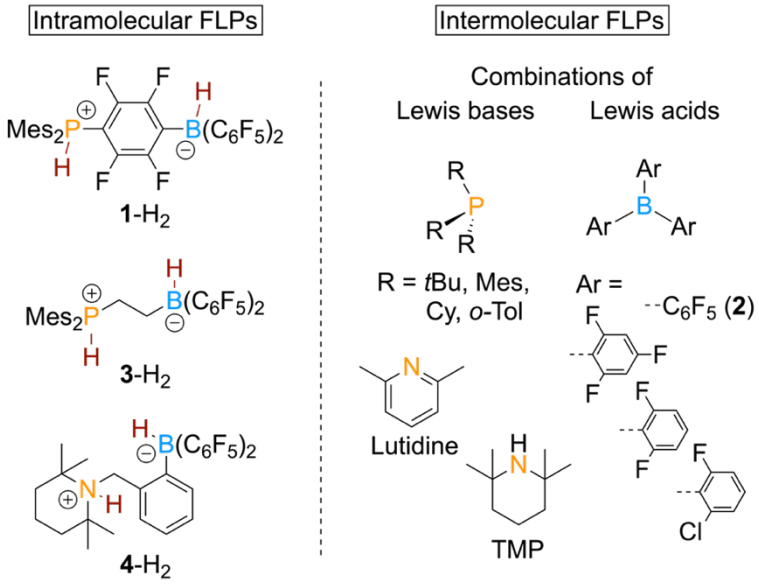

Figure 1. Selected examples of intra- and intermolecular frustrated Lewis pairs. Note that intramolecular FLPs are usually stored and handled in their "H_2 salt" state (denoted by "-H_2") and are thus shown in this form. TMP = 2,2,6,6-tetramethylpiperidine.

The hydrogenation of more challenging substrates relied on the improvement of existing systems and the development of new types of FLPs. A second generation of FLP catalysts was thus developed with Lewis bases or acids with a tuned reactivity, adapted to the type of substrates targeted. In 2012, the group of Paradies in collaboration with Stephan reported the first hydrogenation of olefins.[44] For this transformation, they used deactivated Lewis bases such as $P(C_6F_5)(Ph)_2$ (Scheme 7a). Upon hydrogen activation, these weaker bases generate a phosphonium cation with enhanced Brønsted acidity, able to protonate a carbon-carbon double bond. The carbenium ion formed after protonation is stabilized by conjugation with either aryl substituents or neighboring unsaturated bonds in the substrate. The borohydride then adds on the carbocation to yield the alkane as product. These FLP systems appear not to react spontaneously with dihydrogen at room temperature, and low temperatures (between -60°C and -80°C) are needed to observe the phosphonium and borohydride by NMR spectroscopy. However, it does not prevent the hydrogenation to proceed at room temperature, and olefins are reduced in reaction times between 12 h and 96 h, with longer times and higher temperatures required for less reactive double bonds (up to 240h and 70°C). Interestingly, Stephan showed that dialkylethers/$B(C_6F_5)_3$ combinations can catalyze 1,1-diphenylethylene hydrogenation, although requiring higher pressures of H_2 to proceed.[45] Similarly, polycyclic aromatic cycles and N-heteroaromatics are partially reduced with these FLP catalysts.[46-49]

In contrast to this reactivity, Alcarazo showed that olefins can also act as hydride acceptors if the resulting carbanion is stabilized by electron-withdrawing groups (Scheme 7b). In this case, the hydride transfer happens first and is followed by the protonation step.[50-52]

While not technically an FLP catalyst, Wang's hydrogenation of aliphatic olefins catalyzed by Piers' borane [bis(pentafluorophenyl)borane, $HB(C_6F_5)_2$)] is worth mentioning (Scheme 7c).[53] These less reactive alkenes are not readily hydrogenated by standard FLP systems. Their formal hydrogenation is achieved by initial hydroboration of the alkene by the borane, followed by σ-bond metathesis with H_2, or hydrogenolysis, of the carbon-boron bond (Scheme 7d). The metal-free catalytic hydrogenation of olefins was already known in the literature (Scheme 7e), dating back to the 1960's,[54-55] but the reaction of Wang *et al.*, performed at 140°C under 6 bar of hydrogen pressure and 20 mol% catalyst, constitutes the first reported example of metal-free catalyzed

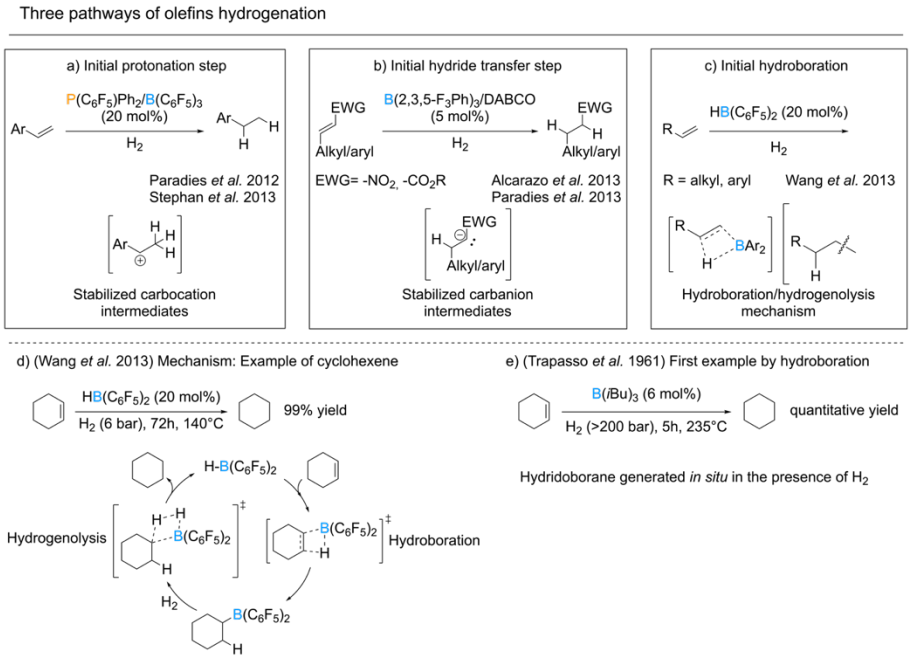

Scheme 7. Metal-free-catalyzed hydrogenations of olefins, either by FLPs or Piers' borane. DABCO = 1,4-diazabicyclo[2.2.2.]octane.

hydrogenation of aliphatic, unactivated alkenes, under relatively mild conditions. They took advantage of the better reactivity of Piers' borane for hydroborations compared to classical boranes to perform this challenging reaction.[56]

The first step toward the hydrogenation of alkynes was reported by the group of Erker. Their intramolecular FLP **3** reduced ynones into the corresponding enones.[57] The hydrogenation of simple alkynes however was reported later by Repo and coworkers. Using an *ansa*-aminoborane system **6**, they performed the hydrogenation of alkynes to *cis*-alkenes under mild conditions (Scheme 8). The actual catalyst **6** is generated by reacting the pre-catalyst **5** at 80°C under H_2 atmosphere. The new B-H bond allows the following hydroboration of the substrate, generating a bulky bifunctional system **7** which cleaves H_2 to form the corresponding ammonium hydridoborate salt **7**-H_2, eventually releasing the *cis*-alkene *via* protodeborylation. Hydrogenation with this system only yields the *cis*-alkene (Z). Subsequent work by Du described the selective hydrogenation to *cis*- or *trans*-alkenes catalyzed by $HB(C_6F_5)_2$, in a similar fashion as Wang for unactivated alkenes.[58]

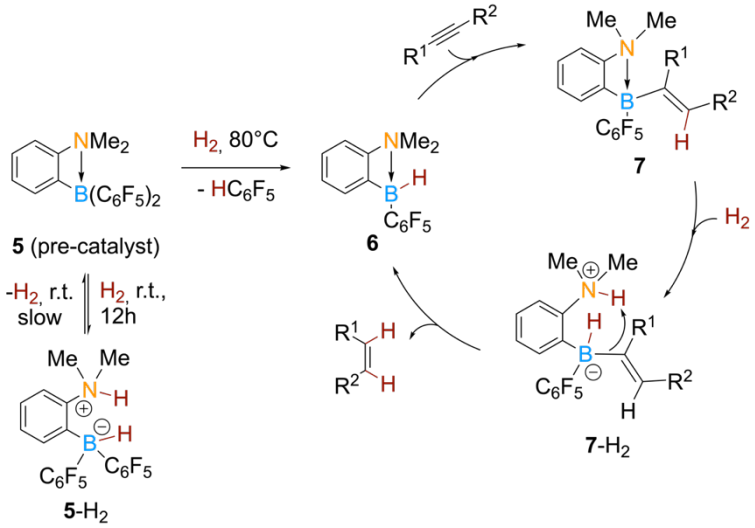

*Scheme 8. Formation of the catalyst **6** and mechanism of FLP-catalyzed hydrogenation of alkynes to cis-alkenes.*

1.2.2 Hydrogenation of carbonyl derivatives

The use of ethereal solvents developed by Stephan and Ashley allowed the hydrogenation of aldehydes and ketones. These substrates turned out to be more challenging than their imines analogues due to the lower basicity of the oxygen atom. By computational investigation, Privalov reported that the process of activating H_2 with a ketone in combination with $B(C_6F_5)_3$ was possible.[59] Early efforts however were unsuccessful and only led to the formation of the corresponding alkoxyboranes and the deactivation of the catalyst.[60-61] Eventually, the groups of Ashley and Stephan solved this problem by using respectively THF or diethyl ether/diisopropyl ether as solvents (Scheme 9).[62-63]

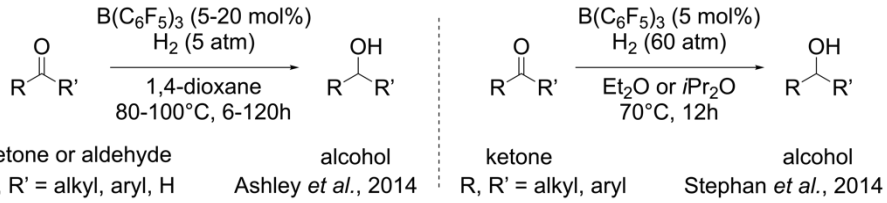

Scheme 9. FLP-catalyzed hydrogenation of ketones and aldehydes by Ashley and Stephan.

Investigating the reactivity of the Lewis acid also expanded the scope of FLP chemistry. Soós *et al.* reported the use of bulkier and weaker Lewis acids for the hydrogenation of Michael acceptors, previously limited by their coordination to the oxygen atom, and carbonyl compounds.[40, 43, 64] The first water-tolerant FLPs

were developed this way, allowing the catalysis of a new reaction by FLPs, reductive aminations, not considered earlier since it generates water as by-product.[65-66]

The reduction of amides is one of the major ways to form functionalized amines.[67] The use of transition metal catalysts is well-developed but poses issues of selectivity (formation of a mixture of the corresponding amine and alcohol) and of tolerance with sensitive functional groups (*e.g.* halogens, alkynes, nitro). Paradies reported the first hydrogenation of amides by FLPs.[68] This reaction required $(COCl)_2$ as additive to convert the amide in the corresponding chloroiminium ion before reduction to the ammonium (Scheme 10).[69] Later improvements using a phosphine oxide in combination with triphosgene $[CO(OCCl_3)_2]$ to generate the chloroiminium intermediate were reported.[70] Similarly, esters eluded FLP hydrogenation until recently, when Ashley reported their direct hydrogenation catalyzed by an organotin Lewis acid in combination with lutidine.[71]

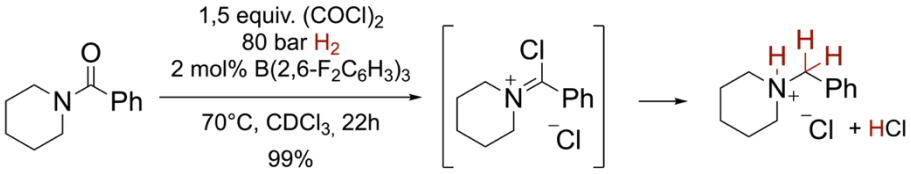

Scheme 10. Paradies' hydrogenation of amide through a chloroiminium intermediate.

1.2.3 Enantioselective hydrogenations catalyzed by FLPs

In 2008, Klankermayer and his group opened the door of asymmetric catalysis with FLP catalysts when they used an alkenylborane derived from (+)-α-pinene (**8**, Scheme 11) to catalyze the enantioselective hydrogenation of imines.[39] This first chiral catalyst only led to limited enantiomeric excess (13% *ee*) but later improvements using a camphor scaffold (**9**, Scheme 11) led to *ee* values up to 83% for the same reaction.[72-73] Other chiral FLP systems were developed as well, Erker *et al*. used a ferrocene-based catalyst (**10**, Scheme 11) for asymmetric imine reduction with up to 69% *ee*.[74-75] Building on earlier work with intramolecular FLPs,[41] Repo and coworker synthesized a series of *ansa*-ammonium borates systems including some chiral versions (**11**, Scheme 11) able to yield up to 35% *ee*.[76] Notably, the group of Du reported a straightforward method to access chiral Lewis acid catalysts based on the binaphtyl chiral scaffold.[77] Their catalyst **12** (Scheme 11) is generated *in situ* by double hydroboration of binaphtyl diene with Piers' borane $[HB(C_6F_5)_2]$ and displays

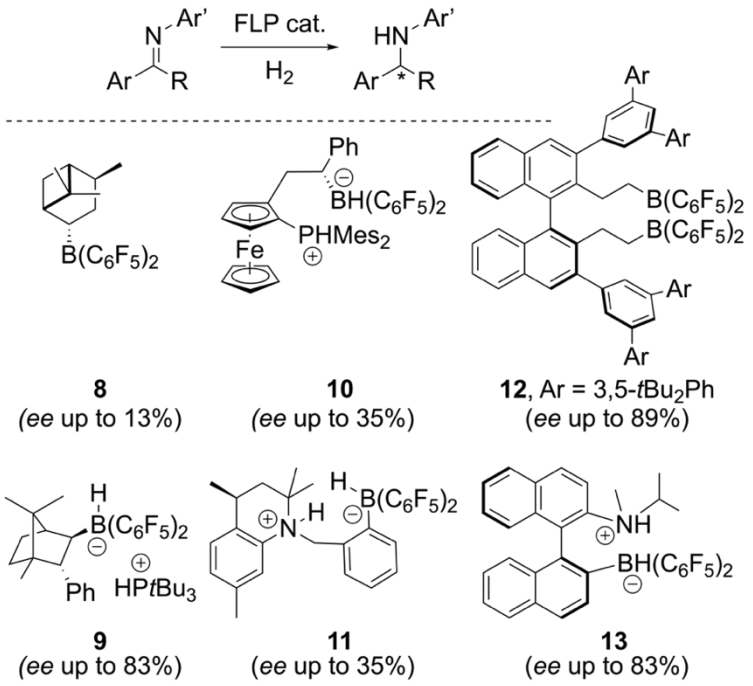

Scheme 11. General reaction of asymmetric hydrogenation of imines and selected examples of chiral FLP systems.

good enantioselectivity with up to 89% *ee*. Another well-performing system for asymmetric imine hydrogenation based on the naphtyl scaffold (**13**, Scheme 11) was reported by Repo. These bifunctional "chiral molecular tweezers" led to *ee* values up to 83% for imines and up to 99% for enamines.[78]

Other substrates were targeted as well, for example variations of Du's catalyst allowed the hydrogenation of silyl enol ethers (**14**, Scheme 12) and N-heterocycles with good enantioselectivity.[79-83]

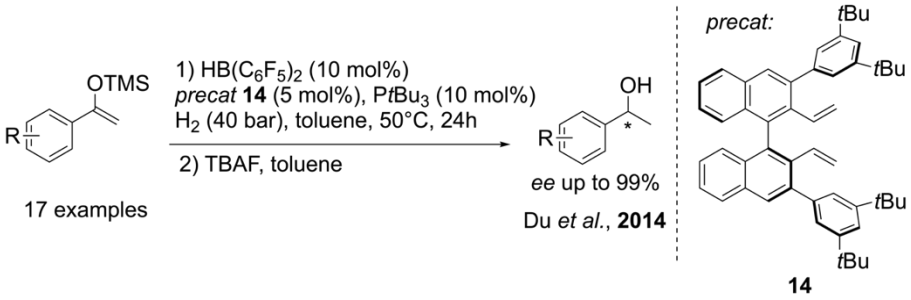

Scheme 12. Asymmetric hydrogenation of silyl enol ethers and deprotection to the secondary alcohol by Du et al*. TBAF= tetrabutylammonium fluoride, TMS = trimethylsilyl.*

1.2.4 Investigations on the mechanism of H_2 activation

Quantum chemical investigations are a useful tool to support and guide experimental work. In this field, Density functional Theory (DFT) became the pillar of theoretical support for organic chemists because it displayed the best compromise between computational cost and accuracy of the results. A summary of the main principles of DFT and the equations that define it is presented in the Annex II of this work.

Understanding the reactivity of frustrated Lewis pairs and the mechanism of hydrogen activation remains a challenge. To this end, many research groups have undertaken computational studies, mostly employing Density Functional Theory, to gain insight into the complex reactivity of FLPs.[84-91] In particular, the mechanism of H_2 activation by acid-base combinations was a source of long-lasting debates. Shortly after the seminal discoveries of Stephan, in 2008, Pápai and co-workers reported a quantum chemical study of the activation of dihydrogen by the typical FLP tris(*tert*-butyl)phosphine (P*t*-Bu_3) and tris(pentafluorophenyl)borane ($B(C_6F_5)_3$).[84] They pointed out that the splitting of the hydrogen molecule is neither due to a preliminary borane-H_2 or phosphine-H_2 complexation but to a concerted mechanism: a simultaneous breaking of the H-H bond and formations of P-H and B-H covalent bonds. The preliminary borane-H_2 complex was initially hypothesized because $H_3B{\leftarrow}H_2$ interactions were previously observed experimentally.[92-93] In the case of $B(C_6F_5)_3$ however, the weak electron-donation from the π-system to the vacant boron orbital is sufficient to prevent this interaction, due to Pauli repulsions. Instead, they suggested that the Lewis acid and the Lewis base associate first through weak interactions, without direct P-B charge transfer (mainly dispersion interactions and C-H···F hydrogen bonds), to form a cavity in which H_2 can be inserted (Figure 2). The H-H bond heterolytic cleavage happens subsequently through a transition state stabilized by the same weak intermolecular interactions between the phosphine and the borane to form the product, itself further stabilized by a P-H···H-B electrostatic interaction.

Their mechanism was later detailed based on a molecular orbital approach.[94] The LA-LB complex retains the HOMO of the base and the LUMO of the acid mostly unchanged but aligned in a way to ease orbital overlaps with H_2. The latter molecule inserted in the cavity undergoes a significant polarization

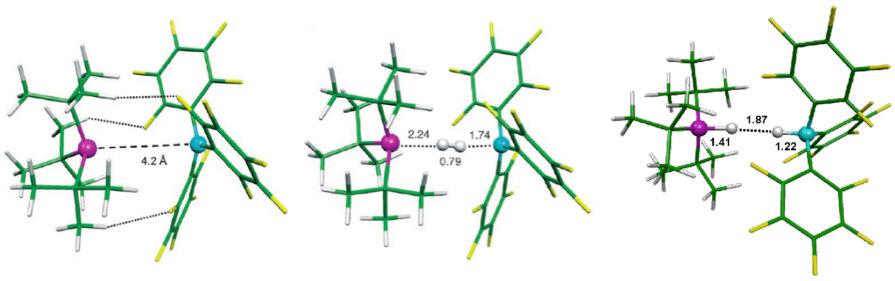

a b c

Figure 2. a) Structure of the t-Bu$_3$P···B(C$_6$F$_5$)$_3$ complex (a) with C-H···F hydrogen bonds ($d_{H\text{-}F}$ <2.4 Å) dotted, b) transition-state of the hydrogen cleavage and c) product complex. Distances given in Å. Structures optimized at the B3LYP/6-31G(d) level of theory reprinted from reference 84 with permission from John Wiley and Sons. Colors: Purple = Phosphorus; White = Hydrogen; Yellow = Fluorine; Green = Carbon; Blue = Boron.

(symmetry breaking) that alters its orbital configuration (mixing between the HOMO and LUMO of H_2) resulting in a H_2 molecule acting both as a better electron pair acceptor and electron pair donor than in the unperturbed system (Scheme 13, left). The actual heterolytic splitting happens next through a simultaneous $LP_P \rightarrow \sigma^*_{H_2}$ and $\sigma_{H_2} \rightarrow p^*_B$ electron transfer, resulting in the phosphonium and borohydride ion pair. H_2 acts as a bridge between the acid and base centers, breaking its σ bond to release the frustration. Interestingly, they drew a parallel between this reactivity and the other modes of H_2 splitting, homolytic or heterolytic, in metal complexes or by singlet carbenes, identifying FLP-H_2 activation as the newest member in this category (Scheme 13, right). In view of all these results and the stabilization occurring in the product of the reaction, they could explain why, experimentally, this reaction happened quantitatively and under mild conditions.

Similarly, Guo and Li invoked the same mechanism to explain the splitting of H_2 by Stephan's first intramolecular FLP system **1**,[95] contrary to the mechanism proposed in that initial report.[13]

Next were investigated the factors influencing the thermodynamics of H_2 activation by several acid-base combinations.[85] To this end, a partitioning of reaction energies was undertaken, identifying several unfavorable and favorable contributions, the former consisting in the H_2 cleavage itself and the preparation energy of the Lewis pair (breaking of eventual dative LA-LB bonds or weak interactions to "make space" for H_2 insertion), the latter consisting in the

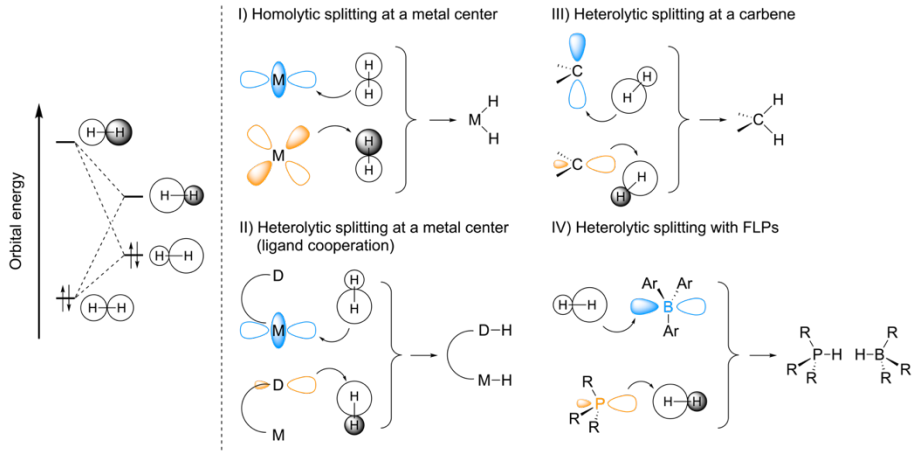

Scheme 13. (left) Orbital deformation resulting from mixing between HOMO and LUMO. (right) Modes of H_2 splitting in a metal complex (I, II), at a carbene (III) and by FLPs (IV). In orange and in blue are shown filled and empty orbitals respectively, filled orbital of H_2 shown in full white, empty in black and white. Heterolytic splitting modes involve a polarized H_2 moiety. Scheme adapted from reference 94 with permission from John Wiley and Sons.

stabilizations brought by proton attachment to the Lewis base, the hydride attachment to the acid and the coulombic interactions in the ion pair product. Isolating these contributions allowed to pinpoint the individual effect of the acid, the base, and the nature of the FLP itself (either intra- or intermolecular). A notable conclusion from the report was that intermolecular FLPs displayed a good correlation between the strength of the acid-base combination and the ease of H_2 cleavage, while intramolecular FLPs benefited from a reduced entropy penalty, so that weaker intramolecular acid-base combinations were still able to activate H_2. In a later report, Vankova *et al*. drew similar conclusions for reaction kinetics.[89] Both articles stress the importance of tuning of the size and properties of the Lewis base and the Lewis acid to best exploit the reactivity with H_2.

In 2010, Grimme and Erker challenged the so-called "electron transfer" mechanism of Papaï, described above.[96] Their initial claim was that the previous work of Papaï was questionable, mainly due to a poor theoretical treatment (namely the small, poorly flexible, basis set, the use of the B3LYP functional, and the lack of proper benchmark study for the method) that did not (sufficiently) consider the interactions between the bulky substituents, mainly London dispersion forces, and led to inaccurate transition state structures. Using the

B97-D[97]/TZVPP'[1][98] method in combination with single point calculations at the higher-level SCS-MP2[99]/CBS[100-101], they probed the potential energy surface in the cavities (Figure 2a) created in FLP systems at several P-B and H-H distances and concluded that once H_2 was inside the cavity, its dissociation was practically barrierless. They attributed the observed kinetic barrier to the H_2 entrance into the cavity. According to their mechanism, the electric field generated between the acid and the base centers is sufficient to split the H_2 molecule, the phosphorus and boron then acting merely as the hydride acceptor and donor. To support this view, they simulated a strong electric field acting on H_2, without FLP system, and showed that the heterolytic splitting was spontaneous (Figure 3). According to them, there is no need to invoke orientation and deformation of molecular orbitals to explain FLP reactivity.

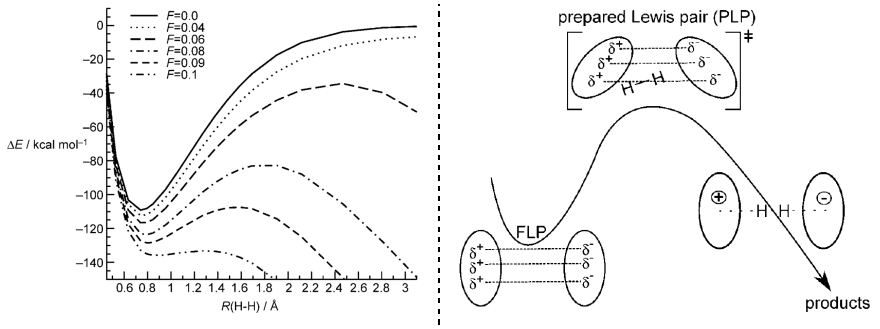

Figure 3. (left) Potential energy curves of H_2 dissociation (computed at the FCI/aug-cc-pVQZ) in electric fields of varying strength, note that for a strong enough field ≥0.1 a.u. (1 a.u.= 5.1422.10[11] V.M[-1]), the dissociation is almost barrierless. (right) Representation of FLP H_2 activation with the electric field model, a typical range of field strength inside a FLP is between 0.04 and 0.06 a.u. Schemes reprinted from reference 96 with permission from John Wiley and Sons.

To summarize both conceptual views, in the electron transfer mechanism, FLPs activate H_2 by adequate orbital overlaps, allowing electron transfer. The reaction barrier is due to the transition state of H_2 splitting. In the electric field mechanism, FLPs activate H_2 through its polarization owing to the electric field generated by the LA and LB moieties. The reaction barrier is due to preparation or entrance of H_2 in the cavity.

Investigations in the following years discussed the possibilities of both mechanisms. Camaioni *et al*. studied a series of small molecules combinations

[1] TZVPP' corresponding to Alrich's triple ζ valence basis set with either two sets of polarization functions for P, B and H (TZVPP) or one set for all other atoms (TZVP).

(NH_3/BX_3, X= H, F, Cl) in their reaction with H_2.[102] They optimized their structures using B3LYP-D/DZVP2 method and refined electronic energies at the G3(MP2)-B3LYP[103] and CCSD(T) levels of theory. Given the study was not experimental, they could decide to ignore the fact that the small molecules would normally form Lewis adducts and focused instead on the energy decomposition analysis of their reaction with H_2. They concluded that favorable orbital overlaps were the main stabilizing factor in reaction energy. Electrostatic interactions, which include the interactions through the electric field generated by the FLP, were significant as well but could not alone be accountable for the reactivity of the system.

Rokob, Papaï and co-workers eventually addressed the previous comments of Grimme on the theoretical method. New in-depth studies, extensively comparing both conceptual views, were reported.[88, 104] Inter- and intramolecular FLPs with several types of Lewis acids and bases were considered, eventually supporting the electron-transfer mechanism, and highlighting the limitations of the electric field view. To further support their claim, they performed a preliminary benchmark study, investigating the effect of the method on the results and settled on the use of the ωB97X-D exchange correlation functional, a range-separated hybrid functional including an empirical dispersion correction term, with the 6-311G(d,f) basis set. Eventually, they proposed a general mechanism for intermolecular FLP systems, regardless of the nature of the LA and LB considered, divided in three main steps: i) preorganization through weak interactions, ii) simultaneous interaction of H_2 with both LA and LB (*i.e.* H_2 polarization) and iii) electron transfer through cooperative $LP_{LB} \rightarrow \sigma^*_{H_2}$ and $\sigma_{H_2} \rightarrow p^*_{LA}$. The mechanism differs between systems in the way H_2, the electron donor and the acceptor are positioned.

These discussions pointed out the need for a robust computational method and how inappropriate exchange-correlation functionals or basis sets can lead to inaccurate structures, energies, or scientific conclusions. Even though the electron transfer model has been generally adopted overtime, especially since the molecular orbital approach allowed a deeper understanding and the establishment of guidelines for the development of new systems, continuous improvements and contributions were added over the years. The addition of Molecular Dynamics studies are worth mentioning, which allowed the group of Ensing to shed light on the asynchronous nature of the transition state and the individual roles of the acid and base on the kinetics.[105-107] Giving more depth to

the established models, Privalov described more complex orbital interactions, in which both σ and σ* orbitals of H_2 in the cavity are coupled with the HOMO and LUMO respectively of the FLP system.[108]

The understanding of reaction mechanisms and the interactions between all involved compounds through computational studies is crucial to predict the properties of FLPs and to design new ones. In the present work, quantum chemical investigations were performed to guide and support experimental work.

1.2.5 Small molecules capture, carbon dioxide hydrogenation and methane activation

The reactivity of FLP systems is not limited to dihydrogen, several small molecules can be captured by FLPs, such as CO, CO_2, SO_2 and N_2O (Figure 4).[109-115] Reactions conditions are similar to the original H_2 reports:[14] the FLP spontaneously traps these small molecules at room temperature and atmospheric pressure of the gas. Contrary to H_2 however, no catalytic system has yet been developed with these molecules. They require a stoichiometric amount of phosphine-borane, which is why one talks of small molecules "capture" instead of "activation".

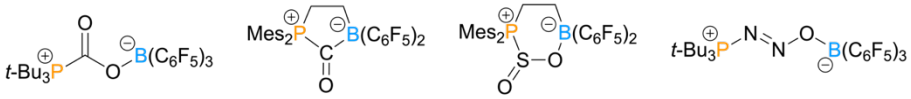

Figure 4. CO_2, CO, SO_2 and N_2O molecules captured by FLPs.

The activation of CO_2, a potent greenhouse gas,[116] is a very attractive transformation, which led researchers to further investigate its reactivity with FLP catalysts. Its conversion with dihydrogen into formic acid or methanol is an attractive method to generate C_1 building blocks in chemical synthesis or as a chemical storage of H_2 in the context of renewable energy management.[117-119] This transformation is well-studied in heterogenous catalysis,[120-121] with electrochemical reduction[122] as well as with transition metal in homogeneous catalysis (Scheme 14a),[123] but an efficient metal-free alternative is still lacking.[124] Wang reported a $B(C_6F_5)_3$-catalyzed hydrogenation of carbon dioxide without transition metal but using instead potassium metal (K) in the reaction mixture under harsh conditions (Scheme 14b). A first proof of concept that CO_2 can be hydrogenated into methanol in low yield with a FLP in stoichiometric amount (Scheme 14c) was described[125] by Ashley but ultimately led to the destruction of

the FLP catalyst. Another stoichiometric reaction was reported by Stephan and Fontaine in 2015.[126]

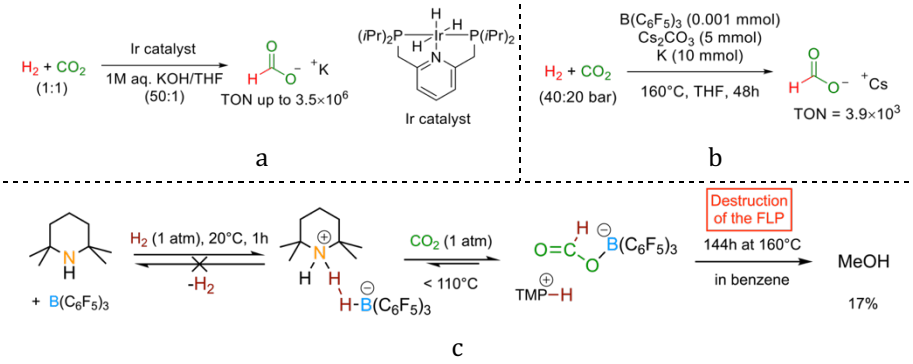

Scheme 14. Hydrogenation of carbon dioxide to formate or methanol with an iridium catalyst (a), $B(C_6F_5)_3$ catalyst (b) or stoichiometrically with an FLP system (c).

More recent computational investigations hinted at the feasibility of the catalytic transformation of CO_2 into formic acid by FLPs, which is encouraging.[127-129] Eventually, Stephan's group reported the hydrogenation of CO_2 with H_2 in the presence of silyl halides, leading selectively to either disilyl acetals or methoxysilanes.[130]

Another compound of great interest that cannot yet be activated by FLPs is methane (CH_4). Methane is, alongside carbon dioxide, one the major gases responsible for global warming and its conversion into value-added products would be most profitable. Again, transition metals proved to be efficient catalysts for this challenging transformation. Periana and coworkers developed the first catalytic conversion of methane into a methanol derivative using a Pt (II) complex.[131] More recently, the groups of Sanford and Mindiola developed catalytic C-H borylations of methane using Ir, Rh and Ru complexes (Scheme 15).[132-133]

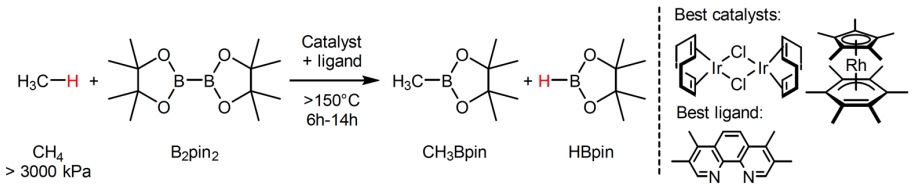

Scheme 15. Transition-metal-catalyzed selective monoborylation of methane by Sanford et al.*[132]*

FLPs were obvious candidates for developing metal-free alternatives for the activation of methane. However, while carbon dioxide displays some reactivity

with FLP systems, no reaction with methane was reported to this day. Several theoretical studies tried to address this problem by understanding the reasons behind this difficulty.[86, 134-135] Alternatively, the group of Wang reported more recently that the activation and functionalization of methane can be achieved with a borenium cation complex, effecting its borylation (Scheme 16) and its addition on a silyl acetylene, demonstrating that reactivity with methane is possible without transition metal complexes.[136]

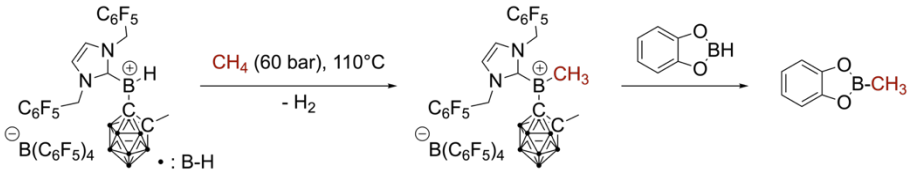

Scheme 16. Activation and borylation of methane by a borenium complex.

The activation of methane by FLP systems will be the focus of one section of this work (Chapter VI), more details on this transformation and a state-of-the-art will be provided there.

As shown in above-detailed examples, the hydrogenation of, or the reactivity with, new and challenging substrates is strongly reliant on the development of new Lewis acids and Lewis bases, specifically designed to address limitations in the field.[137-139] In parallel, it is also crucial to understand these limitations and the parameters affecting their reactivity, for which quantum chemical calculations are necessary. Phosphines are ideal Lewis base candidates in FLP chemistry and were widely used and studied in this field,[44, 140] and their development is an important field of research, especially since they can also be applied as ligands in organometallic chemistry. This thesis details the development and application in FLP chemistry of an understudied class of phosphine, 9-phosphatriptycenes, which is why the following introduction section gives more details into their nature, reactivity, and applications.

2. Phosphines

Phosphines (PR_3) constitute an important class of Lewis bases which display a high propensity to form bonds with a wide variety of electrophiles, or to oxidize into phosphine oxides, owing to the lone pair of electrons of the P atom. The oxidation of phosphines is the driving force of several important organic reactions such as the Mitsunobu, the Appel or the Staudinger reactions.[141-144]

The phosphorus being below the nitrogen in the periodic table, there is a strong similarity between the reactivity of amines (NR_3) and phosphines as their valence configuration is the same (one lone pair of electrons and three unpaired electrons). For similar substituents, phosphines are generally weaker Brønsted bases, due to their high polarizability and low electronegativity, and are more nucleophilic than amines.[145] Tertiary phosphines PR_3 and amines NR_3 are pyramidal, but the latter will easily undergo inversion ("flipping") at room temperature whereas the former retain their configuration even above room temperature.[146] P-chirogenic phosphines (phosphines with the chiral center on the phosphorus) are thus configurationally stable.

The steric and electronic properties of phosphines can be readily modulated by varying the nature of the groups linked to the phosphorus atom (alkyl, aryl, halogen, …, see subsection 2.1). These modulable properties make them particularly useful as ligands in organometallic chemistry, which has ever been their main field of applications (see subsection 2.2).[147] In recent years, the use of phosphines as organocatalysts (*i.e.* where the phosphine itself acts as catalyst) has received increasing interest from organic chemists, as discussed in subsection 2.3.[11, 148]

2.1 Measurements of the steric and electronic properties of phosphines

The quantification of the steric and electronic properties of phosphines is necessary to rationalize and predict their reactivity. Chemists have thus endeavored to develop new measurements of these properties. Most notably, Chadwick A. Tolman studied both electronic and steric factors of ligands in organometallic chemistry and defined in 1970 the phosphine cone angle, still in use today to describe steric effects of phosphines and any other type of ligands.[149] From a zerovalent nickel atom at 2.28 Å of the phosphorus atom of the ligand, he constructed a cone that comprises the entirety of the ligand (Figure

5). To quote, the measurement corresponds to "*the apex angle of a cone, centered on the metal, just large enough to enclose the van der Waals radii of the outermost atoms of the ligand*". The cone angle is a direct measure of the steric effect of the ligand: the larger the angle value, the bulkier the ligand. The "percent buried volume" (%V_{bur}), introduced by Nolan, is another example of steric descriptor. Calculated using crystallographic data, it is defined as the percent of the total volume of a sphere (of predefined radius and centered on the metal) occupied by a ligand.[150]

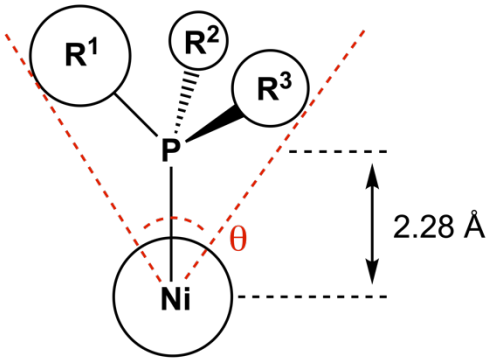

Figure 5. Cone angle θ as defined by Tolman.

In parallel to the cone angle, Tolman also developed a measure of the electronic parameter of phosphine ligands: in a mixed ligands nickel complex $NiL(CO)_3$, the influence of the phosphine ligand L on the infrared stretching frequency of the carbonyl ligands can be measured.[151] The C-O stretching frequency decreases with stronger ligands (Figure 6).

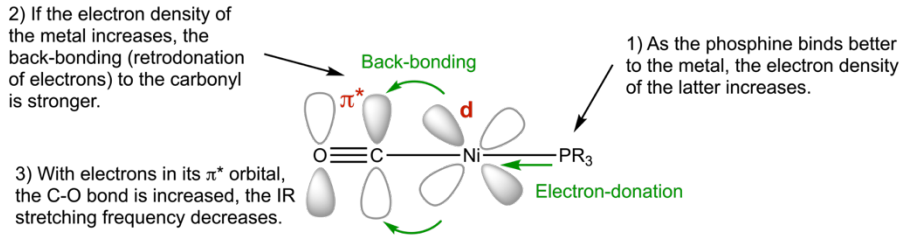

Figure 6. Principle of the measurement of the Tolman electronic parameter.

Other strategies to assess the electronic parameter of phosphine ligands include ^{31}P NMR measurements of the $^{1}J_{P\text{-}C}$ and $^{1}J_{P\text{-}Se}$ coupling constants of the corresponding methylated phosphine and phosphine selenide, respectively.[152]

To evaluate the reactivities of phosphines commonly used as organocatalysts, Lewis basicity scales were developed for comparing the affinity of a multitude of

Lewis bases to a selected reference Lewis acid. Several scales are based on quantum chemical calculations such as the methyl cation affinity (MCA)[153] and the halenium (F^+, Cl^+, Br^+, I^+) affinity (*HalA*) scales.[154] Experimental Lewis basicity scales are based on equilibrium constants of association of Lewis bases with reference Lewis acids such as benzhydrylium cations (Ar_2CH^+) for the Mayr scale[155] or BF_3 for the BF_3 affinity scale (BF_3A).[156] The former scale links the equilibrium constant to a Lewis acidity (*LA*) and a basicity (*LB*) parameter. With known *LA* parameters for the reference, one can determine the *LB* parameter with a simple mathematical relation (Figure 7).

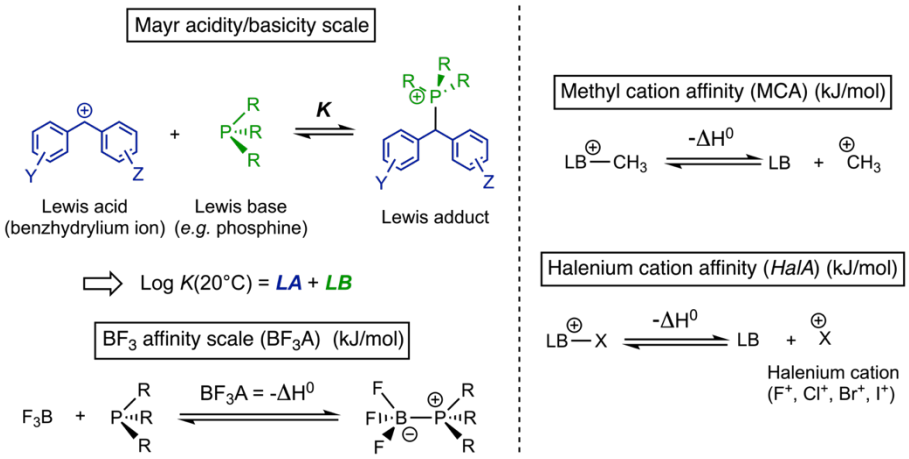

Figure 7. Common Lewis basicity scales.

2.2 Phosphines in transition metal catalysis

As mentioned earlier, phosphines are widely used as ligands in organometallic catalysis owing to their strong coordinating properties towards transition metals. The orbitals of the phosphorus atom are well adapted for an efficient binding with metals through two distinct modes: σ-donation and retro-donation (or back-bonding). The latter is due to the overlap between the partially filled *d* orbitals of the metal and the antibonding orbitals of the P-R bonds (σ*) (Figure 8).[10]

Ligands that accept back-bonding such as phosphines are called π-acceptors or π-acids. This property, among other factors, distinguishes phosphines in terms of ligand ability from amines (NR_3), which are not (or weakly) π-acidic.

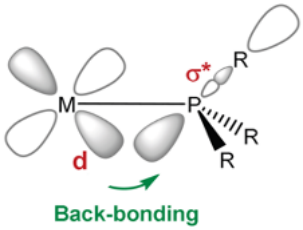

Figure 8. Overlap between a partially filled d *orbital of the metal and the σ* orbital of one of the P-R bonds.*

The functional groups around the phosphorus tune the steric and electronic properties of the phosphine and subsequently its bonding with metals. For examples, electron-withdrawing groups such as fluorine atoms will enhance the π-acidity of the phosphine[10] or sterically demanding groups like *i*-propyl substituents will limit the number of ligands bonded to the metal in what are called "sterically stabilized" species.[157]

Numerous major organic reactions are catalyzed by transition metal complexes with phosphine ligands. Notably, a wide range of coupling reactions such as the Suzuki-Miyaura, the Hiyama-Denmark and the Negishi couplings.[158-161] A nice example of phosphine ligand tuning is the development of the Buchwald-Hartwig coupling with Buchwald's dialkylbiarylphosphines. This reaction uses a palladium complex with a phosphine ligand (initially such as triphenylphosphine or tris(*o*-tolyl)phosphine) to carry out a C-N bond formation between an aryl halide and an amine to form a tertiary aryl amine (Scheme 17).[162-163]

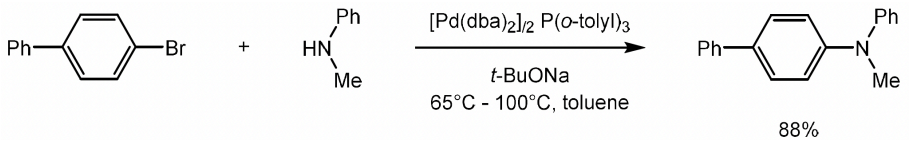

Scheme 17. Example of a Buchwald-Hartwig C-N coupling reaction.

Later improvements of these reactions by Buchwald led to the development of a new class of phosphines (Scheme 18) which are bulky, electron-rich monodentate ligands with high activity in C-N[162, 164], C-O[165]and C-C coupling reactions (Scheme 18).[166-167] Phosphine ligands also possess a wide application in asymmetric catalysis. Since the pioneer work of Kagan on the asymmetric hydrogenation of ethylene derivatives using chiral diphosphines,[168] they have become ligands of choice in enantioselective transition-metal-catalyzed reactions.[169] One such ligand is the bidentate BINAP ligand (Scheme 18).[170]

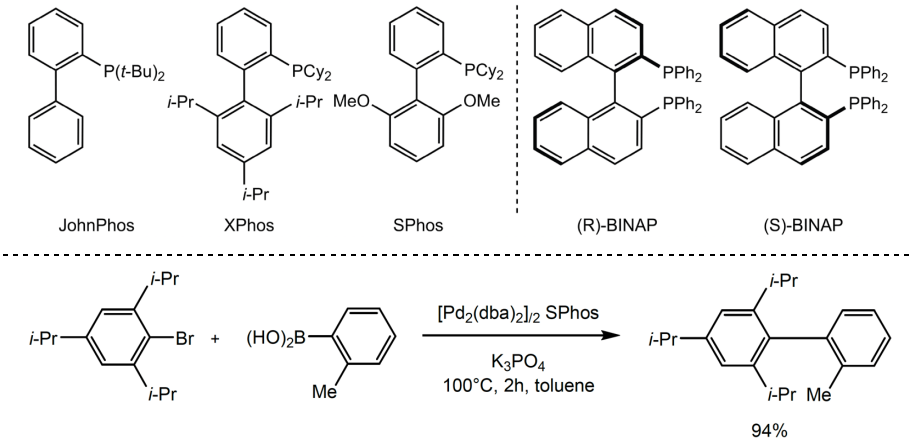

Scheme 18. (up, left) Examples of Buchwald's dialkylbiarylphosphine ligands (JohnPhos, XPhos, SPhos);[167] (up, right) (S)- or (R)-BINAP (2,2′-bis(diphenylphosphino)-1,1′-binaphthyl) ligand, the limited rotation around the bond between the naphthyl groups induces an axial chirality in the molecule (i.e. a locked spatial arrangement without chiral center that is non-superposable to its mirror image); (down) Example of a palladium-catalyzed Suzuki-Miyaura cross-coupling reaction with the SPhos ligand.

To further demonstrate the importance of phosphines in organometallic chemistry, a few examples of popular transition metal catalysts with phosphine ligands can be put forward (Table 1).

Table 1. Examples of prominent transition metal complexes with phosphine ligands and some of their applications.

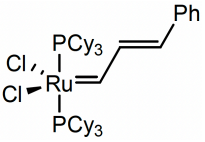 (Grubbs' Catalyst)	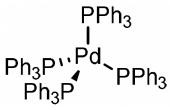 "Palladium tetrakis"	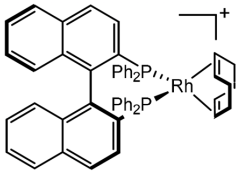	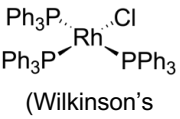 (Wilkinson's Catalyst)
Ring-closing and olefins metathesis[171]	Widely used in cross-coupling reactions[172]	Industrial synthesis of (-)-menthol [173-174]	Industrial hydrogenations of olefins[175]

2.3 Phosphines as organocatalysts

Phosphines are also involved as catalysts in many transition-metal-free organic reactions, hence defined as "organocatalysts". In most cases, they perform Michael-type additions to many types of electrophilic C-C multiple bonds such as alkenes, allenes and alkynes (through a $n_P \rightarrow \pi^*$ HOMO-LUMO overlap). During the last few years, the use of phosphines as organocatalysts has grown significantly, both in standard and asymmetric catalysis, as extensively reviewed by the groups of Kwon and Lu.[176-177]

As an example of phosphine-catalyzed transformation, the Morita-Baylis-Hillman (MBH) reaction consists in a Lewis base-catalyzed C-C bond formation between the α-position of an electron-deficient alkene and an aldehyde (Scheme 19).

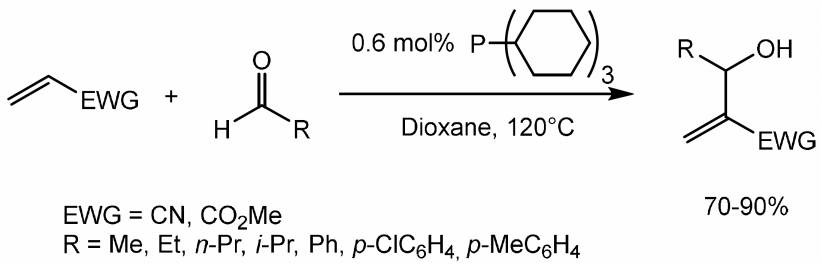

Scheme 19. Morita-Baylis-Hillman reaction as reported by Morita in 1968. EWG = electron-withdrawing group.

This reaction was first described by Morita in 1968 with a phosphine catalyst [178] and later, in 1972, by Baylis and Hillman with an amine catalyst.[179] The mechanism of this reaction is a Michael-type addition-elimination sequence (Scheme 20).[180]

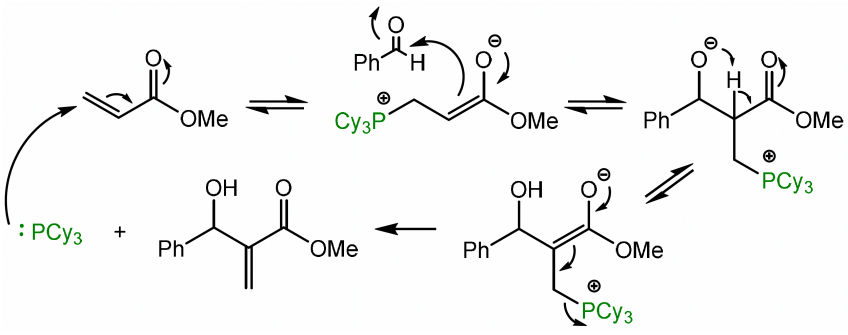

Scheme 20. Mechanism of the MBH reaction.[180]

The main drawback of this reaction was the high dependence of the yields and conversions on the substrate.[148] At first, this limited the applications in complex syntheses but new developments after the 90's, in particular the design of better catalysts, overcame these problems until the MBH became a prominent method for the synthesis of new C-C bonds.[180] Tertiary amines are more often used as catalysts because of their low costs and less toxic character although phosphines usually perform better and in easier conditions.[148] The asymmetric variant of the MBH reaction has been extensively developed in later years.[181] Notably, multifunctional chiral phosphine catalysts based on the BINOL scaffold were developed to increase the stability of the reaction intermediates as well as enantio- or diastereoselectively form the desired product.[182]

P-chiral phosphines also serve as catalysts for asymmetric acylation reactions and give moderate to good enantiomeric excess.[177] The utility of chiral phosphines in asymmetric organocatalysis (either P-chiral phosphines or phosphines in a chiral structure) has increased in the last decade. New chiral phosphines were developed to maximize the nucleophilicity of the catalyst in a chiral scaffold (Figure 9).[48]

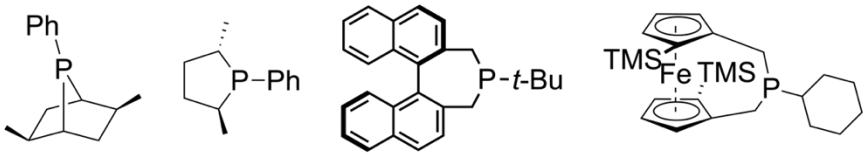

a b c d

Figure 9. Examples of chiral phosphines, bearing a bridged skeleton (a), cyclic (b), with a biaryl scaffold (c) and based on ferrocene (d).

Frustrated Lewis pair chemistry proved to be an important new field of phosphine organocatalysis. From the use of simple alkyl or aryl phosphines such as P*t*Bu$_3$ and PMes$_3$ to deactivated ones like (C_6F_5)Ph_2P and intramolecular systems, the development of new Lewis bases is crucial to broaden the scope of FLP chemistry. In this regard, 9-phosphatriptycene derivatives are promising new candidates, their unique properties detailed below could prove useful in the hydrogenation of challenging substrates.

2.4 The 9-phosphatriptycene and its derivatives

Synthesized by Bartlett in 1942, the triptycene is the simplest member of the iptycene family of molecules.[183-184] This scaffold consists in arene units fused to the central bicyclo[2.2.2]octatriene bridgehead system, forming a rigid system. Due to their unique 3D structure (Figure 10), triptycene derivatives have mainly been used in molecular machines, supramolecular chemistry, and material science.[185-186]

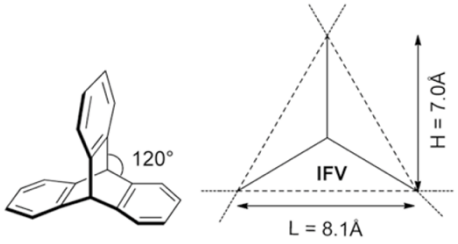

Figure 10. Structure of the triptycene, figure reprinted from reference 184. IFV refers to the "Internal Free Volume" defined by Swager.[187]

An understudied and yet promising class of phosphines are 9-phosphatriptycene derivatives. The 9-phosphatriptycene is a strongly pyramidalized ring-strained phosphine with its phosphorus atom in the bridgehead 9-position of the tricyclic [2.2.2]-octatriene inner motif. While heteroderivatives of the triptycene were synthesized in the decades following the parent triptycene, they found little applications until their use as ligands in the early 2000's.[188-190] Among them, the 9-phosphatriptycene was first synthesized in 1974 by Bickelhaupt in five steps with 3% overall yield (Scheme 21).[189]

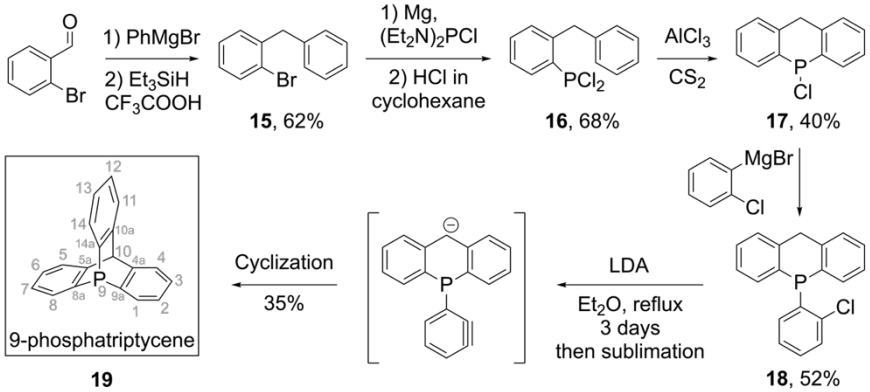

Scheme 21. Bickelhaupt's synthesis of 9-phosphatriptycene (overall yield 3%). The atomic numbering shown in grey is introduced by Chen and Ma in reference 184 and is used throughout this manuscript. Note that the "a" subscripts refer to the carbons connected to the bridgehead positions that cannot bear substituents.

In the past two decades, several new developments and syntheses were made on the phosphatriptycene and its derivatives. A new synthetic pathway was designed by the group of Kawashima in 2003 that uses phosphatriptycene oxides intermediates to access methoxy substituted phosphatriptycenes (**20**, Figure 11).[191] Other oxide derivatives were later described by the same group.[192] Tsuji, Tamao *et al*. reported the synthesis of new 9-phospha-10-silatriptycenes **21** and derivatives as well as a study of their structure and properties.[193] In order to have a better solubility in common organic solvents, the group of Mazaki introduced methyl groups on phosphorus- and antimony-based diheteratriptycenes.[194] These methyl groups were added on the 2, 3, 6, 7, 12 and 13-positions (**22**).

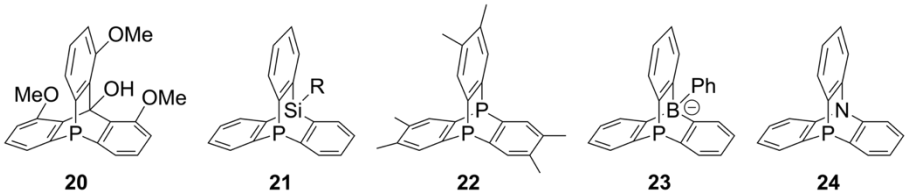

Figure 11. Phosphatriptycene derivatives: Kawashima's phosphatriptycene derivative (a), Tsuji's 9-phospha-10-silatriptycene (b), Mazaki's methylated 9,10-diphosphatriptycene (c), Sawamura's 9-phospha-10-boratriptycene derivative (d) and Shionoya's 9-phospha-10-azatriptycene (e).

A significantly greater challenge, however, is to add substituents in positions 1, 8 and 14 (*i.e.* in *ortho*-position relative to the phosphorus), and no example of triptycenes with this interesting substitution pattern has been reported so far.

To this day, the applications of phosphatriptycenes are limited to being used as ligands in organometallic chemistry. These strong π-acids and weak σ-donors were shown to be effective ligands in palladium-catalyzed reactions, Stille coupling and Heck reactions.[195] Recently, the group of Sawamura reported the synthesis of a 9-phospha-10-boratriptycene (**23**), used as ligand in a Pd-catalyzed Suzuki-Miyaura cross-coupling.[196] In heterogeneous catalysis, a silica-supported 9-phosphatriptycene has also displayed good ligand properties in Pd-catalyzed Suzuki-Miyaura cross-couplings[197] and Rh-catalyzed selective C-H borylations.[198] Shionoya *et al.* described the synthesis of azaphosphatriptycene (**24**) as a rotor in a palladium-centered molecular gear.[199]

The 9-phosphatriptycene was never reportedly tested as a Lewis base in FLPs or in any other organocatalysis. It possesses however interesting properties. The scaffold is very robust and can be heated to high temperatures without

degradation. *Ortho*-substituents in the unique structure of the triptycene would be fixed in a rigid position, pointing forward. This could be very useful in a number of applications. The steric and electronic properties of the 9-phosphatriptycenes could be modulated by changing the groups in this position.

In 2018, before the start of the present PhD thesis, our group published, with the work of Dr. Lei Hu, two new synthetic approaches to the parent 9-phosphatriptycene, as well as a combined experimental and theoretical investigation of its steric and electronic properties.[200] On the one hand, it can be obtained *via* an *ortho*-tribrominated phosphine precursor that undergoes a triple lithium-halogen exchange, then cyclizes on phenylchloroformate to give a 9-phospha-10-hydroxytriptycene that is further reduced into the target 9-phosphatriptycene in two steps using a Barton-McCombie deoxygenation (Scheme 22, Pathway 1). On the other hand, a trihalogenated triphenylmethane precursor[201] can be used for lithiation and cyclization on a phosphorus-based electrophile, namely PCl_3, to obtain 9-phosphatriptycene (Scheme 22, Pathway 2).

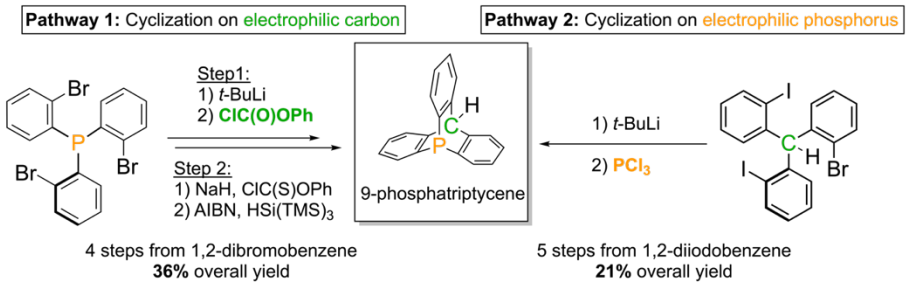

Scheme 22. Formation of 9-phosphatriptycene via two synthetic pathways.

The cage-like structure of the 9-phosphatriptycene **19** imposes a strong pyramidalization on the phosphorus center with respect to other triarylphosphines. This structural constraint impacts the electronic configuration of the phosphorus and induces a high *s* character of its lone pair. Interestingly, it was highlighted that this triptycene scaffold effected a weakening of the Lewis basicity of the phosphorus atom compared to the reference triphenylphosphine (PPh_3). This was evidenced computationally[2] by a lower proton affinity and methyl cation affinity of **19** than PPh_3 and

[2] M06-2X/6-311+G**//B3LYP-D3/6-31+G* (benzene, polarizable continuum-Poisson method) using the Jaguar 8.5 pseudospectral program package. Quantum chemical calculations performed by Lei Hu.

experimentally by the evaluation of the Lewis Basicity (*LB*) parameter, as introduced by Mayr, with a *LB* value 7.63 for **19** with respect to 14.27 for PPh_3, corresponding to a $\sim 10^6$ times weaker Lewis basicity towards C-centered Lewis acids.[155] Finally, the pK_a in water of the conjugate acid of PPh_3 was estimated at -1.5 by linear correlation between computed proton affinities and experimental pK_a of reference phosphines (w.r.t. 3.28 for PPh_3).[3]

[3] Correlation between B3LYP-D3/6-31+G* (benzene) proton affinities and pK_a in water of three triarylphosphines (PPh_3 [3.28], P(*p*-Cl-C_6H_4)$_3$ [0.87] and P(*p*-CF_3-C_6H_4)$_3$ [-1.39]; R^2 = 0.9994)

3. Objectives of the research project

This PhD thesis aims at developing and studying a promising class of weakly basic phosphines, 9-phosphatriptycene derivatives, and probe their application in frustrated Lewis pair chemistry. At a fundamental level, the goal of this investigation is to develop our understanding of structure-property relationships in cage-shaped phosphines, especially at the electronic level. This study will be supported by experimental work as well as quantum chemical calculations performed using Density Functional Theory. For the latter part of the research, a specific objective is to develop and apply a robust theoretical method as well as new tools that can be useful even beyond the scope of this work. From an applied perspective, the new molecules developed during this PhD thesis are employed to target specific limitations in the field of frustrated Lewis pair chemistry, offering alternatives to transition metal catalysts, which is a major societal issue. This aims at broadening the current scope of reactions available in main group chemistry.

This manuscript is divided into several chapters, each aiming at answering one targeted objective described above. Specifically, the research on 9-phosphatriptycene derivatives has long been hampered by the difficulty to synthesize them, the synthesis of the parent compound was reported long ago and requires hazardous reactions with harsh conditions.[189] Developing a new convenient synthetic pathway was thus an obvious prerequisite to any research on this family of compounds. Building from a previous reported work on the unsubstituted 9-phosphatriptycene from our group,[200] the first chapter focuses on the synthesis of *ortho*-substituted 9-phosphatriptycenes and a primary investigation of their electronic properties and coordinating ability.

Next, a fundamental investigation of the structure-property relationships in 9-phosphatriptycenes is undertaken to understand the origins of their unique reactivity. An important reactivity parameter of phosphines to consider in FLP chemistry is the pK_a of their conjugate phosphonium cation. The latter is still unknown for 9-phosphatriptycene derivatives, which is why a new DFT tool is also developed for its accurate estimation.

The low basicity of 9-phosphatriptycenes is what sets them apart from other phosphines. In addition, they have a high thermal stability. This unique reactivity can be taken advantage of in the context of FLP-catalysis, in which the hydrogenation of unactivated olefins is still a challenge. Upon hydrogen

activation and given favorable experimental conditions, 9-phosphatriptycenes could provide a suitable solution to this problem. The third chapter of the manuscript thus focuses on the optimization of the FLP-catalyzed hydrogenation of unactivated alkenes and the DFT study of their mechanism.

Beyond the field of FLP catalysis, the reactivity displayed by 9-phosphatriptycenes and studied in the previous chapters could serve to advance other aspects of main group chemistry. As a proof of concept, their application in the field of electrophilic fluorinations is probed in Chapter IV. Fluorophosphonium cations are known to be Lewis acids, but the cage-scaffold of 9-phosphatriptycenes should prevent this reactivity, allowing for the first time their use as electrophilic fluorinating agents.

Finally, in parallel to the main work of this research project on 9-phosphatriptycenes, a significant part of this PhD was dedicated to DFT investigations on boron Lewis acids in the context of collaborations among the research group of Prof. Berionni, as a support for the experimental work of other researchers. Each time, the objective was the same however: the establishment of structure-property relationships in these boranes as well as a characterization of their Lewis acidity through the means of quantum chemical calculations. This work aims at supporting and guiding experimental endeavors in the lab. The fifth chapter of this manuscript summarizes these contributions, while the sixth and last chapter gives details on the development of a new catalyst predicted to be able to activate methane (1-aza-9-boratriptycene), a great challenge in main group chemistry. The aim of this last contribution is still to advance our fundamental understanding of the reactivity of these main group compounds while finding relevant applications to societal issues.

A summary of the content and objectives of each chapter is given below:

	Content	Objectives
Chapter I	Five-step synthesis of *ortho*-substituted 9-phosphatriptycenes and primary investigation of their coordinating abilities.	Provide a solution to access 9-phospha-triptycenes for further research.
Chapter II	Investigation of structure-property relationships in 9-phosphatriptycenes and development of a pK_a prediction method.	Understand the origin of the reactivity of 9-phosphatriptycenes and quantify its impact on their reactivity.
Chapter III	Optimization and scope of FLP-catalyzed hydrogenation of olefins with 9-phospha-triptycenes.	Find alternatives to transition metal catalysts and solutions to current limitations in the field of FLP catalysis.
Chapter IV	Preliminary study on the synthesis and reactivity of 9-phosphatriptycene-derived difluoro-phosphoranes and fluorophosphonium cations.	Exploit the 9-phosphatriptycene scaffold to expand phosphorus reactivity in main group chemistry.
Chapter V	DFT study on boron Lewis acids synthesized in the research group.	Establish structure-reactivity relationships in non-planar boranes and characterize their Lewis acidity.
Chapter VI	DFT study of the reactivity of 1-aza-9-bora-triptycene with methane and comparison with other reported systems.	Understand the reactivity of methane with FLPs, provide guidelines to develop new solutions to a societal issue.

4. References

[1] G. N. Lewis, *Valence and the structure of atoms and molecules*, American Chemical Society, **1923**.

[2] H. Yamamoto (Ed.), *Lewis acid reagents: a practical approach*, Oxford University Press, New-York, **1999**.

[3] E. Y. Chen, T. J. Marks, "Cocatalysts for metal-catalyzed olefin polymerization: activators, activation processes, and structure-activity relationships", *Chem. Rev.* **2000**, *100*, 1391-1434.

[4] H. Yamamoto (Ed.), *Lewis acids in organic synthesis*, Wiley-VCH, Weinheim, **2000**.

[5] A. Corma, H. Garcia, "Lewis acids: from conventional homogeneous to green homogeneous and heterogeneous catalysis", *Chem. Rev.* **2003**, *103*, 4307-4365.

[6] W. E. Piers, T. Chivers, "Pentafluorophenylboranes: from obscurity to applications", *Chem. Soc. Rev.* **1997**, *26*.

[7] K. Ishihara, H. Yamamoto, "Arylboron compounds as acid catalysts in organic synthetic transformations", *Eur. J. Org. Chem.* **1999**, *1999*, 527-538.

[8] G. Erker, "Tris(pentafluorophenyl)borane: a special boron Lewis acid for special reactions", *Dalton Trans.* **2005**, 1883-1890.

[9] T. Chivers, "Pentafluorophenylboron halides: 40 years later", *J. Fluorine Chem.* **2002**, *115*, 1-8.

[10] R. H. Crabtree (Ed.), *The organometallic chemistry of the transition metals*, 6th ed., John Wiley & Sons, Inc., Hoboken, **2014**.

[11] S. E. Denmark, G. L. Beutner, "Lewis base catalysis in organic synthesis", *Angew. Chem. Int. Ed.* **2008**, *47*, 1560-1638.

[12] H. C. Brown, H. I. Schlesinger, S. Z. Cardon, "Studies in stereochemistry. I. Steric strains as a factor in the relative stability of some coordination compounds of boron", *J. Am. Chem. Soc.* **1942**, *64*, 325-329.

[13] G. C. Welch, R. R. San Juan, J. D. Masuda, D. W. Stephan, "Reversible, metal-free hydrogen activation", *Science* **2006**, *314*, 1124-1126.

[14] G. C. Welch, D. W. Stephan, "Facile heterolytic cleavage of dihydrogen by phosphines and boranes", *J. Am. Chem. Soc.* **2007**, *129*, 1880-1881.

[15] D. W. Stephan, ""frustrated Lewis pairs": A concept for new reactivity and catalysis", *Org. Biomol. Chem.* **2008**, *6*, 1535-1539.

[16] J. S. McCahill, G. C. Welch, D. W. Stephan, "Reactivity of "frustrated Lewis pairs": three-component reactions of phosphines, a borane, and olefins", *Angew. Chem. Int. Ed.* **2007**, *46*, 4968-4971.

[17] P. A. Chase, G. C. Welch, T. Jurca, D. W. Stephan, "Metal-free catalytic hydrogenation", *Angew. Chem. Int. Ed.* **2007**, *46*, 8050-8053.

[18] D. W. Stephan, ""Frustrated Lewis pair" hydrogenations", *Org. Biomol. Chem.* **2012**, *10*, 5740-5746.

[19] C. H. Bartholomew, R. J. Farrauto, *Fundamentals of industrial catalytic processes*, 2nd ed., John Wiley & sons, Inc., Hoboken (NJ), USA, **2006**.

[20] H.-U. Blaser, C. Malan, B. Pugin, F. Spindler, H. Steiner, M. Studer, "Selective hydrogenation for fine chemicals: recent trends and new developments", *Adv. Synth. Catal.* **2003**, *345*, 103-151.

[21] P. Sabatier, "How I have been led to the direct hydrogenation method by metallic catalysts", *Ind. Eng. Chem.* **1926**, *18*, 1005-1008.

[22] J. G. de Vries, C. J. Elsevier (Ed.), *The handbook of homogeneous hydrogenation*, Wiley-VCH, Weinheim, **2006**.

[23] R. Morris Bullock (Ed.), *Catalysis without precious metals*, Wiley-VCH, Weinheim, Germany, **2010**.

[24] B. K. Sovacool, S. H. Ali, M. Bazilian, B. Radley, B. Nemery, J. Okatz, D. Mulvaney, "Sustainable minerals and metals for a low-carbon future", *Science* **2020**, *367*, 30-33.

[25] E. Lebre, M. Stringer, K. Svobodova, J. R. Owen, D. Kemp, C. Cote, A. Arratia-Solar, R. K. Valenta, "The social and environmental complexities of extracting energy transition metals", *Nature Communications* **2020**, *11*, 4823.

[26] K. S. Egorova, V. P. Ananikov, "Toxicity of metal compounds: knowledge and myths", *Organometallics* **2017**, *36*, 4071-4090.

[27] W. Cheves, L. Bollyky, "Homogeneous hydrogenation in the absence of transition-metal catalysts", *J. Am. Chem. Soc.* **1964**, *86*, 3750-3752.

[28] A. Berkessel, T. J. Schubert, T. N. Muller, "Hydrogenation without a transition-metal catalyst: on the mechanism of the base-catalyzed hydrogenation of ketones", *J. Am. Chem. Soc.* **2002**, *124*, 8693-8698.

[29] P. I. Dalko, L. Moisan, "In the golden age of organocatalysis", *Angew. Chem. Int. Ed.* **2004**, *43*, 5138-5175.

[30] J. W. Yang, M. T. Hechavarria Fonseca, B. List, "A metal-free transfer hydrogenation: organocatalytic conjugate reduction of alpha,beta-unsaturated aldehydes", *Angew. Chem. Int. Ed.* **2004**, *43*, 6660-6662.

[31] H. Adolfsson, "Organocatalytic hydride transfers: a new concept in asymmetric hydrogenations", *Angew. Chem. Int. Ed.* **2005**, *44*, 3340-3342.

[32] M. Rueping, A. P. Antonchick, T. Theissmann, "A highly enantioselective Brønsted acid catalyzed cascade reaction: organocatalytic transfer hydrogenation of quinolines and their application in the synthesis of alkaloids", *Angew. Chem. Int. Ed.* **2006**, *45*, 3683-3686.

[33] J. B. Tuttle, S. G. Ouellet, D. W. MacMillan, "Organocatalytic transfer hydrogenation of cyclic enones", *J. Am. Chem. Soc.* **2006**, *128*, 12662-12663.

[34] C. Zheng, S. L. You, "Transfer hydrogenation with Hantzsch esters and related organic hydride donors", *Chem. Soc. Rev.* **2012**, *41*, 2498-2518.

[35] J. Paradies, "Frustrated Lewis pair catalyzed hydrogenations", *Synlett* **2013**, *24*, 777-780.

[36] J. Lam, K. M. Szkop, E. Mosaferi, D. W. Stephan, "FLP catalysis: main group hydrogenations of organic unsaturated substrates", *Chem. Soc. Rev.* **2019**, *48*, 3592-3612.

[37] R. Zhou, Z. Tavandashti, J. Paradies, "Frustrated Lewis pair catalysed reactions", *SynOpen* **2023**.

[38] P. A. Chase, T. Jurca, D. W. Stephan, "Lewis acid-catalyzed hydrogenation: $B(C_6F_5)_3$-mediated reduction of imines and nitriles with H_2", *Chem. Commun.* **2008**, 1701-1703.

[39] D. Chen, J. Klankermayer, "Metal-free catalytic hydrogenation of imines with tris(perfluorophenyl)borane", *Chem. Commun.* **2008**, 2130-2131.

[40] G. Erös, K. Nagy, H. Mehdi, I. Pápai, P. Nagy, P. Király, G. Tárkányi, T. Soõs, "Catalytic hydrogenation with frustrated Lewis pairs: Selectivity achieved by size-exclusion design of Lewis acids", *Chem. Eur. J.* **2012**, *18*, 574-585.

[41] V. Sumerin, F. Schulz, M. Atsumi, C. Wang, M. Nieger, M. Leskela, T. Repo, P. Pyykko, B. Rieger, "Molecular tweezers for hydrogen: synthesis, characterization, and reactivity", *J. Am. Chem. Soc.* **2008**, *130*, 14117-14119.

[42] S. Tussing, L. Greb, S. Tamke, B. Schirmer, C. Muhle-Goll, B. Luy, J. Paradies, "Autoinduced catalysis and inverse equilibrium isotope effect in the frustrated Lewis pair catalyzed hydrogenation of imines", *Chem. Eur. J.* **2015**, *21*, 8056-8059.

[43] D. J. Scott, M. J. Fuchter, A. E. Ashley, "Metal-free hydrogenation catalyzed by an air-stable borane: use of solvent as a frustrated Lewis base", *Angew. Chem. Int. Ed.* **2014**, *53*, 10218-10222.

[44] L. Greb, P. Oña-Burgos, B. Schirmer, S. Grimme, D. W. Stephan, J. Paradies, "Metal-free catalytic olefin hydrogenation: Low-temperature H_2 activation by frustrated Lewis pairs", *Angew. Chem. Int. Ed.* **2012**, *51*, 10164-10168.

[45] L. J. Hounjet, C. Bannwarth, C. N. Garon, C. B. Caputo, S. Grimme, D. W. Stephan, "Combinations of ethers and $B(C_6F_5)_3$ function as hydrogenation catalysts", *Angew. Chem. Int. Ed.* **2013**, *52*, 7492-7495.

[46] S. J. Geier, P. A. Chase, D. W. Stephan, "Metal-free reductions of N-heterocycles via Lewis acid catalyzed hydrogenation", *Chem. Commun.* **2010**, *46*, 4884-4886.

[47] Y. Segawa, D. W. Stephan, "Metal-free hydrogenation catalysis of polycyclic aromatic hydrocarbons", *Chem. Commun.* **2012**, *48*, 11963-11965.

[48] T. Mahdi, Z. M. Heiden, S. Grimme, D. W. Stephan, "Metal-free aromatic hydrogenation: Aniline to cyclohexyl-amine derivatives", *J. Am. Chem. Soc.* **2012**, *134*, 4088-4091.

[49] G. Li, Y. Liu, H. Du, "$B(C_6F_5)_3$-catalyzed metal-free hydrogenation of naphthylamines", *Org. Biomol. Chem.* **2015**, *13*, 2875-2878.

[50] B. Ines, D. Palomas, S. Holle, S. Steinberg, J. A. Nicasio, M. Alcarazo, "Metal-free hydrogenation of electron-poor allenes and alkenes", *Angew. Chem. Int. Ed.* **2012**, *51*, 12367-12369.

[51] J. A. Nicasio, S. Steinberg, B. Ines, M. Alcarazo, "Tuning the Lewis acidity of boranes in frustrated Lewis pair chemistry: implications for the hydrogenation of electron-poor alkenes", *Chem. Eur. J.* **2013**, *19*, 11016-11020.

[52] L. Greb, C. G. Daniliuc, K. Bergander, J. Paradies, "Functional-group tolerance in frustrated Lewis pairs: hydrogenation of nitroolefins and acrylates", *Angew. Chem. Int. Ed.* **2013**, *52*, 5876-5879.

[53] Y. Wang, W. Chen, Z. Lu, Z. H. Li, H. Wang, "Metal-free $HB(C_6F_5)_2$-catalyzed hydrogenation of unfunctionalized olefins and mechanism study of borane-mediated σ-bond metathesis", *Angew. Chem. Int. Ed.* **2013**, *52*, 7496-7499.

[54] F. L. Ramp, E. J. DeWitt, L. E. Trapasso, "Homogeneous hydrogenation catalyzed by boranes", *J. Am. Chem. Soc.* **1961**, *83*, 4672.

[55] F. L. Ramp, E. J. DeWitt, L. E. Trapasso, "Homogeneous hydrogenation catalyzed by boranes", *J. Org. Chem.* **1962**, *27*, 4368-4372.

[56] D. J. Parks, W. E. Piers, G. P. A. Yap, "Synthesis, properties, and hydroboration activity of the highly electrophilic borane bis(pentafluorophenyl)borane, $HB(C_6F_5)_2$", *Organometallics* **1998**, *17*, 5492-5503.

[57] B. H. Xu, G. Kehr, R. Frohlich, B. Wibbeling, B. Schirmer, S. Grimme, G. Erker, "Reaction of frustrated Lewis pairs with conjugated ynones-selective hydrogenation of the carbon-carbon triple bond", *Angew. Chem. Int. Ed.* **2011**, *50*, 7183-7186.

[58] Y. Liu, L. Hu, H. Chen, H. Du, "An alkene-promoted borane-catalyzed highly stereoselective hydrogenation of alkynes to give Z- and E-alkenes", *Chem. Eur. J.* **2015**, *21*, 3495-3501.

[59] J. Nyhlen, T. Privalov, "On the possibility of catalytic reduction of carbonyl moieties with tris(pentafluorophenyl)borane and H_2: a computational study", *Dalton Trans.* **2009**, 5780-5786.

[60] M. Lindqvist, N. Sarnela, V. Sumerin, K. Chernichenko, M. Leskela, T. Repo, "Heterolytic dihydrogen activation by $B(C_6F_5)_3$ and carbonyl compounds", *Dalton Trans.* **2012**, *41*, 4310-4312.

[61] L. E. Longobardi, C. Tang, D. W. Stephan, "Stoichiometric reductions of alkyl-substituted ketones and aldehydes to borinic esters", *Dalton Trans.* **2014**, *43*, 15723-15726.

[62] D. J. Scott, M. J. Fuchter, A. E. Ashley, "Non-metal catalyzed hydrogenation of carbonyl compounds", *J. Am. Chem. Soc.* **2014**, *136*, 15813-15816.

[63] T. Mahdi, D. W. Stephan, "Enabling catalytic ketone hydrogenation by frustrated Lewis pairs", *J. Am. Chem. Soc.* **2014**, *136*, 15809-15812.

[64] G. Erős, H. Mehdi, I. Pápai, T. A. Rokob, P. Király, G. Tárkányi, T. Soós, "Expanding the scope of metal-free catalytic hydrogenation through frustrated Lewis pair design", *Angew. Chem. Int. Ed.* **2010**, *122*, 6709-6713.

[65] É. Dorkó, M. Szabó, B. Kótai, I. Pápai, A. Domján, T. Soós, "Expanding the boundaries of water-tolerant frustrated Lewis pair hydrogenation: Enhanced back strain in the Lewis acid enables the reductive amination of carbonyls", *Angew. Chem. Int. Ed.* **2017**, *56*, 9512-9516.

[66] Á. Gyömöre, M. Bakos, T. Földes, I. Pápai, A. Domján, T. Soós, "Moisture-tolerant frustrated Lewis pair catalyst for hydrogenation of aldehydes and ketones", *ACS Catal.* **2015**, *5*, 5366-5372.

[67] A. M. Smith, R. Whyman, "Review of methods for the catalytic hydrogenation of carboxamides", *Chem. Rev.* **2014**, *114*, 5477-5510.

[68] N. A. Sitte, M. Bursch, S. Grimme, J. Paradies, "Frustrated Lewis pair catalyzed hydrogenation of amides: halides as active Lewis base in the metal-free hydrogen activation", *J. Am. Chem. Soc.* **2019**, *141*, 159-162.

[69] H. Zhu, Z. W. Qu, S. Grimme, "Borane-catalyzed hydrogenation of tertiary amides activated by oxalyl chloride: DFT mechanistic insights", *Eur. J. Org. Chem.* **2019**, *2019*, 4609-4612.

[70] L. Koring, N. A. Sitte, M. Bursch, S. Grimme, J. H. H. Paradies, "Hydrogenation of secondary amides using phosphane oxide and frustrated Lewis pair catalysis", *Chem. Eur. J.* **2021**.

[71] J. S. Sapsford, D. Csókás, R. C. Turnell-Ritson, L. A. Parkin, A. D. Crawford, I. Pápai, A. E. Ashley, "Transition metal-free direct hydrogenation of esters via a frustrated Lewis pair", *ACS Catal.* **2021**, 9143-9150.

[72] D. Chen, Y. Wang, J. Klankermayer, "Enantioselective hydrogenation with chiral frustrated Lewis pairs", *Angew. Chem. Int. Ed.* **2010**, *49*, 9475-9478.

[73] G. Ghattas, D. Chen, F. Pan, J. Klankermayer, "Asymmetric hydrogenation of imines with a recyclable chiral frustrated Lewis pair catalyst", *Dalton Trans.* **2012**, *41*, 9026-9028.

[74] X. Wang, G. Kehr, C. G. Daniliuc, G. Erker, "Internal adduct formation of active intramolecular C_4-bridged frustrated phosphane/borane Lewis pairs", *J. Am. Chem. Soc.* **2014**, *136*, 3293-3303.

[75] K. Y. Ye, X. Wang, C. G. Daniliuc, G. Kehr, G. Erker, "A ferrocene-based phosphane/borane frustrated Lewis pair for asymmetric imine reduction", *Eur. J. Inorg. Chem.* **2016**, *2017*, 368-371.

[76] V. Sumerin, K. Chernichenko, M. Nieger, M. Leskelä, B. Rieger, T. Repo, "Highly active metal-free catalysts for hydrogenation of unsaturated nitrogen-containing compounds", *Adv. Synth. Catal.* **2011**, *353*, 2093-2110.

[77] Y. Liu, H. Du, "Chiral dienes as "ligands" for borane-catalyzed metal-free asymmetric hydrogenation of imines", *J. Am. Chem. Soc.* **2013**, *135*, 6810-6813.

[78] M. Lindqvist, K. Borre, K. Axenov, B. Kotai, M. Nieger, M. Leskela, I. Papai, T. Repo, "Chiral molecular tweezers: synthesis and reactivity in asymmetric hydrogenation", *J. Am. Chem. Soc.* **2015**, *137*, 4038-4041.

[79] S. Wei, H. Du, "A highly enantioselective hydrogenation of silyl enol ethers catalyzed by chiral frustrated Lewis pairs", *J. Am. Chem. Soc.* **2014**, *136*, 12261-12264.

[80] X. Ren, G. Li, S. Wei, H. Du, "Facile development of chiral alkenylboranes from chiral diynes for asymmetric hydrogenation of silyl enol ethers", *Org. Lett.* **2015**, *17*, 990-993.

[81] Z. Zhang, H. Du, "Enantioselective metal-free hydrogenations of disubstituted quinolines", *Org. Lett.* **2015**, *17*, 6266-6269.

[82] Z. Zhang, H. Du, "*Cis*-selective and highly enantioselective hydrogenation of 2,3,4-trisubstituted quinolines", *Org. Lett.* **2015**, *17*, 2816-2819.

[83] Z. Zhang, H. Du, "A highly *cis*-selective and enantioselective metal-free hydrogenation of 2,3-disubstituted quinoxalines", *Angew. Chem. Int. Ed.* **2015**, *54*, 623-626.

[84] T. A. Rokob, A. Hamza, A. Stirling, T. Soós, I. Pápai, "Turning frustration into bond activation: A theoretical mechanistic study on heterolytic hydrogen splitting by frustrated Lewis pairs", *Angew. Chem. Int. Ed.* **2008**, *47*, 2435-2438.

[85] T. A. Rokob, A. Hamza, I. Pápai, "Rationalizing the reactivity of frustrated Lewis pairs: Thermodynamics of H_2 activation and the role of acid–base properties", *J. Am. Chem. Soc.* **2009**, *131*, 10701-10710.

[86] H. Li, L. Zhao, G. Lu, Y. Mo, Z. X. Wang, "Insight into the relative reactivity of "frustrated Lewis pairs" and stable carbenes in activating H_2 and CH_4: a comparative computational study", *Phys. Chem. Chem. Phys.* **2010**, *12*, 5268-5275.

[87] S. Gao, W. Wu, Y. Mo, "Steric and electronic effects on the heterolytic H_2-splitting by phosphine-boranes R_3B/PR'_3 (R = C_6F_5, Ph; R′ = $C_6H_2Me_3$, tBu, Ph, C_6F_5, Me, H): a computational study", *Int. J. Quantum Chem* **2011**, *111*, 3761-3775.

[88] T. A. Rokob, I. Papai, "Hydrogen activation by frustrated Lewis pairs: insights from computational studies", *Top. Curr. Chem.* **2013**, *332*, 157-212.

[89] L. L. Zeonjuk, N. Vankova, A. Mavrandonakis, T. Heine, G.-V. Röschenthaler, J. Eicher, "On the mechanism of hydrogen activation by frustrated Lewis pairs", *Chem. Eur. J.* **2013**, *19*, 17413-17424.

[90] J. Paradies, "Mechanisms in frustrated Lewis pair-catalyzed reactions", *Eur. J. Org. Chem.* **2019**, *2019*, 283-294.

[91] G. Sharma, P. D. Newman, J. A. Platts, "A review of quantum chemical studies of frustrated Lewis pairs", *J. Mol. Graphics Modell.* **2021**, *105*, 107846.

[92] T. J. Tague, L. Andrews, "Reactions of pulsed-laser evaporated boron atoms with hydrogen. Infrared spectra of boron hydride intermediate species in solid argon", *J. Am. Chem. Soc.* **1994**, *116*, 4970-4976.

[93] J. D. Watts, R. J. Bartlett, "On the existence of BH_5", *J. Am. Chem. Soc.* **1995**, *117*, 825-826.

[94] A. Hamza, A. Stirling, T. András Rokob, I. Pápai, "Mechanism of hydrogen activation by frustrated Lewis pairs: A molecular orbital approach", *Int. J. Quantum Chem* **2009**, *109*, 2416-2425.

[95] Y. Guo, S. Li, "Unusual concerted Lewis acid-Lewis base mechanism for hydrogen activation by a phosphine-borane compound", *Inorg. Chem.* **2008**, *47*, 6212-6219.

[96] S. Grimme, H. Kruse, L. Goerigk, G. Erker, "The mechanism of dihydrogen activation by frustrated Lewis pairs revisited", *Angew. Chem. Int. Ed.* **2010**, *49*, 1402-1405.

[97] S. Grimme, "Semi-empirical GGA-type density functional constructed with a long-range dispersion correction", *J. Comput. Chem.* **2006**, *27*, 1787-1799.

[98] A. Schäfer, C. Huber, R. Ahlrichs, "Fully optimized contracted Gaussian basis sets of triple *zeta* valence quality for atoms Li to Kr", *J. Chem. Phys.* **1994**, *100*, 5829-5835.

[99] S. Grimme, "Improved second-order Møller–Plesset perturbation theory by separate scaling of parallel- and antiparallel-spin pair correlation energies", *J. Chem. Phys.* **2003**, *118*, 9095-9102.

[100] G. A. Petersson, M. Braunstein, "Complete basis set correlation energies. IV. The total correlation energy of the water molecule", *J. Chem. Phys.* **1985**, *83*, 5129-5134.

[101] J. W. Ochterski, G. A. Petersson, K. B. Wiberg, "A comparison of model chemistries", *J. Am. Chem. Soc.* **2002**, *117*, 11299-11308.

[102] D. M. Camaioni, B. Ginovska-Pangovska, G. K. Schenter, S. M. Kathmann, T. Autrey, "Analysis of the activation and heterolytic dissociation of H_2 by frustrated Lewis pairs: NH_3/BX_3 (X = H, F, and Cl)", *J. Phys. Chem. A* **2012**, *116*, 7228-7237.

[103] A. G. Baboul, L. A. Curtiss, P. C. Redfern, K. Raghavachari, "Gaussian-3 theory using density functional geometries and zero-point energies", *J. Chem. Phys.* **1999**, *110*, 7650-7657.

[104] T. A. Rokob, I. Bako, A. Stirling, A. Hamza, I. Papai, "Reactivity models of hydrogen activation by frustrated Lewis pairs: synergistic electron transfers or polarization by electric field?", *J. Am. Chem. Soc.* **2013**, *135*, 4425-4437.

[105] M. Pu, T. Privalov, "*Ab initio* dynamics trajectory study of the heterolytic cleavage of H_2 by a Lewis acid $[B(C_6F_5)_3]$ and a Lewis base $[P(t\text{Bu})_3]$", *J. Chem. Phys.* **2013**, *138*, 154305.

[106] L. Liu, B. Lukose, B. Ensing, "Hydrogen activation by frustrated Lewis pairs revisited by metadynamics simulations", *The Journal of Physical Chemistry C* **2017**, *121*, 2046-2051.

[107] J. Daru, I. Bakó, A. Stirling, I. Pápai, "Mechanism of heterolytic hydrogen splitting by frustrated Lewis pairs: comparison of static and dynamic models", *ACS Catal.* **2019**, *9*, 6049-6057.

[108] M. Heshmat, T. Privalov, "H_2 cleavage by frustrated Lewis pairs characterized by the energy decomposition analysis of transition states: An alternative to the electron transfer and electric field models", *J. Phys. Chem. A* **2018**, *122*, 7202-7211.

[109] D. W. Stephan, G. Erker, "Frustrated Lewis pairs: metal-free hydrogen activation and more", *Angew. Chem. Int. Ed.* **2010**, *49*, 46-76.

[110] D. W. Stephan, "The broadening reach of frustrated Lewis pair chemistry", *Science* **2016**, *354*, 1248-1256.

[111] D. W. Stephan, G. Erker, "Frustrated Lewis pair chemistry of carbon, nitrogen and sulfur oxides", *Chem. Sci.* **2014**, *5*, 2625-2641.

[112] C. M. Mömming, E. Otten, G. Kehr, R. Fröhlich, S. Grimme, D. W. Stephan, G. Erker, "Reversible metal-free carbon dioxide binding by frustrated Lewis pairs", *Angew. Chem. Int. Ed.* **2009**, *48*, 6643-6646.

[113] M. Sajid, A. Klose, B. Birkmann, L. Liang, B. Schirmer, T. Wiegand, H. Eckert, A. J. Lough, R. Fröhlich, C. G. Daniliuc, S. Grimme, D. W. Stephan, G. Kehr, G. Erker, "Reactions of phosphorus/boron frustrated Lewis pairs with SO_2", *Chem. Sci.* **2013**, *4*, 213-219.

[114] E. Otten, R. C. Neu, D. W. Stephan, "Complexation of nitrous oxide by frustrated Lewis pairs", *J. Am. Chem. Soc.* **2009**, *131*, 9918-9919.

[115] A. J. P. Cardenas, B. J. Culotta, T. H. Warren, S. Grimme, A. Stute, R. Fröhlich, G. Kehr, G. Erker, "Capture of NO by a frustrated Lewis pair: a new type of persistent N-oxyl radical", *Angew. Chem. Int. Ed.* **2011**, *50*, 7567-7571.

[116] T. R. Karl, K. E. Trenberth, "Modern global climate change", *Science* **2003**, *302*, 1719-1723.

[117] G. A. Olah, A. Goeppert, G. K. Prakash, "Chemical recycling of carbon dioxide to methanol and dimethyl ether: from greenhouse gas to renewable,

environmentally carbon neutral fuels and synthetic hydrocarbons", *J. Org. Chem.* **2009**, *74*, 487-498.

[118] D. Mellmann, P. Sponholz, H. Junge, M. Beller, "Formic acid as a hydrogen storage material - development of homogeneous catalysts for selective hydrogen release", *Chem. Soc. Rev.* **2016**, *45*, 3954-3988.

[119] B. Grignard, S. Gennen, C. Jérôme, A. W. Kleij, C. Detrembleur, " Advances in the use of CO_2 as a renewable feedstock for the synthesis of polymers ", *Chem. Soc. Rev.* **2019**, *48*, 4466-4514.

[120] X. Jiang, X. Nie, X. Guo, C. Song, J. G. Chen, "Recent Advances in Carbon Dioxide Hydrogenation to Methanol via Heterogeneous Catalysis", *Chem. Rev.* **2020**, *120*, 7984-8034.

[121] W. Taifan, J. F. Boily, J. Baltrusaitis, "Surface chemistry of carbon dioxide revisited", *Surf. Sci. Rep.* **2016**, *71*, 595-671.

[122] C. Costentin, M. Robert, J. M. Savéant, "Catalysis of the electrochemical reduction of carbon dioxide", *Chem. Soc. Rev.* **2013**, *42*, 2423-2436.

[123] R. Tanaka, M. Yamashita, K. Nozaki, "Catalytic hydrogenation of carbon dioxide using Ir(III)-pincer complexes", *J. Am. Chem. Soc.* **2009**, *131*, 14168-14169.

[124] T. Zhao, X. Hu, Y. Wu, Z. Zhang, "Hydrogenation of CO_2 to formate with H_2 : Transition metal free catalyst based on a Lewis pair", *Angew. Chem. Int. Ed.* **2019**, *58*, 722-726.

[125] A. E. Ashley, A. L. Thompson, D. O'Hare, "Non-metal-mediated homogeneous hydrogenation of CO_2 to CH_3OH", *Angew. Chem. Int. Ed.* **2009**, *48*, 9839-9843.

[126] M.-A. Courtemanche, A. P. Pulis, É. Rochette, M.-A. Légaré, D. W. Stephan, F.-G. Fontaine, "Intramolecular B/N frustrated Lewis pairs and the hydrogenation of carbon dioxide", *Chem. Commun.* **2015**, *51*, 9797-9800.

[127] L. Liu, N. Vankova, T. Heine, "A kinetic study on the reduction of CO_2 by frustrated Lewis pairs: from understanding to rational design", *Phys. Chem. Chem. Phys.* **2016**, *18*, 3567-3574.

[128] B. Jiang, Q. Zhang, L. Dang, "Theoretical studies on bridged frustrated Lewis pair (FLP) mediated H_2 activation and CO_2 hydrogenation", *Organic Chemistry Frontiers* **2018**, *5*, 1905-1915.

[129] M. Ghara, P. K. Chattaraj, "A computational study on hydrogenation of CO_2, catalyzed by a bridged B/N frustrated Lewis pair", *Struct. Chem.* **2019**, *30*, 1067-1077.

[130] T. Wang, M. Xu, A. R. Jupp, Z. W. Qu, S. Grimme, D. W. Stephan, "Selective catalytic frustrated Lewis pair hydrogenation of CO_2 in the presence of silylhalides", *Angew. Chem. Int. Ed.* **2021**, *60*, 25771-25775.

[131] R. A. Periana, D. J. Taube, S. Gamble, H. Taube, T. Satoh, H. Fujii, "Platinum catalysts for the high-yield oxidation of methane to a methanol derivative", *Science* **1998**, *280*, 560-564.

[132] A. K. Cook, S. D. Schimler, A. J. Matzger, M. S. Sanford, "Catalyst-controlled selectivity in the C-H borylation of methane and ethane", *Science* **2016**, *351*, 1421-1424.

[133] K. T. Smith, S. Berritt, M. González-Moreiras, S. Ahn, M. R. Smith, M. H. Baik, D. J. Mindiola, "Catalytic borylation of methane", *Science* **2016**, *351*, 1424-1427.

[134] S. Frömel, C. G. Daniliuc, C. Bannwarth, S. Grimme, K. Bussmann, G. Kehr, G. Erker, "Indirect synthesis of a pair of formal methane activation products at a phosphane/borane frustrated Lewis pair", *Dalton Trans.* **2016**, *45*, 19230-19233.

[135] N. Villegas-Escobar, A. Toro-Labbé, M. Becerra, M. Real-Enriquez, J. R. Mora, L. Rincon, "A DFT study of hydrogen and methane activation by $B(C_6F_5)_3$/P(t-Bu)$_3$ and $Al(C_6F_5)_3$/P(t-Bu)$_3$ frustrated Lewis pairs", *J. Mol. Model.* **2017**, *23*.

[136] Y. Liu, W. Dong, Z. H. Li, H. Wang, "Methane activation by a borenium complex", *Chem* **2021**, *7*, 1843-1851.

[137] S. Mukherjee, P. Thilagar, "Frustrated Lewis pairs: Design and reactivity", *Journal of Chemical Sciences* **2015**, *127*, 241-255.

[138] D. J. Scott, M. J. Fuchter, A. E. Ashley, "Designing effective 'frustrated Lewis pair' hydrogenation catalysts", *Chem. Soc. Rev.* **2017**, *46*, 5689-5700.

[139] J. Paradies, "From structure to novel reactivity in frustrated Lewis pairs", *Coord. Chem. Rev.* **2019**, *380*, 170-183.

[140] L. Greb, S. Tussing, B. Schirmer, P. Oña-Burgos, K. Kaupmees, M. Lõkov, I. Leito, S. Grimme, J. Paradies, "Electronic effects of triarylphosphines in metal-free hydrogen activation: a kinetic and computational study", *Chem. Sci.* **2013**, *4*, 2788.

[141] O. Mitsunobu, "The use of diethyl azodicarboxylate and triphenylphosphine in synthesis and transformation of natural products", *Synthesis* **1981**, *1981*, 1-28.

[142] R. Appel, "Tertiary phosphane/tetrachloromethane, a versatile reagent for chlorination, dehydration, and P-N linkage", *Angew. Chem. Int. Ed.* **1975**, *14*, 801-811.

[143] H. Staudinger, J. Meyer, "Über neue organische phosphorverbindungen III. Phosphinmethylenderivate und phosphinimine", *Helv. Chim. Acta* **1919**, *2*, 635-646.

[144] J. E. Leffler, R. D. Temple, "Staudinger reaction between triarylphosphines and azides. Mechanism", *J. Am. Chem. Soc.* **1967**, *89*, 5235-5246.

[145] R. G. Pearson, J. Songstad, "Application of the principle of hard and soft acids and bases to organic chemistry", *J. Am. Chem. Soc.* **1967**, *89*, 1827-1836.

[146] A. Rauk, L. C. Allen, K. Mislow, "Pyramidal inversion", *Angew. Chem. Int. Ed.* **1970**, *9*, 400-414.

[147] D. H. Valentine Jr., J. H. Hillhouse, "Electron-rich phosphines in organic synthesis II. Catalytic applications", *Synthesis* **2003**, 2437-2460.

[148] J. L. Methot, W. R. Roush, "Nucleophilic phosphine organocatalysis", *Adv. Synth. Catal.* **2004**, *346*, 1035-1050.

[149] C. A. Tolman, "Phosphorus ligand exchange equilibriums on zerovalent nickel. Dominant role for steric effects", *J. Am. Chem. Soc.* **1970**, *92*, 2956-2965.

[150] H. Clavier, S. P. Nolan, "Percent buried volume for phosphine and N-heterocyclic carbene ligands: steric properties in organometallic chemistry", *Chem. Commun.* **2010**, *46*, 841-861.

[151] P. C. J. Kamer, P. W. N. M. van Leeuwen, *Phosphorus(III) ligands in homogeneous catalysis: design and synthesis*, John Wiley & Sons, Ltd, **2012**.

[152] Z. L. Niemeyer, A. Milo, D. P. Hickey, M. S. Sigman, "Parameterization of phosphine ligands reveals mechanistic pathways and predicts reaction outcomes", *Nat. Chem.* **2016**, *8*, 610-617.

[153] C. Lindner, R. Tandon, B. Maryasin, E. Larionov, H. Zipse, "Cation affinity numbers of Lewis bases", *Beilstein J. Org. Chem.* **2012**, *8*, 1406-1442.

[154] K. D. Ashtekar, N. S. Marzijarani, A. Jaganathan, D. Holmes, J. E. Jackson, B. Borhan, "A new tool to guide halofunctionalization reactions: The halenium affinity (HalA) scale", *J. Am. Chem. Soc.* **2014**, *136*, 13355-13362.

[155] H. Mayr, J. Ammer, M. Baidya, B. Maji, T. A. Nigst, A. R. Ofial, T. Singer, "Scales of Lewis basicities toward C-centered Lewis acids (Carbocations)", *J. Am. Chem. Soc.* **2015**, *137*, 2580-2599.

[156] C. Laurence, J. Graton, J.-F. Gal, "An overview of Lewis basicity and affinity scales", *J. Chem. Educ.* **2011**, *88*, 1651-1657.

[157] J. E. Huheey, E. A. Keiter, R. L. Keiter, *Inorganic chemistry: Principles of structures and reactivity*, HarperCollins College Publishers, New-York, **1994**.

[158] E.-i. Negishi, "Palladium- or nickel-catalyzed cross coupling. A new selective method for carbon-carbon bond formation", *Acc. Chem. Res.* **1982**, *15*, 340-348.

[159] T. Hiyama, Y. Hatanaka, S. Fukushima, "A convenient synthesis of substituted heteroaromatic compounds via the palladium-catalyzed cross-coupling reaction od organosilicon compounds", *Heterocycles* **1990**, *30*, 303.

[160] N. Miyaura, A. Suzuki, "Palladium-catalyzed cross-coupling reactions of organoboron compounds", *Chem. Rev.* **1995**, *95*, 2457-2483.

[161] S. E. Denmark, R. F. Sweis, "Design and implementation of new, silicon-based, cross-coupling reactions: importance of silicon-oxygen bonds", *Acc. Chem. Res.* **2002**, *35*, 835-846.

[162] A. S. Guram, R. A. Rennels, S. L. Buchwald, "A simple catalytic method for the conversion of aryl bromides to arylamines", *Angew. Chem. Int. Ed.* **1995**, *34*, 1348-1350.

[163] J. F. Hartwig, J. Louie, "Palladium-catalyzed synthesis of arylamines from aryl halides. Mechanistic studies lead to coupling in the absence of tin reagents", *Tetrahedron Lett.* **1995**, *36*, 3609-3612.

[164] J. P. Wolfe, H. Tomori, J. P. Sadighi, J. Yin, S. L. Buchwald, "Simple, efficient catalyst system for the palladium-catalyzed amination of aryl chlorides, bromides, and triflates", *The Journal of Organic Chemistry* **2000**, *65*, 1158-1174.

[165] A. Aranyos, D. W. Old, A. Kiyomori, J. P. Wolfe, J. P. Sadighi, S. L. Buchwald, "Novel electron-rich bulky phosphine ligands facilitate the palladium-catalyzed preparation of diaryl ethers", *J. Am. Chem. Soc.* **1999**, *121*, 4369-4378.

[166] T. E. Barder, S. D. Walker, J. R. Martinelli, S. L. Buchwald, "Catalysts for Suzuki–Miyaura coupling processes: Scope and studies of the effect of ligand structure", *J. Am. Chem. Soc.* **2005**, *127*, 4685-4696.

[167] R. Martin, S. L. Buchwald, "Palladium-catalyzed Suzuki–Miyaura cross-coupling reactions employing dialkylbiaryl phosphine ligands", *Acc. Chem. Res.* **2008**, *41*, 1461-1473.

[168] T. P. Dang, H. B. Kagan, "The asymmetric synthesis of hydratropic acid and amino-acids by homogeneous catalytic hydrogenation", *J. Chem. Soc. D* **1971**, 481.

[169] T. P. Yoon, E. N. Jacobsen, "Privileged chiral catalysts", *Science* **2003**, *299*, 1691-1693.

[170] J. P. Wolfe, S. Wagaw, S. L. Buchwald, "An improved catalyst system for aromatic carbon-nitrogen bond formation: The possible involvement of bis(phosphine) palladium complexes as key intermediates", *J. Am. Chem. Soc.* **1996**, *118*, 7215-7216.

[171] T. M. Trnka, R. H. Grubbs, "The development of $L_2X_2Ru{=}CHR$ olefin metathesis catalysts: an organometallic success story", *Acc. Chem. Res.* **2001**, *34*, 18-29.

[172] M. Schlosser (Ed.), *Organometallics in synthesis*, John Wiley & Sons, Chichester, England, **1994**.

[173] K. Tani, T. Yamagata, S. Otsuka, S. Akutagawa, H. Kumobayashi, T. Taketomi, H. Takaya, A. Miyashita, R. Noyori, "Highly enantioselective isomerization of prochiral allylamines catalyzed by chiral diphosphine rhodium(I) complexes. Preparation of optically active enamines", *J. Am. Chem. Soc.* **1984**, *106*, 5208-5217.

[174] S. Akutagawa, "Ch. 16. A practical synthesis of (-)-menthol with the Rh-BINAP catalyst" in *Chirality in industry: the commercial manufacture and applications of optically active compounds* (Eds.: A. N. Collins, G. N. Sheldrake, J. Crosby), John Wiley & Sons, Chichester, England, **1992**.

[175] J. F. Young, J. A. Osborn, F. H. Jardine, G. Wilkinson, "Hydride intermediates in homogeneous hydrogenation reactions of olefins and acetylenes using rhodium catalysts", *Chem. Commun.* **1965**.

[176] H. Guo, Y. C. Fan, Z. Sun, Y. Wu, O. Kwon, "Phosphine organocatalysis", *Chem. Rev.* **2018**, *118*, 10049-10293.

[177] H. Ni, W. L. Chan, Y. Lu, "Phosphine-catalyzed asymmetric organic reactions", *Chem. Rev.* **2018**, *118*, 9344-9411.

[178] K.-i. Morita, Z. Suzuki, H. Hirose, "A tertiary phosphine-catalyzed reaction of acrylic compounds with aldehydes", *Bull. Chem. Soc. Jpn.* **1968**, *41*, 2815-2815.

[179] A. B. Baylis, M. E. D. Hillman, "Reaction of acrylic type compounds with aldehydes and certain ketones", Patent DE2155113, Germany, **1972**.

[180] D. Basavaiah, A. J. Rao, T. Satyanarayana, "Recent advances in the Baylis−Hillman reaction and applications", *Chem. Rev.* **2003**, *103*, 811-892.

[181] G. Masson, C. Housseman, J. Zhu, "The enantioselective Morita-Baylis-Hillman reaction and its aza counterpart", *Angew. Chem. Int. Ed.* **2007**, *46*, 4614-4628.

[182] Y. Wei, M. Shi, "Multifunctional chiral phosphine organocatalysts in catalytic asymmetric morita-baylis-hillman and related reactions", *Acc. Chem. Res.* **2010**, *43*, 1005-1018.

[183] P. D. Bartlett, M. J. Ryan, S. G. Cohen, "Triptycene (9,10-*o*-benzenoanthracene)", *J. Am. Chem. Soc.* **1942**, *64*, 2649-2653.

[184] Y. X. Ma, C. F. Chen, *Iptycenes chemistry: from synthesis to applications*, Springer-Verlag, Berlin, **2013**.

[185] J. H. Chong, M. J. MacLachlan, "Iptycenes in supramolecular and materials chemistry", *Chem. Soc. Rev.* **2009**, *38*, 3301-3315.

[186] T. M. Swager, "Iptycenes in the design of high performance polymers", *Acc. Chem. Res.* **2008**, *41*, 1181-1189.

[187] T. M. Long, T. M. Swager, "Minimization of free volume: Alignment of triptycenes in liquid crystals and stretched polymers", *Adv. Mater.* **2001**, *13*, 601-604.

[188] G. Wittig, G. Steinhoff, "Azatriptycene", *Angew. Chem. Int. Ed.* **1963**, *2*, 396-396.

[189] C. Jongsma, J. P. de Kleijn, F. Bickelhaupt, "Phosphatriptycene", *Tetrahedron* **1974**, *30*, 3465-3469.

[190] F. J. M. Freijee, C. H. Stam, "Arsatriptycene and phosphatriptycene", *Acta Crystallogr. A* **1980**, *36*, 1247-1249.

[191] J. Kobayashi, T. Agou, T. Kawashima, "A novel and convenient synthetic route to a 9-phosphatriptycene and systematic comparisons of 9-phosphatriptycene derivatives", *Chem. Lett.* **2003**, *32*, 1144-1145.

[192] T. Agou, J. Kobayashi, T. Kawashima, "Synthesis, structure, and reactivity of a symmetrically substituted 9-phosphatriptycene oxide and Its derivatives", *Heteroat. Chem* **2004**, *15*, 437-446.

[193] H. Tsuji, T. Inoue, Y. Kaneta, S. Sase, A. Kawachi, K. Tamao, "Synthesis, structure, and properties of 9-phospha-10-silatriptycenes and their derivatives", *Organometallics* **2006**, *25*, 6142-6148.

[194] Y. Uchiyama, J. Sugimoto, M. Shibata, G. Yamamoto, Y. Mazaki, "Bromine adducts of 9,10-diheteratriptycene derivatives", *Bull. Chem. Soc. Jpn.* **2009**, *82*, 819-828.

[195] T. Agou, J. Kobayashi, T. Kawashima, "Evaluation of σ-donating ability of a 9-phosphatriptycene and its application to catalytic reactions", *Chem. Lett.* **2004**, *33*, 1028-1029.

[196] S. Konishi, T. Iwai, M. Sawamura, "Synthesis, properties, and catalytic application of a triptycene-type borate-phosphine ligand", *Organometallics* **2018**, *37*, 1876-1883.

[197] T. Iwai, S. Konishi, T. Miyazaki, S. Kawamorita, N. Yokokawa, H. Ohmiya, M. Sawamura, "Silica-supported triptycene-type phosphine. Synthesis, characterization, and application to Pd-catalyzed suzuki–miyaura cross-coupling of chloroarenes", *ACS Catal.* **2015**, *5*, 7254-7264.

[198] S. Kawamorita, T. Miyazaki, H. Ohmiya, T. Iwai, M. Sawamura, "Rh-catalyzed *ortho*-selective C–H borylation of N-functionalized arenes with silica-supported bridgehead monophosphine ligands", *J. Am. Chem. Soc.* **2011**, *133*, 19310-19313.

[199] H. Ube, Y. Yasuda, H. Sato, M. Shionoya, "Metal-centred azaphosphatriptycene gear with a photo- and thermally driven mechanical switching function based on coordination isomerism", *Nature Communications* **2017**, *8*, 14296-14301.

[200] L. Hu, D. Mahaut, N. Tumanov, J. Wouters, R. Robiette, G. Berionni, "Complementary synthetic approaches toward 9-phosphatriptycene and structure–reactivity investigations of its association with sterically hindered Lewis acids", *J. Org. Chem.* **2019**, *84*, 11268-11274.

[201] S. E. Creutz, J. C. Peters, "Catalytic reduction of N_2 to NH_3 by an Fe–N_2 complex featuring a C-atom anchor", *J. Am. Chem. Soc.* **2014**, *136*, 1105-1115.

Chapter I
Sterically hindered *ortho*-substituted phosphatriptycenes as configurationally stable P-chirogenic triarylphosphines

---

The previously reported synthesis of 9-phosphatriptycene is expanded to its *ortho*-substituted derivatives. The strategy based on triarylmethane precursors bearing the substituents of the final molecules is adopted.

This chapter is based on the following article published in the journal *Dalton Transactions* on March 12, 2021 and reproduced (adapted) with permission from the Royal Society of Chemistry.

L. Hu, D. Mahaut, N. Tumanov, J. Wouters, L. Collard, R. Robiette, G. Berionni, "Sterically hindered *ortho*-substituted phosphatriptycenes as configurationally stable P-chirogenic triarylphosphines", *Dalton Trans.* **2021**, *50*, 4772-4777.

Note that Dr. Lei Hu is the main contributor to this article, my contribution is limited to triarylmethane syntheses of 9-phosphatriptycenes and metal complexes presented in schemes 26, 27, 28 and 30.

Dalton Transactions

ROYAL SOCIETY OF CHEMISTRY

COMMUNICATION

View Article Online
View Journal | View Issue

Check for updates

Cite this: *Dalton Trans.*, 2021, **50**, 4772

Received 11th March 2021,
Accepted 12th March 2021

DOI: 10.1039/d1dt00816a

rsc.li/dalton

Sterically hindered *ortho*-substituted phosphatriptycenes as configurationally stable *P*-chirogenic triarylphosphines†

Lei Hu,[a,b] Damien Mahaut,[b] Nikolay Tumanov,[b] Johan Wouters,[b] Laurent Collard,[a] Raphaël Robiette *[a] and Guillaume Berionni *[b]

***ortho*-Substituted and unsymmetrical 9-phospha-triptycenes were synthesized *via* two synthetic approaches involving densely functionalized *ortho*-halogenated triarylmethane or phosphine precursors. *ortho*-Substituents imposed a considerable steric shielding due to the tricyclic cage-shaped structure with the aryl rings p-systems orthogonal to the phosphorus electron pair. A series of Au(I) and Rh(I) complexes were analysed in the solid state to determine Tolman electronic parameters, cone angles and buried volumes of these unprecedented functionalized phosphines. Quantum chemical calculations of electronic and steric descriptors revealed that these cage-shaped phosphines are electron-poor and that single methyl substituent is enough to provide the largest effect on steric shielding reported so far in triarylphosphines. An unsymmetrically substituted 9-phosphatriptycene was resolved by chiral HPLC, opening the avenue towards stable *P*-chirogenic triarylphosphines with unlimited configurational stability for new catalyst development in asymmetric transition-metal catalysis.**

Phosphatriptycenes and their heteroatom bridged analogues **1–6** are increasingly used as ligands in Rh,[1] Ir,[2] Pt[3] and Pd[4] organometallic complexes applied in homogeneous and heterogeneous transition-metal catalysis.[5] Meta-substituted 9-phosphatriptycenes such as **4–6** are readily accessible in a few steps,[6] but this type of substitution has a small impact on the steric hindrance around the phosphorus atom, as indicated by the Tolman cone angle of 151° for **6**,[7] only slightly higher than in triphenylphosphine (145°) (Scheme 1).[8]

In contrast, the synthesis of *ortho*-substituted 9-phospha-triptycenes **7–11** (Scheme 2) with better shielding of phosphorus is much more challenging, and since the first report on 9-phosphatriptycene **1** in 1974, no examples of *ortho*-substituted 9-phosphatriptycenes have been reported so far.[9]

We now achieved the first synthesis of the sterically hindered *ortho*-substituted 9-phosphatriptycenes **7–10** *via* two synthetic approaches involving densely functionalized *ortho*-halogenated triarylmethanes or phosphines precursors (Scheme 2). Owing to their P atom embedded in a tricyclic cage-shape scaffold, no inversion,[10] rotation or flipping at P is allowed in the unsymmetrically substituted 9-phosphatriptycenes **9–11**, opening the path to a new configurationally stable *P*-chirogenic triaryphosphines.[11]

The steric and electronic properties of the *ortho*-substituted 9-phosphatriptycenes **7–11** were determined by characterizing their Rh and Au complexes by X-ray diffraction analysis and by NMR and IR spectroscopies, giving access to their σ-donating and π-accepting abilities (Tolman electronic parameters), and steric hindrance (cone angles, buried volumes).[12]

Quantum chemical calculations were performed to evaluate their Brønsted and Lewis basicities, and their $\%V_{Bur}$ and He_s_ring steric descriptors were computed to probed the steric hindrance imposed by the *ortho*-substituents. The resolution of both enantiomers of an unsymmetrical phosphatriptycene

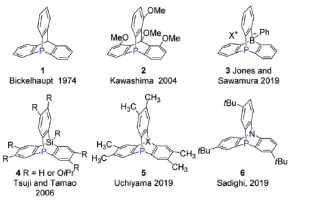

Scheme 1 Reported 9-phospha and phospha-hetero triptycenes.

[a]*Université catholique de Louvain, Institute of Condensed Matter and Nanosciences, Place Louis Pasteur 1 box L4.01.02, 1348 Louvain-la-Neuve, Belgium. E-mail: raphael.robiette@uclouvain.be*
[b]*University of Namur, Department of Chemistry, Namur Institute of Structured Matter, rue de Bruxelles 61, 5000 Namur, Belgium. E-mail: guillaume.berionni@unamur.be*

† Electronic supplementary information (ESI) available. CCDC 2061849–2061862. For ESI and crystallographic data in CIF or other electronic format see DOI: 10.1039/d1dt00816a

1. Abstract

Ortho-substituted and unsymmetrical 9-phosphatriptycenes were synthesized via two synthetic approaches involving densely functionalized *ortho*-halogenated triarylmethane or phosphine precursors. *Ortho*-substituents impose a considerable steric shielding due to the tricyclic cage-shaped structure with the aryl rings π-systems orthogonal to the phosphorus electron pair. A series of Au(I) and Rh(I) complexes were analyzed in the solid state to determine Tolman electronic parameters, cone angles and buried volumes of these unprecedented functionalized phosphines. Quantum chemical calculations of electronic and steric descriptors revealed that these cage-shaped phosphines are electron-poor and that a single methyl substituent is enough to provide the largest effect on steric shielding reported so far in triarylphosphines. An unsymmetrically substituted 9-phosphatriptycene was resolved by chiral HPLC, opening the avenue towards stable P-chirogenic triarylphosphines with unlimited configurational stability for new catalysts development in asymmetric transition metal catalysis.

2. Introduction

9-Phosphatriptycenes and their heteroatom bridged analogues **I.1**-**I.6** (Figure 12) are increasingly used as ligands in Rh,[1] Ir,[2-4] Pt[5] and Pd[6-9] organometallic complexes applied in homogeneous and heterogeneous transition metal catalysis.[1-3, 8, 10] *Meta*-substituted 9-phosphatriptycenes such as **I.4**-**I.6** are readily accessible in a few steps,[10-14] but this type of substitution has a small impact on the steric hindrance around the phosphorus atom, as indicated by the Tolman cone angle of 151° for **I.6**,[15] only slightly higher than in triphenylphosphine (145°).[16-17]

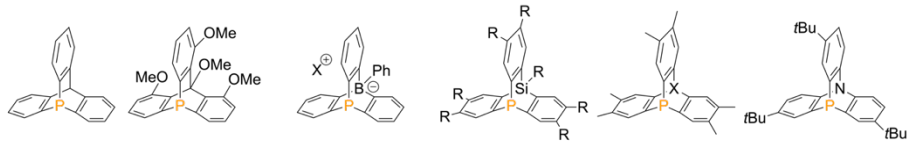

I.1 Bickelhaupt 1974 | **I.2** Kawashima 2004 | **I.3** $X^+ = Na^+, NBu_4^+$ Sawamura, Peters 2018 | **I.4** R = H, O*i*Pr Tsuji, Tamao 2006 | **I.5** X = P, Sb Uchiyama 2019 | **I.6** Sadighi 2019

Figure 12. Reported 9-phospha- and 9-phospha-10-heterotriptycenes.

In contrast, the synthesis of *ortho*-substituted 9-phosphatriptycenes **I.7**-**I.11** (Scheme 23) with better shielding of phosphorus is much more challenging, and

since the first report on 9-phosphatriptycene **I.1** in 1974,[18] no examples of *ortho*-substituted 9-phosphatriptycenes have been reported so far.[19]

We now achieved the first synthesis of the sterically hindered *ortho*-substituted 9-phosphatriptycenes **I.7**-**I.10** via two synthetic approaches involving densely functionalized *ortho*-halogenated triarylmethanes or phosphines precursors (Scheme 23). Owing to their P atom embedded in a tricyclic cage-shaped scaffold, no inversion,[20] rotation or flipping at P is allowed in the unsymmetrically substituted 9-phosphatriptycenes **I.9**-**I.11**, opening the path to new configurationally stable P-chirogenic triarylphosphines.[21-26]

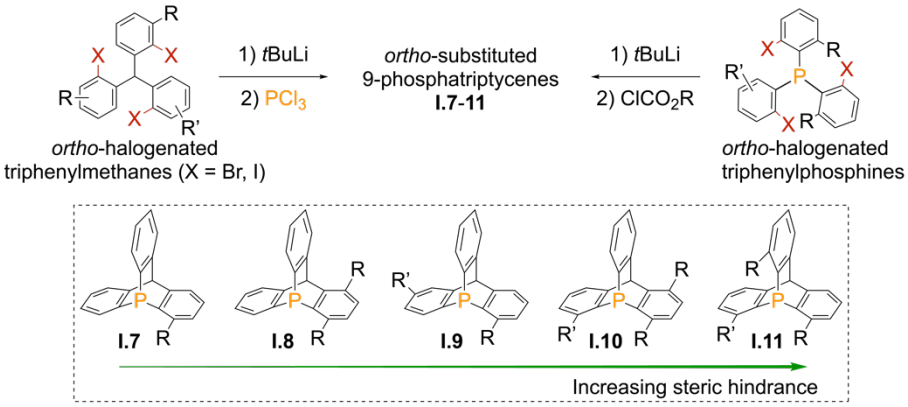

*Scheme 23. 9-Phosphatriptycene derivatives **I.7**-**I.11** synthesized and studied in this work (**I.11**: attempted synthesis).*

The steric and electronic properties of the *ortho*-substituted 9-phosphatriptycenes **I.7**-**I.11** were determined by characterizing their Rh and Au complexes by X-ray diffraction analysis and by NMR and IR spectroscopies, giving access to their σ-donating and π-accepting abilities (Tolman electronic parameters), and steric hindrance (cone angles, buried volumes).[27]

Quantum chemical calculations were performed to evaluate their Brønsted and Lewis basicities, and their $\%V_{Bur}$ and He_8_ring steric descriptors were computed to probe the steric hindrance imposed by the *ortho*-substituents. The resolution of both enantiomers of an unsymmetrical 9-phosphatriptycene was performed by chiral HPLC, giving access to enantiopure 9-phosphatriptycenes with unlimited configurationally stability.

3. Results and discussion

The first step in our synthetic approach to obtain tris-*ortho*-substituted phosphatriptycene **I.11** was the preparation of the sterically crowded *ortho*-substituted halogenated triarylphosphines **I.14** (Scheme 24). The directed *ortho*-lithiation of **I.12a-b** with lithium amides was performed at low temperature to avoid benzyne formation. However, quenching the intermediate aryl-lithium species with PCl_3 did not lead to expected hexa-*ortho*-substituted phosphines **I.14a-b** (Scheme 24).

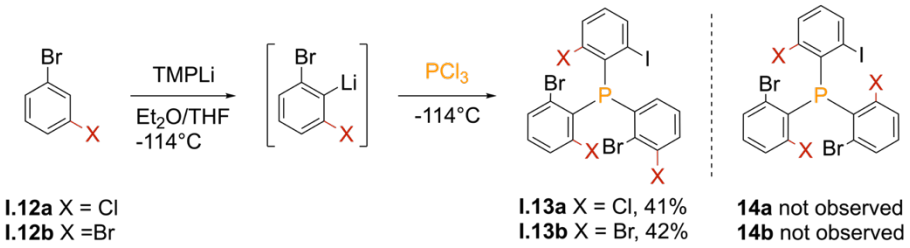

*Scheme 24. Synthesis of ortho-halogenated triarylphosphines **I.13a-b**. For their single-crystal X-ray structures, see the SI.*

Instead, NMR spectroscopy and single-crystal X-ray diffraction (SC-XRD) revealed the formation of the arylphosphines **I.13a-b** with only five halogens in *ortho*-positions, the sixth halogen being located in the *meta* position, presumably due to an halogen migration occurring even at this low temperature.[28]

Although we failed to obtain the hexa-*ortho*-substituted phosphines I.**14a-b**, which are the direct precursors to the tris-*ortho*-substituted 9-phosphatriptycene **I.11**, we still decided to show that **I.13a** can be converted into *ortho*-substituted 9-phosphatriptycenes such as **I.16** (Scheme 25). The triple Br/Li exchange on **I.13a** with *t*BuLi followed by quenching with phenyl chloroformate produced either the phosphinofluorene **I.15a** or the substituted 9-phosphatriptycene **I.16** depending on the reaction temperature.

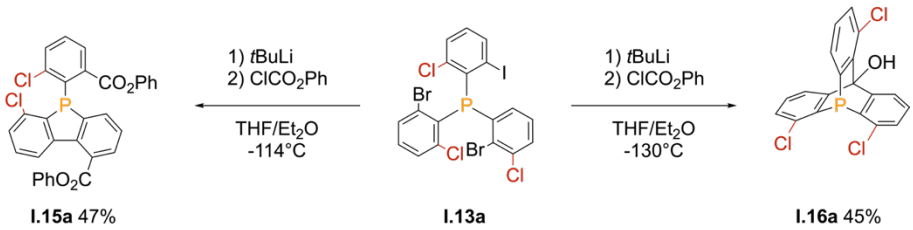

*Scheme 25. Synthesis of unsymmetrical phosphinofluorene **I.15a** and triptycene **I.16a**. For the crystal structure of **I.15a** and synthetic details, see the SI.*

Since the initially planned synthetic approach toward *ortho*-substituted phosphatriptycenes suffered from several limitations and low yields, we focused on the second synthetic approach involving *ortho*-halogenated triphenylmethane precursors.

Based on the method of Moran,[29] the Friedel-Crafts reactions of **I.17a-c** produced **I.18a-c** in good yields (Scheme 26). Consecutive iodine oxidation with *m*CPBA, regioselective intramolecular S_EAr cyclization and TfO^-/I^- anion metathesis[30] led to the cyclic iodonium salts **I.19a-c** in high yields. Thermally induced ring-opening of **I.19a-c** by S_NAr reactions with iodide[30] provided the halogenated triarylmethanes **I.20a-c** in good isolated yields. Then, a triple halogen/lithium exchange and the trapping with PCl_3 yielded the novel *ortho*-substituted 1-fluoro-, 1-chloro- and 1-trifluoromethyl-9-phosphatriptycenes (**I.7a-c**).

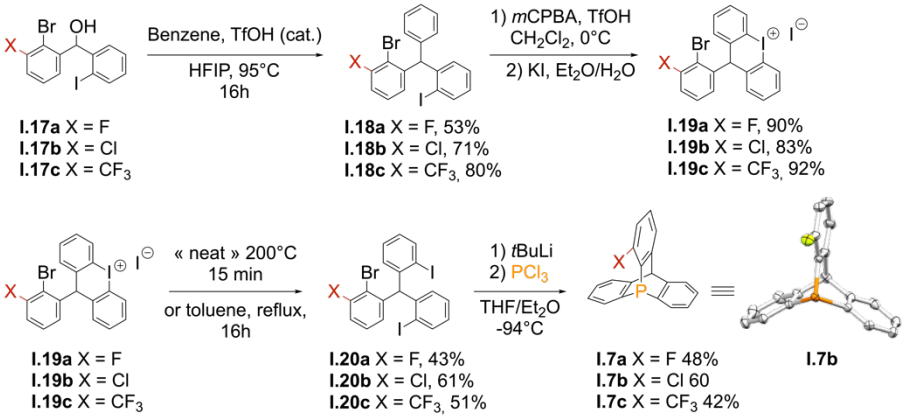

*Scheme 26. Synthesis of ortho-substituted 9-phosphatriptycene **I.7a-c** and X-ray structure of **I.7b** with ellipsoids represented at the 50% level.*

We next extended our synthetic method to produce 1,4-disubstituted 9-phosphatriptycenes. The Friedel-Crafts alkylation of *p*-xylene with the benzhydrylium ion, generated from **I.21**, and triflic acid gave access to **I.22** in good yield (Scheme 27). Oxidation of the iodine atom of **I.22** with *m*CPBA and intramolecular S_EAr cyclization gave the iodonium salt **I.23**. Subsequent S_NAr substitution provided **I.24**, which after triple halogen/lithium exchange and trapping with PCl_3 led to **I.8a**.

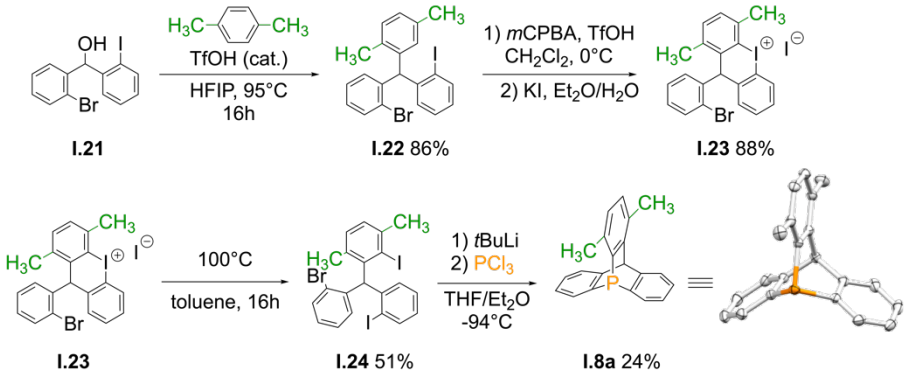

*Scheme 27. Synthesis of the 1,4-disubstituted 9-phosphatriptycene **I.8a** and its crystal structure with ellipsoids represented at the 50% level.*

To evaluate the steric and electronic properties of these cage-shaped phosphines, we prepared the Au(I) and Rh(I) complexes of 9-phosphatriptycene **I.1** and of its substituted analogues **I.7**-**I.8** and characterized them by NMR, FTIR and SC-XRD (Scheme 28).

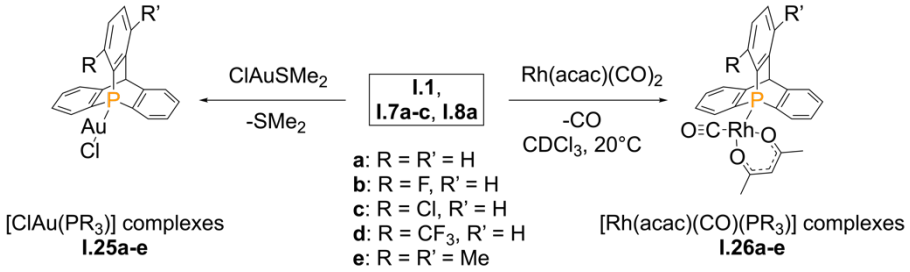

*Scheme 28. Formation of the gold(I) complexes [AuCl(R3P)] and rhodium(I) complexes [Rh(acac)(CO)(R3P)] of 9-phosphatriptycenes **I.1** and **I.7**-**I.8**. All reactions were quantitative except for **I.7c**, see the SI.*

The σ-donating and π-accepting abilities (Tolman electronic parameters) of the 9-phosphatriptycenes were derived from the IR stretching frequency (ν_{CO}) of the *cis* carbonyl ligand in the Rh complexes **I.26** in CH_2Cl_2 solutions (Table 2). The frequencies are comparable to these in the complexes of the electron-poor P(*p*-CF_3-C_6H_4)$_3$ and P(*p*-Cl-C_6H_4)$_3$ phosphines, showing that 9-phosphatriptycenes are weak σ electron-donor but strong π-acceptor ligands. *Ortho*- substituents were found to have minor effects on the electronic properties of 9-phosphatriptycenes (maximum deviation of ν_{CO} is of 5 cm^{-1}) since their aryl ring π-systems are orthogonal and not conjugated to the P lone pair.

*Table 2. Selected spectroscopic data and computed[a] reactivity parameters for PPh_3 and 9-phosphatriptycenes **I.1** and **I.7-I.8**. The $^3J_{P-F}$ coupling constants in Hz are indicated in square brackets.*

Parameters	PPh_3	**I.1** (-H)	**I.7a** (-F)	**I.7b** (-Cl)	**I.7c** (-CF_3)	**I.8a** (-CH_3)
^{31}P NMR/ppm [$^3J_{P-F}$/Hz]	22.2	-64.4	-83.4 [*d* 36.1]	-72.5	-69.7 [*q* 51.7]	-74.9
^{31}P NMR in Au(R_3P)Cl	33.3[b]	-1.9	-19.4 [*d* 22.8]	-10.7	-5.6 [*q* 17.2]	-13.4
^{31}P NMR in Rh complex	48.6[c]	4.4	-11.6 [*d* 11.4]	-0.5	0.5 [*q* 11.7]	-3.0
J_{P-Rh} / Hz	177[c]	189	192	196	200	188
ν_{CO} / Rh (cm^{-1})	1978[c]	1985[d]	1983	1983	1980	1982
PA[e]	248	236	233	234	232	237
pK_a[f]	3.28	-0.42	-1.24	-1.17	-1.58	0.03
MCA[e]	113	103	101	101	99	104

[a] Calculations carried out at the M06-2X/6-311+G*(benzene)//M06-2X/6-31+G* level of theory using the Jaguar 8.5 pseudospectral program package (Jaguar 8.5, Schrodinger, Inc., New York, NY, 2014). See the SI for full computational details. [b] Ref. 31; [c] Ref. 32; [d] Ref. 33; [e] PA and MCA stand for the proton and methyl cation affinities, in kcal/mol; [f] Obtained by linear correlation of PA versus pK_a of selected reference phosphines, see SI.

To evaluate the Brønsted and Lewis basicities of these phosphines, we performed quantum chemical calculations of the proton affinity (PA) and methyl cation affinity (MCA). The Brønsted and Lewis basicities of **I.7**-**I.8** turned out to be only moderately affected by *ortho*-substitution (see Table 2). Linear correlation of PA versus pK_a (see SI) indicated that pK_a(H_2O) ranges from -1.58 to 0.03 between **I.7c** and **I.8a**, which are all weaker Brønsted bases than PPh_3 and comparable to P(*p*-CF_3-C_6H_4)$_3$.[34]

Thus, *ortho*-substituents have a negligible effect on the electronic properties of 9-phosphatriptycenes due to the near absence of conjugation between the triptycene aryl rings orbitals and the orthogonal P lone pair.[4] In contrast, a huge impact on the steric shielding is anticipated since *ortho*-substituents are maintained in very close proximity to the P-lone pair, and aryl rings are prevented from rotating by the cage-shaped structure.

[4] This is supported by a NBO analysis which provides an estimation of the conjugation between the lone pair and the π systems (E2 energy) of 4.2-4.9 kcal/mol for all studied triptycene derivatives.

SC-XRD showed that the 9-phosphatriptycene Rh complexes are square planar with P-Rh bonds of 2.22 Å, and the Au complexes are linear with P-Au bonds also of 2.22 Å on average (Figure 13 and Table 3). The crystallographic cone angle of 160° for the 9-phosphatriptycene **I.1** increases up to 187° for the methyl-substituted triptycene **I.8a**, representing one of the largest impacts known on the sterics of phosphines due to a single CH_3 substituent; for comparison, the effect of a CH_3 group substituent on PPh_3 becoming PPh_2(*o*-Tol) is only 6° (Table 3).

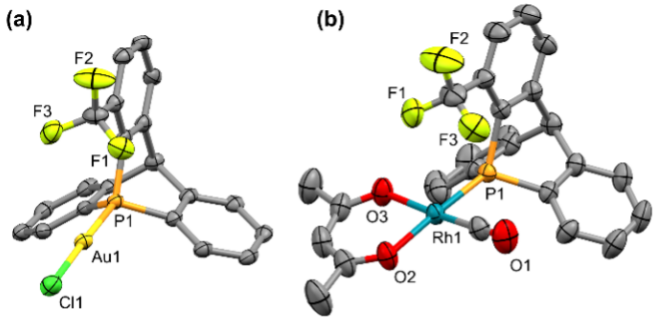

*Figure 13. Structure of the Au (a) and Rh complexes (b) of **I.7c** in the solid state. Here and further structures are represented with ellipsoids at the 50% level; hydrogen atoms and solvate molecules are omitted for clarity. Labels are shown only for heteroatoms.*

Due to the cage-shaped strained structure of these phosphines, the Tolman cone angles and buried volumes of the free and metal-complexed phosphatriptycenes are nearly identical, as shown by the similar buried volume of the free 9-phosphatriptycene **I.1** (30.7%), and in its complexes with Au (31.8%) and Rh (31.3%). The high steric bulk of -CF_3 and -Me substituted phosphatriptycenes **I.7c** and **I.8a** is also evidenced by the computed He_8_ring descriptor (21.1 and 18.5 kcal/mol, respectively), which is designed to mimic the non-bonded interactions between a P-donor ligand and other *cis* ligands in an octahedral complex (see SI for full details).[35]

Capitalizing on our new synthetic strategy toward *ortho*-substituted 9-phosphatriptycenes, we undertook the synthesis of the first unsymmetrically derivative **I.9a**. Treatment of the trityl precursor **I.28** with an excess of *t*BuLi followed by a trapping with PCl_3 provided **I.9a** in good isolated yield (Scheme 29).

*Table 3. Steric descriptors for 9-phosphatriptycenes **I.1**, **I.7-I.8** and **I.10**. The buried volume values (%V_{bur}) are calculated for M–P length at 2.00 Å with a sphere radius of 3.5 Å and bonds radii scaled by 1.17 as standard method.*[36-37]

Parameters	PPh_3	PPh_2(*o*-Tol)	P(*o*-Tol)$_3$	**I.1** (-H)	**I.7a** (-F)
Cone angle (°)	145[a]	151[b]	194[a]	160[c]	167
P-Rh (Å)	2.242(2)[d]	2.242(2)[c]	-	2.225(1) 2.228(2)[h]	2.223(2) 2.232(1)[h]
P-Au (Å)	2.231(1)[d]	2.231(1)[d]	2.243(2)[e]	2.213(1)	-
%V_{Bur}	29.6[a]	29.6[a]	46.7[a]	31.3[f]	33.5
He_8_steric (kcal/mol)	8.0[g]	8.0[g]	30.1[g]	9.3	12.5
Parameters	**I.7b** (-Cl)	**I.7c** (-CF_3)	**I.8a** (-CH_3)	**I.9a** (-Cl, -*t*Bu)	**I.10a** (-Cl, -CH_3)
Cone angle (°)	173	186	187	174	196
P-Rh (Å)	2.225(2)	2.230(1)	-	-	-
P-Au (Å)	-	2.220(1) 2.215(1)[h]	-	-	-
%V_{Bur}	36.3	41.3	36.0	37.0	41.9
He_8_steric (kcal/mol)	18.6	21.1	18.5	18.4	35.2

[a] Cone angles and %V_{Bur} values from ref. [36-37] (the %V_{Bur} values were calculated with the SambVca 2.1 program); [b] ref. [38]; [c] ref. 33; [d] ref. 32 and ref. [39]; [e] ref. [40]; [f] Average value based on three solid-state structures: structure of the free 9-phosphatriptycene **1** (30.7%) from reference 33, and of its complexes **I.25a** with Au (31.8%) and **I.26a** with Rh (31.3%). All other %V_{bur} parameters from the free phosphatriptycenes; [g] He_8_ring values from ref. 27; h) two values are indicated if the crystal mesh displays two unidentical structures.

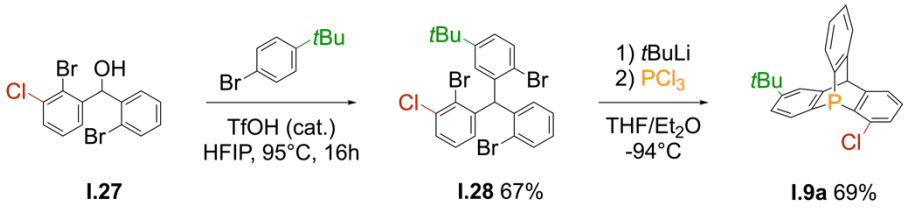

*Scheme 29. Synthesis of unsymmetrically substituted phosphatriptycene **I.9a**.*

Using the same strategy, the bulky bis-*ortho*-substituted 9-phosphatriptycene **10a** with two different substituents in *ortho*-position could be obtained in four synthetic steps (Scheme 30).

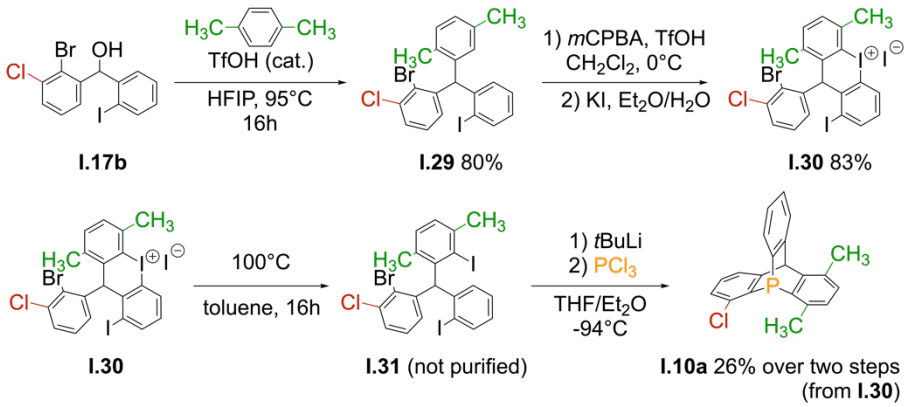

*Scheme 30. Synthesis of trisubstituted 9-phosphatriptycenes **10a**.*

Single-crystal X-ray diffraction analyses provided the structures of the unsymmetrical 9-phosphatriptycenes **9a** and **10a** (Figure 14), which were used for the determination of their crystallographic cone angle (Table 3). Whereas the chiral resolution of **10a** was not effective, both enantiomers of **9a** were resolved by chiral HPLC with a good resolution (see the SI) illustrating the potential to obtain enantiopure P-chirogenic triarylphosphines with unlimited configurationally stability and with completely unprecedent electronic and steric properties, opening new physico-chemical spaces in P-ligands for transition metal catalysis.

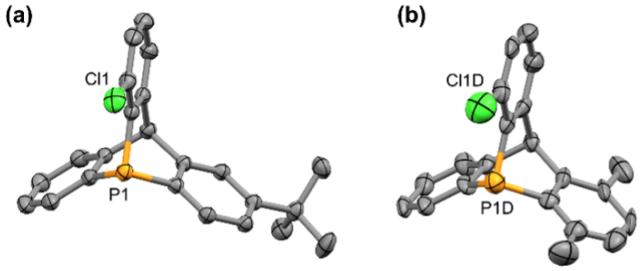

*Figure 14. Structure of **I.9a** (a) and **I.10a** (b) in the solid state with ellipsoids represented at the 50% level. H atoms and toluene solvate molecules omitted.*

4. Conclusions

Using highly functionalized triphenylmethanes allowed us to access to *ortho*-substituted 9-phosphatriptycenes. As the P lone pair is not conjugated with the triptycene aryl rings, their Brønsted and Lewis basicities are less affected by substituents than in common triaryl-phosphines.

With their substituents parallel to the P-lone pair axis in a cage-shaped strained 9-phosphatriptycene core, the P environment becomes exceptionally shielded, resulting in completely new types of rigid and bulky phosphines with high potential in Au, Rh and Pd catalysis.

In conclusion, the investigation of *ortho*-substituted 9-phosphatriptycenes as electron-poor and bulky P-ligands in cross-coupling reactions,[41-42] or for the design of electrophilic phosphonium cations[43-44] is ongoing in our laboratories. Owing to their tricyclic cage-shaped structures, *ortho* triptycenes constitute a new class of configurationally stable P-chirogenic phosphines, with highly modular steric hindrance, opening the way to further applications in asymmetric transition metal catalysis and frustrated Lewis pairs catalyzed hydrogenations.

5. References

[1] S. Kawamorita, T. Miyazaki, H. Ohmiya, T. Iwai, M. Sawamura, "Rh-catalyzed *ortho*-selective C–H borylation of N-functionalized arenes with silica-supported bridgehead monophosphine ligands", *J. Am. Chem. Soc.* **2011**, *133*, 19310-19313.

[2] S. Kawamorita, T. Miyazaki, T. Iwai, H. Ohmiya, M. Sawamura, "Rh-catalyzed borylation of N-adjacent C(sp^3)-H bonds with a silica-supported triarylphosphine ligand", *J. Am. Chem. Soc.* **2012**, *134*, 12924-12927.

[3] S. Kawamorita, R. Murakami, T. Iwai, M. Sawamura, "Synthesis of primary and secondary alkylboronates through site-selective C(sp^3)-H activation with silica-supported monophosphine-Ir catalysts", *J. Am. Chem. Soc.* **2013**, *135*, 2947-2950.

[4] R. Murakami, K. Tsunoda, T. Iwai, M. Sawamura, "Stereoselective C-H borylations of cyclopropanes and cyclobutanes with silica-supported monophosphane-Ir catalysts", *Chem. Eur. J.* **2014**, *20*, 13127-13131.

[5] H. Ube, Y. Yasuda, H. Sato, M. Shionoya, "Metal-centred azaphosphatriptycene gear with a photo- and thermally driven mechanical switching function based on coordination isomerism", *Nature Communications* **2017**, *8*, 14296-14301.

[6] S. Konishi, T. Iwai, M. Sawamura, "Synthesis, properties, and catalytic application of a triptycene-type borate-phosphine ligand", *Organometallics* **2018**, *37*, 1876-1883.

[7] M. W. Drover, K. Nagata, J. C. Peters, "Fusing triphenylphosphine with tetraphenylborate: introducing the 9-phosphatriptycene-10-phenylborate (PTB) anion", *Chem. Commun.* **2018**, *54*, 7916-7919.

[8] T. Iwai, S. Konishi, T. Miyazaki, S. Kawamorita, N. Yokokawa, H. Ohmiya, M. Sawamura, "Silica-supported triptycene-type phosphine. Synthesis, characterization, and application to Pd-catalyzed suzuki–miyaura cross-coupling of chloroarenes", *ACS Catal.* **2015**, *5*, 7254-7264.

[9] T. Agou, J. Kobayashi, T. Kawashima, "Evaluation of σ-donating ability of a 9-phosphatriptycene and its application to catalytic reactions", *Chem. Lett.* **2004**, *33*, 1028-1029.

[10] H. Tsuji, T. Inoue, Y. Kaneta, S. Sase, A. Kawachi, K. Tamao, "Synthesis, structure, and properties of 9-phospha-10-silatriptycenes and their derivatives", *Organometallics* **2006**, *25*, 6142-6148.

[11] Y. Uchiyama, T. Ohtsuki, R. Murakami, M. Shibata, J. Sugimoto, "(E)-selective Wittig reactions between a nonstabilized phosphonium ylide bearing a phosphastibatriptycene skeleton and benzaldehydes", *Eur. J. Org. Chem.* **2017**, *2017*, 159-174.

[12] Y. Uchiyama, S. Kuniya, R. Watanabe, T. Ohtsuki, "Heteroatom effects toward isomerization of intermediates in Wittig reactions of non-stabilized phosphonium ylides bearing a phosphaheteratriptycene skeleton with benzaldehyde", *Heteroat. Chem* **2018**, *29*.

[13] Y. Uchiyama, S. Kuniya, R. Watanabe, T. Ohtsuki, "Wittig reactions of non-stabilized phosphonium ylides bearing a phosphaheteratriptycene skeleton containing group 14 and 15 elements with benzaldehyde", *Phosphorus, Sulfur, and Silicon and the Related Elements* **2018**, *194*, 277-278.

[14] Y. Uchiyama, S. Kuniya, R. Watanabe, T. Ohtsuki, "Observation of intermediates in Wittig reactions of non-stabilized phosphonium ylides bearing a phosphaheteratriptycene skeleton containing Group 15 elements with benzaldehyde", *Phosphorus, Sulfur, and Silicon and the Related Elements* **2019**, *194*, 281-284.

[15] Y. Cao, J. W. Napoline, J. Bacsa, P. Pollet, J. D. Soper, J. P. Sadighi, "Synthesis of an azaphosphatriptycene and its rhodium carbonyl complex", *Organometallics* **2019**, *38*, 1868-1871.

[16] C. A. Tolman, "Phosphorus ligand exchange equilibriums on zerovalent nickel. Dominant role for steric effects", *J. Am. Chem. Soc.* **1970**, *92*, 2956-2965.

[17] T. E. Müller, D. M. P. Mingos, "Determination of the Tolman cone angle from crystallographic parameters and a statistical analysis using the crystallographic data base", *Transition Met. Chem.* **1995**, *20*, 533-539.

[18] C. Jongsma, J. P. de Kleijn, F. Bickelhaupt, "Phosphatriptycene", *Tetrahedron* **1974**, *30*, 3465-3469.

[19] J. P. Sadighi, "New ligands for catalysis through elaboration of the phosphatriptycene framework", *PRF ACS Annual Report* **2015**, *ND3*, 54739.

[20] J. Holz, H. Jiao, M. Gandelman, A. Börner, "About the Inversion Barriers of P-Chirogenic Triaryl-Substituted Phosphanes", *Eur. J. Org. Chem.* **2018**, *2018*, 2984-2994.

[21] V. Diemer, A. Berthelot, J. Bayardon, S. Juge, F. R. Leroux, F. Colobert, "Stereoselective synthesis of P-chirogenic dibenzophosphole-boranes via aryne intermediates", *J. Org. Chem.* **2012**, *77*, 6117-6127.

[22] M. Dutartre, J. Bayardon, S. Jugé, "Applications and stereoselective syntheses of P-chirogenic phosphorus compounds", *Chem. Soc. Rev.* **2016**, *45*, 5771-5794.

[23] J. Holz, K. Rumpel, A. Spannenberg, R. Paciello, H. Jiao, A. Börner, "P-chirogenic Xantphos ligands and related ether diphosphines: Synthesis and application in rhodium-catalyzed asymmetric hydrogenation", *ACS Catal.* **2017**, *7*, 6162-6169.

[24] J. Holz, G. Wenzel, A. Spannenberg, M. Gandelman, A. Börner, "New P-chirogenic *tert*-butyl-Xantphos ligands and their application in asymmetric hydrogenation and alkylation", *Tetrahedron* **2020**, *76*.

[25] R. Huber, A. Passera, A. Mezzetti, "Which future for stereogenic phosphorus? Lessons from P* pincer complexes of iron(II)", *Chem. Commun.* **2019**, *55*, 9251-9266.

[26] C. Muller, E. A. Pidko, A. J. Staring, M. Lutz, A. L. Spek, R. A. van Santen, D. Vogt, "Developing a new class of axial chiral phosphorus ligands: preparation and characterization of enantiopure atropisomeric phosphinines", *Chem. Eur. J.* **2008**, *14*, 4899-4905.

[27] D. J. Durand, N. Fey, "Computational ligand descriptors for catalyst design", *Chem. Rev.* **2019**, *119*, 6561-6594.

[28] W. Erb, F. Mongin, "Halogen 'dance': a way to extend the boundaries of arene deprotolithiation", *Tetrahedron* **2016**, *72*, 4973-4988.

[29] V. D. Vuković, E. Richmond, E. Wolf, J. Moran, "Catalytic Friedel–Crafts reactions of highly electronically deactivated benzylic alcohols", *Angew. Chem. Int. Ed.* **2017**, *56*, 3085-3089.

[30] S. E. Creutz, J. C. Peters, "Catalytic reduction of N_2 to NH_3 by an Fe–N_2 complex featuring a C-atom anchor", *J. Am. Chem. Soc.* **2014**, *136*, 1105-1115.

[31] F. della Sala, E. R. Kay, "Reversible control of nanoparticle functionalization and physicochemical properties by dynamic covalent exchange", *Angew. Chem. Int. Ed.* **2015**, *54*, 4187-4191.

[32] A. Brink, A. Roodt, G. Steyl, H. G. Visser, "Steric vs. electronic anomaly observed from iodomethane oxidative addition to tertiary phosphine modified rhodium(I) acetylacetonato complexes following progressive phenyl replacement by cyclohexyl [PR_3 = PPh_3, PPh_2Cy, $PPhCy_2$ and PCy_3]", *Dalton Trans.* **2010**, *39*, 5572-5578.

[33] L. Hu, D. Mahaut, N. Tumanov, J. Wouters, R. Robiette, G. Berionni, "Complementary synthetic approaches toward 9-phosphatriptycene and structure–reactivity investigations of its association with sterically hindered Lewis acids", *J. Org. Chem.* **2019**, *84*, 11268-11274.

[34] A. J. Poe, D. H. Farrar, Y. Zheng, "Systematic kinetics of high nuclearity metal carbonyl clusters. Associative substitution reactions of $Ru_6C(CO)_{17}$ with P-donor nucleophiles", *J. Am. Chem. Soc.* **1992**, *114*, 5146-5152.

[35] J. Jover, N. Fey, M. Purdie, G. C. Lloyd-Jones, J. N. Harvey, "A computational study of phosphine ligand effects in Suzuki-Miyaura coupling", *J. Mol. Catal. A: Chem.* **2010**, *324*, 39-47.

[36] H. Clavier, S. P. Nolan, "Percent buried volume for phosphine and N-heterocyclic carbene ligands: steric properties in organometallic chemistry", *Chem. Commun.* **2010**, *46*, 841-861.

[37] L. Falivene, Z. Cao, A. Petta, L. Serra, A. Poater, R. Oliva, V. Scarano, L. Cavallo, "Towards the online computer-aided design of catalytic pockets", *Nat. Chem.* **2019**, *11*, 872-879.

[38] H. Riihimäki, P. Suomalainen, H. K. Reinius, J. Suutari, S. Jääskeläinen, A. O. I. Krause, T. A. Pakkanen, J. T. Pursiainen, "*o*-Alkyl-substituted aromatic phosphanes for hydroformylation studies: synthesis, spectroscopic characterization and *ab initio* investigations", *J. Mol. Catal. A: Chem.* **2003**, *200*, 69-79.

[39] A. O. Borissova, A. A. Korlyukov, M. Y. Antipin, K. A. Lyssenko, "Estimation of dissociation energy in donor-acceptor complex AuCl·PPh_3 via topological analysis of the experimental electron density distribution function", *J. Phys. Chem. A* **2008**, *112*, 11519-11522.

[40] C. S. W. Harker, E. R. T. Tiekink, "Chloro[tris(*o*-tolyl)phosphine]gold(I)", *Acta Crystallogr. C* **1990**, *46*, 1546-1547.

[41] K. Abe, M. Kitamura, H. Fujita, M. Kunishima, "Development of highly electron-deficient and less sterically-hindered phosphine ligands possessing 1,3,5-triazinyl groups", *Molecular Catalysis* **2018**, *445*, 87-93.

[42] S. Zhao, T. Gensch, B. Murray, Z. L. Niemeyer, M. S. Sigman, M. R. Biscoe, "Enantiodivergent Pd-catalyzed C-C bond formation enabled through ligand parameterization", *Science* **2018**, *362*, 670-674.

[43] A. J. Stepen, M. Bursch, S. Grimme, D. W. Stephan, J. Paradies, "Electrophilic phosphonium cation-mediated phosphane oxide reduction using oxalyl chloride and hydrogen", *Angew. Chem. Int. Ed.* **2018**, *57*, 15253-15256.

[44] M. Vogler, L. Süsse, J. H. W. LaFortune, D. W. Stephan, M. Oestreich, "Electrophilic phosphonium cations as Lewis acid catalysts in Diels–Alder reactions and Nazarov cyclizations", *Organometallics* **2018**, *37*, 3303-3313.

Chapter I

Chapter II
9-phosphatriptycene derivatives: from their weak basicity to their application in frustrated Lewis pair chemistry

---

A DFT method is developed for the prediction of pK_a values of phosphines in water and acetonitrile, highlighting the weak basicity of 9-phosphatriptycene derivatives and providing insight into the factors explaining their reactivity.

D. Mahaut, G. Berionni, B. Champagne, "9-Phosphatriptycene derivatives: from their weak basicity to their application in frustrated Lewis pair chemistry", *J. Phys. Chem. A* **2022**, *126*, 2794-2801.

THE JOURNAL OF PHYSICAL CHEMISTRY A
A JOURNAL OF THE AMERICAN CHEMICAL SOCIETY

pubs.acs.org/JPCA Article

9-Phosphatriptycene Derivatives: From Their Weak Basicity to Their Application in Frustrated Lewis Pair Chemistry

Damien Mahaut, Guillaume Berionni, and Benoît Champagne*

Cite This: *J. Phys. Chem. A* 2022, 126, 2794–2801 Read Online

ACCESS | Metrics & More | Article Recommendations | Supporting Information

ABSTRACT: The accurate prediction of the basicity of tertiary phosphines in acetonitrile and water is reported by the linear correlation between computed ΔpK_a's obtained by density functional theory (DFT) and experimental values extracted from the literature. This method is applied to the prediction of pK_a values of 9-phosphatriptycene derivatives and showed that they are weaker Brønsted bases than their triphenylphosphine analogues. This lower reactivity is attributed to their high pyramidalization that increases their lone pair 3s character, stabilizing its energy level. Their potential application in frustrated Lewis pair chemistry is then considered by investigating the hydrogenation of 1,1-diphenylethylene by the tris(pentafluorophenyl)borane/1-chloro-9-phosphatriptycene frustrated Lewis pair.

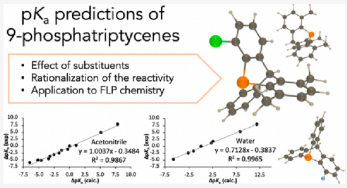

INTRODUCTION

Tertiary phosphines are widely used as Lewis bases and ligands for applications spanning from organometallic complexes to organocatalysts or in frustrated Lewis pair chemistry.[1−7] 9-Phosphatriptycenes constitute a lesser-known family of phosphines characterized by a caged-shaped structure where the three phenyl groups are linked by a single carbon atom. The parent 9-phosphatriptycene was first synthesized by Bickelhaupt in 1974 and was only seldom studied afterward due to its tedious synthesis.[8] Several new developments were reported over the years, especially for the synthesis of analogues of 9-phosphatriptycenes, 9-phospha-10-heterotriptycenes, and 9,10-diheteratriptycene.[9−12] To this day the applications of such compounds were limited to being used as ligands in organometallic chemistry. Due to their caged structure, 9-phosphatriptycenes are known for being strong π-acceptors and weak σ-donors and were shown to be effective ligands in palladium-catalyzed processes such as the Stille coupling or the Heck reaction.[13] Other organometallic applications were also reported in homogeneous[14] or heterogenous[15,16] catalysis and as the rotor in palladium-centered molecular gears.[17]

We have recently reported novel synthetic approaches toward the parent 9-phosphatriptycene.[18] Investigations of its steric and electronic properties showed that the 9-phosphatriptycene was slightly bulkier and had a weaker Lewis base than triphenylphosphine. A linear correlation between the proton affinity of reference triarylphosphines and the pK_a of the corresponding protonated forms allowed the estimation of its aqueous pK_a of −1.5. In addition, the Lewis basicity (LB = 7.6) of the 9-phosphatriptycene relative to benzhydrylium ions, determined according to the Mayr scale, is significantly lower than that of triphenylphosphine (LB = 14.3), further supporting the lower reactivity of 9-phosphatriptycene derivatives compared to other triarylphosphines. Later, an extension of the synthetic approach toward 9-phosphatriptycenes allowed for the production of a set of ortho-substituted derivatives, a substitution pattern never reported before.[19] The new substituents span from electron-donating groups (methyl groups, Me) to various electron-withdrawing ones (F, Cl, and CF_3) and a combination of both Cl and Me to further increase steric hindrance (Figure 1). Investigations of their ligand ability in Rh- and Au- complexes indicated that ortho-substituents had a limited effect on the reactivity of the phosphorus center, which was attributed to the lack of conjugation between the phosphorus lone pair, and the π-system of the neighboring aryl rings.

In order to compare quantitatively the Brønsted basicity of these phosphines, an accurate prediction of their pK_a is an essential tool. The pK_a of an acid characterizes the equilibrium of a proton transfer reaction in a given solvent, aqueous or organic.[20] Its measurement finds numerous applications in chemical and biochemical processes.[21−25] The basicity of a

Received: February 24, 2022
Revised: April 23, 2022
Published: May 4, 2022

https://doi.org/10.1021/acs.jpca.2c01339
J. Phys. Chem. A 2022, 126, 2794−2801

1. Abstract

The accurate prediction of the basicity of tertiary phosphines in acetonitrile and water is reported by linear correlation between computed ΔpK_a's obtained by density functional theory (DFT) and experimental values extracted from the literature. This method is applied to the prediction of pK_a values of 9-phosphatriptycene derivatives and showed that they are weaker Brønsted bases than their triphenylphosphine analogues. This lower reactivity is attributed to their high pyramidalization that increases their lone pair *3s* character, stabilizing its energy level. Their potential application in frustrated Lewis pair chemistry is then considered by investigating the hydrogenation of 1,1-diphenylethylene by the tris(pentafluorophenyl)borane/1-chloro-9-phosphatriptycene frustrated Lewis pair.

2. Introduction

Tertiary phosphines are widely used as Lewis bases and ligands for applications spanning from organometallic complexes to organocatalysts or in frustrated Lewis pair chemistry.[1-7] 9-phosphatriptycenes constitute a lesser-known family of phosphines characterized by a caged-shaped structure where the three phenyl groups are linked by a single carbon atom. The parent 9-phosphatriptycene was first synthesized by Bickelhaupt in 1974 and was only seldom studied afterwards due to its tedious synthesis.[8] Several new development were reported over the years, especially for the synthesis of analogues of 9-phosphatriptycenes, 9-phospha-10-heterotriptycenes and 9,10-dihetera-triptycene.[9-12] To this day the applications of such compounds were limited to being used as ligands in organometallic chemistry. Due to their caged structure, 9-phosphatriptycenes are known for being strong π-acceptors and weak σ-donors and were shown to be effective ligands in palladium-catalyzed processes such as the Stille coupling or the Heck reaction.[13] Other organometallic applications were also reported in homogeneous[14] or heterogenous[15-16] catalysis and as rotor in palladium-centered molecular gears.[17]

We have recently reported novel synthetic approaches toward the parent 9-phosphatriptycene.[18] Investigations of its steric and electronic properties showed that the 9-phosphatriptycene was slightly bulkier and a weaker Lewis base than triphenylphosphine. A linear correlation between the proton affinity

of reference triarylphosphines and the pK_a of the corresponding protonated forms allowed the estimation of its aqueous pK_a of -1.5. In addition, the Lewis basicity (LB = 7.6) of the 9-phosphatriptycene relative to benzhydrylium ions, determined according to the Mayr scale, is significantly lower than that of triphenylphosphine (LB = 14.3), further supporting the lower reactivity of 9-phosphatriptycene derivatives compared to other triarylphosphines. Later, an extension of the synthetic approach toward 9-phosphatriptycenes allowed to produce a set of *ortho*-substituted derivatives, a substitution pattern never reported before.[19] The new substituents span from electron donating groups (methyl groups, Me) to various electron-withdrawing ones (F, Cl, CF_3) and a combination of both Cl and Me to further increase steric hindrance (Figure 15). Investigations of their ligand ability in Rh- and Au- complexes indicated that *ortho*-substituents had a limited effect on the reactivity of the phosphorus center, which was attributed to the lack of conjugation between the phosphorus lone pair, and the π-system of the neighboring aryl rings.

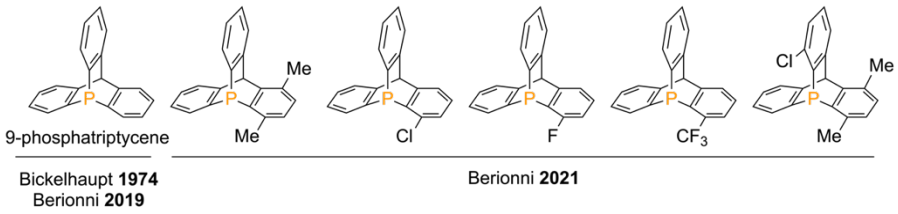

Figure 15. Structures of the parent 9-phosphatriptycene and ortho-substituted derivatives synthesized by Berionni et al.[18-19]

In order to compare quantitatively the Brønsted basicity of these phosphines, an accurate prediction of their pK_a is an essential tool. The pK_a of an acid characterizes the equilibrium of a proton transfer reaction in a given solvent, aqueous or organic.[20] Its measurement finds numerous applications in chemical and biochemical processes.[21-25] The basicity of a base B is characterized by the pK_a value of its conjugated acid [Eq. (1)], BH^+ and is denoted p$K_a(BH^+)$:[26]

$$BH^+ \rightleftharpoons \mathrm{B} + H^+ \qquad (1)$$

$$\mathrm{p}K_a(BH^+) = -log\frac{a(B)\,a(H^+)}{a(BH^+)} \qquad (2)$$

where *a(X)* is the activity of the appropriate entity. It only differs from that of neutral acids in that the global charge remains positive on both sides of the

equilibrium. pK_a values allow direct comparison between selected bases: the stronger the base the higher the pK_a.

Predicting pK_a's by employing quantum chemistry methods is crucial because it enables the investigation of the reactivity of compounds that are still unmeasured, not synthesized experimentally or purely theoretical. Among the strategies developed over the years for the quantum chemical prediction of pK_a's, relative pK_a calculations is generally preferred over absolute pK_a predictions (involving thermodynamic cycles and free energies of solvation determination for the proton), especially when experimental data are available.[27-29] The former method avoids tedious and often unprecise free energy changes associated to the proton in the thermodynamic cycles necessary for absolute pK_a calculations.

In this article, we substantiate the accurate prediction of pK_a values of phosphines by linear correlation between experimental and computed $\Delta \mathrm{p}K_a(BH^+) = \mathrm{p}K_a(BH^+) - \mathrm{p}K_a(Ref.)$ in water and acetonitrile. Experimental values are taken from the litterature[30-32] while computational ones are obtained by density functional theory calculations using an implicit solvation method for water and acetonitrile. This method is then employed to investigate the substituent effect on the basicity of 9-phosphatriptycenes for the first time and to compare them with other phosphines. In addition, the structural impact of the triptycene scaffold on the electronic properties of the phosphorus atom is discussed. Finally, a 9-phosphatriptycene derivative is used in combination with the bulky Lewis acid $B(C_6F_5)_3$ to demonstrate that the resulting FLP can be used as catalyst in the model hydrogenation of 1,1-diphenylethylene.

3. Computational methods

All calculations were performed using the Gaussian16 package.[33] Full geometry optimizations followed by vibrational frequency calculations were done at the M06-2X/6-311G(d) level of theory.[34] Tight convergence thresholds were used for geometry optimizations, *e.g.* for the residual forces on the atoms, 1.5×10^{-5} Hartree/Bohr or Hartree/radian. This method was shown previously to give satisfying results in thermochemistry when compared to higher-level methods such as double-hybrid DFT with a more extended and flexible basis set.[35] Calculations were performed at the temperature and pressure of 298.15 K and 1 atm. For ground state equilibrium structures, all vibrational frequencies of the optimized stationary points are real, demonstrating that the structures are

minima on the potential energy surface. All transition state geometries were obtained by optimization to a saddle point using the Berny algorithm[36-39] and are characterized by a single imaginary frequency. Solvent effects (acetonitrile or water for pK_a determination, dichloromethane for NBO and other reactivity investigations) were taken into account using the implicit solvation IEFPCM method.[40] Natural atomic orbital and natural bond orbital analyses were performed using the Gaussian NBO 3.1 program[41] at the M06-2X/6-311G(d) level of theory on the optimized structures in solvent.

The nature of rotamers was shown to have a strong influence on the reactivity of the phosphonium in the case of phosphines with one or several fluorine atoms in *ortho*-position (see Annex I). For these compounds, a weighed proportion of each rotamer was taken into account using Boltzmann populations.

4. Results and discussion

4.1 Calibration of pK_a determinations

The pK_a's were determined by performing correlations between experimental and computed $\Delta pK_a(BH^+)$'s. Considering equilibrium (3) between two phosphines A and B, one of known experimental p$K_a(AH^+)$ (AH^+/A), the other of unknown p$K_a(BH^+)$ (BH^+/B),

$$A + BH^+ \rightleftharpoons AH^+ + B \qquad (3)$$

its reaction ΔG^0 was determined by quantum chemical calculations (with the abovementioned method), allowing to determine the $K(BH^+ \rightarrow AH^+)$ equilibrium constant (4) and thus to compute $\Delta pK_a(BH^+)$ *via* equation (5).

$$K_{calc}(BH^+ \rightarrow AH^+) = \frac{a(AH^+)\,a(B)}{a(A)\,a(BH^+)} = e^{-\frac{\Delta G^0}{RT}} \qquad (4)$$

$$\Delta pK_a(BH^+) = pK_a(BH^+) - pK_a(AH^+) = -\log K_{calc}(BH^+ \rightarrow AH^+) \qquad (5)$$

The calculated $\Delta pK_a(BH^+)$ [$\Delta pK_a(calc.)$] is then corrected to an estimated experimental $\Delta pK_a(BH^+)$ [$\Delta pK_a(est.)$] value by using a predetermined linear correlation relationship. The latter is obtained by linear regression between calculated (at the same level) and experimental $\Delta pK_a(BH^+)$ values of a training set of compounds:

$$\Delta \mathrm{p}K_a(exp.) = \alpha\ \Delta \mathrm{p}K_a(calc.) + \beta \qquad (6)$$

so that for any unknown phosphine (7), the estimated value reads:

$$\Delta \mathrm{p}K_a(est.) = \alpha\ \Delta \mathrm{p}K_a(calc.) + \beta \qquad (7)$$

This quantity is finally employed to predict the unknown pK_a by using equation (8):

$$\mathrm{p}K_a(BH^+, est.) = \mathrm{p}K_a(AH^+, exp.) + \Delta \mathrm{p}K_a(BH^+, est.) \qquad (8)$$

For each solvent (MeCN and H_2O), a single reference phosphine of known pK_a is selected (triphenylphosphine, PPh_3 **II.1** was arbitrarily selected although the final result is independent of the choice of reference phosphine) from which all $\Delta \mathrm{p}K_a(BH^+)'$s are calculated. The linear correlation is drawn by taking advantage of the vast experimental databank of phosphine pK_a's in acetonitrile, available thanks to the efforts of Leito's group (Table 4).[31-32] Phosphines with the lowest pK_a were selected as references since 9-phosphatriptycenes are known for being weak phosphines. They consist in triaryl-, aryl(alkyl)-, and trialkyl-phosphines with electron-withdrawing groups (F and Cl atoms). The correlation coefficient R^2 of 0.987 indicates a good correlation between experimental and computed values, leading to equation (9) for estimating the pK_a of phosphine BH^+ from its calculated $\Delta \mathrm{p}K_a(BH^+)$:

$$\mathrm{p}K_a(BH^+) = 7.62 + [1.00\ \Delta \mathrm{p}K_a(BH^+) - 0.35] \qquad (9)$$

where 7.62 is the experimental pK_a of PPh_3. The accuracy of the method is evaluated by comparing the experimental and predicted p$K_a's$ of the training set, which differ by 0.1 to 1.0 pK_a units with a mean absolute pK_a error of 0.4 pK_a units (Table 4). The same procedure is then applied for a set of trialkyl- and triaryl-phosphines of experimentally known pK_a's in water.[30] These triarylphosphines display electron-withdrawing groups (EWGs, -F, -Cl and $-CF_3$) and electron-donating ones (EDGs, -Me and -OMe).

Another linear correlation between experimental and calculated $\Delta \mathrm{p}K_a(BH^+)'s$ is then established for water as solvent (Table 5). Again, a good correlation coefficient (R^2= 0.997) is found.

Table 4. Experimental and calculated [M06-2X/6-311G(d) IEFPCM(acetonitrile)] ΔpK_a's in acetonitrile at 25°C for the training set of phosphines. $pK_a(est.)$ stands for the corrected pK_a. The bracketed values correspond to the signed error with respect to experiment.

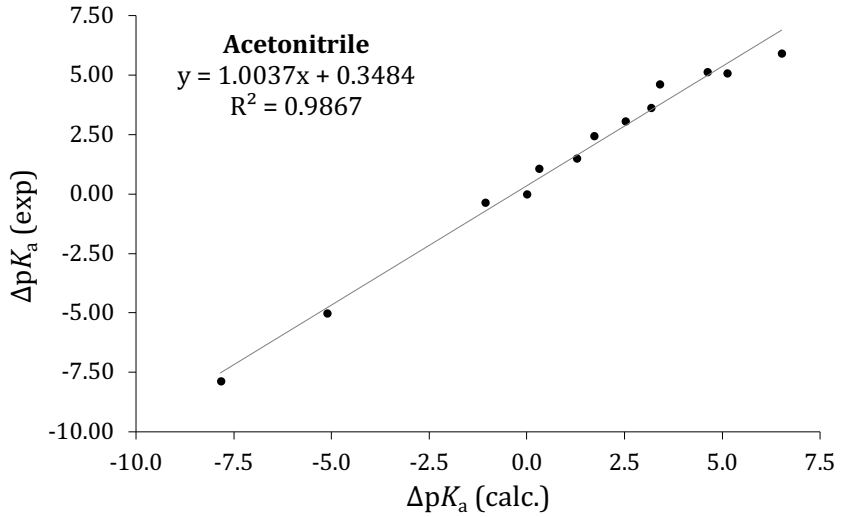

Phosphine	$pK_a(exp.)$	$\Delta pK_a(exp.)$	$\Delta pK_a(calc.)$	$\mathbf{pK_a(est.)}$
$P(2,6\text{-}Cl_2\text{-}C_6H_3)_3$	1.70	-5.92	-6.52	**0.7** [-1.0]
$P(2,6\text{-}F_2\text{-}C_6H_3)_2Ph$	2.50	-5.12	-4.61	**2.6** [+0.1]
$P(C_6F_5)(Ph)_2$	2.54	-5.08	-5.12	**2.1** [-0.4]
$P(2\text{-}F\text{-}C_6H_4)_3$	3.01	-4.61	-3.40	**3.9** [+0.9]
BIPHEP-(H^+)	4.00	-3.62	-3.17	**4.1** [+0.1]
$P(2\text{-}F\text{-}C_6H_4)_2(Ph)$	4.56	-3.06	-2.52	**4.7** [+0.1]
$P(2,6\text{-}F_2\text{-}C_6H_3)Ph_2$	5.17	-2.45	-1.71	**5.6** [+0.4]
$P(2\text{-}FC_6H_4)(Ph)_2$	6.11	-1.51	-1.27	**6.0** [-0.1]
$P(naphtyl)_3$	6.55	-1.07	-0.30	**7.0** [+0.4]
PPh_3 (**II.1**)	7.62	0.00	0.00	**7.3** [-0.3]
BIPHEP	7.99	0.37	1.06	**8.3** [+0.4]
$PMe_2(Ph)$	12.64	5.02	5.11	**12.4** [-0.2]
PMe_3	15.48	7.86	7.84	**15.1** [-0.4]

BIPHEP= 2,2'-bis(diphenylphosphino)biphenyl.

Table 5. Experimental and calculated [M06-2X/6-311G(d) IEFPCM(water)] ΔpK_a's in water at 25°C for a training set of phosphines. $pK_a(est.)$ stands for the corrected pK_a. The bracketed values correspond to the signed error with respect to experiment.

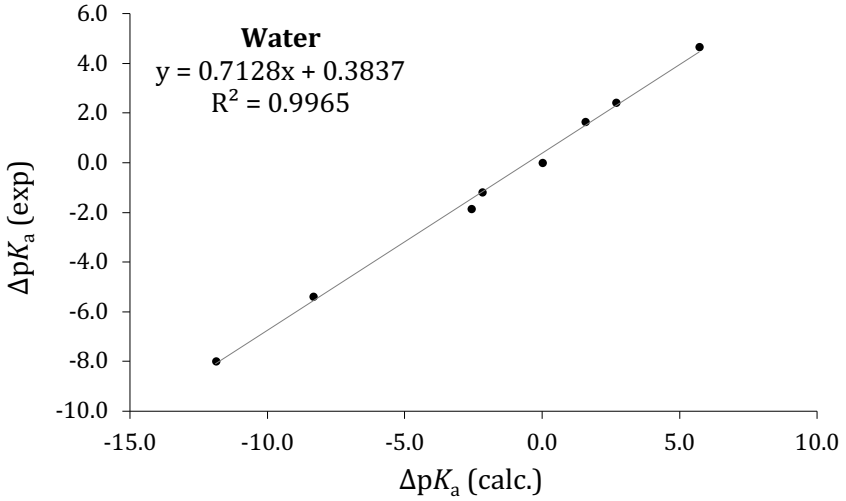

Phosphine	$pK_a(exp.)$	$\Delta pK_a(exp.)$	$\Delta pK_a(calc.)$	$\mathbf{pK_a(est.)}$
PCy_3	11.26	7.98	11.89	**11.4** [+0.1]
PBu_3	8.67	5.39	8.35	**8.8** [+0.2]
$P(4\text{-}MeO\text{-}C_6H_4)_3$	5.13	1.85	2.59	**4.7** [-0.4]
$P(4\text{-}Me\text{-}C_6H_4)_3$	4.46	1.18	2.19	**4.5** [0.0]
PPh_3 (**II.1**)	3.28	0.00	0.00	**2.9** [-0.4]
$P(4\text{-}F\text{-}C_6H_4)_3$	1.63	-1.65	-1.57	**1.8** [+0.1]
$P(4\text{-}Cl\text{-}C_6H_4)_3$	0.87	-2.41	-2.68	**1.0** [+0.1]
$P(4\text{-}CF_3\text{-}C_6H_4)_3$	-1.39	-4.67	-5.71	**-1.2** [+0.2]

The following expression (10) is then derived to predict the pK_a's of new phosphines:

$$pK_a(BH^+) = 3.28 + [0.71\ \Delta pK_a(BH^+) - 0.38] \qquad (10)$$

where 3.28 is the aqueous pK_a of PPh_3. The mean absolute error in predicting these pK_a values amounts to 0.2 and is comprised between 0.0 and 0.4 pK_a units.

In both solvents, the predicted pK_a values are reliable, with a maximum absolute error of one pK_a unit for all systems, while the mean absolute error amounts to 0.4 and 0.2 pK_a units in acetonitrile and water, respectively. In addition, the range of pK_a values is large, between 12 and 14 units in both solvents. In summary, the pK_a estimation by correlation between experimental and computed ΔpK_a's is a robust method for triaryl- and trialkyl-phosphines in acetonitrile and water.

4.1 pK_a predictions of 9-phosphatriptycene derivatives

Using equations (9) and (10), we next predicted the pK_a's of a series of 9-phosphatriptycene derivatives with *ortho*-substituents in acetonitrile and water (Table 6). Compounds **II.3**, **II.4**, **II.5**, and **II.11** are not yet synthesized but are included to investigate the cumulative effect of multiple substituents. Note that the set of reference phosphines is consistent with the list of 9-phosphatriptycene derivatives given that nature of substituents and heteroatoms they display are the same (F, Cl, Me and CF_3). Interestingly, all 9-phosphatriptycene derivatives display lower pK_a values than the other triarylphosphines, regardless of the substituents, demonstrating that they form a distinct family of weakly basic phosphines, even though they also display three aryl rings linked to the phosphorus atom.

The strong effect of the triptycene scaffold on the phosphorus atoms is nicely evidenced when comparing the pK_a's of triphenylphosphine **II.1** and of the unsubstituted 9-phosphatriptycene **II.2**. They display the same substitution pattern (except a single carbon linker at the back of molecule **II.2**) but their pK_a's are differing by -8.3 pK_a units in acetonitrile and -6.2 in water. The same trends are observed in both solvents. When electron-donating groups are added, (one, two, and three methyl groups) the pK_a value increases (-0.5, -0.2, 0.7 in acetonitrile; -2.7, -2.5 and -2.0 in water for one, two and three methyl groups, respectively) and decreases with electron-withdrawing group (-2.6, -2.5, -2.9 in acetonitrile; -4.2, -4.1 and -4.5 in water for Cl, F, and CF_3 respectively). Eventually, when both Cl and two methyl groups are added, as in compound **II.10**, the effects of all groups sum up and result in an intermediate pK_a value of -1.5 in acetonitrile and -3.5 in water. The addition of chlorine substituents is cumulative and has a strong impact on the acidity: going from **II.2** to **II.7** and **II.6** $\rightarrow$ **II.10** $\rightarrow$ **II.11**, approximatively the same drop in pK_a is observed (-1.9, -1.7 and -2.0 pK_a units in acetonitrile; -1.3, -1.3 and -1.5 in water). On the other hand, adding Me groups increases the pK_a but in a less significant way. The series

Table 6. Predicted pK_a values of 9-phosphatriptycene derivatives in acetonitrile and water at 25°C using equations (9) and (10). Functional groups indicated in parentheses. Xyl= xylene.

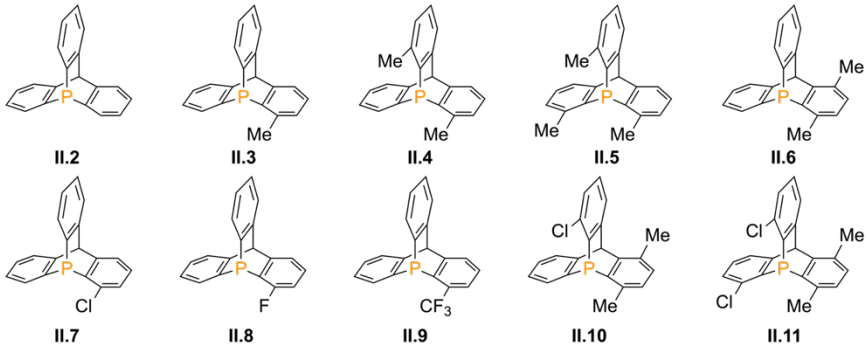

Phosphines	Acetonitrile		Water	
	$\Delta pK_a(calc.)$	$\mathbf{pK_a(est.)}$	$\Delta pK_a(calc.)$	$\mathbf{pK_a(est.)}$
2 (-H)	-7.96	**-0.7**	-8.10	**-2.9**
3 (-Me)	-7.78	**-0.5**	-7.91	**-2.7**
4 (-Me_2)	-7.43	**-0.2**	-7.58	**-2.5**
5 (-Me_3)	-6.53	**0.7**	-6.87	**-2.0**
6 (-Xyl)	-7.03	**0.2**	-7.22	**-2.2**
7 (-Cl)	-9.84	**-2.6**	-10.02	**-4.2**
8 (-F)	-9.69	**-2.5**	-9.85	**-4.1**
9 (-CF_3)	-10.17	**-2.9**	-10.34	**-4.5**
10 (Cl, Xyl)	-8.71	**-1.5**	-8.91	**-3.5**
11 (Cl_2, Xyl)	-10.75	**-3.5**	-11.03	**-5.0**

II.2 → **II.3** → **II.4** → **II.5** results in smaller increases of +0.2, +0.2 and +0.9 pK_a units in acetonitrile and +0.2, +0.2 and +0.5 in water. **6** is a synthetic analogue of **3** but slightly more reactive, with one additional methyl group and a pK_a value intermediate between that of **II.4** and **II.5** (0.2 in acetonitrile and -2.2 in water).

4.2 Rationalizing the weak basicity of 9-phosphatriptycenes

The triptycene scaffold forces a large strain on the phosphine, which results in an increase in the pyramidalization of 9-phosphatriptycene derivatives compared to their triphenyl- analogues. This structural change brings an electronic reorganization of the atom, modifying the *s*/*p* orbital hybridization of the phosphorus lone pair and hence affecting its reactivity (Figure 16).

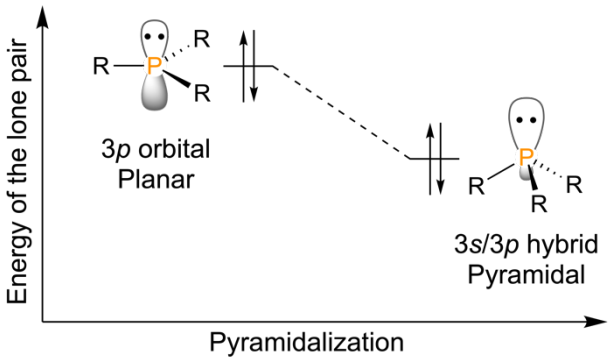

Figure 16. Schematic Welsh diagram illustrating the effect of pyramidalization and hybridization on the energy of the phosphorus lone pair.

A higher pyramidalization increases the *s* character of the lone pair, using the spherical shape of *s* orbitals to widen the frontal lobe of the lone pair and reduce its back lobe, leaving space for the neighboring carbon atoms. Since *s* orbitals are lower in energy than *p* orbitals (for a given quantum number *n*), the global energy of the lone pair is reduced, along with the reactivity of the phosphorus. This assumption was verified by NBO calculations, that allow quantifying the *s*/*p* hybridization of a given natural bond orbital (Table 7, further discussed in Annex I). These were confronted to the pyramidalization of phosphorus compounds defined as the distance between the phosphorus and the plane drawn by its three neighboring carbons divided by the mean P-C distance (*Pyr* parameter in Table 7).

4.3 Application of 9-phosphatriptycenes in frustrated Lewis pair chemistry

The addition of substituents also impacts the lone pair energy and affects the reactivity of the phosphorus. Actually, this is the strategy systematically preferred when one wants to tune the reactivity of a given compound. However,

Table 7. NBO results. ε_{LP} is the energy of the lone pair of the phosphorus, Pyr is the pyramidalization, s_{LP} (%) and p_{LP} (%) are respectively its 3s and 3p components [$3d_{LP}$ (%) is neglected since typically <0.01%], $Occ._{LP}$ is its electronic occupancy and Q_P is the natural charge of the phosphorus atom (expressed as multiple of the fundamental charge, e).

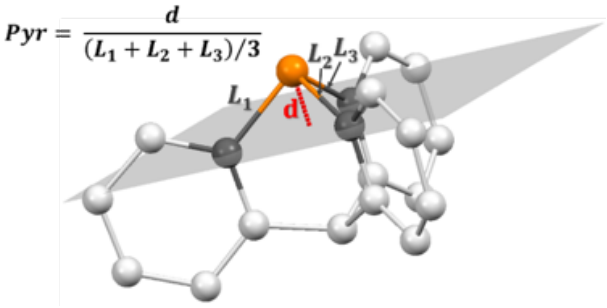

Compounds	ε_{LP} (eV)	*Pyr*	$3s_{LP}$ (%)	$3p_{LP}$ (%)	$Occ._{LP}$	Q_P
II.1	-11.66	0.452	45.4	54.6	1.917	0.82
II.2	-12.78	0.536	49.9	50.1	1.961	0.79
II.3	-12.74	0.534	50.0	50.0	1.960	0.79
II.4	-12.69	0.533	50.0	50.0	1.959	0.78
II.5	-12.65	0.532	50.1	49.9	1.958	0.78
II.6	-12.71	0.534	49.9	50.1	1.960	0.79
II.7	-12.95	0.538	50.8	49.2	1.960	0.81
II.8	-12.93	0.540	50.7	49.3	1.962	0.81
II.9	-12.99	0.538	50.9	49.1	1.960	0.81
II.10	-12.88	0.536	50.8	49.2	1.959	0.81
II.11	-13.05	0.537	51.6	48.3	1.957	0.83

with the prediction of 9-phosphatriptycenes pK_a's, this study has demonstrated that the same result can also be obtained by only changing structural parameters. In our research group, this strategy was already successfully applied to enhance the reactivity of triarylboranes, developing a new family of non-planar Lewis acids.[35, 42-44]

One domain in which weak Brønsted bases like 9-phosphatriptycenes can find application is frustrated Lewis pairs (FLPs) chemistry.[5, 45-46] When associated with tris(pentafluorophenyl)borane [$B(C_6F_5)_3$], these bifunctional systems constituted of sterically hindered Lewis acids and bases are behaving as transition-metal-free catalysts for the hydrogenation of unsaturated

substrates.[47] Combined with tris(pentafluorophenyl)borane ($B[C_6F_5]_3$), Lewis bases such as bulky phosphines (*e.g.* P*t*Bu$_3$, PMes$_3$) or amines (*e.g.* TMP, 2,6-lutidine) are suitable to reduce electron rich polarized double bonds such as in imines, enamines, or silyl enol ethers.[6, 48-49] More challenging substrates however, olefins, ketones and aldehydes, require instead much weaker Lewis bases as catalysts. Deactivated phosphines or ethereal solvents were employed.[50-51] The latter are necessary to generate strongly acidic protons (phosphonium or oxonium) able to partially protonate the C=C double bond or the carbonyl group. In this context, 9-phosphatriptycenes are promising candidates as sterically hindered Lewis bases for H_2 activation and for FLP-catalyzed hydrogenations of challenging substrates. Their *ortho*-substitution will increase their steric hindrance and prevent the adduct formation with Lewis acids while their weak Brønsted basicity will result in the generation of more acidic (hence more reactive) phosphonium ions upon hydrogen splitting.

As a proof of concept, the energy profile of hydrogenation of 1,1-diphenylethylene **II.12**, a substrate that is reportedly hydrogenated by other phosphines deactivated by the addition of multiple EWGs,[50] was then described at the IEFPCM(dichloromethane)/M06-2X/6-311G(d) level of theory and is shown below (Figure 17).

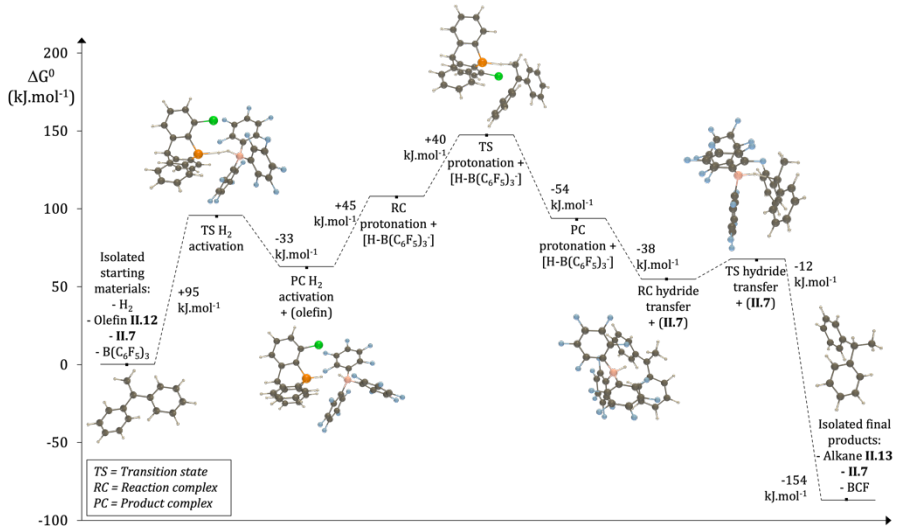

*Figure 17. Gibbs free energy profile of 1,1-diphenylethylene **II.12** hydrogenation by 1-chloro-9-phosphatriptycene **II.7** and tris(pentafluorophenyl)borane computed at the IEFPCM(dichloromethane)/M06-2X/6-311G(d) level of theory at 25°C.*

Since the unsubstituted 9-phosphatriptycene is known to form a Lewis adduct with $B(C_6F_5)_3$,[18] a chlorine *ortho*-substituent was considered (1-chloro-9-phosphatriptycene **II.7**) owing to its electron-withdrawing ability combined with the increase in steric hindrance (the Lewis adduct formation with $B(C_6F_5)_3$ is prevented, with a computed ΔG^0 value of +4 kJ.mol^{-1}). The overall scheme of the reaction is shown in Figure 18. The hydrogenation of alkenes proceeds in a stepwise manner: first, a protonation of the double bond by the phosphonium occurs and is followed by hydride transfer from the borohydride to the carbocation intermediate. The preliminary hydrogen activation is endergonic, with a ΔG^0 of 62 kJ.mol^{-1} and an activation barrier of 95 kJ.mol^{-1}, which was expected given the weak nature of the Lewis base. The proton transfer to the

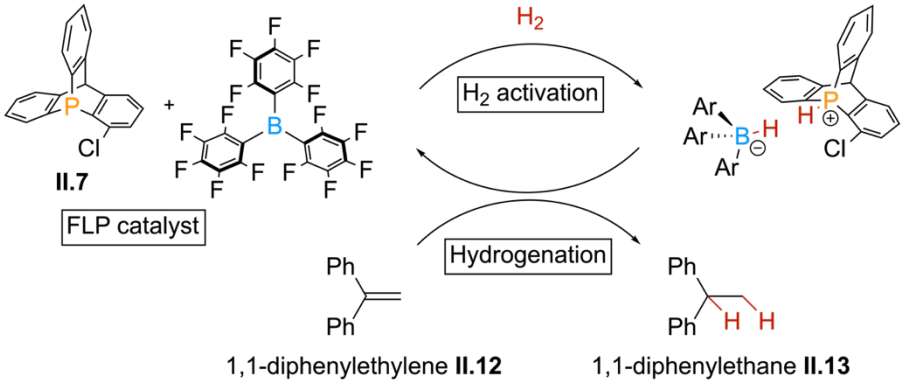

*Figure 18. Scheme of the model hydrogenation reaction of 1,1-diphenylethylene **12** with the 1-chloro-9-phosphatriptycene/$B(C_6F_5)_3$ FLP.*

olefin is the rate-limiting step of the reaction, with a total activation energy of 147 kJ.mol^{-1}. It is preceded by a free energy penalty necessary for separating the ion pair (PC-1 → RC-2, +45 kJ.mol^{-1}), later compensated by the following ion pair formation (PC-2 → RC-3, -38 kJ.mol^{-1}). Eventually, the driving force is the borohydride transfer, with a Gibbs free energy variation of -142 kJ.mol^{-1} from the carbocation intermediate and -87 kJ.mol^{-1} overall. The potential of 9-phosphatriptycenes as catalysts for hydrogenations was further demonstrated experimentally: guided by the quantum chemistry results, we started our investigations of FLP-catalyzed hydrogenations with the Lewis pair consisting of 1-chloro-9-phosphatriptycene **II.7** and $B(C_6F_5)_3$. An NMR analysis with 1 equivalent of both compounds in $CDCl_3$ showed no formation of Lewis adduct and confirmed that they behave like a FLP. Then, the hydrogenation of 1,1-diphenylethylene was performed at room temperature and under pressure of dihydrogen. After optimization of the conditions (detailed in Annex I), a

conversion of 98% and a yield of 88% were obtained with 20 mol% catalyst for 16h at 40 bar of H_2, demonstrating the potential of 9-phosphatriptycene derivatives in FLP catalysis.

5. Conclusions and outlooks

In conclusion, a reliable method for predicting pK_a's of phosphines in acetonitrile and water has been developed by linear correlation between DFT-computed ΔpK_a's and experimental values extracted from the literature. This method allowed to estimate the pK_a's of a series of 9-phosphatriptycenes and indicate that they are weaker Brønsted bases than their unstrained triarylphosphine analogues. Structural and electronic investigations suggested that the strain and increased pyramidalization forced by the triptycene scaffold on the phosphorus atom increases the *3s* character of its lone pair, stabilizing it and reducing its basicity, even without strong electron-withdrawing groups. These bulky yet electron-poor phosphines were then used to design new frustrated Lewis pairs which were used in the model hydrogenation reaction of 1,1-diphenylethylene. The latter application, although a proof-of-concept since 1,1-diphenylethylene is easily reduced by simpler acid-base combinations, showed that 9-phosphatriptycenes are good candidates for FLP chemistry. Furthermore, this study demonstrates that increasing the pyramidalization of phosphines by constraining their geometry can be also used as a new tool for reactivity tuning in contrast to the classical addition of electron-withdrawing groups currently used as the main strategy to decrease their basicity. Investigations are ongoing in our lab for the use of 9-phosphatriptycenes in FLP chemistry in the hydrogenation of challenging substrates.

6. References

[1] P. C. J. Kamer, P. W. N. M. van Leeuwen, *Phosphorus(III) ligands in homogeneous catalysis: design and synthesis*, John Wiley & Sons, Ltd, **2012**.

[2] J. L. Methot, W. R. Roush, "Nucleophilic phosphine organocatalysis", *Adv. Synth. Catal.* **2004**, *346*, 1035-1050.

[3] H. Guo, Y. C. Fan, Z. Sun, Y. Wu, O. Kwon, "Phosphine organocatalysis", *Chem. Rev.* **2018**, *118*, 10049-10293.

[4] H. Ni, W. L. Chan, Y. Lu, "Phosphine-catalyzed asymmetric organic reactions", *Chem. Rev.* **2018**, *118*, 9344-9411.

[5] G. C. Welch, R. R. San Juan, J. D. Masuda, D. W. Stephan, "Reversible, metal-free hydrogen activation", *Science* **2006**, *314*, 1124-1126.

[6] D. W. Stephan, "The broadening reach of frustrated Lewis pair chemistry", *Science* **2016**, *354*, 1248-1256.

[7] L. Greb, S. Tussing, B. Schirmer, P. Oña-Burgos, K. Kaupmees, M. Lõkov, I. Leito, S. Grimme, J. Paradies, "Electronic effects of triarylphosphines in metal-free hydrogen activation: a kinetic and computational study", *Chem. Sci.* **2013**, *4*, 2788.

[8] C. Jongsma, J. P. de Kleijn, F. Bickelhaupt, "Phosphatriptycene", *Tetrahedron* **1974**, *30*, 3465-3469.

[9] J. Kobayashi, T. Agou, T. Kawashima, "A novel and convenient synthetic route to a 9-phosphatriptycene and systematic comparisons of 9-phosphatriptycene derivatives", *Chem. Lett.* **2003**, *32*, 1144-1145.

[10] T. Agou, J. Kobayashi, T. Kawashima, "Synthesis, structure, and reactivity of a symmetrically substituted 9-phosphatriptycene oxide and Its derivatives", *Heteroat. Chem* **2004**, *15*, 437-446.

[11] H. Tsuji, T. Inoue, Y. Kaneta, S. Sase, A. Kawachi, K. Tamao, "Synthesis, structure, and properties of 9-phospha-10-silatriptycenes and their derivatives", *Organometallics* **2006**, *25*, 6142-6148.

[12] Y. Uchiyama, J. Sugimoto, M. Shibata, G. Yamamoto, Y. Mazaki, "Bromine adducts of 9,10-diheteratriptycene derivatives", *Bull. Chem. Soc. Jpn.* **2009**, *82*, 819-828.

[13] T. Agou, J. Kobayashi, T. Kawashima, "Evaluation of σ-donating ability of a 9-phosphatriptycene and its application to catalytic reactions", *Chem. Lett.* **2004**, *33*, 1028-1029.

[14] S. Konishi, T. Iwai, M. Sawamura, "Synthesis, properties, and catalytic application of a triptycene-type borate-phosphine ligand", *Organometallics* **2018**, *37*, 1876-1883.

[15] T. Iwai, S. Konishi, T. Miyazaki, S. Kawamorita, N. Yokokawa, H. Ohmiya, M. Sawamura, "Silica-supported triptycene-type phosphine. Synthesis, characterization, and application to Pd-catalyzed suzuki–miyaura cross-coupling of chloroarenes", *ACS Catal.* **2015**, *5*, 7254-7264.

[16] S. Kawamorita, T. Miyazaki, H. Ohmiya, T. Iwai, M. Sawamura, "Rh-catalyzed *ortho*-selective C–H borylation of N-functionalized arenes with silica-supported bridgehead monophosphine ligands", *J. Am. Chem. Soc.* **2011**, *133*, 19310-19313.

[17] H. Ube, Y. Yasuda, H. Sato, M. Shionoya, "Metal-centred azaphosphatriptycene gear with a photo- and thermally driven mechanical switching function based on coordination isomerism", *Nature Communications* **2017**, *8*, 14296-14301.

[18] L. Hu, D. Mahaut, N. Tumanov, J. Wouters, R. Robiette, G. Berionni, "Complementary synthetic approaches toward 9-phosphatriptycene and structure–reactivity investigations of its association with sterically hindered Lewis acids", *J. Org. Chem.* **2019**, *84*, 11268-11274.

[19] L. Hu, D. Mahaut, N. Tumanov, J. Wouters, L. Collard, R. Robiette, G. Berionni, "Sterically hindered *ortho*-substituted phosphatriptycenes as configurationally stable P-chirogenic triarylphosphines", *Dalton Trans.* **2021**, *50*, 4772-4777.

[20] R. P. Bell, *The Proton in Chemistry*, Springer, Boston, MA, **1976**.

[21] P. S. Charifson, W. P. Walters, "Acidic and basic drugs in medicinal chemistry: a perspective", *J. Med. Chem.* **2014**, *57*, 9701-9717.

[22] P. Gilli, L. Pretto, G. Gilli, "PA/pK_a equalization and the prediction of the hydrogen-bond strength: A synergism of classical thermodynamics and structural crystallography", *J. Mol. Struct.* **2007**, *844-845*, 328-339.

[23] M. H. Huynh, T. J. Meyer, "Proton-coupled electron transfer", *Chem. Rev.* **2007**, *107*, 5004-5064.

[24] K. Izutsu, *Electrochemistry in Nonaqueous Solutions*, Wiley-VCH, Weinheim, **2009**.

[25] B. Thapa, K. Raghavachari, "Accurate pK_a Evaluations for Complex Bio-Organic Molecules in Aqueous Media", *J. Chem. Theory Comput.* **2019**, *15*, 6025-6035.

[26] A. Kütt, S. Selberg, I. Kaljurand, S. Tshepelevitsh, A. Heering, A. Darnell, K. Kaupmees, M. Piirsalu, I. Leito, "pK_a values in organic chemistry – Making maximum use of the available data", *Tetrahedron Lett.* **2018**, *59*, 3738-3748.

[27] G. C. Shields, P. G. Seybold, *Computational approaches for the determination of pKa values*, CRC Press, Boca Raton, **2014**.

[28] J. Ho, "Predicting pK_a in implicit solvents: current status and future directions", *Aust. J. Chem.* **2014**, *67*, 1441-1460.

[29] L. Xu, M. L. Coote, "Methods to improve the calculations of solvation model density solvation free energies and associated aqueous pK_a values: Comparison between choosing an optimal theoretical level, solute cavity scaling, and using explicit solvent molecules", *J. Phys. Chem. A* **2019**, *123*, 7430-7438.

[30] A. J. Poe, D. H. Farrar, Y. Zheng, "Systematic kinetics of high nuclearity metal carbonyl clusters. Associative substitution reactions of Ru6C(CO)17 with P-donor nucleophiles", *J. Am. Chem. Soc.* **1992**, *114*, 5146-5152.

[31] K. Haav, J. Saame, A. Kütt, I. Leito, "Basicity of phosphanes and diphosphanes in acetonitrile", *Eur. J. Org. Chem.* **2012**, *2012*, 2167-2172.

[32] S. Tshepelevitsh, A. Kütt, M. Lõkov, I. Kaljurand, J. Saame, A. Heering, P. G. Plieger, R. Vianello, I. Leito, "On the basicity of organic bases in different media", *Eur. J. Org. Chem.* **2019**, *2019*, 6735-6748.

[33] M. J. Frisch, G. W. Trucks, H. B. Schlegel, G. E. Scuseria, M. A. Robb, J. R. Cheeseman, G. Scalmani, V. Barone, G. A. Petersson, H. Nakatsuji, X. Li, M. Caricato, A. V. Marenich, J. Bloino, B. G. Janesko, R. Gomperts, B. Mennucci, H. P. Hratchian, J. V. Ortiz, A. F. Izmaylov, J. L. Sonnenberg, D. Williams-Young, F. Ding, F. Lipparini, F. Egidi, J. Goings, B. Peng, A. Petrone, T. Henderson, D. Ranasinghe, V. G. Zakrzewski, J. Gao, N. Rega, G. Zheng, W. Liang, M. Hada, M. Ehara, K. Toyota, R. Fukuda, J. Hasegawa, M. Ishida, T. Nakajima, Y. Honda, O. Kitao, H. Nakai, T. Vreven, K. Throssell, J. A. Montgomery, Jr., J. E. Peralta, F. Ogliaro, M. J. Bearpark, J. J. Heyd, E. N. Brothers, K. N. Kudin, V. N. Staroverov, T. A. Keith, R. Kobayashi, J. Normand, K. Raghavachari, A. P. Rendell, J. C. Burant, S. S. Iyengar, J. Tomasi, M. Cossi, J. M. Millam, M. Klene, C. Adamo, R. Cammi, J. W. Ochterski, R. L. Martin, K. Morokuma, O. Farkas, J. B. Foresman, D. J. Fox, *Gaussian 16, Revision A.03*, Gaussian Inc., Wallingford CT, **2016**.

[34] Y. Zhao, D. G. Truhlar, "The M06 suite of density functionals for main group thermochemistry, thermochemical kinetics, noncovalent interactions, excited states, and transition elements: Two new functionals and systematic testing of four M06-class functionals and 12 other functionals", *Theor. Chem. Acc.* **2008**, *120*, 215-241.

[35] D. Mahaut, A. Chardon, L. Mineur, G. Berionni, B. Champagne, "Rational development of a metal-free bifunctional system for the C-H activation of methane: a density functional theory investigation", *ChemPhysChem* **2021**, *22*, 1958-1966.

[36] C. Peng, P. Y. Ayala, H. B. Schlegel, M. J. Frisch, "Using redundant internal coordinates to optimize equilibrium geometries and transition states", *J. Comput. Chem.* **1996**, *17*, 49-56.

[37] P. Pulay, G. Fogarasi, "Geometry optimization in redundant internal coordinates", *J. Chem. Phys.* **1992**, *96*, 2856-2860.

[38] P. Pulay, G. Fogarasi, F. Pang, J. E. Boggs, "Systematic *ab initio* gradient calculation of molecular geometries, force constants, and dipole moment derivatives", *J. Am. Chem. Soc.* **1979**, *101*, 2550-2560.

[39] X. Li, M. J. Frisch, "Energy-represented direct inversion in the iterative subspace within a hybrid geometry optimization method", *J. Chem. Theory Comput.* **2006**, *2*, 835-839.

[40] J. Tomasi, B. Mennucci, R. Cammi, "Quantum mechanical continuum solvation models", *Chem. Rev.* **2005**, *105*, 2999-3094.

[41] E. D. Glendening, A. E. Reed, J. E. Carpenter, F. Weinhold, *NBO Version 3.1*, Gaussian Inc., Pittsburgh, **2003**.

[42] A. Ben Saida, A. Chardon, A. Osi, N. Tumanov, J. Wouters, A. I. Adjieufack, B. Champagne, G. Berionni, "Pushing the Lewis acidity boundaries of boron compounds with non-planar triarylboranes derived from triptycenes", *Angew. Chem. Int. Ed.* **2019**, *58*, 16889-16893.

[43] A. Chardon, A. Osi, D. Mahaut, A. Ben Saida, G. Berionni, "Non-planar boron Lewis acids taking the next step: Development of tunable Lewis acids, Lewis superacids and bifunctional catalysts", *Synlett* **2020**, *31*, 1639-1648.

[44] A. Chardon, A. Osi, D. Mahaut, T. H. Doan, N. Tumanov, J. Wouters, L. Fusaro, B. Champagne, G. Berionni, "Controlled generation of 9-boratriptycene by Lewis adduct dissociation: Accessing a non-planar triarylborane", *Angew. Chem. Int. Ed.* **2020**, *59*, 12402-12406.

[45] G. C. Welch, D. W. Stephan, "Facile heterolytic cleavage of dihydrogen by phosphines and boranes", *J. Am. Chem. Soc.* **2007**, *129*, 1880-1881.

[46] D. W. Stephan, ""frustrated Lewis pairs": A concept for new reactivity and catalysis", *Org. Biomol. Chem.* **2008**, *6*, 1535-1539.

[47] J. Lam, K. M. Szkop, E. Mosaferi, D. W. Stephan, "FLP catalysis: main group hydrogenations of organic unsaturated substrates", *Chem. Soc. Rev.* **2019**, *48*, 3592-3612.

[48] D. W. Stephan, ""Frustrated Lewis pair" hydrogenations", *Org. Biomol. Chem.* **2012**, *10*, 5740-5746.

[49] D. W. Stephan, "Frustrated Lewis pairs: from concept to catalysis", *Acc. Chem. Res.* **2015**, *48*, 306-316.

[50] L. Greb, P. Oña-Burgos, B. Schirmer, S. Grimme, D. W. Stephan, J. Paradies, "Metal-free catalytic olefin hydrogenation: Low-temperature H_2 activation by frustrated Lewis pairs", *Angew. Chem. Int. Ed.* **2012**, *51*, 10164-10168.

[51] D. J. Scott, M. J. Fuchter, A. E. Ashley, "Non-metal catalyzed hydrogenation of carbonyl compounds", *J. Am. Chem. Soc.* **2014**, *136*, 15813-15816.

Chapter III
Frustrated Lewis pair-catalyzed hydrogenation of unactivated alkenes with sterically hindered 9-phosphatriptycenes

---

9-phosphatriptycene derivatives in combination with tris(pentafluorophenyl)-borane are used as FLP catalysts for the metal-free hydrogenation of unactivated olefins.

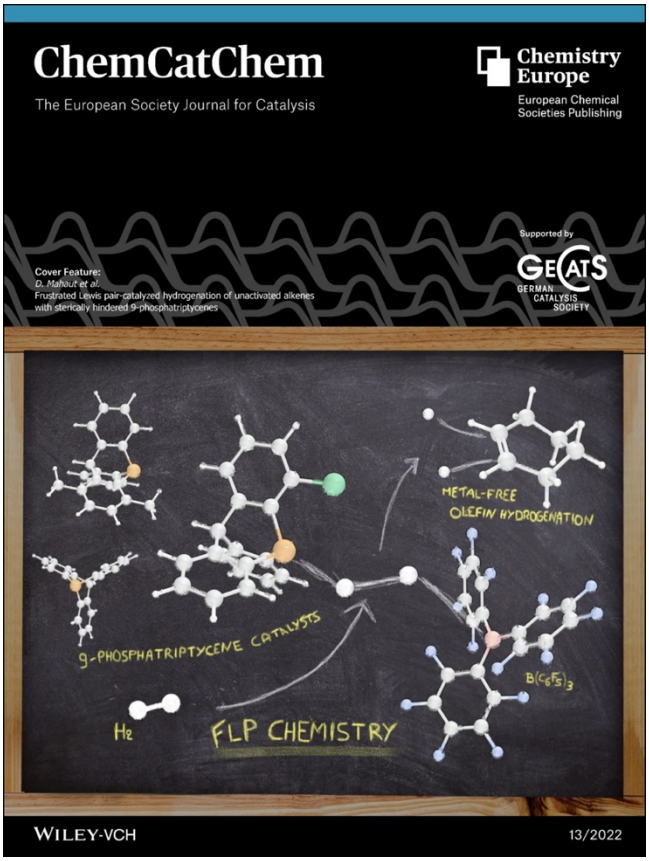

This chapter is based on the following article published in the journal *ChemCatChem* on May 4, 2022 and reproduced with permission from John Wiley and Sons.

D. Mahaut, B. Champagne, G. Berionni, "Frustrated Lewis pair-catalyzed hydrogenation of unactivated alkenes with sterically hindered 9-phosphatriptycenes", *ChemCatChem* **2022**, *14*, e202200294.

ChemCatChem | Research Article
doi.org/10.1002/cctc.202200294
Check for updates
ChemistryEurope
European Chemical Societies Publishing
www.chemcatchem.org

Frustrated Lewis pair-catalyzed hydrogenation of unactivated alkenes with sterically hindered 9-phosphatriptycenes

Damien Mahaut,[a] Benoît Champagne,[a] and Guillaume Berionni*[a]

The frustrated Lewis pair-catalyzed hydrogenation of unactivated alkenes with H_2 is reported. The weak Lewis basicity and high steric hindrance of *ortho*-substituted 9-phosphatriptycene derivatives is taken as an advantage to catalyze this reaction in combination with tris(pentafluorophenyl)borane. A scope of unsaturated substrates is described. The thermodynamics and kinetics of hydrogenation investigated by density functional theory show that the protonation of the olefin by the strongly acidic phosphonium cation is the critical step of the reaction.

Introduction

Since its discovery in 2006 by Stephan and co-workers, the reactivity of frustrated Lewis pairs (FLPs), especially toward dihydrogen, opened new doors in acid/base catalysis.[1] These bifunctional systems consist in a combination of sterically hindered acids and bases that cannot form a classical Lewis adduct due to steric repulsions.[2] The acid and base components then act synergistically on a third smaller molecule (*e.g.* H_2, CO_2, SO_2, N_2O),[3] allowing the development of unprecedented reactivities. This is exemplified with the heterolytic splitting of H_2 and subsequent FLP-catalyzed hydrogenations, used as metal-free alternatives for catalytic transformations that were traditionally requiring transition-metal complexes.[4] The first FLP systems, typically consisting of a bulky phosphine (*e.g.* tris(*tert*-butyl)phosphine, tris(mesityl)phosphine) or amine (*e.g.* 2,6-lutidine, 2,2-6,6-tetramethylpiperidine) combined with B(C_6F_5)$_3$, were restricted to the hydrogenation of imines, enamines or silyl enol ether.[5] Over the years, the substrate scope was largely expanded due to a careful tuning of the reaction conditions and the electronic and steric properties of the Lewis acids and bases. On one hand, bulkier and weaker Lewis acids than B(C_6F_5)$_3$ allowed the hydrogenation of Michael acceptors, previously limited by the strong coordination between the boron and the oxygen in enones,[6] as well as the hydrogenation of electron-poor allenes and alkenes due to easier hydride transfer steps.[7] It also enabled the development of water-tolerant FLPs, able to catalyze reductive amination of carbonyls, prevented before by the coordination of the generated water to the Lewis acid.[8] On the other hand, olefins, ketones or aldehydes can be reduced by targeting the reactivity of the Lewis base catalyst. Ashley, Stephan and Soós and their respective groups used ethereal solvents to catalyze the hydrogenation of ketones and aldehydes with B(C_6F_5)$_3$, taking advantage of the weak basicity of the ethers and their strong conjugate Brønsted acids to promote protodeborylation of the alkoxyborate intermediate.[9] Similarly, the group of Paradies first showed that deactivated phosphines generate in solution strongly acidic phosphonium cations, able to protonate olefins that display allylic stabilization or that bear aryl groups such as 1,1-diphenylethylene (Scheme 1a).[10] Ethers can also be used for the same transformation.[11] Targeting even more challenging substrates, the group of Wang developed a strategy of hydrogenation based on an initial hydroboration using Piers' borane HB(C_6F_5)$_2$,[12] constituting the first example of non-metal-cata-

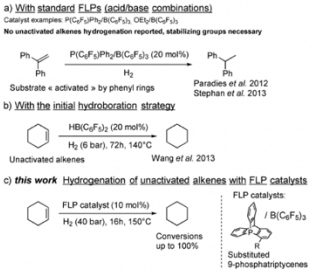

Scheme 1. Previous and current works on hydrogenation reactions of unactivated alkenes.

[a] D. Mahaut, Prof. B. Champagne, Prof. G. Berionni
Department of Chemistry
NISM (Namur Institute of Structured Matter)
University of Namur
Rue de Bruxelles 61
B-5000, Namur (Belgium)
E-mail: guillaume.berionni@unamur.be

Supporting information for this article is available on the WWW under https://doi.org/10.1002/cctc.202200294

This publication is part of a joint Special Collection with EurJIC on "Main Group Catalysis". Please check the ChemCatChem homepage for more articles in the collection.

1. Abstract

The frustrated Lewis pair-catalyzed hydrogenation of unactivated alkenes with H_2 is reported. The weak Lewis basicity and high steric hindrance of *ortho*-substituted 9-phosphatriptycene derivatives is taken as an advantage to catalyze this reaction in combination with tris(pentafluorophenyl)borane. A scope of unsaturated substrates is described. The thermodynamics and kinetics of hydrogenation investigated by density functional theory show that the protonation of the olefin by the strongly acidic phosphonium cation is the critical step of the reaction.

2. Introduction

Since its discovery in 2006 by Stephan and co-workers, the reactivity of frustrated Lewis pairs (FLPs), especially toward dihydrogen, opened new doors in acid/base catalysis.[1-4] These bifunctional systems consist in a combination of sterically hindered acids and bases that cannot form a classical Lewis adduct due to steric repulsions.[5] The acid and base components then act synergistically on a third smaller molecule (*e.g.* H_2, CO_2, SO_2, N_2O),[6-10] allowing the development of unprecedented reactivities. This is exemplified with the heterolytic splitting of H_2 and subsequent FLP-catalyzed hydrogenations, used as metal-free alternatives for catalytic transformations that were traditionally requiring transition metal complexes.[11-15] The first FLP systems, typically consisting of a bulky phosphine (*e.g.* tris(*tert*-butyl)phosphine, tris(mesityl)phosphine) or amine (*e.g.* 2,6-lutidine, 2,2-6,6-tetramethylpiperidine) combined with $B(C_6F_5)_3$, were restricted to the hydrogenation of imines, enamines or silyl enol ether.[16-18] Over the years, the substrate scope was largely expanded due to a careful tuning of the reaction conditions and the electronic and steric properties of the Lewis acids and bases. On one hand, bulkier and weaker Lewis acids than $B(C_6F_5)_3$ allowed the hydrogenation of Michael acceptors, previously limited by the strong coordination between the boron and the oxygen in enones,[19] as well as the hydrogenation of electron-poor allenes and alkenes due to easier hydride transfer steps.[20-21] It also enabled the development of water-tolerant FLPs, able to catalyze reductive amination of carbonyls, prevented before by the coordination of the generated water to the Lewis acid.[22] On the other hand, olefins, ketones or aldehydes can be reduced by targeting the reactivity of the Lewis base catalyst. Ashley, Stephan and Soós and their respective groups used

ethereal solvents to catalyze the hydrogenation of ketones and aldehydes with $B(C_6F_5)_3$, taking advantage of the weak basicity of the ethers and their strong conjugate Brønsted acids to promote protodeborylation of the alkoxyborate intermediate.[23-25] Similarly, the group of Paradies first showed that deactivated phosphines generate in solution strongly acidic phosphonium cations, able to protonate olefins that display allylic stabilization or that bear aryl groups such as 1,1-diphenylethylene (Scheme 31a).[26-27] Ethers can also be used for the same transformation.[28] Targeting even more challenging substrates, the group of Wang developed a strategy of hydrogenation based on an initial hydroboration using Piers' borane $HB(C_6F_5)_2$,[29] constituting the first example of non-metal-catalyzed reduction of aliphatic unactivated olefins in relatively mild conditions (Scheme 31b), where unactivated alkenes bear no stabilizing groups allowing delocalization (*e.g.* aryl, vinyl, nitro groups or acrylates).[30] This approach of initial hydroboration was eventually adopted for the development of new types of metal-free catalysts and the hydrogenation of alkynes.[31-34]

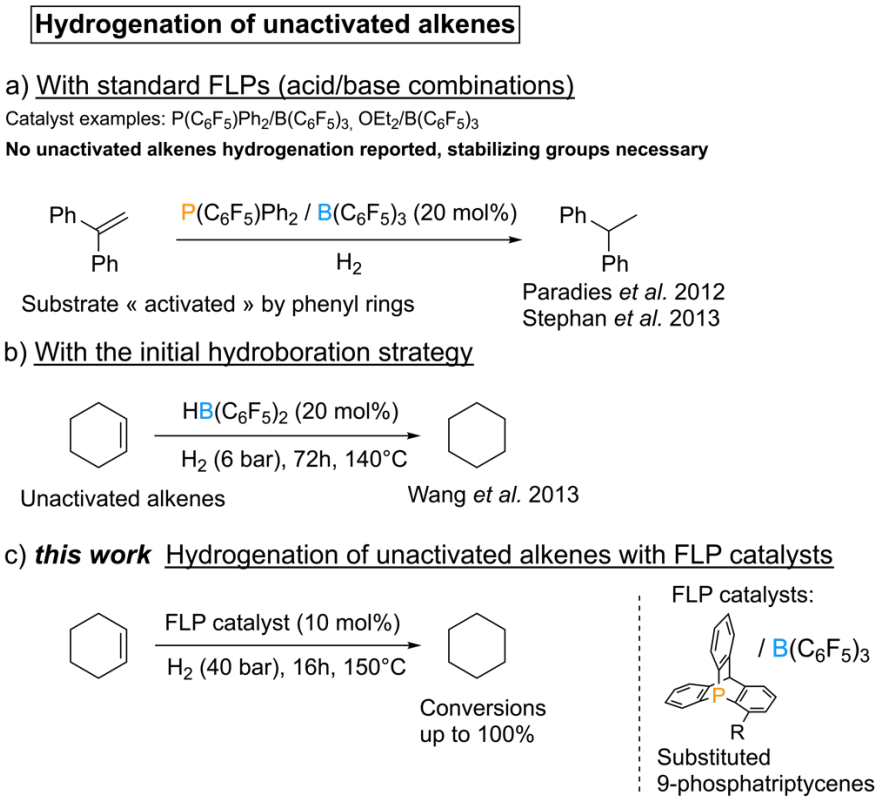

Scheme 31. Previous and current works on hydrogenation reactions of unactivated alkenes.

In contrast to the work of Wang, the hydrogenation of aliphatic olefins such as cyclohexene or other "unactivated" alkenes, a desirable transformation,[11] remains a current limitation and has not been so far performed by standard FLP systems due to the difficulty of protonating the double bond. The synthesis of new sterically hindered Lewis bases is crucial for the development of new types of FLP catalysts able to tackle this challenge. Our group has reported the synthesis of the 9-phosphatriptycene and *ortho*-substituted 9-phospha-triptycene derivatives.[35-36] These strained triarylphosphines display a carbon bridging atom between their three phenyl rings, resulting in more steric bulk and a reduced reactivity compared to triphenylphosphine analogues. The aqueous pK_a of the parent 9-phosphatriptycene was estimated at -1.5 pK_a unit, almost 5 units lower than triphenylphosphine (evaluated as the pK_a of the conjugate phosphonium). In addition, its Lewis basicity relative to benzhydrylium ions (determined according to the Mayr scale)[37] is also significantly impacted, with a LB value of 7.6 with respect to LB = 14.3 for triphenylphosphine. To the best of our knowledge, applications of 9-phosphatriptycene derivatives have so far been restricted to ligands in organometallic chemistry, either in homogeneous[38-39] and heterogeneous[40-41] catalysis or as rotor in palladium-centered molecular gears[42] but never as components of frustrated Lewis pairs. Their unique reactivity however, induced by the triptycene scaffold, makes them promising candidates in this field where the high steric hindrance brought by *ortho*-substituents is a crucial asset.

We now report the applications of FLP catalysts constituted of *ortho*-substituted 9-phosphatriptycenes in combination with tris(pentafluorophenyl)borane for the hydrogenation reaction of olefins, including unactivated aliphatic alkenes (Scheme 31c). Taking advantage of the weak basicity of 9-phosphatriptycenes, resulting in the generation of strongly acidic phosphonium cations after hydrogen activation, and the careful optimization of reaction conditions, the hydrogenation of challenging olefinic substrates that are not yet reported with other Lewis acid-base combinations was performed. In addition, the thermodynamics and kinetics of hydrogen activation and the hydrogenation reaction of cyclohexene are computed using density functional theory (DFT) and discussed.

3. Results and discussion

Our initial investigation for the hydrogenation of unactivated alkenes started with the design of a FLP catalyst. The parent 9-phosphatriptycene **III.1** is known to bind covalently with the commercially available Lewis acid tris(pentafluorophenyl)borane ($B(C_6F_5)_3$, BCF).[35] While Lewis adducts are still able to catalyze FLP-like hydrogenation reactions,[23-24, 28] the energy required to dissociate the adduct (allowing the free acid and base to act in a FLP-manner) impedes the global thermodynamics of the reaction and further heating is thus required. So, *ortho*-substituted 9-phosphatriptycenes **III.2**-**III.6** were considered instead since they are more sterically hindered than **III.1**. The adducts formation with BCF, computed at the M06-2X/6-311G(d) (IEFPCM, dichloromethane) level (Table 8), showed that **III.1** and **III.2** are predicted to spontaneously form a stable Lewis adduct, which is attributed to their lack of significant steric hindrance. The remaining Lewis base candidates **III.3**- **III.6** are suitable for FLP catalysis. **III.3** and **III.5** display slightly positive Gibbs free energy values close to 0 $kJ.mol^{-1}$ at 25°C indicating no generation of a stable Lewis adduct, its formation is in a dynamic equilibrium with a majority of free acid and base species present in solution, especially if heating is required. **III.4** and **III.6** on the other hand display highly endergonic values of ΔG^0_{adduct}, showing no adduct formation. Among these, 1-chloro-9-phosphatriptycene **III.3** was selected because it displays the highest yield of synthesis and the basicity of the phosphine is further reduced by the chlorine atom.[36] After hydrogen activation with BCF, the phosphonium cation generated will be more acidic than the unsubstituted 9-phosphatriptycene or derivatives bearing electron-donating groups, which will favor the protonation of the olefin in the next step of the catalytic cycle. The reaction conditions for the hydrogenation of unactivated alkenes were thus investigated with the FLP constituted of 3 and BCF. A simple ^1H, ^{31}P, ^{11}B, ^{19}F NMR experiment consisting of a 1:1 mixture of 3 and BCF in $CDCl_3$ showed no formation of Lewis adduct (see Annex I), confirming experimentally their FLP behavior. Cyclohexene was selected as model unactivated alkene since it is readily available and its hydrogenation into cyclohexane is easily followed by ^1H NMR spectroscopy, with a singlet at 1.43 ppm. The optimization is shown in Table 9.

*Table 8. IEFPCM(dichloromethane)/M06-2X/6-311G(d) Gibbs free energy of adduct formation between a series of 9-phosphatriptycene derivatives **III.1**- **III.6** and BCF at 25°C (298.15 K). ΔG_{adduct} values at 150°C (423.15 K) are shown in brackets.*

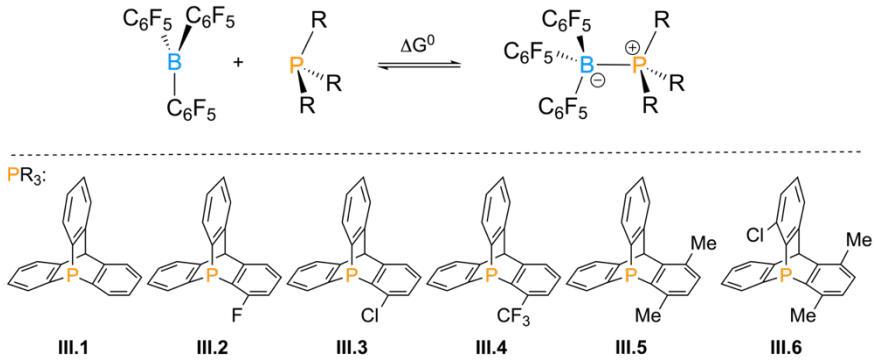

III.1 III.2 III.3 III.4 III.5 III.6

9-phosphatriptycene	*o*-substituent	ΔG^0_{adduct} (kJ.mol^{-1})
III.1	-H	-38 (-13)
III.2	-F	-23 (1.3)
III.3	-Cl	4 (30)
III.4	-CF_3	34 (62)
III.5	-Me	2 (28)
III.6	-Me, -Cl	46 (76)

Stephan *et al*. illustrated with the hydrogenation of arenes that high pressures of dihydrogen are required for the hydrogenation of substrates with low reactivity, even with deactivated phosphines.[43] Even so, no reaction is occurring at 40 bar of H_2 pressure at room temperature (entry 1, Table 9) overnight (16h). Heating is necessary to start the reaction, cyclohexene is first detected at 80°C (entry 2). To our delight, further heating up to 150°C (entry 3-5) allowed to increase conversion until a satisfactory value of 96%, confirming the potential of 9-phoshatriptycene derivatives in FLP chemistry. Full conversion can be reached by increasing the reaction time (entry 6). Reducing the reaction time to 4h (entry 7) or the pressure down to 20 bar (entry 8) results in a lowered conversion of 34% and 27% respectively. The conditions of 150°C, 16h and 40 bar of H_2 pressure (entry 5) were selected for the following investigations.

*Table 9. Optimization of the reaction conditions for the hydrogenation of cyclohexene with 1-chloro-9-phosphatriptycene **III.3** and BCF as catalyst. r.t.= room temperature. In bold are highlighted the selected optimized conditions.*

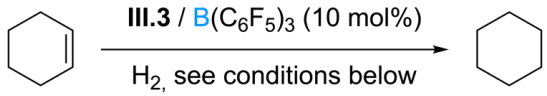

Entry	Conditions[a]			Results
	T (°C)	Time (h)	H_2 (bar)	Conversion[b] (%)
1	r.t.	16	40	0
2	80	16	40	0[c]
3	120	16	40	9
4	140	16	40	23
5	**150**	**16**	**40**	**96**
6	150	72	40	100
7	150	4	40	34
8	150	16	20	27

[a] 10 mol% catalyst, 1 mmol of cyclohexene, reactions performed in $CDCl_3$. [b] Conversions are evaluated without ^1H NMR internal standard as the ratio between the cyclohexane integration (normalized to 1 proton) and the sum of cyclohexane and cyclohexene (both normalized to 1 proton). [c] Traces of cyclohexane are detected.

The influence of the amount and nature of catalyst employed was next investigated to evaluate the effect of the substitution pattern of 9-phosphatriptycene or the use of other triarylphosphines on reactions yields (Table 10). Increasing the catalyst loading was not attempted since the conditions were optimized for 10 mol% of catalyst (entry 1). Reducing to 5 mol% results in a significantly lower yield of 13% (entry 2). A blank test showed the need for catalyst in this transformation since no cyclohexane was detected without one (entry 3). Using a Lewis adduct instead of an actual FLP impedes the reaction, in these conditions employing **III.1** as catalyst lead to almost no hydrogenation reaction (entry 4). Changing the 9-phosphatriptycene substituent with electron-donating methyl groups (entry 5) results in a lowering of the reaction yield down to 35%. This is attributed to the less acidic character of the conjugated phosphonium originating from **III.5** than from **III.3**, which is slowing

down the rate-limiting step of protonation of cyclohexene. Entry 5 shows that a 9-phosphatriptycene, even with electron-donating groups, is still a more potent catalyst for this reaction than triarylphosphines (with activating tolyl, mesityl or deactivating bromine and chlorine substituents, entries 6, 7, 8 and 9 respectively), demonstrating that there is indeed a deactivating effect on the phosphorus reactivity intrinsic to the triptycene scaffold, regardless of additional electronic and steric effects brought by substituents. In addition, the catalysts consisting of BCF and either **III.3** or **III.5** perform better than the deactivated phosphine $P(C_6F_5)Ph_2$ (entry 10) which is typically used for the hydrogenation of olefins or arenes.[26, 43]

Table 10. Influence of the catalyst for the hydrogenation of cyclohexene.

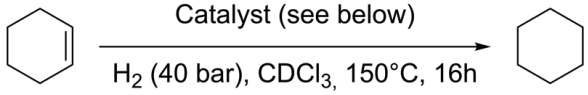

Entry	Catalyst			Results[a]	
	LB	LA	Catalyst loading (mol%)	Conversion (%)[b]	^{1}H NMR yield (%)[b]
1	**III.3**	BCF	10	94	88
2	**III.3**	BCF	5	19	13
3	-	-	-	0	0
4	**III.1**	BCF	10	5	1
5	**III.5**	BCF	10	43	35
6	$P(2\text{-tol})_3$	BCF	10	25	10
7	$PMes_3$	BCF	10	0	0
8	$P(2\text{-}BrC_6H_4)_3$	BCF	10	14	0
9	$P(4\text{-}ClC_6H_4)_3$	BCF	10	6	1
10	$P(C_6F_5)Ph_2$	BCF	10	14	8

[a] 1 mmol of cyclohexene, reactions performed in $CDCl_3$ at 150°C, 40 bar of H_2 and for 16h. [b] Triphenylmethane or 1,3,5-trimethoxybenzene used as ^{1}H internal standard for conversion and yield determination.

With these optimized conditions and the optimal catalyst in hand, the scope of unactivated alkene was investigated (Table 11). Full conversion of the starting material was observed with other cyclic olefins as cyclopentene and the deactivated olefin 3-bromocyclohex-1-ene, and the acyclic hex-1-ene (entry 1-3). These were reduced in moderate to good yields ranging from 60 to 72%. The hydrogenation of cyclohex-2-en-1-one to cyclohexanone with 76% (entry 4) shows complete selectivity towards to the C=C bond with no C=O bond hydrogenation, due to the presence of conjugation with the carbonyl group, its hydrogenation can proceed through an initial hydride transfer.[19] Increasing the

*Table 11. Substrate scope of hydrogenation with 1-chloro-9-phosphatriptycene **III.3** and BCF as catalyst.*

Entry	Substrate	Product	Conversion (%)[a]	^{1}H NMR yield (%)[a]
1			100	72
2	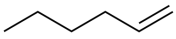		100	60
3			100	70
4			84	76
5			61[b]	57[b]
6	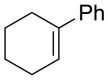	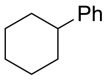	0	0
7	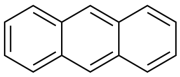	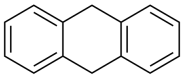	33	20
8			26	3

Conditions: 10 mol% catalyst, Solvent= $CDCl_3$, 150°C, 16h, 40 bar H_2. [a] Triphenylmethane or 1,3,5-trimethoxybenzene used as ^{1}H internal standard for yield determination. [b] Reaction time increased to 72h.

steric hindrance of the olefin with the trisubstituted 1-methyl-1-cyclohexene results in a slower reaction (72h) to 61% of conversion and a yield of 57% (entry 5). Further increasing the steric hindrance with the trisubstituted alkenes (1-phenylcyclohexene) prevents completely the hydrogenation (entry 6). With these conditions, the hydrogenation of anthracene was attempted as well, resulting in a low yield of 20%. Considering previous results by Stephan *et al.*, a significantly higher pressure of H_2 is necessary to reach full conversion of this substrate and other arenes (up to 102 atm H_2).[43] Eventually, the tetrasubstituted 2,3-dimethylbut-2-ene, a substrate challenging even for transition metal catalysts,[44] was tested but only traces of the hydrogenated product were detected and mainly side-products were observed (entry 8). The scope of this method is thus limited to di- and tri-substituted alkenes displaying moderate steric hindrance.

Since 9-phosphatriptycene derivatives are stable to air, moisture and high temperatures, they are recovered intact at the end of the reaction and recycled (see SI), even after long reaction times at 150°C or higher temperatures. Typical ^{1}H, ^{31}P, ^{11}B and ^{19}F NMR spectra after the reaction (exemplified with entry 1 of Table 10 show the presence of several peaks of degradation in ^{11}B and ^{19}F relative to the starting tris(pentafluorophenyl)borane (corresponding to derivatives of the borinic and boronic acids)[45] while the ^{31}P spectrum remains unchanged with a singlet at -72 ppm and a new minor impurity at 11 ppm. Integration in ^{1}H spectrum shows that 0.08 equivalents of 1-chloro-9-phosphatriptycene are remaining in the spectrum over the 0.10 equivalent loaded at the beginning of the reaction. This is consistent with a quantitative recovery experiment performed over the course of several hydrogenation reactions: from a total of 232mg of 1-chloro-9-phosphatriptycene **III.3** loaded, 187mg (81%) were recovered after silica gel column chromatography over the collected crude reaction mixtures.

The computation of the hydrogenation reaction profile of cyclohexene catalyzed by **III.3**/BCF at the DFT [IEFPCM (dichloromethane)/M06-2X/6-311G(d)] level of theory allowed to investigate its mechanism. The most straightforward process is stepwise. It involves the heterolytic splitting of H_2, generating of the phosphonium borohydride ion pair, followed by protonation of the cyclohexene by the phosphonium Brønsted acid (Figure 19). The resulting unstable carbenium ion immediately reacts with the borohydride in a seemingly barrier-less process to form cyclohexane. Indeed, no stationary point corresponding to

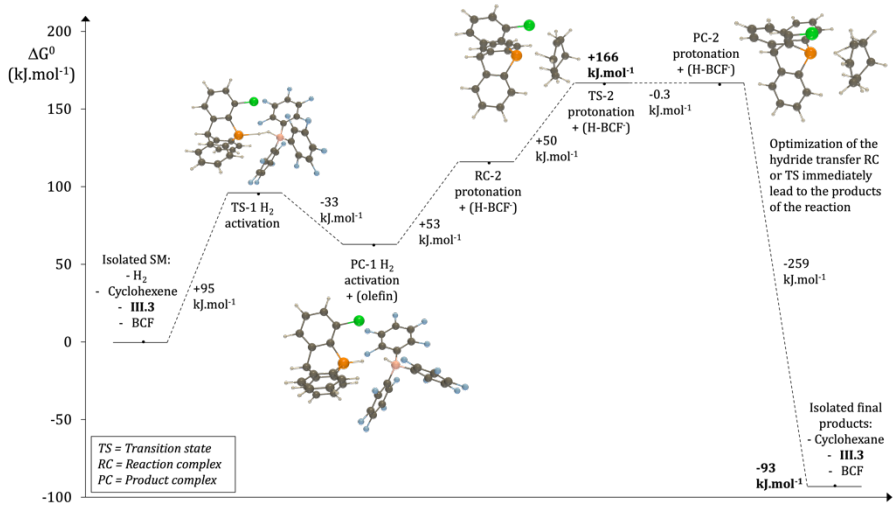

*Figure 19. Gibbs free energy profile of the hydrogenation of cyclohexene by the **III.3**/BCF FLP catalyst at 25°C according to the mechanism involving the direct hydride transfer after the protonation step.*

either the product complex nor the transition state of hydride transfer could be isolated, all attempts at optimization eventually led to the products of the reaction. After the protonation step, an alternative mechanism is also possible, it differs from the first in that the phosphine and the carbenium ion generated after proton transfer immediately react to form the product of hydrophosphination (Figure 20).[46-47] This transient product formation is highly spontaneous and could be further driven by the close proximity of the two reagents after the previous step. The weakly basic character of **3** and its high steric hindrance destabilizes this intermediate sufficiently for the reaction to continue to the most stable product, cyclohexane. The high-energy position of the following hydride transfer transition state is then explained by the three-molecule character of the reaction and the associated large entropic penalty. Both mechanisms lead to the same final product, and change only after the protonation step. In both situations, the rate-limiting step is the protonation of the olefin by the conjugate phosphonium of **III.3** (the value of ΔG^0=+166 kJ.mol^{-1} should be considered as an upper limit of the reaction barrier since the counter anion is not considered in the reaction system, see Annex I for details), which was expected given the challenging character of the substrate and the need for weak bases as catalysts. In consequence, it is possible that the reaction proceeds simultaneously *via* the two mechanisms. The hydride transfer step to form the alkane is the driving

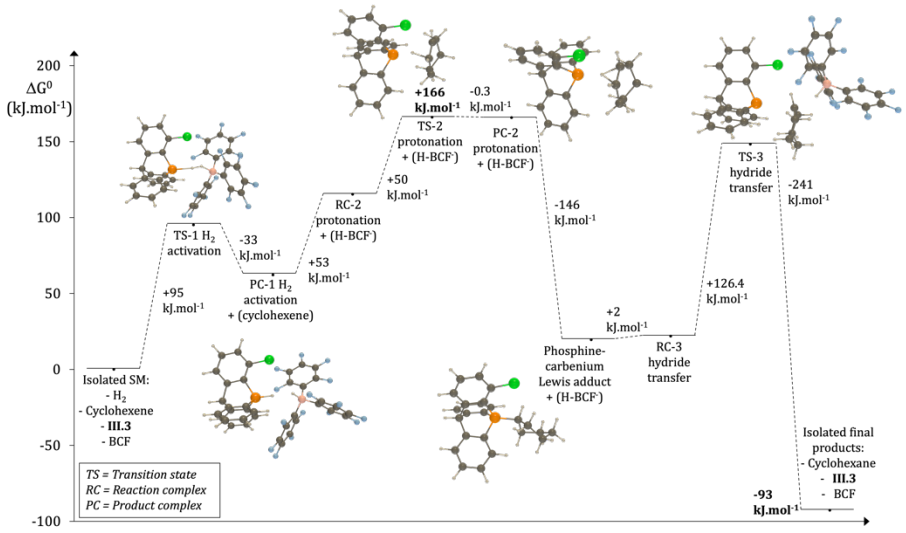

*Figure 20. Gibbs free energy profile of the hydrogenation of cyclohexene by the **III.3**/BCF FLP catalyst at 25°C according to the mechanism involving the formation of a cyclohexyl phosphonium cation after reaction between **III.3** and the carbenium intermediate.*

force of the reaction (ΔG^0=-71 kJ.mol^{-1} from the cyclohexyl-phosphonium intermediate). The overall reaction ΔG^0 amounts to -93 kJ.mol^{-1}. Changing the base affects its proton-transfer ability (the Brønsted acidity of its conjugate acid), the transition state of the rate-limiting step is thus changed as well and stands higher in energy for less acidic phosphoniums, rationalizing the slower character of the reaction (or potentially the absence of reaction) when stronger bases such as **III.5** or other phosphines are used (Table 10). Using Lewis adducts (**III.1**/BCF) instead of FLP combinations implies that the starting energy of the reaction profile is no longer defined by the sum of the energies of the isolated reactants but is lowered by the stabilization energy of the adduct formation. The position of the highest TS is *de facto* increased by the same amount, hence a significantly slower reaction. The endergonic initial H_2 activation explains the need for high dihydrogen pressures, needed to increase its concentration in solution and to drive the disfavorable equilibrium toward the formation of the ion pair and subsequent steps.

4. Conclusions and outlooks

In conclusion, the hydrogenation of unactivated alkenes, a current limitation in frustrated Lewis pair catalysis, was performed for the first time by FLPs consisting of *ortho*-substituted 9-phosphatriptycene derivatives and tris(pentafluorophenyl)borane $B(C_6F_5)_3$. The weak Lewis basicity of this family of cage-shaped triarylphosphines induced by the triptycene scaffold and the steric hindrance associated with the *ortho*-substituents make them ideal candidates for FLP-catalyzed hydrogenation reactions. The subsequent optimization of reaction conditions allowed to perform the hydrogenation of cyclohexene and a series of unactivated olefins at medium pressures of H_2 (up to 40 bar) and 150°C. The substrate scope found limitations in sterically hindered trisubstituted and tetrasubstituted olefins. 1-chloro-9-phosphatriptycene **III.3** was found to be the best-performing catalyst, with the *ortho*-chlorine atom further deactivating the phosphorus while maintaining enough steric hindrance to prevent the Lewis adduct formation with $B(C_6F_5)_3$. The computation at the DFT level [M06-2X/6-311G(d)] of the reaction profile showed that the protonation of the olefin by the phosphonium of the 9-phosphatriptycene catalyst is the rate-limiting step of the reaction and in consequence the rate of the reaction is dictated by the acidity of the conjugate phosphonium. This work demonstrates that 9-phosphatriptycene derivatives have a good potential in FLP chemistry or organocatalysis as weak and bulky Lewis bases. In addition, their steric and electronic properties can be tuned by the choice of their substituents. Further investigations are ongoing into the reactivity of 9-phosphatriptycenes and to expand the reach of applications of this unique family of triarylphosphines.

5. References

[1] G. C. Welch, R. R. San Juan, J. D. Masuda, D. W. Stephan, "Reversible, metal-free hydrogen activation", *Science* **2006**, *314*, 1124-1126.

[2] P. A. Chase, G. C. Welch, T. Jurca, D. W. Stephan, "Metal-free catalytic hydrogenation", *Angew. Chem. Int. Ed.* **2007**, *46*, 8050-8053.

[3] G. C. Welch, D. W. Stephan, "Facile heterolytic cleavage of dihydrogen by phosphines and boranes", *J. Am. Chem. Soc.* **2007**, *129*, 1880-1881.

[4] P. A. Chase, D. W. Stephan, "Hydrogen and amine activation by a frustrated Lewis pair of a bulky N-heterocyclic carbene and $B(C_6F_5)_3$", *Angew. Chem. Int. Ed.* **2008**, *47*, 7433-7437.

[5] D. W. Stephan, ""frustrated Lewis pairs": A concept for new reactivity and catalysis", *Org. Biomol. Chem.* **2008**, *6*, 1535-1539.

[6] D. W. Stephan, G. Erker, "Frustrated Lewis pair chemistry of carbon, nitrogen and sulfur oxides", *Chem. Sci.* **2014**, *5*, 2625-2641.

[7] C. M. Mömming, E. Otten, G. Kehr, R. Fröhlich, S. Grimme, D. W. Stephan, G. Erker, "Reversible metal-free carbon dioxide binding by frustrated Lewis pairs", *Angew. Chem. Int. Ed.* **2009**, *48*, 6643-6646.

[8] M. Sajid, A. Klose, B. Birkmann, L. Liang, B. Schirmer, T. Wiegand, H. Eckert, A. J. Lough, R. Fröhlich, C. G. Daniliuc, S. Grimme, D. W. Stephan, G. Kehr, G. Erker, "Reactions of phosphorus/boron frustrated Lewis pairs with SO_2", *Chem. Sci.* **2013**, *4*, 213-219.

[9] E. Otten, R. C. Neu, D. W. Stephan, "Complexation of nitrous oxide by frustrated Lewis pairs", *J. Am. Chem. Soc.* **2009**, *131*, 9918-9919.

[10] A. J. P. Cardenas, B. J. Culotta, T. H. Warren, S. Grimme, A. Stute, R. Fröhlich, G. Kehr, G. Erker, "Capture of NO by a frustrated Lewis pair: a new type of persistent N-oxyl radical", *Angew. Chem. Int. Ed.* **2011**, *50*, 7567-7571.

[11] J. G. de Vries, C. J. Elsevier (Ed.), *The handbook of homogeneous hydrogenation*, Wiley-VCH, Weinheim, **2006**.

[12] J. F. Young, J. A. Osborn, F. H. Jardine, G. Wilkinson, "Hydride intermediates in homogeneous hydrogenation reactions of olefins and acetylenes using rhodium catalysts", *Chem. Commun.* **1965**.

[13] W. S. Knowles, M. J. Sabacky, "Catalytic asymmetric hydrogenation employing a soluble, optically active, rhodium complex", *Chem. Commun.* **1968**.

[14] R. R. Schrock, J. A. Osborn, "Catalytic hydrogenation using cationic rhodium complexes. II. The selective hydrogenation of alkynes to *cis* olefins", *J. Am. Chem. Soc.* **1976**, *98*, 2143-2147.

[15] R. H. Crabtree, H. Felkin, G. E. Morris, "Cationic iridium diolefin complexes as alkene hydrogenation catalysts and the isolation of some related hydrido complexes", *J. Organomet. Chem.* **1977**, *141*, 205-215.

[16] D. W. Stephan, ""Frustrated Lewis pair" hydrogenations", *Org. Biomol. Chem.* **2012**, *10*, 5740-5746.

[17] D. W. Stephan, "Frustrated Lewis pairs: from concept to catalysis", *Acc. Chem. Res.* **2015**, *48*, 306-316.

[18] D. W. Stephan, "The broadening reach of frustrated Lewis pair chemistry", *Science* **2016**, *354*, 1248-1256.

[19] G. Erős, H. Mehdi, I. Pápai, T. A. Rokob, P. Király, G. Tárkányi, T. Soós, "Expanding the scope of metal-free catalytic hydrogenation through frustrated Lewis pair design", *Angew. Chem. Int. Ed.* **2010**, *122*, 6709-6713.

[20] J. A. Nicasio, S. Steinberg, B. Ines, M. Alcarazo, "Tuning the Lewis acidity of boranes in frustrated Lewis pair chemistry: implications for the hydrogenation of electron-poor alkenes", *Chem. Eur. J.* **2013**, *19*, 11016-11020.

[21] L. Greb, C. G. Daniliuc, K. Bergander, J. Paradies, "Functional-group tolerance in frustrated Lewis pairs: hydrogenation of nitroolefins and acrylates", *Angew. Chem. Int. Ed.* **2013**, *52*, 5876-5879.

[22] É. Dorkó, M. Szabó, B. Kótai, I. Pápai, A. Domján, T. Soós, "Expanding the boundaries of water-tolerant frustrated Lewis pair hydrogenation: Enhanced back strain in the Lewis acid enables the reductive amination of carbonyls", *Angew. Chem. Int. Ed.* **2017**, *56*, 9512-9516.

[23] D. J. Scott, M. J. Fuchter, A. E. Ashley, "Non-metal catalyzed hydrogenation of carbonyl compounds", *J. Am. Chem. Soc.* **2014**, *136*, 15813-15816.

[24] T. Mahdi, D. W. Stephan, "Enabling catalytic ketone hydrogenation by frustrated Lewis pairs", *J. Am. Chem. Soc.* **2014**, *136*, 15809-15812.

[25] Á. Gyömöre, M. Bakos, T. Földes, I. Pápai, A. Domján, T. Soós, "Moisture-tolerant frustrated Lewis pair catalyst for hydrogenation of aldehydes and ketones", *ACS Catal.* **2015**, *5*, 5366-5372.

[26] L. Greb, P. Oña-Burgos, B. Schirmer, S. Grimme, D. W. Stephan, J. Paradies, "Metal-free catalytic olefin hydrogenation: Low-temperature H_2 activation by frustrated Lewis pairs", *Angew. Chem. Int. Ed.* **2012**, *51*, 10164-10168.

[27] L. Greb, S. Tussing, B. Schirmer, P. Oña-Burgos, K. Kaupmees, M. Lõkov, I. Leito, S. Grimme, J. Paradies, "Electronic effects of triarylphosphines in metal-free hydrogen activation: a kinetic and computational study", *Chem. Sci.* **2013**, *4*, 2788.

[28] L. J. Hounjet, C. Bannwarth, C. N. Garon, C. B. Caputo, S. Grimme, D. W. Stephan, "Combinations of ethers and $B(C_6F_5)_3$ function as hydrogenation catalysts", *Angew. Chem. Int. Ed.* **2013**, *52*, 7492-7495.

[29] E. A. Patrick, W. E. Piers, "Twenty-five years of bis-pentafluorophenyl borane: a versatile reagent for catalyst and materials synthesis", *Chem. Commun.* **2020**, *56*, 841-853.

[30] Y. Wang, W. Chen, Z. Lu, Z. H. Li, H. Wang, "Metal-free $HB(C_6F_5)_2$-catalyzed hydrogenation of unfunctionalized olefins and mechanism study of borane-mediated σ-bond metathesis", *Angew. Chem. Int. Ed.* **2013**, *52*, 7496-7499.

[31] V. Sumerin, F. Schulz, M. Atsumi, C. Wang, M. Nieger, M. Leskela, T. Repo, P. Pyykko, B. Rieger, "Molecular tweezers for hydrogen: synthesis, characterization, and reactivity", *J. Am. Chem. Soc.* **2008**, *130*, 14117-14119.

[32] K. Chernichenko, A. Madarasz, I. Papai, M. Nieger, M. Leskela, T. Repo, "A frustrated-Lewis-pair approach to catalytic reduction of alkynes to *cis*-alkenes", *Nat. Chem.* **2013**, *5*, 718-723.

[33] U. Gellrich, "Reversible Hydrogen Activation by a Pyridonate Borane Complex: Combining Frustrated Lewis Pair Reactivity with Boron-Ligand Cooperation", *Angew. Chem. Int. Ed.* **2018**, *57*, 4779-4782.

[34] M. Hasenbeck, U. Gellrich, "Boron-Ligand Cooperation: The Concept and Applications", *Chem. Eur. J.* **2021**, *27*, 5615-5626.

[35] L. Hu, D. Mahaut, N. Tumanov, J. Wouters, R. Robiette, G. Berionni, "Complementary synthetic approaches toward 9-phosphatriptycene and structure–reactivity investigations of its association with sterically hindered Lewis acids", *J. Org. Chem.* **2019**, *84*, 11268-11274.

[36] L. Hu, D. Mahaut, N. Tumanov, J. Wouters, L. Collard, R. Robiette, G. Berionni, "Sterically hindered *ortho*-substituted phosphatriptycenes as configurationally stable P-chirogenic triarylphosphines", *Dalton Trans.* **2021**, *50*, 4772-4777.

[37] H. Mayr, J. Ammer, M. Baidya, B. Maji, T. A. Nigst, A. R. Ofial, T. Singer, "Scales of Lewis basicities toward C-centered Lewis acids (Carbocations)", *J. Am. Chem. Soc.* **2015**, *137*, 2580-2599.

[38] T. Agou, J. Kobayashi, T. Kawashima, "Evaluation of σ-donating ability of a 9-phosphatriptycene and its application to catalytic reactions", *Chem. Lett.* **2004**, *33*, 1028-1029.

[39] S. Konishi, T. Iwai, M. Sawamura, "Synthesis, properties, and catalytic application of a triptycene-type borate-phosphine ligand", *Organometallics* **2018**, *37*, 1876-1883.

[40] T. Iwai, S. Konishi, T. Miyazaki, S. Kawamorita, N. Yokokawa, H. Ohmiya, M. Sawamura, "Silica-supported triptycene-type phosphine. Synthesis, characterization, and application to Pd-catalyzed suzuki–miyaura cross-coupling of chloroarenes", *ACS Catal.* **2015**, *5*, 7254-7264.

[41] S. Kawamorita, T. Miyazaki, H. Ohmiya, T. Iwai, M. Sawamura, "Rh-catalyzed *ortho*-selective C–H borylation of N-functionalized arenes with silica-supported bridgehead monophosphine ligands", *J. Am. Chem. Soc.* **2011**, *133*, 19310-19313.

[42] H. Ube, Y. Yasuda, H. Sato, M. Shionoya, "Metal-centred azaphosphatriptycene gear with a photo- and thermally driven mechanical switching function based on coordination isomerism", *Nature Communications* **2017**, *8*, 14296-14301.

[43] Y. Segawa, D. W. Stephan, "Metal-free hydrogenation catalysis of polycyclic aromatic hydrocarbons", *Chem. Commun.* **2012**, *48*, 11963-11965.

[44] R. P. Yu, J. M. Darmon, J. M. Hoyt, G. W. Margulieux, Z. R. Turner, P. J. Chirik, "High-Activity Iron Catalysts for the Hydrogenation of Hindered, Unfunctionalized Alkenes", *ACS Catal.* **2012**, *2*, 1760-1764.

[45] C. Bergquist, B. M. Bridgewater, C. J. Harlan, J. R. Norton, R. A. Friesner, G. Parkin, "Aqua, Alcohol, and Acetonitrile Adducts of Tris(perfluorophenyl)borane: Evaluation of Brønsted Acidity and Ligand Lability with Experimental and Computational Methods", *J. Am. Chem. Soc.* **2000**, *122*, 10581-10590.

[46] O. Delacroix, A. Gaumont, "Hydrophosphination of Unactivated Alkenes, Dienes and Alkynes: A Versatile and Valuable Approach for the Synthesis of Phosphines", *Curr. Org. Chem.* **2005**, *9*, 1851-1882.

[47] V. Koshti, S. Gaikwad, S. H. Chikkali, "Contemporary avenues in catalytic PH bond addition reaction: A case study of hydrophosphination", *Coord. Chem. Rev.* **2014**, *265*, 52-73.

Chapter IV
Synthesis and reactivity of difluorophosphoranes and fluorophosphonium cations derived from 9-phosphatriptycene

---

This preliminary investigation describes the synthesis and the geometry of difluorophosphoranes and fluorophosphonium cations based on the 9-phosphatriptycene, the application of the latter as Lewis acids or potential electrophilic fluorinating agents is discussed.

1. Introduction

The triptycene scaffold has a significant impact on the reactivity of heteroatoms embedded in it. The previous chapters highlighted how the increased pyramidalization brought by the strain generated by the scaffold leads to a weakening of the basicity of the phosphorus compared to other aryl phosphines. This aspect of main group chemistry is little explored since the general strategy is to tune the reactivity by successive additions of electron-withdrawing or -donating groups. Here, the conjugate phosphonium of 9-phosphatriptycene is a strong acid, without needing to add numerous electron-withdrawing substituents.

Regardless of the electronic effect on the bridgehead heteroatom, another aspect of the reactivity inherent to the triptycene scaffold that could be exploited is the cage shape itself. The backbone and the bridgehead carbon atom should prevent any "backside" attack on the phosphorus (*i.e.* on the inner side of the triptycene cage). In the last decade, Stephan reported the use of fluorophosphonium cations as Lewis acids (see below). A notable feature of this reactivity is that the Lewis acidic site of these compounds lies at the opposite side of the P-F bond (*i.e.* the P-F σ* orbital). Consequently, Lewis bases bind to the phosphorus on the side opposite to the P-F bond. This binding scheme should be prevented in the case of fluorophosphonium cations derived from 9-phosphatriptycene, potentially resulting in another unique reactivity of these compounds. This hypothesis prompted us to explore the chemistry of 9-phosphatriptycene-derived fluorophosphonium cations.

Stephan recently reviewed the reactivity of phosphorus Lewis acids.[1] As detailed in previous sections, phosphorus derivatives are typically used as Lewis bases because of their lone pair of electrons in neutral P(III) compounds. Phosphenium cations (of the form R_2P^+) are rare examples of P(III) compounds capable of displaying a Lewis acid reactivity, despite possessing a lone pair of electrons.[2] In this family, Nieger developed N-heterocyclic phosphenium (NHP) cations (Figure 21a), that are analogues of N-heterocyclic carbenes, but with more electron-accepting ability than donating ability.[3-4] Interestingly, an intramolecular FLP featuring a NHP as Lewis acid was reported by Ragogna *et al.* (Figure 21b).[5] Phosphorus (V) compounds can also exhibit Lewis acidic properties. Among those, reagents of the form $R_3P{=}CHR'$, popularized by Wittig, were shown to be electrophilic at the phosphonium and allow alkene formation

from ketones or aldehydes.[6] Pentacoordinate phosphorus (V), typically PF_5 and PCl_5, are also known Lewis acids and were shown to form Lewis adducts with numerous bases including phosphines, pyridines, ammonia and other amines (Figure 21c).[7]

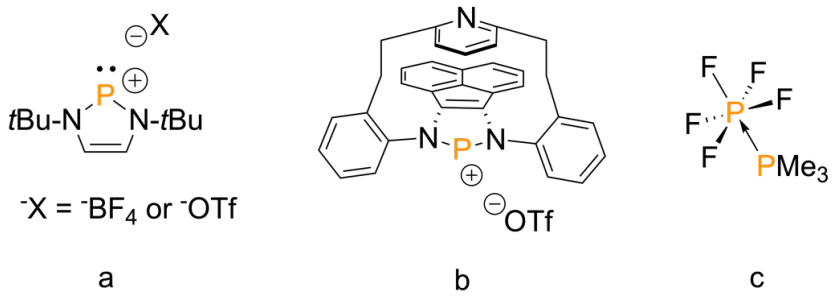

Figure 21. Example of a) a N-heterocyclic phosphenium (NHP) cation; b) intramolecular FLP featuring a phosphenium Lewis acid, and c) adduct between the PF_5 Lewis acid and PMe_3, example of a P(III)-P(V) bond.

More recently, phosphonium cations (R_4P^+) have attracted more attention in the field of main group chemistry, especially in organocatalysis, as reviewed by Werner and Guo.[8-9] Their Lewis acidity arises from the low-lying σ* orbital located opposite to the bond between the phosphorus and its most electron-withdrawing group (Scheme 32).[10]

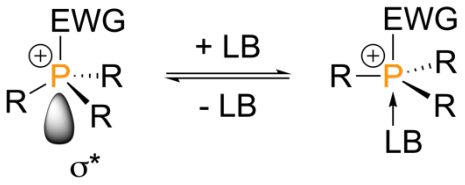

Scheme 32. σ orbital from which arises the Lewis acidity of phosphonium cations and bonding with a Lewis base. Scheme adapted from ref. 10. Upon bonding, the geometry around the phosphorus switches from a tetrahedral one to a trigonal bipyramid, the latter displaying in apical positions the electron-withdrawing group (EWG) and the bonded Lewis base, while the three R groups are now in a planar alignment.*

Notably, the group of Stephan popularized this category of phosphorus Lewis acids with the synthesis of electrophilic phosphonium cations (EPCs), easily accessible Lewis acids generated from phosphines, and their use as catalysts for the hydrodefluorination of fluoroalkanes.[11-12] Typically, a triarylphosphine (*e.g.* PPh_3) is first oxidized by XeF_2, yielding a P(V) difluorophosphorane (Ph_3PF_2), followed by fluoride abstraction by $B(C_6F_5)_3$ or by a silylium cation to generate the fluorophosphonium salt (Scheme 33).[13]

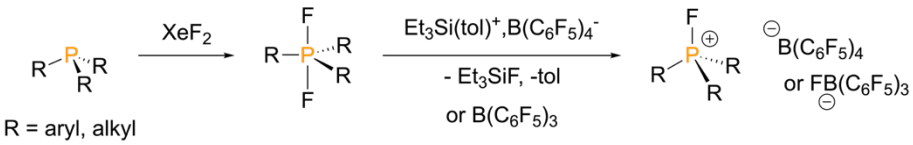

Scheme 33. Synthesis of difluorophosphoranes (R_3PF_2) and fluorophosphonium salts reported by Stephan. tol = toluene molecule. Note that the difluorophosphorane displays its two fluorine atoms at the apical positions (top and down) of the trigonal bipyramid, with the three R group in a plane.

These compounds were subsequently used as Lewis acid catalysts for numerous reactions, mainly on olefins: from their isomerization, hydrosilylation,[14] hydroarylation and hydrothiolation [15] to their FLP-catalyzed hydrogenations.[16] The hydrosilylation was later expanded to its application to ketones imines and nitriles.[17] Very recently, a new strategy for the mono-fluorination of sulfoxides and phosphines with the salt [F-Xe$^+$,$^-$OTf], generated *in situ* as reactive species, was published by Panossian *et al.*[18-19]

Given the ease of application of the method reported by Stephan and its straightforward character, we decided to apply it to the 9-phosphatriptycene (**IV.1**). The shape of the molecule should prevent any reactivity on the inner side of the triptycene core, therefore one could wonder a) whether the difluorophosphorane and fluorophosphonium derivatives of 9-phospha-triptycene can even be formed, b) or whether this would result in a lack of Lewis acidic character in the fluorophosphonium and c) if so, whether the fluorophosphonium then behaves as an group 5-based electrophilic fluorinating agent, a reactivity currently limited to nitrogen derivatives (N-F fluorinating agents[20]) (Scheme 34). These points are discussed below.

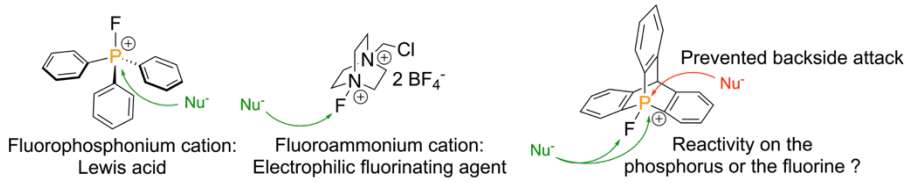

Scheme 34. Behavior in the presence of an electron-rich species of classical fluorophosphonium cations, fluoroammonium cations (example of the Selectfluor[21]), and hypothesized reactivity of the fluorophosphonium cation derived from 9-phosphatriptycene.

2. Results and discussion

The oxidation of the 9-phosphatriptycene (**IV.1**) to its difluorophosphorane derivative was achieved with 1 equivalent of xenon difluoride under inert atmosphere (glovebox) (Scheme 35). The ^{31}P NMR shows full conversion of the starting material and the isolated yield is 95%.

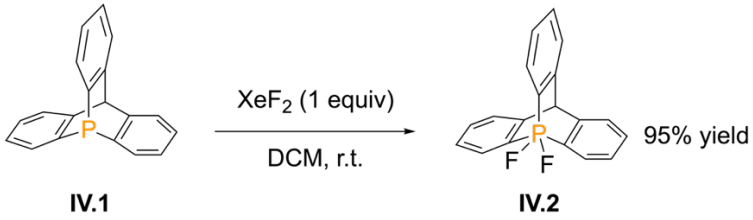

*Scheme 35. Synthesis of difluoro-9-phosphoranetriptycene **IV.2**.*

The reaction is instantaneous, with an effervescence in solution upon addition of XeF_2 due to the release of Xe gas. Similar to reported ^{31}P and ^{19}F NMR values for difluorophosphoranes,[13] the "difluoro-9-phosphoranetriptycene" (**IV.2**) displays a triplet with a large coupling constant of 865 Hz at -44.4 ppm, coupled with a ^{19}F doublet at -57.3 ppm (*d*, J = 865 Hz), typical of a P-F_2 bonding, while ^{1}H NMR displays a classical triptycene pattern, with a characteristic benzylic proton on the carbon bridgehead position at 5.25 ppm (although shielded compared to the 5.60 ppm of the parent compound **IV.1**) and three aromatic multiplets centered at 7.18, 7.43 and 7.90 ppm and accounting respectively for 6, 3 and 3 protons.

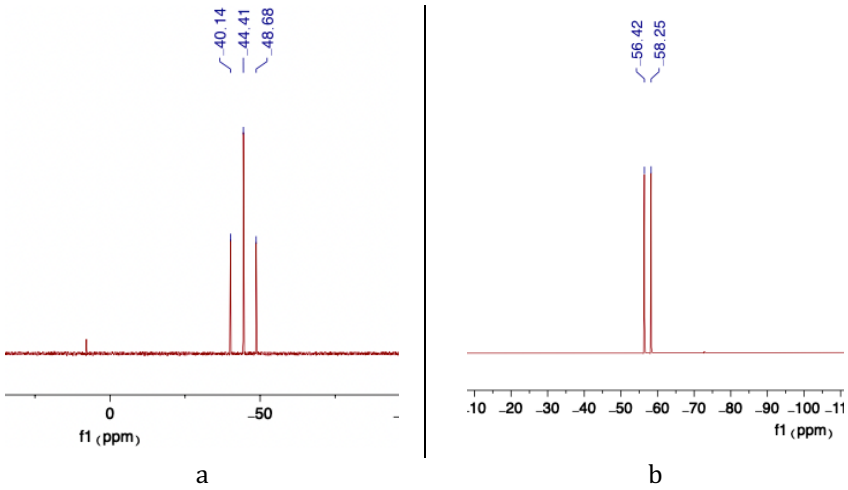

*Figure 22. ^{31}P (a) and ^{19}F (b) spectra of **IV.2** in $CDCl_3$.*

Single crystals of the difluoro-9-phosphoranetriptycene (**IV.2**) were obtained and single-crystal X-ray diffraction data were collected. The compound crystallizes as a 3+1D incommensurately modulated crystal with one modulation vector (0.373, 0, 0.445). The proper refinement is not finished, but the structure was preliminary refined in 3D approximation. Unfortunately, the quality of preliminary refinement is not sufficient to discuss its solid-state geometry with accuracy. Therefore, the M06-2X/6-311G(d)//IEFPCM(CH_2Cl_2) optimized structure is used for discussions instead (Figure 23).

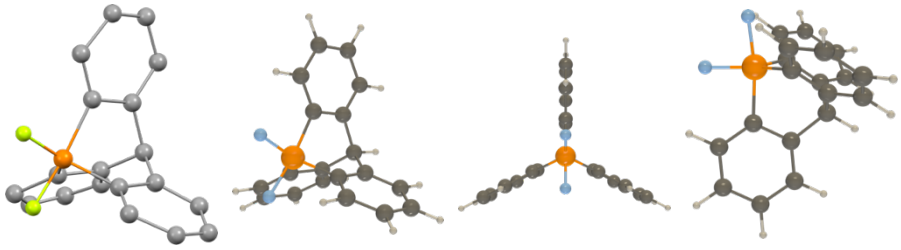

a b c d

*Figure 23. a) Preliminary solid-state structure of **IV.2** (hydrogen atoms ignored) and b-d) three viewpoints of its M06-2X/6-311G(d)//IEFPCM(DCM) optimized geometry (see Annex I for details on the quantum chemical methods).*

The preliminary solid-state structure (Figure 23a) still attests for the right identification of the compound, as well as its main features, which is the position of the fluorine atoms relative to the phosphorus and the P-F bonds of different lengths. Interestingly, the two fluorine atoms are found on the same face of the phosphorus and not, as is usually the case in difluorophosphoranes, on both sides of a new PCCC plane. Classical triarylphosphines undergo a geometry change when oxidized to the difluorophosphorane, the three aryl groups form a plane with the phosphorus while the two fluorine atoms are found in the two apical positions of the new trigonal bipyramid. The triptycene scaffold prevents this reorganization, the energy cost of moving the three neighboring carbons in a plane with the phosphorus as well as bringing a fluorine atom inside the cage would be far too high (Scheme 36). Instead, another trigonal bipyramid is formed, displaying a fluorine in equatorial position and one apical aryl ring, as shown in Figure 23d and drawn in Scheme 36. The latter P-C bond is significantly elongated compared to the two others (1.884 *vs* 1.816 Å). The apical P-F bond is also longer than the equatorial one (P-F_{ap} = 1.687 Å, P-F_{eq} = 1.624 Å).

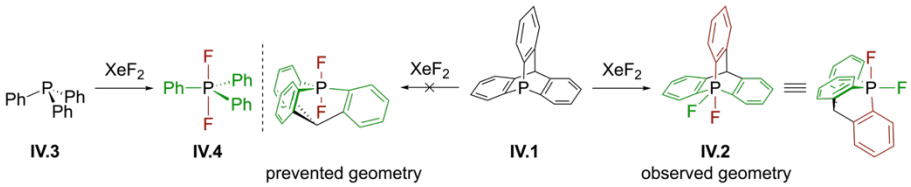

Scheme 36. Geometry of the difluorophosphorane bipyramids for triphenylphosphine and the 9-phosphatriptycene. Apical and equatorial groups are shown in red and green respectively.

The most stable conformer of hypervalent phosphorus compounds such as **IV.4** is typically displaying their most electron-withdrawing groups (*e.g.* fluorine atoms) in apical position because of the highly ionic bond character with these groups, which allows a stabilization by conjugation in the three-center-four-electron (*3c4e*$^-$) between the phosphorus and the two apical groups.[22] For this reason, forcing an aryl group in apical position instead of the fluorine probably destabilizes compound **IV.2** which is why a fast degradation is observed outside of the glovebox. Even inside a closed NMR tube, a sample of **IV.2** showed an almost complete disappearance of its characteristic ^{31}P and ^{19}F peaks of the PF_2 moiety after 3h, resulting in the formation of a phosphine oxide (probably with ambient air and moisture) and the appearance of a new triplet in ^{19}F NMR at -172.67 ppm (Figure 24).

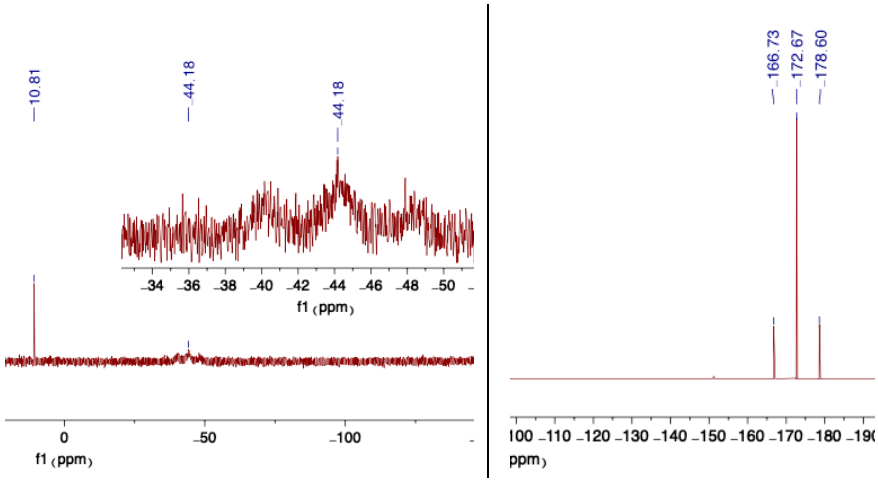

a b

*Figure 24. ^{31}P (a) and ^{19}F (b) spectra of **IV.2** in $CDCl_3$ after 3h in an NMR tube.*

A computation of the relative Gibbs free energies of two isomers of **IV.4**, one displaying two apical fluorine atoms (isomer I) and one displaying one apical phenyl group (isomer II) was undertaken and further supports this hypothesis.

The isomer with two apical F atoms was significantly more stable than the other (Figure 25).

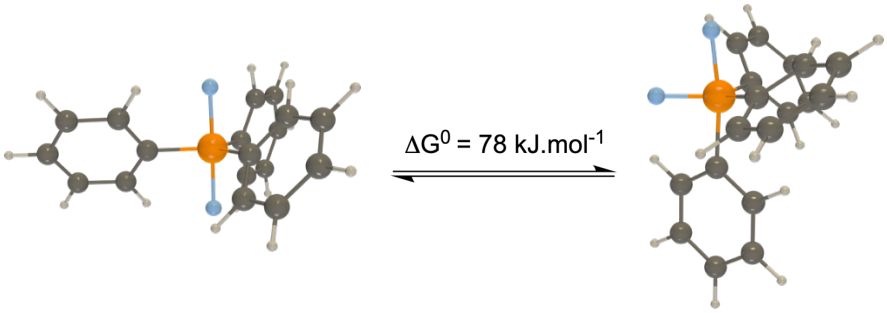

Figure 25. Relative M06-2X/6-311G(d) (IEFPCM scheme for CH_2Cl_2) Gibbs free energies between two isomers (I and II) of difluorotriphenylphosphorane at 25°C.

Next, the abstraction of the fluoride was attempted to generate the fluorophosphonium derivative **IV.5**. Given the unstable character of **IV.2**, a weaker and more convenient Lewis acid than a silylium cation was considered, the sodium tetrakis[3,5-bis(trifluoromethyl)phenyl]borate (Na^+,BAr_F^-). For the same reason and since the formation of **IV.2** from XeF_2 is instantaneous, the reaction was attempted in one-pot from the **IV.1**. Fortunately, the reaction ran smoothly and the "9-fluorophosphoniumtriptycene tetrakis(2,3-bis(trifluoromethyl)phenyl)borate" **IV.5** was obtained in 92% yield (Scheme 37) with full conversion of the starting material.

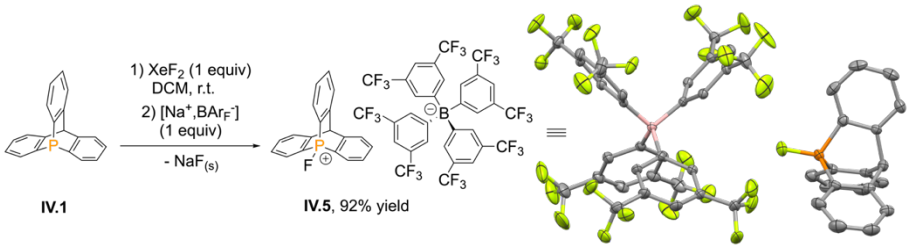

*Scheme 37. Synthesis of the fluorophosphonium salt **IV.5** and its solid-state structure obtained by single-crystal X-ray crystallography (50% probability ellipsoids shown, hydrogen atoms ignored).*

Crystals suitable for X-ray diffraction crystallography were obtained by slow evaporation of a saturated solution of **IV.5** in a 1:1 mixture of DCM and *n*-hexane in the glovebox. A tetrahedral geometry for the phosphonium cation **IV.5** was observed, like in other classical fluorophosphonium cations derived from triarylphosphines. Also in line with reported fluorophosphonium chemical shifts,[13] the ^{31}P NMR of **IV.5** displays a doublet (*d*, J = 1143 Hz) centered at

83.75 ppm, coupled with a ^{19}F doublet centered at -189.50 ppm (*d*, J = 1142 Hz) (Figure 26). The P-F bond distance of **IV.5** is shorter than those of **IV.2** ($P\text{-}F_{crystal}$ = 1.529 Å; $P\text{-}F_{computed}$ = 1.554 Å *vs* 1.687 and 1.624 Å in **IV.2**). The fluorophosphonium cation derived from the 9-phosphatriptycene is significantly more stable than the difluorophosphorane. Degradation is slow outside of the glovebox.

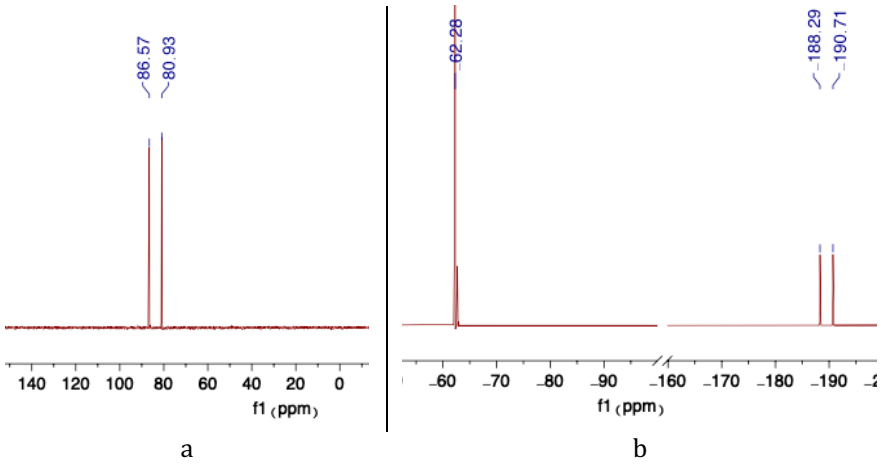

*Figure 26. ^{31}P (a) and ^{19}F (b) spectra of **IV.5** in $CDCl_3$.*

The previous syntheses (Scheme 35 and Scheme 37) were applied to the 1-chloro-9-phosphatriptycene **IV.6**, and the same reactivity as the parent compound was observed, yielding difluorophosphorane **IV.7** and **IV.8** (Scheme 38). No isolated yields are given since these reactions were performed on a small scale (10 mg) directly in the deuterated solvent, but a quantitative conversion to the product was observed by NMR.

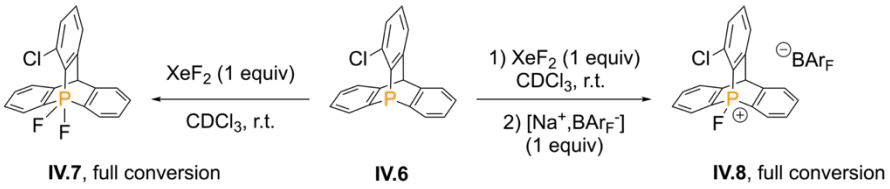

*Scheme 38. Synthesis of the difluorophosphorane **IV.7** and fluorophosphonium salt **IV.8**.*

As a starting point for the investigation on the reactivity of 9-fluorophosphoniumtriptycene cations, the fluoride abstraction of **IV.2** by tris(pentafluorophenyl)borane **IV.9** was attempted, starting from **IV.1** (Scheme 39). While the reaction was not clean and significant amounts of impurities and degradation products were observed in ^{1}H and ^{19}F NMR, the ^{31}P spectrum clearly

shows a full consumption of **IV.1** and the formation of **IV.10** as the major product.

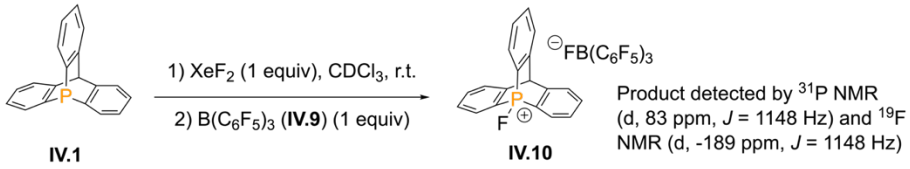

*Scheme 39. Fluoride abstraction of **IV.2** generated from **IV.1** by $B(C_6F_5)_3$ (**IV.9**).*

The fact that **IV.9** is able to abstract a fluoride anion from the *in situ* generated **IV.4** means that is it a stronger acid than the 9-fluorophosphoniumtriptycene **IV.10**, as it was shown that when the fluorophosphonium cation is a stronger acid than **IV.9**, this reaction no longer happens.[13] However, it does not prove that **IV.5** cannot display Lewis acidic properties at all. Next was attempted the coordination of triethylphosphine oxide (Et_3PO) to allow the measurement of its Lewis acidity according to the Guttman-Beckett scale, but the reaction did not yield a $Et_3PO \rightarrow P^+$ Lewis adduct but a mixture of products including a large amount of oxidized phosphine. Again, no conclusion regarding the absence of Lewis acidic character can be drawn from this result. Stephan also reported a lack of reactivity of fluorophosphonium cations with the triethylphosphine oxide.[13] Further reactivity experimentations must be undertaken to investigate the Lewis acid character of **IV.5**.

Finally, to probe the potential electrophilic fluorinating agent of **IV.5**, the reaction with a relatively large Lewis base, PPh_3, was attempted in the presence of **IV.5** (Scheme 40). Due to steric hindrance, the P-P Lewis adduct bond formation is unlikely to happen. In this situation instead, fluorophosphonium cations bearing electron-withdrawing perfluorophenyl groups were shown to undergo a side reaction, namely an aromatic substitution at the fluorine atom in *para*-position relative to the phosphonium, creating a new P-C bond and ultimately yielding a new difluorophosphorane.[11] This side-reaction is not possible in the case of the 9-phosphatriptycene, because there are not fluorine atoms on the phenyl rings. Instead, no reaction at all happens with PPh_3. To our delight, using the more electron-rich phosphines P(4-Tol)$_3$ and P(4-$MeOC_6H_4$) in the presence of **IV.5** resulted in the quantitative formation of the fluorophosphonium cations **IV.12** and **IV.13**, formally effecting their fluorination and regenerating the 9-phosphatriptycene **IV.1**.

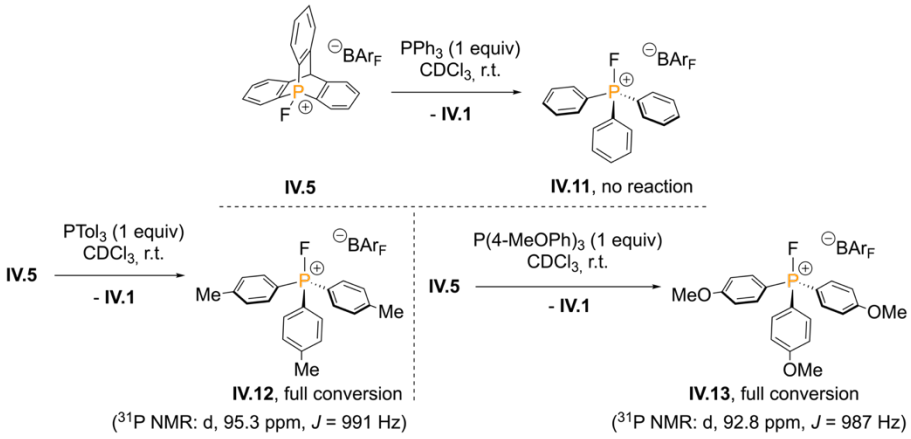

*Scheme 40. Fluorinations of $PTol_3$, $P(4\text{-}MeOC_6H_4)_3$ and attempt at fluorination of PPh_3 by **IV.5**.*

This is a proof of concept that fluorophosphonium cations derived from 9-phosphatriptycene can at least achieve the fluorination of large Lewis bases when the adduct formation and side-reactions are prevented. Further investigations must be undertaken, varying the type of Lewis bases, to continue probing the reactivity of this family of compounds.

3. Conclusions

This preliminary work on the chemistry of difluorophosphoranes and fluorophosphonium cations derived from 9-phosphatriptycene showed that they can be generated similarly to classical arylphosphines, employing strategies reported in the litterature.[13] Contrary to classical phosphines however, they display unusual geometries in their trigonal bipyramid structure, with an aryl ring forced in apical position due to the strained nature of the scaffold. In addition, the triptycene structure also prevents addition of Lewis bases on the side opposite to the P-F bond of fluorophosphonium cations. This limited coordination ability can be exploited to achieve the fluorination of electron-rich phosphines, the fluorine atom becoming *de facto* the most electrophilic site of the molecule. These promising results demonstrate that the chemistry of difluorophosphoranes and fluorophosphonium cations derived from 9-phosphatriptycene is worth exploring and need further investigations, both on the Lewis acidic character of the phosphonium, especially with small Lewis bases, and on the electrophilic character of the fluorine atom in **IV.5**.

4. References

[1] J. M. Bayne, D. W. Stephan, "Phosphorus Lewis acids: emerging reactivity and applications in catalysis", *Chem. Soc. Rev.* **2016**, *45*, 765-774.

[2] A. H. Cowley, R. A. Kemp, "Synthesis and reaction chemistry of stable two-coordinate phosphorus cations (phosphenium ions)", *Chem. Rev.* **1985**, *85*, 367-382.

[3] D. Gudat, A. Haghverdi, H. Hupfer, M. Nieger, "Stability and electrophilicity of phosphorus analogues of arduengo carbenes - an experimental and computational study", *Chem. Eur. J.* **2000**, *6*, 3414-3425.

[4] N. Burford, P. J. Ragogna, "New synthetic opportunities using Lewis acidic phosphines", *Dalton Trans.* **2002**, 4307-4315.

[5] A. L. Brazeau, C. A. Caputo, C. D. Martin, N. D. Jones, P. J. Ragogna, "A new approach to internal Lewis pairs featuring a phosphenium acid and a pyridine base", *Dalton Trans.* **2010**, *39*, 11069-11073.

[6] G. Wittig, U. Schöllkopf, "Über Triphenyl-phosphin-methylene als olefinbildende Reagenzien", *Chem. Ber.* **1954**, *87*, 1318-1330.

[7] C. Y. Wong, D. K. Kennepohl, R. G. Cavell, "Neutral six-coordinate phosphorus", *Chem. Rev.* **1996**, *96*, 1917-1952.

[8] T. Werner, "Phosphonium salt organocatalysis", *Adv. Synth. Catal.* **2009**, *351*, 1469-1481.

[9] H. Li, H. Liu, H. Guo, "Recent advances in phosphonium salt catalysis", *Adv. Synth. Catal.* **2021**, *363*, 2023-2036.

[10] M. Terada, M. Kouchi, "Novel metal-free Lewis acid catalysis by phosphonium salts through hypervalent interaction", *Tetrahedron* **2006**, *62*, 401-409.

[11] L. J. Hounjet, C. B. Caputo, D. W. Stephan, "The Lewis acidity of fluorophosphonium salts: access to mixed valent phosphorus(III)/(V) species", *Dalton Trans.* **2013**, *42*, 2629-2635.

[12] C. B. Caputo, L. J. Hounjet, R. Dobrovetsky, D. W. Stephan, "Lewis acidity of organofluorophosphonium salts: hydrodefluorination by a saturated acceptor", *Science* **2013**, *341*, 1374-1377.

[13] C. B. Caputo, D. Winkelhaus, R. Dobrovetsky, L. J. Hounjet, D. W. Stephan, "Synthesis and Lewis acidity of fluorophosphonium cations", *Dalton Trans.* **2015**, *44*, 12256-12264.

[14] M. Pérez, L. J. Hounjet, C. B. Caputo, R. Dobrovetsky, D. W. Stephan, "Olefin isomerization and hydrosilylation catalysis by Lewis acidic organofluorophosphonium salts", *J. Am. Chem. Soc.* **2013**, *135*, 18308-18310.

[15] M. Pérez, T. Mahdi, L. J. Hounjet, D. W. Stephan, "Electrophilic phosphonium cations catalyze hydroarylation and hydrothiolation of olefins", *Chem. Commun.* **2015**, *51*, 11301-11304.

[16] T. Vom Stein, M. Perez, R. Dobrovetsky, D. Winkelhaus, C. B. Caputo, D. W. Stephan, "Electrophilic fluorophosphonium cations in frustrated Lewis pair hydrogen

activation and catalytic hydrogenation of olefins", *Angew. Chem. Int. Ed.* **2015**, *54*, 10178-10182.

[17] M. Pérez, Z.-W. Qu, C. B. Caputo, V. Podgorny, L. J. Hounjet, A. Hansen, R. Dobrovetsky, S. Grimme, D. W. Stephan, "Hydrosilylation of ketones, imines and nitriles catalysed by electrophilic phosphonium cations: functional group selectivity and mechanistic considerations", *Chem. Eur. J.* **2015**, *21*, 6491-6500.

[18] J. Berreur, A. Diez-Varga, A. Manel, F. R. Leroux, A. Panossian, "One-step oxidative monofluorination of electron-deficient sulfoxides to access highly Lewis acidic sulfur(VI) cations", *Chem. Eur. J.* **2022**, *28*, e202202564.

[19] J. Berreur, "Accès à des acides de Lewis par Umpolung de bases de Lewis chirales : applications en synthèse asymétrique", PhD thesis, University of Strabourg (France), **2020**.

[20] G. S. Lal, G. P. Pez, R. G. Syvret, "Electrophilic NF fluorinating agents", *Chem. Rev.* **1996**, *96*, 1737-1756.

[21] P. T. Nyffeler, S. G. Duron, M. D. Burkart, S. P. Vincent, C. H. Wong, "Selectfluor: mechanistic insight and applications", *Angew. Chem. Int. Ed.* **2004**, *44*, 192-212.

[22] F. Weinhold, C. R. Landis, "Molecular bonding in *s*/*p*-block elements" in *Valency and bonding - a natural bond orbital donor-acceptor perspective*, Cambridge University Press, New-York, **2005**.

Chapter V
Establishing structure-property relationships in non-classical boranes through DFT investigations

---

Density functional theory was employed to characterize and explain the reactivity of a series of boranes outside of the classical trigonal planar structure, as a support to experimental work ongoing in parallel.

This chapter is based on the following articles, reproduced (adapted) with permission from John Wiley and Sons, published throughout the PhD thesis, in which computational support, in the form of DFT calculations and analyses, was employed to complement experimental work performed by other lab members.

1. A. Chardon, A. Osi, D. Mahaut, T. H. Doan, N. Tumanov, J. Wouters, L. Fusaro, B. Champagne, G. Berionni, "Controlled generation of 9-boratriptycene by Lewis adduct dissociation: accessing a non-planar triarylborane", *Angew. Chem. Int. Ed.* **2020**, *59*, 12402-12406.

2. T. H. Doan, A. Chardon, A. Osi, D. Mahaut, N. Tumanov, J. Wouters, B. Champagne, G. Berionni, "Methylene bridging effect on the structures, Lewis acidities and optical properties of semi-planar triarylboranes", *Chem. Eur. J.* **2021**, *27*, 1736-1743.

3. A. Osi, D. Mahaut, N. Tumanov, L. Fusaro, J. Wouters, B. Champagne, A. Chardon, G. Berionni, "Taming the Lewis superacidity of non-planar boranes: C-H bond activation and non-classical binding modes at boron", *Angew. Chem. Int. Ed.* **2022**, *61*, e202112342.

1. Introduction

Organoboranes (BR_3) are the most archetypical representatives of trigonal planar Lewis acids.[1-2] As such, they found several applications in chemistry, first as Lewis acid catalysts,[1, 3-5] but also in material sciences[6-8] or as sensors for electron-rich species.[9-11] Notably, the last two decades saw their extensive use in the field of FLP chemistry, especially for electron-deficient triarylboranes. [12-15]

The steric and electronic properties of boranes, and therefore their reactivity, are determined by their geometry and the nature of their substituents.[16] The latter affect the boron center by the strength of their electron-withdrawing or donating ability, the conjugation with the neighboring π-systems in arylboranes or the electron donation to the boron vacant orbital in boronates or haloboranes. Upon coordination to a Lewis base, boranes adopt a tetrahedral geometry, the energy cost required to switch from their initial planar structure to the final tetrahedral one is called "reorganization energy" and constitutes a significant part of the total reaction energy to the Lewis base. This parameter for example is part of what differentiates boron Lewis acids to their aluminum counterparts in terms of reactivity: alanes are usually more reactive than boranes for a given Lewis base because their reorganization energy cost is lower.[17]

In order to tune the reactivity of organoboron compounds, the established strategy is to change the nature of their substituents. An alternative strategy however is to tune the reactivity of boron compounds by constraining their geometry, affecting their reorganization energy when reacting with a given Lewis base. On the one hand, constraining to a planar structure will reduce their acidity and increase their stability because the structural reorganization will require a larger cost of energy.[8] On the other hand, constraining the borane to a non-planar structure significantly increases its Lewis acidity because of a reduced reorganization energy.[17-20] Many research groups strove to develop non-planar boranes such as the 1-boraadamantane (**V.1**),[18] 1-borabarrelene[21] (**V.2**) or 9-boratriptycene[22] (**V.3**, Figure 27) to exploit their reactivity, and although several derivatives were synthesized,[21, 23-24] they still represent challenges in experimental chemistry.

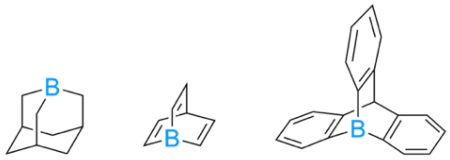

V.1 **V.2** **V.3**

*Figure 27. Structures of the 1-boraadamantane (**V.1**), 1-borabarrelene (**V.2**) and 9-boratriptycene (**V.3**), three examples of non-planar boranes.*

In order to characterize the Lewis acidity of these compounds and compare them to classical boranes, several descriptors of reactivity are necessary. These can be experimental, such as the Gutmann-Beckett scale, the Lappert or the Childs method.[25-28] These methods have in common to consider the reactivity of a given reference Lewis base, respectively triethylphosphine oxide, ethyl acetate and crotonaldehyde and to measure by spectroscopy (NMR for Gutmann-Beckett and Childs or IR for Lappert) the variation of a parameter from the initial uncoordinated base to the Lewis adduct product. The larger the shift, the stronger the Lewis acid. Other probes such as pyridine or acetonitrile can be used as well. Despite the ease of application, these methods come with drawbacks, such as the dependence of reaction trends to the "hardness" or "softness" of the LA (HSAB principle of reactivity[29]), or the steric hindrance in bulky LA.[30] More fundamentally, these methods only consider the effect of the LA on the spectroscopic properties of the LB and are thus missing some key elements in their reactivity such as the reorganization energy of the Lewis acid.

Convenient alternatives or complement to experimental measurements of Lewis acidity are quantum chemical methods. The most common one and the most widely established is the Fluoride Ion Affinity (FIA). The Lewis acidity is determined through the opposite of the Lewis adduct formation enthalpy in standard conditions (FIA = $-\Delta H_f^0$) between the fluoride anion and the Lewis acid. In addition to the fluoride anion, considered a hard and strong LB, other probes can be used as well, yielding further information such as the behavior when reacting with softer Lewis bases (H^-), weaker and neutral bases (NH_3, pyridine) or bulkier bases such as triphenylphosphine (PPh_3).

Finally, intrinsic properties of the Lewis acids (in its free, uncoordinated form) are often considered as well as indicator of their reactivity. These include the energy level of the LUMO or (global) electrophilicity indexes (defined in the next section).[31-33] These multiple parameters allow to grasp the Lewis acidity in its

multidimensionality, since no single scale of acidity can provide a global overview of the reactivity of a given LA.[30, 34]

Quantum chemical calculations allow to characterize Lewis acidity in an easy and reproducible way, as well as predicting experimental properties (namely, NMR chemical shifts) as a support to experimental work. This chapter details DFT investigations performed on a series of boranes with unusual structures and reactivity.

2. Computational methods

Using the Gaussian16 package,[35] geometry optimizations and vibrational frequency calculations were performed at the M06-2X/6-311G(d) level of theory. A tight convergence threshold on the residual forces on the atoms (1.5×10^{-5} Hartree/Bohr or Hartree/radian) was used for geometry optimization. For each compound, all vibrational frequencies are real, demonstrating that the structures are minima on the potential energy surface. When indicated, solvent (dichloromethane, DCM) effects were modelled using the Polarizable Continuum Model put into Integral Equation Formalism (IEFPCM).[36] For fluoride (FIA) and hydride (HIA) affinities, isodesmic reactions were employed, using respectively G3 reference values as anchor points, according to the scheme of Krossing *et al.*[37] (*i.e.* $FSiMe_3 \xrightarrow{\Delta H^0=958\ kJ.mol^{-1}} SiMe_3^+ + F^-$ and $HSiMe_3 \xrightarrow{\Delta H^0=959\ kJ.mol^{-1}} SiMe_3^+ + H^-$). The natural atomic orbital and natural bond orbital analyses were performed in gas phase using the Gaussian NBO 3.1 program[38] at the M06-2X/6-311G(d) level of theory, on optimized structures. NMR chemical shifts (obtained using the GIAO method) were evaluated at the B3LYP/6-311+G(2d,p) level of theory (see Annex II) on structures optimized at the M06-2X/6-311G(d) level of theory, in both cases simulating dichloromethane as solvent.

The global and local electrophilicity indexes are computed using the following expressions. The global electrophilicity index (ω, in eV) was first introduced by Parr and is defined as:[33]

$$\omega = {\chi^2}/{2\eta} \text{ with } \chi = {-1}/{2}\,(\varepsilon_{HOMO} + \varepsilon_{LUMO}) \text{ and } \eta\ \varepsilon_{LUMO} - \varepsilon_{HOMO}$$

where χ is the electronegativity of Mulliken and η the chemical hardness. The local electrophilicity index ω_X can be defined as the product of the global electrophilicity ω with a local Fukui function f_k^+ (on the atomic site k):[32, 39-40]

$$\omega_k = \omega\ f_k^+$$

the latter Fukui function can be conveniently expressed from the electron population of atom *k* in the system of N and N+1 electrons:[31]

$$f_k^+ = Q_k(N+1) - Q_k(N) = \Delta Q_k$$

The natural charges of the boron Q_B (N) and Q_B (N+1) are obtained after NBO analysis (respectively with molecular charge= 0, spin multiplicity= 1 and molecular charge=-1, spin multiplicity= 2) on the same (Q= 0) geometrical structures and at the same level of theory. The detailed values are shown in Table S26 of Annex I.

3. 9-boratriptycene

Initially, the 9-boratriptycene was studied theoretically by Timoshkin and Frenking who predicted that its non-planar structure would lead to an increased Lewis acidity, especially when combined with electron-withdrawing fluorine substituents.[17] In following publications, 9-boratriptycene and other derivatives were predicted to have potential applications as cryptands,[41] in FLP chemistry[42] and to effect complexation of noble gases.[43] Building from a previous synthesis of the related 9-bora-10-phosponium triptycene derivatives, the 9-boratriptycene was generated from the 9-*tert*-butylphenyl-boratriptycene "-ate" complex **V.4** in the presence of triflimidic acid [$HNTf_2$, bis(trifluoromethane-sulfonyl)imide] (Scheme 41). While not isolated, the reactivity of **V.3** is observed indirectly when generated in the presence of Lewis bases, ultimately yielding the Lewis adducts **V.5**-**V.9**. **V.3** exists in equilibrium with the weakly coordinating triflimidate anion NTf_2^-.

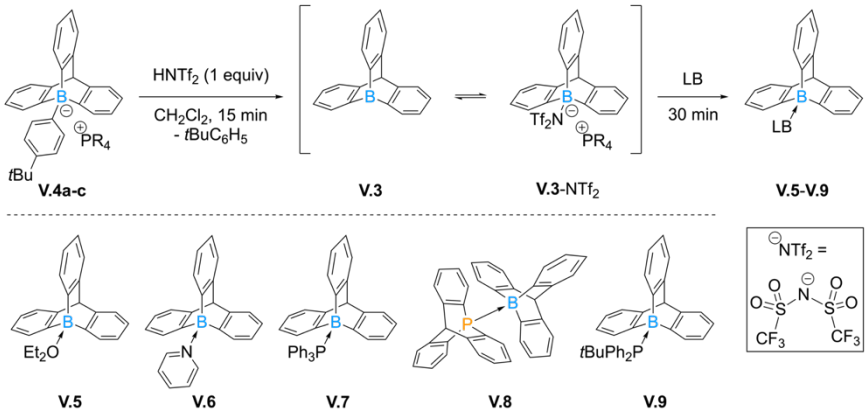

*Scheme 41. Generation of 9-boratriptycene by triflimidic acid in the presence of Lewis bases. Experiments carried out by Arnaud Osi. R_4P^+ in **V.4a-c** are respectively $MePh_3P^+$, $MePh_3P^+$ and $MePh_3P^+$.*

The presence of this equilibrium is key to the reactivity of 9-boratriptycene and was suggested by NMR predictions. Using the GIAO method (see Annex II), NMR chemical shifts were evaluated at the B3LYP/6-311+G(2d,p) on M06-2X/6-311G(d) optimized structures for several experimentally characterized 9-boratriptycene derivatives and were correlated to experimental values. The resulting calibration of the NMR prediction and the associated data are given in Table 12.

*Table 12. Calibration between experimental and computed values for ^{11}B NMR, associated data and predicted experimental chemical shifts of 9-boratriptycene **V.3** and its two adducts with NTf_2^-. Solvent effects for dichloromethane taken into account using the IEFPCM scheme.*

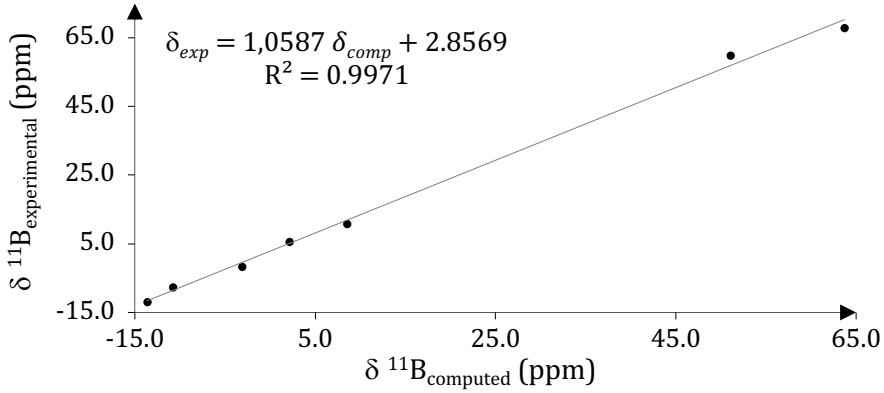

Compounds	δ_{comp} ^{11}B (ppm)	δ_{exp} ^{11}B (ppm)
V.3-Pyridine	-3.2	-1.5
V.3-OEt_2	8.5	10.9
V.3-MeCN	-10.8	-7.6
V.3-PPh_3	-13.6	-11.9
V.3-AcOEt	2.2	5.7
BPh_3 **V.10**	51.0	60.0
$B(C_6F_5)_3$ **V.11**	63.7	68.0
V.3	84.9	**Predicted: 92 ppm**
V.3-NTf_2 (N-adduct)	0.0	**Predicted: 3 ppm**
V.3-NTf_2 (O-adduct)	5.9	**Predicted: 9 ppm**

Using the calibration equation (11), the ^{11}B NMR peak of the free 9-boratriptycene **V.3** is predicted to be at 92ppm.

$$\delta_{exp} = 1{,}0587\ \delta_{comp} + 2.8569 \qquad (11)$$

The broad ^{11}B NMR signal observed at 60 ppm, that disappears with the addition of the LB, is significantly downshifted from that predicted value, which suggest a reversible coordination, presumably with the NTf_2^- anion, and potentially with a Cl atom the dichloromethane solvent.

To shed light into the reactivity of 9-boratriptycene, its reorganization energy upon complexation with F^-, H^-, NH_3, PPH_3 and pyridine as well as its affinities to these Lewis bases were evaluated and compared to other Lewis acids. These values are put in parallel to the pyramidalization angle α, that defines the non-planar character of the boranes (Figure 28, left). It is calculated as the *arcsin* function of the ratio defined by i) the distance between the boron and the plan drawn by its three neighboring carbons and ii) the mean boron-carbon bond length. The following relation (12) is used (α given in radian, apply the $180/\pi$ factor for degrees):

$$\alpha = \sin^{-1}\left(\frac{d_{B-plan}}{\bar{d}_{B-C}}\right) \qquad (12)$$

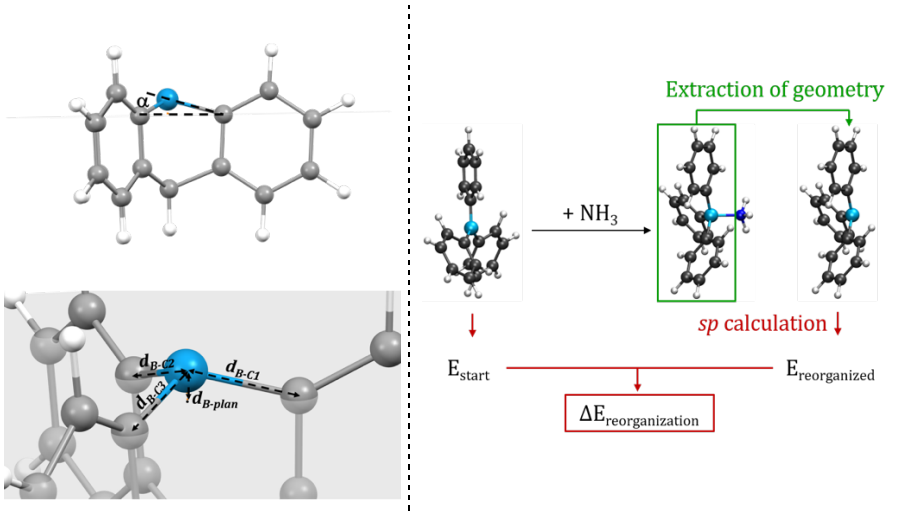

Figure 28. Pyramidalization angle α (in degrees) and the parameters that define it (left) and method for the determination of the reorganization energy exemplified with the complexation of ammonia (right).

The reorganization energy, defined as the energy required to transform the geometry of the free Lewis acid into the geometry of the Lewis acid in the donor-acceptor complex, is calculated as the electronic energy difference between the initial and reorganized structure as shown in Figure 28. The results are shown in Table 13.

Table 13. Pyramidalization angles α, reorganization energies (ΔE_{reorg}, kJ.mol^{-1}) and affinities (-ΔH^0, kJ.mol^{-1}) of selected boron Lewis acids with a series of Lewis bases, global (GEI, eV) and local (for the boron atom ω_B, eV) electrophilicity indexes of the Lewis acids. HIA = Hydride Ion Affinity, FIA = Fluoride Ion Affinity.

Boron Lewis acids		Reorganization energies with Lewis bases				
	α (°)	H^-	F^-	NH_3	PPh_3	C_5H_5N
1-boraadamantane **V.1**	11.0	101	91	48	54	59
1-borabarrelene **V.2**	15.4	95	87	45	50	52
9-boratriptycene **V.3**	15.5	92	87	45	55	58
BPh_3 **V.10**	0	130	174	74	69	113
$B(C_6F_5)_3$ **V.11**	0	144	132	97	82	121
Triethylborane (BEt_3)	0.9	125	118	72	81	86

Boron Lewis acids		Lewis base affinities and electrophilicity indexes						
	α (°)	HIA	FIA	NH_3	PPh_3	C_5H_5N	GEI	ω_B
1-boraadamantane **V.1**	11.0	326	282	74	85	116	0.88	-0.57
1-borabarrelene **V.2**	15.4	412	395	172	164	176	1.02	-1.23
9-boratriptycene **V.3**	15.5	496	476	206	194	200	1.20	-1.50
BPh_3 **V.10**	0.0	352	333	88	72	79	1.53	-0.65
$B(C_6F_5)_3$ **V.11**	0.0	516	466	159	133	144	2.79	-1.23
Triethylborane (BEt_3)	0.9	292	285	92	38	86	0.97	-0.67

The reorganization energy (RE) of non-planar boranes is similar for a given LB and significantly lower than that of planar boranes (*e.g.* for F^-, the RE is 91, 87 and 87 kJ.mol^{-1} respectively for **V.1**, **V.2** and **V.3** and lower than that of planar boranes, 174, 132 and 118 kJ.mol^{-1} for **V.10**, **V.11** and BEt_3 respectively). The value of 45 kJ.mol^{-1} for **V.3** with NH_3 is consistent with that reported by Timoshkin.[41] **V.1** being the non-planar borane with the lowest α angle (11.0°) displays the highest RE of the three compounds (**V.1**, **V.2** and **V.3**). The bindings

of H^- and F^- lead to the highest RE values for all compounds, it can be attributed to the stronger character of these bases and their smaller size compared to the others: the shorter the LA-LB bond, the larger the RE. Comparison between the 9-boratriptycene (**V.9**) and its planar analogue BPh_3 (**V.10**) nicely highlights the strong effect of non-planarity on reactivity. **V.9** has lower REs than **V.10** in magnitudes spanning from 14 to 87 kJ.mol^{-1} ($14 = 69 - 55$ kJ.mol^{-1} for PPh_3; $87 = 174 - 87$ kJ.mol^{-1} for F^-). It significantly affects their reactivity, as shown with the affinities to the Lewis bases, systematically higher for **V.9**. The 9-boratriptycene (**V.9**) is predicted to be stronger than $B(C_6F_5)_3$ (**V.11**) for weaker neutral bases NH_3, PPh_3 (confirmed experimentally by competition experiments) and pyridine, their FIA is comparable (predicted to be slightly higher for **V.9** by DFT, a competition experiment suggested the contrary) and the HIA slightly favors **V.11**. The three former affinities indicate that **V.9** is less hindered than **V.11** while the two latter suggests that it is a "harder" acid than **V.11**.

The global electrophilicity index does not reproduce the trends drawn by the affinities to Lewis bases. While it rightly predicts the acidity ranking among non-planar boranes **V.3**, **V.2**, **V.1**, and among planar boranes **V.11**, **V.10** and BEt_3, it fails when mixing planar and non-planar boranes. Indeed, according to the GEI, the 9-boratriptycene **V.3** is a weaker acid than **V.10** and **V.11**. This error probably arises from the intrinsic nature of the GEI, it is a global quantity based on the ground state properties of Lewis acids (highest occupied (HOMO) and lowest unoccupied (LUMO) molecular orbital energy levels) in their initial geometries, reorganization energies are therefore not considered. Interestingly, a better description is achieved with the local electrophilicity index, which correctly reproduces the Lewis acidity trends.

Another factor influencing the reactivity of the 9-boratriptycene (**V.3**) is the lack of π-electron delocalization from the triptycene phenyl rings into the boron empty *2p* orbital. The almost orthogonal position of the boron 2*p* orbital relative to the aromatic π-systems prevents any orbital overlaps and enhances the boron electrophilicity. A NBO population analysis can highlight this phenomenon indirectly. As shown in Table 14, the electron occupancy of the formally vacant *2p* triphenylborane (**V.10**) increases linearly with the number of mesomeric donating group $-NMe_2$ (from 0.22 to 0.26 e^-) in *para* position to the boron. In the case of 9-boratriptycene, the electron occupancy is significantly lower (0.08 e^-) and remains unperturbed by the addition of electron-donating groups. The sum

of these elements demonstrates the absence of orbital overlap between the phenyl rings π-system and the boron vacant orbital, contributing to its high Lewis acidity.

Table 14. Electron occupancy of the formally vacant 2p *orbital of the boron atom and natural charge of the boron (in e, e = elemental charge). Calculations at the M06-2X/6-311G(d) level of theory using the Gaussian NBO 3.1 program on Gaussian16.*[35, 38]

R = H/NMe_2	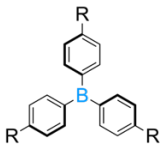				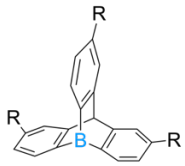			
Number of NMe_2 groups	0 (**V.10**)	1	2	3	0 (**V.3**)	1	2	3
Occupancy of $2p_B$	0.22	0.24	0.25	0.26	0.08	0.08	0.08	0.08
B natural charge	0.92	0.89	0.88	0.86	1.00	1.00	1.00	1.00

In summary, quantum chemical calculations, in the form of NMR predictions, computation of reaction energies and population analyses gave insight into the reactivity of the 9-boratriptycene **V.3**. In a manner that is reminiscent of the effect of the triptycene scaffold on 9-phosphatriptycene, the 9-boratriptycene has an enhanced Lewis acidity compared to its planar analogues due to the strain induced by its geometry. The main contribution arises from its non-planar character that reduces the reorganization energy upon coordination with a Lewis base. Then, the absence of π-$2p_B$ conjugation further increases its electrophilicity. These two factors account for a reactivity that is comparable to that of $B(C_6F_5)_3$ (**V.11**), even exceeding it in some cases, without the need for numerous electron-withdrawing fluorine substituents.

4. 9-sulfonium-10-boratriptycene

The investigations on 9-boratriptycene **V.3** showed that structural effects impacting reorganization energies and π-$2p_B$ conjugation can account for increases in reactivity that are comparable to the addition of electron-withdrawing groups (*e.g.* as for tris(pentafluorophenyl)borane **V.11**). An even higher Lewis acidity can be achieved if these two concepts are combined, as demonstrated by the unique reactivity of the 9-sulfonium-10-boratriptycene (**V.12**). In a similar strategy to **V.3**, **V.12** can be generated by protodeboronation of the "ate" complex **V.13** in the presence of triflidic acid ($HCTf_3$), yielding the Lewis adduct **V.14** (Scheme 42).

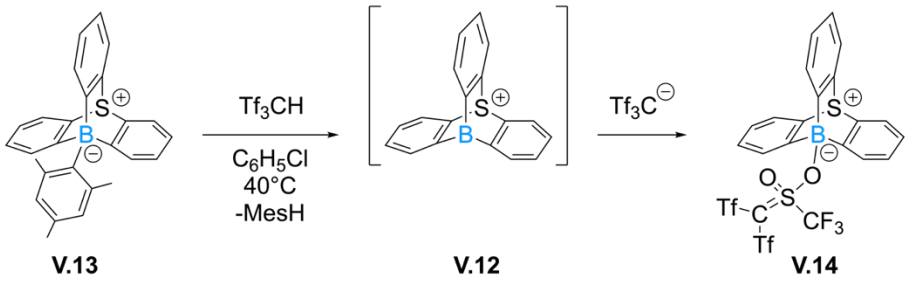

*Scheme 42. Synthesis of the 9-sulfonium-10-boratriptycene Lewis adduct **V.14**. Experimental work carried out by A. Osi.*

The inductive electron-withdrawing nature of the sulfonium cation in bridgehead position of the triptycene scaffold significantly enhances the Lewis acidity of the 9-boratriptycene (Table 15).

Table 15. Pyramidalization angles α, affinities (-ΔH⁰, in kJ.mol⁻¹) of selected boron Lewis acids with a series of Lewis bases, global (GEI, in eV) and local (for the boron atom ω_B, in eV) electrophilicity indexes of the Lewis acids. HIA = Hydride Ion Affinity, FIA = Fluoride Ion Affinity.

Boron Lewis acids		Lewis base affinities and electrophilicity indexes						
	α (°)	HIA	FIA	NH_3	PPh_3	C_5H_5N	GEI	ω_B
V.12 (see above)	13.9	880	854	263	270	269	4.91	-2.28
V.3 (9-bora-triptycene)	15.5	496	476	206	194	200	1.20	-1.50
V.11 $[B(C_6F_5)_3]$	0.0	516	466	159	133	144	2.79	-1.23

HIA and FIA of **V.12** are significantly larger than those of **V.3** and **V.11**, which is mainly due to coulombic attraction between positive and negative charges, and are comparable to those of main group cationic Lewis acids such as $[tolyl{\cdot}Si(CH_3)_3]^+$ (842 kJmol⁻¹), $[Ge(CH_3)_3]^+$ (875 kJmol⁻¹), $[Ga(Me_2)]^+$ (853 kJmol⁻¹), and 9-phosphonium-10-boratriptycene (845 kJ.mol⁻¹).[24, 30] A better comparison, less dependent to charge effects, is achieved with neutral Lewis bases, NH_3, PPh_3 and pyridine, showing a higher reactivity in **V.12**. With a FIA value above the threshold defined as the FIA of SbF_5 (FIA = 506 kJ.mol⁻¹), the 9-sulfonium-10-boratriptycene is considered as a "Lewis superacid". The larger size of the sulfur atom slightly reduces the pyramidalization around the boron atom (13.9° w.r.t. 15.5° in **V.3**), due to longer C-S bonds than the corresponding C-C bonds in the parent 9-boratriptycene **V.3**.

In an effort to generate the free Lewis acid **V.12**, the borohydride **V.15** was exposed to the tritylium cation Ph_3C^+ (acting as hydride acceptor) (Scheme 43). The resulting ^{11}B NMR signal at 8.8 ppm was inconsistent with the one of **V.12** predicted at 82 ppm (using the same GIAO-DFT method shown in Table 12). Surprisingly, compound **V.16** was obtained instead, as revealed by single-crystal X-ray diffraction crystallography.

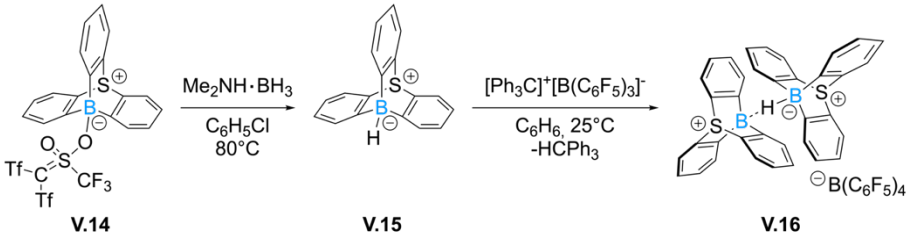

*Scheme 43. Synthesis of the B-H-B bridge compound **V.16**. Experimental work carried out by A. Osi.*

The bonding nature in **V.16** was probed by quantum chemical calculations in the form of a NBO analysis. The symmetry of the bonding situation was indicated by similar partial charges on both boron atom (0.54*e*) and negative charge for the central hydrogen atom (-0.12*e*). The Lewis structure resulting from the NBO calculation shows a hypovalent three-center bond with a electron occupancy slightly lower than two electrons (1.98) (Figure 29).[44-45]

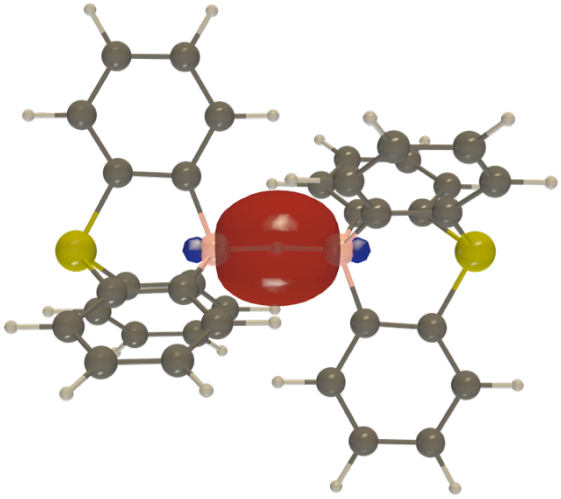

Figure 29. Three centers bonding NBO between the two boron and the central hydrogen atom.

The valence hybrid composition of the NBO expressed from the population analysis describes a main contribution of 55.8% from the hydrogen atom

compared to 22.1% for each boron atom. In summary, the computational data suggest a bonding situation defined as a three-centers-two electrons bonding. **V.16** is likely formed by reaction between the transient species **V.12** and the remaining borohydride **V.15**.

Another example of the unique reactivity of **V.12** is the generation of the unique diborate **V.17** (Scheme 44). In the presence of 2,2,6,6-tetramethylpiperidine (TMPH) with traces of water, the expected reaction with TMPH does not happen but instead, the formation of **V.17** is observed. The expected mechanism involves the trapping of a water molecules followed by twofold deprotonation by TMPH.

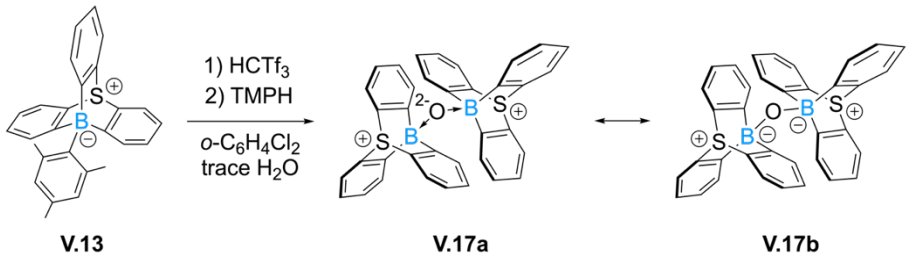

*Scheme 44. Formation of diborane **V.17** following the failed C-H activation of TMPH. Experimental work carried out by A. Osi.*

The bonding situation described by NBO analysis on this unprecedented structure suggests O-B donor-acceptor interactions resulting from partial overlaps between the O lone pairs and formally vacant boron *2p* orbitals rather than the conventional σ-bonding. Therefore, **V.17** should be considered as a dianionic oxygen atom coordinated to two boron atoms, the resonance structure **V.17a** being more adequate than **V.17b**. Inspection of the NBO reveals that there are four lone pairs at the oxygen atom (Figure 30): two have 100% *2p* character while the others are described as 88.5% *2s* - 11.5% *2p* and 11.5% *2p* - 88.5% *2s* respectively. Both boron empty orbitals are sp^2 hybridized, and possess natural charges of 0.70 *e* for B1 and B2 as well as a comparable electron occupancy of 0.4 e^-. The partial charge at the oxygen atom has a significant negative value (-1.0 *e*) which is in agreement with its total valence electron occupancy of 7.0 e^-.

In summary, embedding electron-withdrawing cations such as S^+ on the bridgehead position of the 9-boratriptycene can lead to exceptional levels of Lewis acidity. The resulting non-planar Lewis superacid **V.12** can be generated as a transient species and its reactivity has been exploited to perform C-H bond activation but also leads to the formation of unexpected and unprecedented

structures, such as the bridged B-H-B and B-O-B structures. The type of bonding situations in these compounds was studied by NBO analyses.

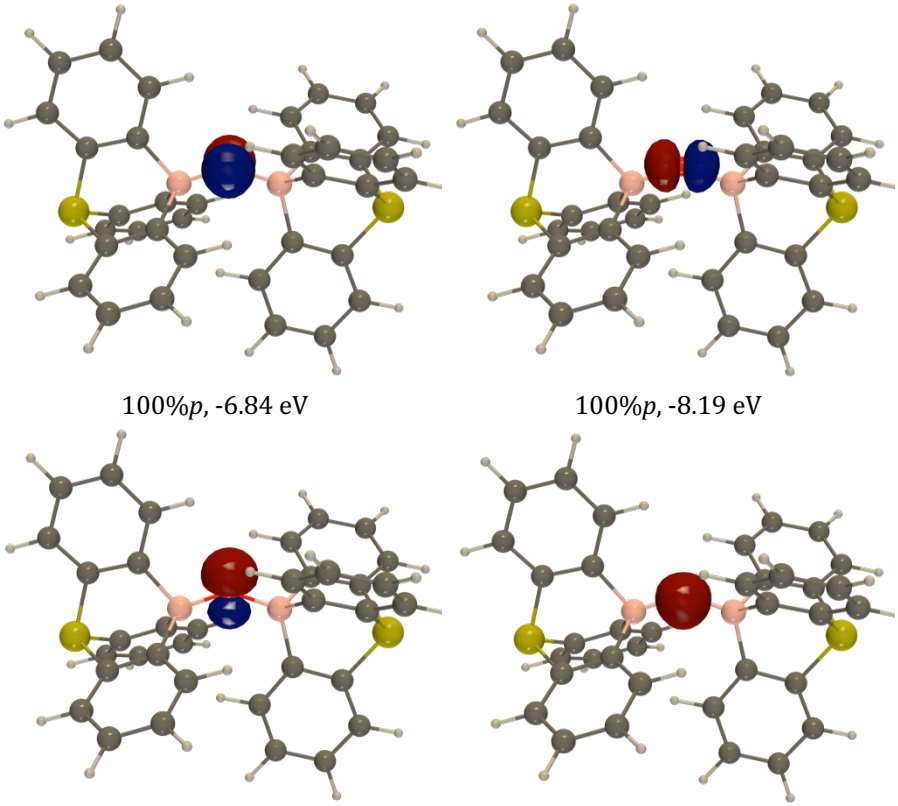

*Figure 30. Plot of the oxygen lone pairs of **V.17** in decreasing order of energy from left to right, with corresponding s/p character (negligible d character is omitted for clarity) and energy in eV: the isovalue for all structures is of 0.1 a.u.*

5. Methylene-bridged triarylboranes

In contrast to the increased Lewis acidity brought by the triptycene scaffold, adding a methylene bridge between aryl rings in planar triarylboranes has a stabilizing effect. As mentioned earlier, forcing the boron into a fully planar situation reduces its Lewis acidity because of an increased reorganization energy compared to classical triarylboranes displaying propeller-like structures (Figure 31).[8] "Semi-planar" boranes, with a methylene bridge, display a reactivity that is intermediate between that of the two aforementioned structures.

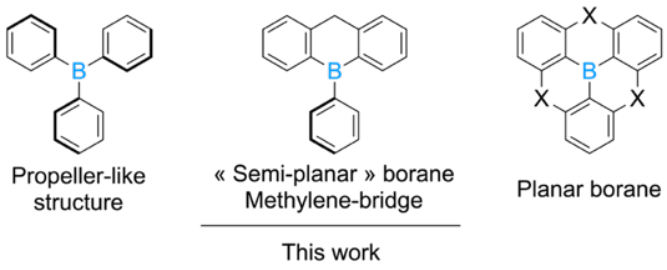

Figure 31. "Semi-planar" boranes compared to planar and propeller-like ones.

Using three different syntheses, a series of semi-planar boranes were prepared, including but not limited to compounds **V.21**-**V.24**. A comparison of their reactivity parameters with the corresponding non-bridged boranes highlights the effect of the structure (Table 16).

While reorganization energies are, as predicted, slightly larger for non-planar boranes, the introduction of the bridging methylene has only a small to negligible effect on the affinity with small bases F^- and NH_3, the latter decreasing only of 4 $kJ.mol^{-1}$ from **V.10** to **V.21**. A slight decrease is also observed for global and local electrophilicity indexes hinting at a weaker Lewis acidity. Increasing the size of the Lewis base clearly reduces its affinity with semi-planar boranes, as seen with triphenylphosphine. This suggests that the difference in reactivity is mostly due to a higher steric hindrance around the boron. Finally, adding fluorine atoms on the exocyclic aryl ring expectedly increased the Lewis acidity of the boron atom, as illustrated by a higher FIA of almost 40 kJ mol^{-1} for **V.24** (Ar = C_6F_5) *versus* **V.21** (Ar = Ph).

*Table 16. M06-2X/6-311G(d) gas phase (FIA, ΔH^0 in kJ.mol^{-1}), affinities with NH_3 and PPh_3 (ΔG^0 in kJ.mol^{-1}) at 25°C, global (ω, in eV) and local (boron, ω_B, in eV) electrophilicity indexes of the borane derivatives **V.10-20** and **V.21-24**. As a comparison, the corresponding affinities (in kJ.mol^{-1}) of $B(C_6F_5)_3$ for F^- (ΔH^0), NH_3 (ΔG^0) and PPh_3 (ΔG^0) are -466, -117 and -62 respectively while its global and local electrophilicity indexes are respectively 2.79 eV and -1.23 eV.[46] In parenthesis are indicated the reorganization energies necessary for the borane to reach its final geometry in the Lewis adduct.*

	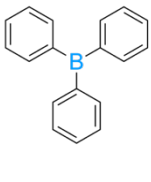	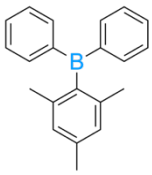	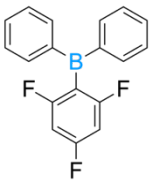	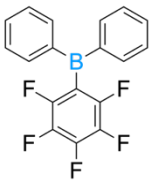
Affinities/index	**V.10**	**V.18**	**V.19**	**V.20**
FIA	-333 (174)	-324 (135)	-353 (159)	-379 (159)
NH_3	-43 (74)	-19 (89)	-63 (92)	-67 (91)
PPh_3	-7 (69)	40 (92)	-3 (93)	8 (103)
GEI	1.53	1.43	1.68	1.86
ω_B	-0.65	-0.69	-0.74	-0.81
	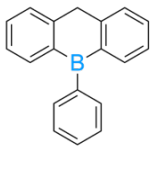	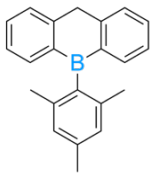	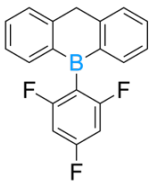	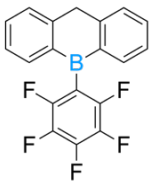
Affinities/index	**V.21**	**V.22**	**V.23**	**V.24**
FIA	-333 (169)	-306 (141)	-349 (176)	-372 (179)
NH_3	-39 (107)	0 (95)	-55 (102)	-58 (102)
PPh_3	20 (136)	43 (100)	31 (159)	-5 (97)
GEI	1.48	1.38	1.61	1.77
ω_B	-0.61	-0.63	-0.67	-0.73

6. Conclusions

Changing the structure of boranes strongly affects their reactivity. Using quantum chemical calculations, their reactivity can be characterized and structure reactivity-relationships established. Deviation from the classical planar structure has mostly an impact on the reorganization energy, which is reduced when reacting with a Lewis base, but it also affects the conjugation with the neighboring π-systems of the aryl rings. These have a stabilizing effect on the

boron atom by donating electrons in its empty *2p* orbital that is prevented in the case of 9-boratriptycene derivatives. Combining these effects with the electron-withdrawing ability of the sulfonium cation leads to an even higher Lewis acidity. In contrast, the structure of semi-planar boranes leads to a weaker Lewis acidity than classical propeller-shape boranes, which is mainly due to a higher steric shielding of the boron atom.

7. References

[1] A. Corma, H. Garcia, "Lewis acids: from conventional homogeneous to green homogeneous and heterogeneous catalysis", *Chem. Rev.* **2003**, *103*, 4307-4365.

[2] E. Fernández, A. Whiting (Ed.), *Synthesis and application of organoboron compounds*, Springer, London, **2015**.

[3] W. E. Piers, "The chemistry of perfluoroaryl boranes" in *Adv. Organomet. Chem.*, Elsevier, **2005**.

[4] J. L. Carden, A. Dasgupta, R. L. Melen, "Halogenated triarylboranes: synthesis, properties and applications in catalysis", *Chem. Soc. Rev.* **2020**, *49*, 1706-1725.

[5] M. A. Legare, C. Pranckevicius, H. Braunschweig, "Metallomimetic chemistry of boron", *Chem. Rev.* **2019**, *119*, 8231-8261.

[6] A. Wakamiya, S. Yamaguchi, "Designs of functional π-electron materials based on the characteristic features of boron", *Bull. Chem. Soc. Jpn.* **2015**, *88*, 1357-1377.

[7] A. Lorbach, A. Hubner, M. Wagner, "Aryl(hydro)boranes: versatile building blocks for boron-doped pi-electron materials", *Dalton Trans.* **2012**, *41*, 6048-6063.

[8] M. Hirai, N. Tanaka, M. Sakai, S. Yamaguchi, "Structurally constrained boron-, nitrogen-, silicon-, and phosphorus-centered polycyclic π-conjugated systems", *Chem. Rev.* **2019**, *119*, 8291-8331.

[9] F. Jakle, "Advances in the synthesis of organoborane polymers for optical, electronic, and sensory applications", *Chem. Rev.* **2010**, *110*, 3985-4022.

[10] M. Li, J. S. Fossey, T. D. James (Ed.), *Boron: Sensing, synthesis and supramolecular self-assembly*, Royal Society of Chemistry, Cambridge, **2015**.

[11] C. R. Wade, A. E. Broomsgrove, S. Aldridge, F. P. Gabbai, "Fluoride ion complexation and sensing using organoboron compounds", *Chem. Rev.* **2010**, *110*, 3958-3984.

[12] G. C. Welch, R. R. San Juan, J. D. Masuda, D. W. Stephan, "Reversible, metal-free hydrogen activation", *Science* **2006**, *314*, 1124-1126.

[13] D. W. Stephan, "Frustrated Lewis pairs", *J. Am. Chem. Soc.* **2015**, *137*, 10018-10032.

[14] D. W. Stephan, "The broadening reach of frustrated Lewis pair chemistry", *Science* **2016**, *354*, 1248-1256.

[15] J. Lam, K. M. Szkop, E. Mosaferi, D. W. Stephan, "FLP catalysis: main group hydrogenations of organic unsaturated substrates", *Chem. Soc. Rev.* **2019**, *48*, 3592-3612.

[16] I. B. Sivaev, V. I. Bregadze, "Lewis acidity of boron compounds", *Coord. Chem. Rev.* **2014**, *270-271*, 75-88.

[17] L. A. Mück, A. Y. Timoshkin, G. Frenking, "Design of neutral Lewis superacids of group 13 elements", *Inorg. Chem.* **2011**, *51*, 640-646.

[18] B. M. Mikhailov, "The chemistry of 1-boraadamantane", *Pure Appl. Chem.* **1983**, *55*, 1439-1452.

[19] A. Y. Timoshkin, G. Frenking, "Gas-phase Lewis acidity of perfluoroaryl derivatives of group 13 elements", *Organometallics* **2008**, *27*, 371-380.

[20] G. Bouhadir, D. Bourissou, "Unusual geometries in main group chemistry", *Chem. Soc. Rev.* **2004**, *33*, 210-217.

[21] T. K. Wood, W. E. Piers, B. A. Keay, M. Parvez, "1-Borabarrelene derivatives via Diels-Alder additions to borabenzenes", *Org. Lett.* **2006**, *8*, 2875-2878.

[22] A. G. Massey, "1,6-Disubstituted Triptycenes", *Adv. Inorg. Chem.* **1989**, *33*, 1-38.

[23] T. E. Wood, B. A. Keay, W. E. Piers, "Boron-containing aromatic compounds: synthesis, characterization and reactivity", PhD thesis, University of Calgary (Canada), **2009**.

[24] A. Ben Saida, A. Chardon, A. Osi, N. Tumanov, J. Wouters, A. I. Adjieufack, B. Champagne, G. Berionni, "Pushing the Lewis acidity boundaries of boron compounds with non-planar triarylboranes derived from triptycenes", *Angew. Chem. Int. Ed.* **2019**, *58*, 16889-16893.

[25] U. Mayer, V. Gutmann, W. Gerger, "The acceptor number - A quantitative empirical parameter for the electrophilic properties of solvents", *Monatsh. Chem.* **1975**, *106*, 1235-1257.

[26] M. A. Beckett, G. C. Strickland, J. R. Holland, K. Sukumar Varma, "A convenient N.M.R. method for the measurement of Lewis acidity at boron centres: correlation of reaction rates of Lewis acid initiated epoxide polymerizations with Lewis acidity", *Polymer* **1996**, *37*, 4629-4631.

[27] M. F. Lappert, "103. Coordination compounds having carboxylic esters as ligands. Part II. Relative acceptor strengths of some Group III and IV halides", *J. Chem. Soc.* **1962**.

[28] R. F. Childs, D. L. Mulholland, A. Nixon, "Lewis acid adducts of α,β-unsaturated carbonyl and nitrile compounds. A calorimetric study", *Can. J. Chem.* **1982**, *60*, 809-812.

[29] R. G. Pearson, J. Songstad, "Application of the principle of hard and soft acids and bases to organic chemistry", *J. Am. Chem. Soc.* **1967**, *89*, 1827-1836.

[30] L. Greb, "Lewis superacids: Classifications, candidates, and applications", *Chem. Eur. J.* **2018**, *24*, 17881-17896.

[31] W. Yang, W. J. Mortier, "The use of global and local molecular parameters for the analysis of the gas-phase basicity of amines", *J. Am. Chem. Soc.* **1986**, *108*, 5708-5711.

[32] P. K. Chattaraj, U. Sarkar, D. R. Roy, "Electrophilicity index", *Chem. Rev.* **2006**, *106*, 2065-2091.

[33] R. G. Parr, L. V. Szentpály, S. Liu, "Electrophilicity index", *J. Am. Chem. Soc.* **1999**, *121*, 1922-1924.

[34] P. Erdmann, L. Greb, "Multidimensional Lewis acidity: A consistent data set of chloride, hydride, methide, water and ammonia affinities for 183 p-block element Lewis acids", *ChemPhysChem* **2021**, *22*, 935-943.

[35] M. J. Frisch, G. W. Trucks, H. B. Schlegel, G. E. Scuseria, M. A. Robb, J. R. Cheeseman, G. Scalmani, V. Barone, G. A. Petersson, H. Nakatsuji, X. Li, M. Caricato, A. V. Marenich, J. Bloino, B. G. Janesko, R. Gomperts, B. Mennucci, H. P. Hratchian, J. V. Ortiz, A. F. Izmaylov, J. L. Sonnenberg, D. Williams-Young, F. Ding, F. Lipparini, F. Egidi, J. Goings, B. Peng, A. Petrone, T. Henderson, D. Ranasinghe, V. G. Zakrzewski, J. Gao, N. Rega, G. Zheng, W. Liang, M. Hada, M. Ehara, K. Toyota, R. Fukuda, J. Hasegawa, M. Ishida, T. Nakajima, Y. Honda, O. Kitao, H. Nakai, T. Vreven, K. Throssell, J. A. Montgomery, Jr., J. E. Peralta, F. Ogliaro, M. J. Bearpark, J. J. Heyd, E. N. Brothers, K. N. Kudin, V. N. Staroverov, T. A. Keith, R. Kobayashi, J. Normand, K. Raghavachari, A. P. Rendell, J. C. Burant, S. S. Iyengar, J. Tomasi, M. Cossi, J. M. Millam, M. Klene, C. Adamo, R. Cammi, J. W. Ochterski, R. L. Martin, K. Morokuma, O. Farkas, J. B. Foresman, D. J. Fox, *Gaussian 16, Revision A.03*, Gaussian Inc., Wallingford CT, **2016**.

[36] J. Tomasi, B. Mennucci, R. Cammi, "Quantum mechanical continuum solvation models", *Chem. Rev.* **2005**, *105*, 2999-3094.

[37] H. Böhrer, N. Trapp, D. Himmel, M. Schleep, I. Krossing, "From unsuccessful H_2-activation with FLPs containing $B(Ohfip)_3$ to a systematic evaluation of the Lewis acidity of 33 Lewis acids based on fluoride, chloride, hydride and methyl ion affinities", *Dalton Trans.* **2015**, *44*, 7489-7499.

[38] E. D. Glendening, A. E. Reed, J. E. Carpenter, F. Weinhold, *NBO Version 3.1*, Gaussian Inc., Pittsburgh, **2003**.

[39] P. Pérez, A. Toro-Labbé, A. Aizman, R. Contreras, "Comparison between experimental and theoretical scales of electrophilicity in benzhydryl cations", *J. Org. Chem.* **2002**, *67*, 4747-4752.

[40] E. Chamorro, P. K. Chattaraj, P. Fuentealba, "Variation of the electrophilicity index along the reaction path", *J. Phys. Chem. A* **2003**, *107*, 7068-7072.

[41] A. Y. Timoshkin, K. Morokuma, "Novel group 13 Lewis superacids and 13-15 donor-acceptor cryptands for hydrogen activation: a theoretical study", *Phys. Chem. Chem. Phys* **2012**, *14*, 14911-14916.

[42] T. M. Gilbert, "Computational studies of complexation of nitrous oxide by borane-phosphine frustrated Lewis pairs", *Dalton Trans.* **2012**, *41*, 9046-9055.

[43] G. N. Lewis, *Valence and the structure of atoms and molecules*, American Chemical Society, **1923**.

[44] F. Weinhold, C. R. Landis, *Discovering chemistry with natural bond orbitals*, Wiley, Hoboken, NJ, **2012**.

[45] F. Weinhold, C. R. Landis, "Molecular bonding in *s*/*p*-block elements" in *Valency and bonding - a natural bond orbital donor-acceptor perspective*, Cambridge University Press, New-York, **2005**.

[46] A. Chardon, A. Osi, D. Mahaut, T. H. Doan, N. Tumanov, J. Wouters, L. Fusaro, B. Champagne, G. Berionni, "Controlled generation of 9-boratriptycene by Lewis adduct dissociation: Accessing a non-planar triarylborane", *Angew. Chem. Int. Ed.* **2020**, *59*, 12402-12406.

Chapter VI
Rational development of a metal-free bifunctional system for the C-H activation of methane: a density functional theory investigation

---

A new boron/nitrogen bifunctional catalyst derived from 9-boratriptycene is considered for the activation of methane and studied through a quantum chemical investigation.

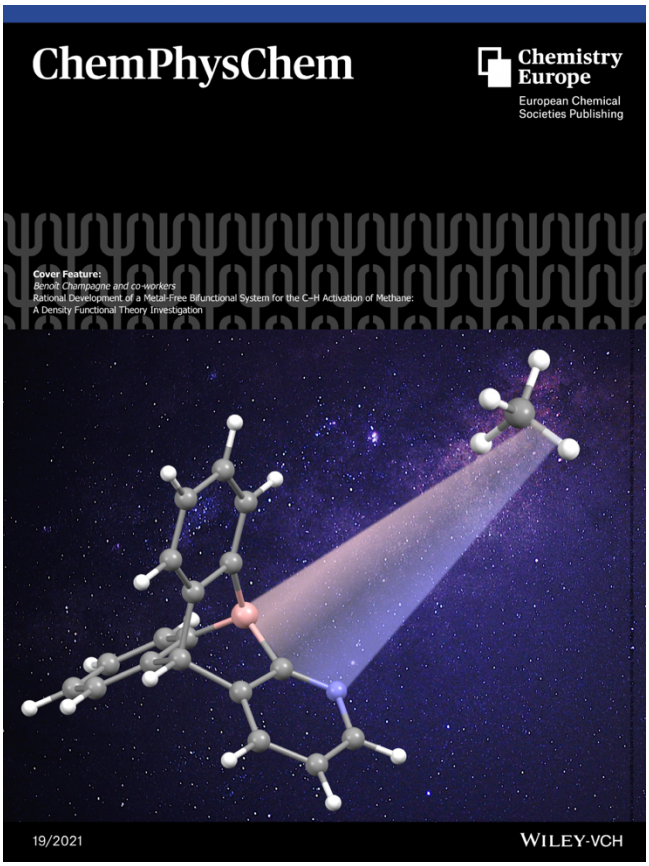

This chapter is based on the following article published in the journal *ChemPhysChem* on July 26, 2021 and reproduced (adapted) with permission from John Wiley and Sons.

D. Mahaut, A. Chardon, L. Mineur, G. Berionni, B. Champagne, "Rational Development of a Metal-Free Bifunctional System for the C-H Activation of Methane: A Density Functional Theory Investigation", *ChemPhysChem* **2021**, *22*, 1958-1966.

ChemPhysChem | Articles
doi.org/10.1002/cphc.202100527

Rational Development of a Metal-Free Bifunctional System for the C–H Activation of Methane: A Density Functional Theory Investigation

Damien Mahaut,[a] Aurélien Chardon,[a] Loïc Mineur,[a] Guillaume Berionni,[a] and Benoît Champagne*[a]

The activation or heterolytic splitting of methane, a challenging substrate usually restricted to transition metals, has so far proven elusive in experimental frustrated Lewis pair (FLP) chemistry. In this article, we demonstrate, using density functional theory (DFT), that 1-aza-9-boratriptycene is a conceptually simple intramolecular FLP for the activation of methane. Systematic comparison with other FLP systems allows to gain insight into their reactivity with methane. The thermodynamics and kinetics of methane activation are interpreted by referring to the analysis of the natural charges and by employing the distortion-interaction/activation strain (DIAS) model. These showed that the nature of the Lewis base influences the selectivity over the reaction pathway, with N Lewis bases favoring the deprotonation mechanism and P bases the hydride abstraction one. The lower barrier of activation for 1-aza-9-boratriptycene and the higher products stability are due to a better interaction energy than its counterparts, itself due to electrostatic interactions with the methane moiety, favorable orbital overlaps allowed by the side-attack, and space proximity between the B and N atoms.

1. Introduction

The pioneering work of Lewis in 1923 on acids and bases led to one of the most important and unifying theories in chemical reactivity.[1] Still today, his definitions of acids as electron pair acceptors, bases as electron pair donors and the formation of donor-acceptor bonds are put forward to explain the mechanism of numerous transformations.[2] Accordingly, both would react to form covalently bonded adducts, effecting a mutual neutralization. The seminal discovery of the metal-free activation and heterolytic splitting of H_2 by Stephan and the subsequent introduction of the concept of frustrated Lewis pairs (FLPs) opened a new dimension to this Lewis acid-base reactivity.[3] FLPs consist in a combination of sterically hindered acid and base that cannot form the covalent Lewis adduct because of steric repulsions, allowing synergistic cooperation for the activation of small molecules.

The main application arising from this discovery is doubtless the small molecules activation (H_2, CO_2, SO_2, N_2O *etc.*).[3a,4] Among these, hydrogen activation was the focus of numerous mechanistic investigations[5] and had by far the most impact, because it enabled the transition-metal-free catalytic hydrogenation of a large range of unsaturated substrates.[6]

A challenging substrate that proved so far elusive in experimental reports of FLP reactions is methane (CH_4). This small molecule has drawn a lot of attention from the research community in the past decades both because of its impact as greenhouse gas in the global warming crisis but also as a fundamental scientific challenge due to its high stability and chemical inertness.[7] For these reasons, the conversion of methane to higher-value products is of paramount importance in modern chemistry. The high reactivity of transition metal complexes made it possible to achieve some remarkable transformations in this domain over the years.[8] Still, so far, the same level of reactivity could not be reached without such compounds and no metal- or transition-metal-free alternative was yet reported in homogeneous catalysis. Unsurprisingly, frustrated Lewis pairs were considered as ideal candidates for this purpose and several of these systems were proposed and, enacting quantum chemistry methods, studied for the activation of methane, shedding light into some of the key factors affecting their reactivity toward methane.[9]

We have recently reported the synthesis, application and DFT investigations of 9-boratriptycene derivatives **1** and **2** (Scheme 1) as Lewis acids, showing that the non-planar structure of boron compounds greatly increases their Lewis

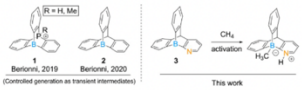

Scheme 1. Structures of 9-(methyl)phosphonium-10-boratriptycenes **1**, 9-boratriptycene **2**, 1-aza-9-boratriptycene **3** and reaction of activation or heterolytic splitting of the methane molecule with **3**. The atomic numbering used in these previous reports, including this one, was introduced by Chen and Ma.[10]

[a] D. Mahaut, Dr. A. Chardon, L. Mineur, Prof. G. Berionni, Prof. B. Champagne
Department of Chemistry, Namur Institute of Structured Matter
University of Namur
Rue de Bruxelles 61, B-5000, Namur, Belgium
E-mail: benoit.champagne@unamur.be

Supporting information for this article is available on the WWW under https://doi.org/10.1002/cphc.202100527

1. Abstract

The activation or heterolytic splitting of methane, a challenging substrate usually restricted to transition metals, has so far proven elusive in experimental frustrated Lewis pair (FLP) chemistry. In this article, we demonstrate, using density functional theory (DFT), that 1-aza-9-boratriptycene is a conceptually simple intramolecular FLP for the activation of methane. Systematic comparison with other FLP systems allows to gain insight into their reactivity with methane. The thermodynamics and kinetics of methane activation are interpreted by referring to the analysis of the natural charges and by employing the distortion-interaction/activation strain (DIAS) model. These showed that the nature of the Lewis base influences the selectivity over the reaction pathway, with N Lewis bases favoring the deprotonation mechanism and P bases the hydride abstraction one. The lower barrier of activation for 1-aza-9-boratriptycene and the higher products stability are due to a better interaction energy than its counterparts, itself due to electrostatic interactions with the methane moiety, favorable orbital overlaps allowed by the side-attack, and space proximity between the B and N atoms.

2. Introduction

The pioneering work of Lewis in 1923 on acids and bases led to one of the most important and unifying theories in chemical reactivity.[1] Still today, his definitions of acids as electron pair acceptors, bases as electron pair donors and the formation of donor-acceptor bonds are put forward to explain the mechanism of numerous transformations.[2-4] Accordingly, both would react to form covalently bonded adducts, effecting a mutual neutralization. The seminal discovery of the metal-free activation and heterolytic splitting of H_2 by Stephan and the subsequent introduction of the concept of frustrated Lewis pairs (FLPs) opened a new dimension to this Lewis acid-base reactivity.[5-9] FLPs consist in a combination of sterically hindered acid and base that cannot form the covalent Lewis adduct because of steric repulsions, allowing synergistic cooperation for the activation of small molecules.

The main application arising from this discovery is doubtless the small molecules activation (H_2, CO_2, SO_2, N_2O *etc.*).[9-14] Among these, hydrogen activation was the focus of numerous mechanistic investigations[15-26] and had by far the most

impact, because it enables the transition-metal-free catalytic hydrogenation of a large range of unsaturated substrates.[27]

A challenging substrate that proved so far elusive in experimental reports of FLP reactions is methane (CH_4). This small molecule has drawn a lot of attention from the research community in the past decades both because of its impact as greenhouse gas in the global warming crisis but also as a fundamental scientific challenge due to its high stability and chemical inertness.[28-30] For these reasons, the conversion of methane to higher-value products is of paramount importance in modern chemistry. The high reactivity of transition metal complexes made it possible to achieve some remarkable transformations in this domain over the years.[31-36] Still, so far, the same level of reactivity could not be reached without such compounds and no metal- or transition-metal-free alternative was yet reported in homogeneous catalysis. Unsurprisingly, frustrated Lewis pairs were considered as ideal candidates for this purpose and several of these systems were proposed and, enacting quantum chemistry methods, studied for the activation of methane, shedding light into some of the key factors affecting their reactivity toward methane.[37-42]

We have recently reported the synthesis, application and DFT investigations of 9-boratriptycene derivatives **VI.1** and **VI.2** (Scheme 45) as Lewis acids, showing that the non-planar structure of boron compounds greatly increases their Lewis acidity due to the lowering of their reorganization (or distortion) energies.[43-44] This drove us to explore the reactivity toward methane of 9-boratriptycenes in combination with a Lewis base, to design a new metal-free bifunctional system for methane activation.

In this report, we propose the 1-aza-9-boratriptycene **VI.3** as an ideal candidate for the heterolytic splitting of the methane molecule (Scheme 45). Since derived from already isolated scaffolds (9-boratriptycene derivatives), we consider this system as realistic and synthetically attainable. This compound is investigated at the DFT level and compared with representative FLP systems applied to the activation of methane and selected from the literature. The thermodynamics and kinetics (transition states) of the reactions are discussed, and the DIAS model[45] is applied to all systems to investigate the effects of the reorganization and interaction energies on the activation of methane along the reaction pathway.

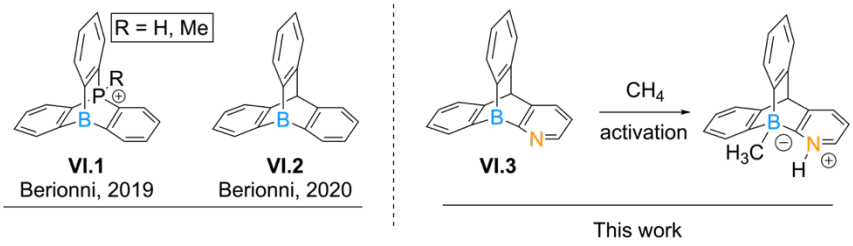

*Scheme 45. Structures of 9-(methyl)phosphonium-10-boratriptycenes **VI.1**, 9-bora-triptycene **VI.2**, 1-aza-9-boratriptycene **VI.3** and reaction of activation or heterolytic spitting of the methane molecule with **VI.3**. The atomic numbering used in these previous reports, including this one, was introduced by Chen and Ma.[46].*

3. State-of-the-art

Only a limited number of research articles have been published on the FLP-mediated activation of methane. In a first contribution in 2010, Wang *et al.* studied the activation of H_2 and CH_4 using stable carbenes in combination with $B(C_6F_5)_3$, reaching gas phase reaction (activation) energies, $\Delta G^0(\Delta G^{\neq})$, of -54(157) kJ.mol^{-1} at the M05-2X/6-311++G(d,p)//M05-2X/6-31G(d,p) level of theory.[37] They showed that the methane activation is a systematically less favorable process than the one of H_2 for a given system and attributed it to weaker orbital interactions and to a larger distortion of methane compared to dihydrogen. In addition, they highlighted the significant impact of the electrostatic interactions in the approach of the methane moiety. In their subsequent report, they designed intramolecular FLPs **VI.4a-c** based on a bora- and aza-adamantane skeleton (Figure 32),[38] where the reaction occurs side-on

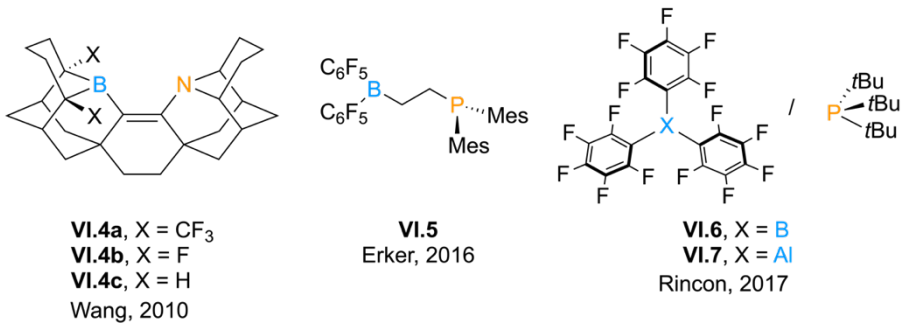

*Figure 32. Selected systems studied theoretically for the activation of methane. a) Representative examples of one of Wang's intramolecular B/N FLPs **VI.4**, b) Erker's intramolecular B/P FLP **VI.5**, and c) Rincon's $B(C_6F_5)_3$ or $Al(C_6F_5)_3/PtBu_3$ FLPs **VI.6** and **VI.7**.*

and without an unfavorable inversion of the -CH_3 moiety. It reduces the activation barrier and reaction energies, down to $\Delta G^0(\Delta G^{\neq})$ = -22(85) kJ.mol^{-1} for their system **VI.4a** at the IEFPCM(cyclohexane)/M05-2X/6-311++G(d,p)// M05-2X/6-31G(d,p).

In 2016, the group of Erker developed an intramolecular FLP (**VI.5**) and indirectly synthesized the products of methane activation. The stability of the latter compounds indicates a substantial barrier of activation since the reaction with methane was predicted to be endergonic, which was confirmed by DFT analysis [$\Delta G^0(\Delta G^{\neq})$ of +15(302) kJ.mol^{-1}] at the PW6B95-D3(BJ)/def2-QZVP level while simulating the dichloromethane solvent with COSMO-RS.[40]

Later, Rincon *et al.* investigated the reactivity of two FLPs, **VI.6** and **VI.7**, based on $B(C_6F_5)_3$ or $Al(C_6F_5)_3$ in combination with P*t*Bu_3, for the dihydrogen and methane activations (Figure 32).[41] Given the similar bond dissociation energies for H_2 and CH_4 and the higher barrier of activation for the latter, they argued that the barrier was more structurally controlled than electronically controlled. They indeed showed that structural rearrangements, mainly of CH_4 and the Lewis acid, accounted for most of the activation barrier. They suggested to use Al-derived FLPs since they displayed lower reorganization energies and, subsequently, a lower barrier of activation than their boron counterparts, down to $\Delta G^0(\Delta G^{\neq})$ of -51(50) kJ.mol^{-1} [ωB97X-D/6–311++G(2d,2p), PCM-SMD scheme for toluene as solvent]. The key factors affecting this reaction highlighted in these reports were taken into account when designing our FLP system.

Other metal-free non-FLP systems were studied as well. In 2016, Ma and Li studied the potential of silylboranes for the activation of methane.[39] Using statistical methods and DFT [M06-2X/6-311+G(d,p)], they correlated the electronic properties of the silylboranes and their reactivity to show that the Lewis acidic boron center plays the major role in the reaction. More recently, Migliaro and Cundari studied the effects of periodicity with Lewis pairs of group 13 trihalides and group 15 pentahalides with ammonia as Lewis base for their reaction with methane.[42] In general, the reaction was favored with heavier elements. Activation energies could be correlated to DFT electronic ground states parameters through machine learning.

4. Design of the FLP system

Reducing activation barriers and reaction energies for the heterolytic splitting of methane can be achieved using intramolecular FLPs instead of intermolecular ones. This allows reducing a) the entropic penalty since it becomes a two-molecule process instead of three and b) the distortion of methane by avoiding the inversion of the $-CH_3$ moiety in the transition state.[38] Owing to its significantly lower reorganization energy upon reaction than other boron compounds, we based our FLP system on the 9-boratriptycene scaffold.[44] Then, since 9-boratriptycene derivatives have similar Lewis acidity as $B(C_6F_5)_3$ (see Annex I) no electron-withdrawing substituents were added to the scaffold to further increase it. A pyridine in *ortho*-position was considered as Lewis base. Nitrogen is more electronegative than carbon and bears a partial negative charge in the molecule on the contrary to its phosphorus analogue, so that the choice of pyridine as Lewis base should favor electrostatic interactions with the approaching partially positive hydrogens of the methane moiety.[37] These considerations allowed us to propose the 1-aza-9-boratriptycene **VI.3** as a conceptually simple and synthetically attainable FLP system for the activation of methane.

5. Computational method

Using the Gaussian16 package,[47] full geometry optimizations and vibrational frequency calculations were performed at the M06-2X/6-311G(d) level of theory.[48] The geometry optimizations were performed using tight convergence thresholds, *e.g.* for the residual forces on the atoms, 1.5×10^{-5} Hartree/Bohr or Hartree/radian. For each non transition state compound, all vibrational frequencies are real, demonstrating that the structures are minima on the potential energy surface. All transition state geometries were obtained by optimization to a saddle point using the Berny algorithm[49-52] and are characterized by a single imaginary frequency. The validity of all transition states was confirmed by performing intrinsic reaction coordinate calculations using the steepest descend approach, systematically leading to the products of methane activation and the isolated reactants. Solvent (cyclohexane) effects were modelled using the implicit solvation IEFPCM approach.[53] Gibbs free energy values, initially obtained considering a reference gas phase pressure of 1 atm were corrected to refer to a standard concentration of 1 $mol.L^{-1}$. Accordingly,

a correction of +7.90 kJ.mol^{-1} corresponding to RTln(24.46) is added to the first computed values.[54] Natural atomic orbital and natural bond orbital analyses were performed using the Gaussian NBO 3.1 program[55] at the M06-2X/6-311G(d) level of theory on the optimized structures in solvent. Reorganization or distortion energies (ΔE_{Dis}) were obtained by extracting the geometry of a given moiety (*i.e.* methane, Lewis acid or Lewis base) in the transition state, product, or at any point of the IRC, and performing a single point calculation to evaluate its total electronic energy and finally subtracting it to its equilibrium-geometry value. Interaction energies were then obtained by subtracting distortion energies to the total electronic energies:

$$\Delta E_{Int} = \Delta E - \Delta E_{Dis}$$

The autoDIAS tool developed by Svatunek and Houk was employed to perform the DIAS analysis along the reaction pathways.[56]

6. Results and discussion

6.1 Thermodynamics and kinetics of methane activation

The C-H bond activation of methane with the bifunctional system **VI.3** can occur *via* two distinct mechanisms, leading to the products **VI.3**-P1 and **VI.3**-P2 (Scheme 46). The reaction of methane activation was evaluated at the M06-2X/6-311G(d) level of theory (Table 17). Of the two possible products of

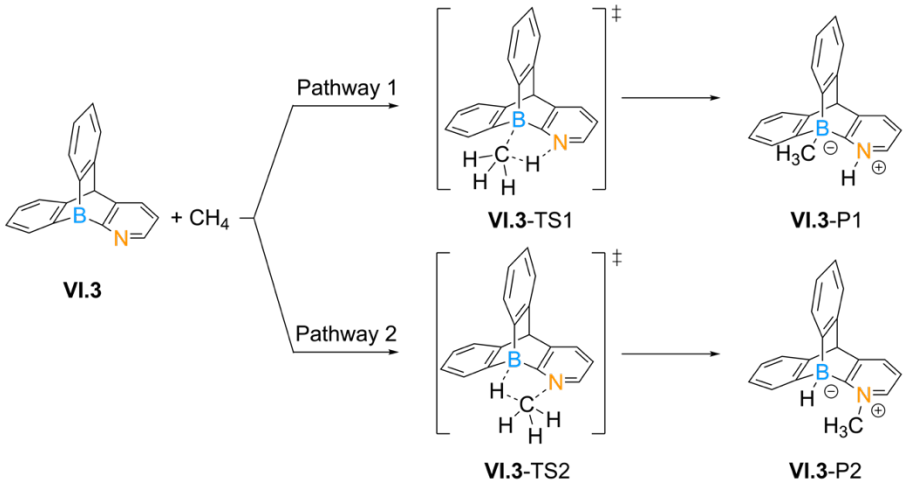

*Scheme 46. Methane C-H bond activation pathways with compound **VI.3**.*

methane splitting, **VI.3**-P1, corresponding to the formation of a formal methyl anion (with the nitrogen acting as a Brønsted base in the transition state, deprotonating the methane moiety) is favored over the competing **VI.3**-P2 product (ΔG^0 = -108 kJ.mol^{-1} *versus* -64 kJ.mol^{-1}). The reaction is exergonic at 25°C, with an expected entropic penalty and an exothermic process.

Kinetically, the formation of **VI.3**-P1 is also favored, with an activation barrier ($\Delta G^{\neq}$) of 76 kJ.mol^{-1} that is much smaller than its **VI.3**-P2 analogue (258 kJ.mol^{-1}). The corresponding transition state (**VI.3**-TS1, Figure 33) displays the methane moiety located in front of the boron atom (B-C distance of 1.799 Å) with an elongated C-H bond (1.354 Å) pointing towards the nitrogen atom (N-H distance of 1.400 Å). The transition state corresponding to the competing pathway (**VI.3**-TS2, Figure 33) displays the CH_3 formal methyl cation in front of the nitrogen atom, (N-C distance of 2.171 Å) with a B-H bond almost formed (B-H distance of 1.318 Å and C-H distance of 1.658 Å).

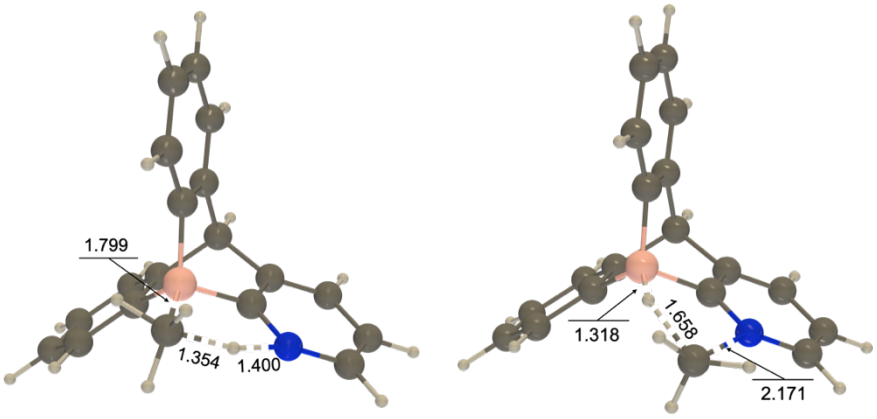

VI.3-TS1 **VI.3**-TS2

*Figure 33. Computed structures of the two transition states for the methane splitting reaction by 1-aza-9-boratriptycene **VI.3** and selected interatomic distances (in Å). Both transition states are characterized by a single imaginary frequency (1430i cm^{-1} and 1036i cm^{-1} for TS1 and TS2, respectively).*

The results obtained with this standard DFT scheme [M06-2X/6-311G(d)] were validated by comparing the energies and geometries of the same two reaction pathways with other calculation methods, including at the double-hybrid B2PLYP-D3/6-311+G(2d,p) level (see Annex I).

Table 17. Variation of electronic energies (ΔE, ΔE≠) and Gibbs free energies (ΔG⁰, ΔG≠) of methane splitting for both pathways as determined at the M06-2X/6-311G(d) level of theory in cyclohexane (IEFPCM) for several FLP systems. All energies are given in kJ.mol-1. P1 and TS1 refer to the product and transition state of the reactions where the P or N atom acts as a Brønsted base and deprotonates the methane moiety. P2 and TS2 refer to the product and the transition state of the competing reaction pathway where the B or Al atom abstracts a hydride from the methane.

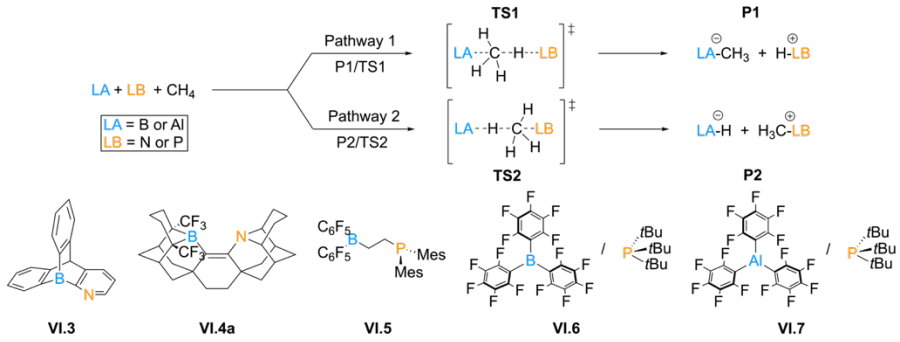

Pathway System	Global reaction			Transition states		
	ΔE	ΔG⁰	$\Delta G^{0}_{corr.}$ [a]	ΔE≠	ΔG≠	$\Delta G^{\neq}_{corr.}$ [a]
P1/TS1 **VI.3**	-156	-108		46	76	
P2/TS2 **VI.3**	-113	-64		227	258	
P1/TS1 **VI.4a**	-85	-24		43	86	
P2/TS2 **VI.4a**	24	87		287	331	
P1/TS1 **VI.5**	-35	13	55	120	158	199
P2/TS2 **VI.5**	-53	6	47	270	303	345
P1/TS1 **VI.6**	-62	22		89	162	
P2/TS2 **VI.6**	-111	-23		91	166	
P1/TS1 **VI.7**	-74	3	45	25	90	132
P2/TS2 **VI.7**	-83	-5	38	86	163	205

[a] $\Delta G^{0}_{corr.}$ and $\Delta G^{\neq}_{corr.}$ are the corrected values of Gibbs free energy for the systems where the adduct formation is spontaneous between the Lewis acid and the base. The ΔG⁰ of adduct formation (-42 kJ.mol-1 for system **VI.5** and -50 kJ.mol-1 for **VI.7**) is subtracted to the original ΔG⁰/ΔG≠ of methane splitting. System **6** has a positive ΔG⁰ of adduct formation (+21 kJ.mol-1) and was not corrected.

The 1-aza-9-boratriptycene system displays reaction and activation energies among the best reported so far by frustrated Lewis pairs (see above). However, direct comparison between results obtained with different computational methods can be misleading. For this reason, representative examples of FLP systems described in the literature (Figure 32) were computed at our standard

DFT level, M06-2X/6-311G(d), and evaluated for both reactions of heterolytic methane splitting (P1/TS1, P2/TS2, Table 17), allowing comparisons. As a matter of fact, 1-aza-9-boratriptycene **VI.3** turns out to be the best performing, both when Gibbs free energies of reaction and activation barriers are considered, even though system **VI.4a** gives similar results for the latter. Though the activation barriers and ΔG^0 reported above are higher than those reported in the literature, the same trends are drawn nonetheless (see Annex I).

For all systems, other antagonistic equilibria should be considered to achieve an overall description of the process. Here, in the case of Lewis acids and bases, the direct acid-base interaction should be taken into account. In the case of systems **VI.5** and **VI.7**, the Lewis adduct formation was found to be spontaneous: ΔG^0 of -42 kJ.mol^{-1} for system **VI.5**, -50 kJ.mol^{-1} for **VI.7,** and +21 kJ.mol^{-1} for **VI.6** (see Table S29 in Annex I). Since the most stable starting state of these systems (the 0 point, from which reaction energies are evaluated) are these Lewis adducts instead of the free Lewis acids and bases, the abovementioned values should be deducted from the ones reported in Table 17 to provide "corrected" values, $\Delta G^0_{corr.}$. The global reaction energies and the barriers of activation are in consequence increased. For system **VI.4a**, the intramolecular Lewis adduct is prevented, but another possibility for self-quenching is the formation of a dimer. Since this eventuality was already discussed and ruled out in the article of Wang *et al.*,[38] it was not investigated here. The same correction should be applied to the 1-aza-9-boratriptycene values since it is predicted to dimerize spontaneously. This reaction is discussed further below.

6.2 Natural charge analysis

A striking feature of the results shown in Table 17 is the difference in selectivity for the reaction pathway (P1/TS1 *versus* P2/TS2) between the FLP systems. The two N-based FLPs **VI.3** and **VI.4a** strongly favor the first pathway kinetically and thermodynamically while P-based FLPs **VI.5**, **VI.6** and **VI.7** favor the first kinetically, but the second thermodynamically. The thermodynamic selectivity for a given nature of Lewis base is attributed to their atomic charges. When comparing the natural charges of the Lewis acid/base sites and of the methane moiety at different stages of the reaction, one can see that the preferred pathway is that which allows favorable electrostatic interactions between partially positive and negative sites (Table 18). The strongest bonds are formed between atoms of opposite partial charges. The difference of selectivity is then explained

Table 18. Natural charge Q (times the fundamental charge e) of the Lewis acid/bases sites at different stages of the reaction with methane (transition states, products).

Pathway-System	Nature of the LB/LA		Natural charges (Q)					
			Free molecules[a]		Transition states			
	LB	LA	LB	LA	LB	LA	C	H
P1/TS1 **VI.3**	N	B	-0.47	0.99	-0.54	0.51	-1.03	0.46
P2/TS2 **VI.3**					-0.42	0.33	-0.32	0.03
P1/TS1 **VI.4a**	N	B	-0.58	1.26	-0.61	0.85	-0.98	0.45
P2/TS2 **VI.4a**					-0.46	0.46	-0.28	-0.02
P1/TS1 **VI.5**	P	B	0.82	0.99	1.04	0.62	-0.98	0.29
P2/TS2 **VI.5**					1.13	0.38	-0.50	0.05
P1/TS1 **VI.6**	P	B	0.85	0.89	1.06	0.65	-1.11	0.30
P2/TS2 **VI.6**					1.25	0.41	-0.62	0.05
P1/TS1 **VI.7**	P	Al	0.85	1.83	1.12	1.63	-1.27	0.24
P2/TS2 **VI.7**					1.29	1.50	-0.68	-0.16

Pathway-System	Nature of the LB/LA		Natural charges (Q)					
			Free molecules[a]		Products			
	LB	LA	LB	LA	LB	LA	C	H
P1/TS1 **VI.3**	N	B	-0.47	0.99	-0.47	0.34	-0.89	0.42
P2/TS2 **VI.3**					-0.34	0.05	-0.33	-0.02
P1/TS1 **VI.4a**	N	B	-0.58	1.26	-0.54	0.60	-0.96	0.52
P2/TS2 **VI.4a**					-0.37	0.24	-0.35	-0.05
P1/TS1 **VI.5**	P	B	0.82	0.99	1.35	0.46	-0.88	0.03
P2/TS2 **VI.5**					1.63	0.13	-0.92	-0.01
P1/TS1 **VI.6**	P	B	0.85	0.89	1.37	0.40	-0.88	0.05
P2/TS2 **VI.6**					1.75	0.08	-1.00	-0.01
P1/TS1 **VI.7**	P	Al	0.85	1.83	1.36	1.57	-1.22	0.05
P2/TS2 **VI.7**					1.75	1.34	-0.99	-0.39

[a] Natural charges of the free methane atoms: C = -0.79*e*; H = 0.20*e*.

by the electronegativity of the N or P atoms, the former being partially negative when linked to the less electronegative carbon atoms while the latter is partially positive. In addition, although electrostatic interactions are attractive both when B-C (or Al-C) and B-H (or Al-H) bonds are formed, the former situation remains more favorable than the latter.

6.3 Distortion/interaction-activation strain analysis

Electronic factors alone cannot wholly explain the reactivity however, especially for transition states, structural parameters must also be taken into account. They are even often considered as the main factor controlling the activation barrier. The DIAS model is a useful tool to investigate reaction barriers[57-58] and was recently employed in the investigations of other small molecules activation and FLP chemistry.[59-61] It decomposes the variations of the total electronic energy of the system along the reaction pathway as the sum of i) the distortion energy, or activation strain, required to modify the structure of the molecules to their transition state geometry, and of ii) the interaction energy. In this model, the transition state is defined as the point where the interaction energy overcomes the structural reorganization. The height of the transition state is determined by the balance between the two curves. An activation barrier can thus be lowered either by reducing the activation strain and/or by lowering the interaction energy curve. For all systems the DIAS model was computed along the reaction pathway and projected on the stretching distance of the breaking C-H bond. It is shown for the 1-aza-9-boratriptycene **VI.3** in Figure 34 while those of other systems are shown in the supporting information (Figure S47).

When comparing the curves of interaction (ΔE_{Int}) and distortion energies (ΔE_{Dis}) in Figure 34, one observes that ΔE_{Int} (green curves) is lower in P1/TS1 than in P2/TS2. On the other hand, the ΔE_{Dis} curves (in red) are closer to one another, but with the P1/TS1 being above the other, which corresponds to lower strain curves for the P2/TS2 pathway. This means that the second reaction pathway is associated with slightly less strain over the reaction mechanism than the first but with comparably even smaller stabilizing interactions, resulting in higher-energy reaction profile and transition state. Subsequently, TS1 happens at an earlier stage than TS2 in the reaction path. This is in agreement with the Hammond's postulate, stating that a more exergonic reaction will have an earlier-stage transition state and less exergonic or endergonic reactions will

have later-stage transition states and P1/TS1 is favored over P2/TS2 (ΔG^0 = -108 *versus* -64 kJ.mol^{-1}).[62]

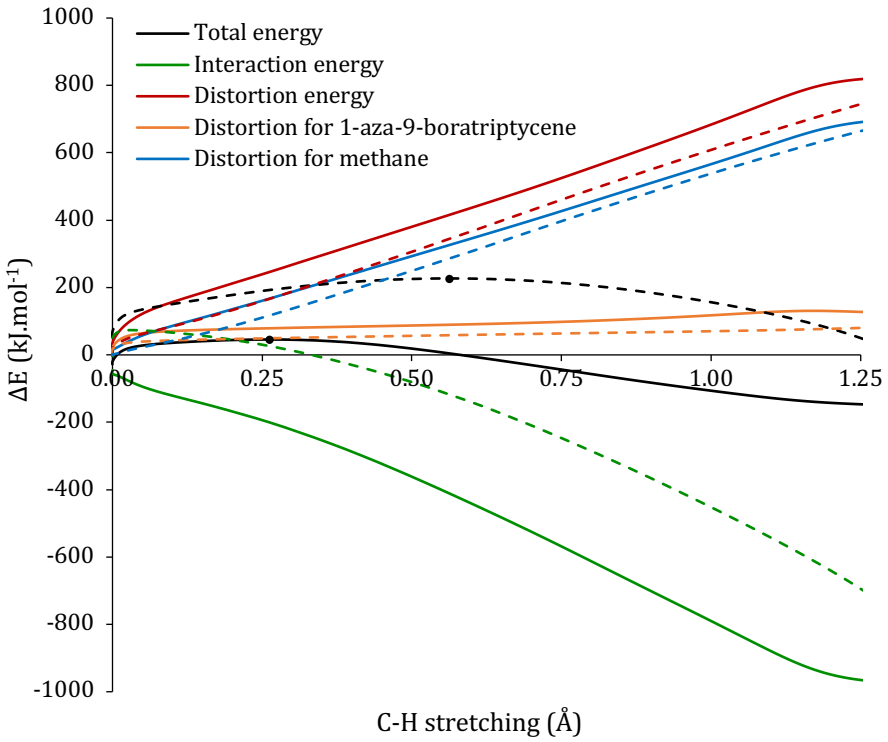

*Figure 34. Activation strain diagrams of system **VI.3** over the stretching distance of the C-H bond that is breaking in the methane activation for the first (P1/TS1, full line) and the second reaction pathway(P2/TS2, dashed). The dots indicate the position of the transition states.*

As for **VI.3** and **VI.4a**, all systems display a repulsive (>0) interaction energy in the first stages of the P2/TS2 pathway, which is consistent with partial charges repulsions, later compensated by stabilizing orbital overlaps. Further investigation of the main orbital interactions at the transition states was performed using a natural bond orbital analysis. The stabilization energy due to resonance effects, (*i.e.* correction energy due to donor-acceptor interactions between filled and vacant orbitals -"Lewis" and "non-Lewis" orbitals respectively in the NBO scheme-) was evaluated within the second-order perturbative analysis.[63-64] TS1 displays two main interactions, between i) the nitrogen lone pair (N LP, Figure 35) and an acceptor orbital located on the hydrogen H LP* (non-Lewis orbital consisting in its vacant *1s* orbital) and ii) between the same acceptor orbital (H LP*) and the neighboring B-C σ-bond. The latter is made

possible by the intramolecular character of **VI.3** that allows the side-on attack of the methane molecule. Similar interactions are present in TS2, although the acceptor orbital is located on the carbon atom of the methane moiety (C-LP*) and the σ-bond is between the boron and hydrogen (B-H).

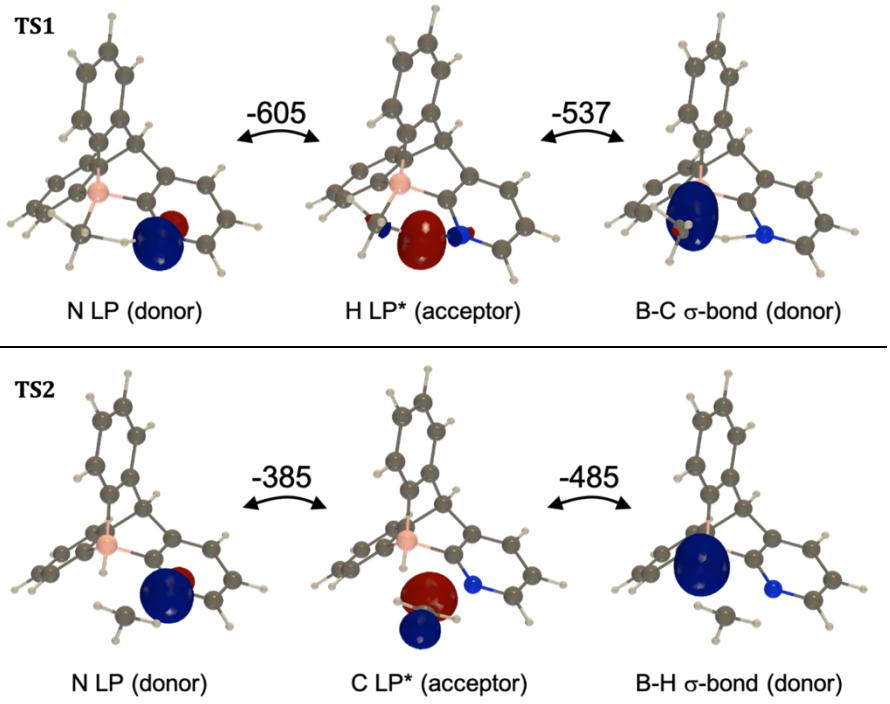

*Figure 35. Natural bond orbitals involved in the main donor-acceptor interactions in **VI.3**-TS1 and **VI.3**-TS2 and interaction energies in kJ.mol^{-1}. The * suffix indicates a non-Lewis (formally vacant) NBO. The LP label stand for Lone Pair. Isosurface value of 0.10 a.u. NBO superpositions showing the spatial overlaps are shown in supporting information.*

TS2 displays less stabilizing orbital overlaps than TS1. The BC σ-bond → H-LP* and BH σ-bond → C-LP* interactions are of similar stabilization energy (-537 *vs* -485 kJ.mol^{-1}) but the interaction of the nitrogen lone pair and the H/C acceptor orbital (LP*) is much more stabilizing in TS1 than TS2 (-605 *vs* -385 kJ.mol^{-1}). Weaker orbital interactions combined with repulsive electrostatic repulsions between the interacting atoms of TS2 (Table 18) explain the large difference of activation energy with TS1. The same trends are observed in other systems, with the main orbital interactions stabilizing TS1.

Putting in parallel these observations with DIAS diagrams projected over the intrinsic reaction coordinate centered on the TS (Figure S47) confirms that, for a given system, i) steeper (gentler) slopes of interaction are associated to earlier-

stage (later-stage) transition states, and ii) pulling lower (higher) the interaction curve or the distortion one results in lower-lying (higher-lying) transition states. So, less stabilizing interactions, translated in higher curves for the P2/TS2 pathway in all systems, is the main explanation behind its systematic higher activation barrier, even though this pathway is associated with slightly less strain. The only exception is for system **VI.6**, where differences in strain and interaction in both pathways compensate each other and similar barriers are observed. The lower TS1 for **VI.3** and **VI.4a** compared to other FLPs is attributed to the nature of the Lewis base, which allows attractive partial charges interactions and the better orbital overlap allowed by their intramolecular character (side-on attack). Both factors significantly lower the interaction energy curve compared to other systems. The only exception is for **7**-TS1, which has a lower activation barrier, resulting from a lower interaction energy curve (due to its high Lewis acidity, see Table S30) and slightly lower activation strain.

Table 19 further shows that the distortion energy of methane is the main contribution to the total distortion of the system for transition states and reaction energies. Furthermore, the strain associated to the Lewis acid is larger than that of the Lewis base.

For similar total distortion in reaction energies (between 806 and 828 kJ.mol^{-1} for **VI.3**, **VI.4a**, **VI.6** and **VI.7**), the lower total reaction energies, and thus higher stability of the products in **VI.3** compared to other systems is again attributed to its stronger interaction energy contribution. The latter is explained in part by the higher Lewis acidity of the boron site, which is enhanced during the reaction by the increasing inductive effect of the neighboring pyridinium formed (*i.e.* a positive charge close in space is generated), thus stabilizing the B-H bond. Indeed, the formally negative boron and positive nitrogen in the products for **VI.3** are separated by only one carbon atom, the inductive effect between the two is thus strong and further stabilizes them. As evidence of this phenomenon, the increase of several Lewis acidity descriptors of the boron atom before and after protonation of the pyridine in **VI.3** (see Table S30) can be put forward. One can also note that the LA/LB contribution to the distortion energy is lower to that of other boron compounds and is more similar to the aluminum Lewis acid [$Al(C_6F_5)_3$ in **VI.7**]. Alanes are generally known for having lower reorganization energies than boranes.[65] In this case, it is attributed to the non-planar character of the boron site in 9-boratriptycene derivatives.

*Table 19. Interaction and distortion energies of methane activation for the transition states and products of the **VI.3**, **VI.4a**, **VI.5**, **VI.6** and **VI.7** FLP systems along both reaction pathways. All quantities are electronic energies given in kJ.mol^{-1}. "Dis." stands for distortion energy; "Int." stands for interaction energy.*

Pathway-System	Transition states					
	Total	Int. total	Dis. total	Dis. CH_4	Dis. LA	Dis. LB
P1/TS1 **VI.3**	**46**	-201	246	167	79	
P2/TS2 **VI.3**	**227**	-117	344	286	58	
P1/TS1 **VI.4a**	**43**	-131	175	115	59	
P2/TS2 **VI.4a**	**287**	-104	391	320	71	
P1/TS1 **VI.5**	**120**	-171	290	190	101	
P2/TS2 **VI.5**	**270**	-90	359	254	106	
P1/TS1 **VI.6**	**89**	-123	211	130	73	8
P2/TS2 **VI.6**	**91**	-110	201	139	54	8
P1/TS1 **VI.7**	**25**	-210	235	172	50	14
P2/TS2 **VI.7**	**86**	-177	263	200	54	9
Pathway-System	Products					
	Total	Int. total	Dis. total	Dis. CH_4	Dis. LA	Dis. LB
P1/TS1 **VI.3**	**-156**	-984	828	709	119	
P2/TS2 **VI.3**	**-113**	-939	827	725	101	
P1/TS1 **VI.4a**	**-85**	-892	806	668	139	
P2/TS2 **VI.4a**	**24**	-811	835	675	160	
P1/TS1 **VI.5**	**-35**	-1049	1014	831	183	
P2/TS2 **VI.5**	**-53**	-1007	954	816	138	
P1/TS1 **VI.6**	**-62**	-884	822	641	133	47
P2/TS2 **VI.6**	**-111**	-938	827	664	132	31
P1/TS1 **VI.7**	**-74**	-882	808	673	88	46
P2/TS2 **VI.7**	**-83**	-895	812	697	83	32

6.4 Dimerization of 1-aza-9-boratriptycene

As mentioned earlier, the 1-aza-9-boratriptycene **VI.3** spontaneously dimerizes *via* the formation of two B-N bonds. The association is favored because the dimer adopts a staggered conformation of the compound which allows bimolecular interlocking with almost no steric constraint. In other words, this system lacks the high steric hindrance usually associated with FLPs. Without substituents, the dimerization is highly exergonic with a ΔG^0 of -472 kJ.mol^{-1}, which far exceeds that of methane splitting (-108 kJ.mol^{-1}). Adding substituents in *ortho*-position to the boron or nitrogen atoms can prevent the formation of dimers (Table 20) but also affects the reaction with methane. With this in mind, the ideal substituted 1-aza-9-boratriptycene will prevent the dimerization while unaffecting or having a positive impact on the activation.

A set of the substituted 1-aza-9-boratriptycene derivatives were thus subjected to calculations in order to assess their methane activation in comparison to their dimerization (Table 20). Other substituents and combinations were tested and are detailed in the supporting information. The addition of one substituent in *ortho*-position to the pyridine (R^1) does not significantly affect the energies of methane activation but the ΔG^0 of dimerization is reduced by ~150-170 kJ.mol^{-1}. Significant differences are observed for one or two additional substituents on the aryl rings (R^2, R^3). *Tert*-butyl (*t*Bu) groups have a strong deactivating effect on both dimerization and methane activation. This energy penalty for the latter is attributed to the large structural deformation (increase in B-C_{Me} bond and dihedral NCB-C_{Me} angle) brought by the *t*Bu group (see Annex I). On the other hand, mesityl (Mes) groups have almost no impact (or even a slightly positive one) on $\Delta G^{\neq}_{methane}$ and a minor effect on $\Delta G^{0}_{methane}$ when multiple groups are added while, in parallel, they completely prevent dimerization with three groups. To summarize, the 1-aza-9-boratriptycene with three mesityl groups grafted in *ortho*-position of the boron and nitrogen is the ideal candidate to activate the methane molecule without self-quenching.

Table 20. Gibbs free energy of dimerization ($\Delta G^{0}_{dimer.}$, in kJ.mol^{-1}) for 1-aza-9-boratriptycene derivatives at the M06-2X/6-311G(d) IEFPCM (cyclohexane) level of theory compared to Gibbs free energy of activation and reaction of/with methane ($\Delta G^{\neq}_{methane}$ and $\Delta G^{0}_{methane}$, in kJ.mol^{-1}). Mes = mesityl or 2,4,6-trimethylphenyl.

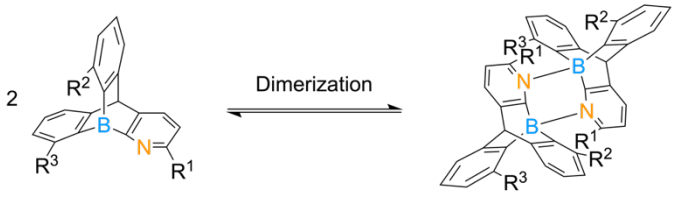

Entry	R^1	R^2	R^3	$\Delta G^{0}_{dimer.}$	$\Delta G^{0}_{methane}$	$\Delta G^{\neq}_{methane}$
1 (**VI.3**)	H	H	H	-472	-108	76
2	Mes	H	H	-319	-112	72
3	*t*Bu	H	H	-295	-105	76
[a]4	H	Mes	H	-487	-102	74
[a]5	H	*t*Bu	H	-310	-38	134
[a]6	Mes	Mes	H	-226	-108	69
[a]7	*t*Bu	*t*Bu	H	-116	-37	131
8	H	Mes	Mes	-399	-85	79
9	H	*t*Bu	*t*Bu	-123	48	207
10	Mes	Mes	Mes	110	-97	77
11	*t*Bu	*t*Bu	*t*Bu	203	46	204

[a] With different R^2 and R^3 substituents on the triptycene scaffold, it becomes chiral, with two enantiomers A and B, leading to two possible dimers (AA or AB, BB is ignored), both were computed and the most stable is reported here.

The DIAS analysis of the first pathway of methane activation by compound **VI.10** was compared to that of compound **VI.3** (Figure 36). The differences between the respective strain and interaction curves are small and compensate each other, resulting in almost superimposed total energy curves.

The small increase in distortion in **VI.10** may be attributed in part to the breaking of stabilizing π-π stacking between mesityl groups present in the starting compound while the slightly lower interaction curve is attributed to new C-H/π interactions between the methane and the mesityl groups (Figure 37).

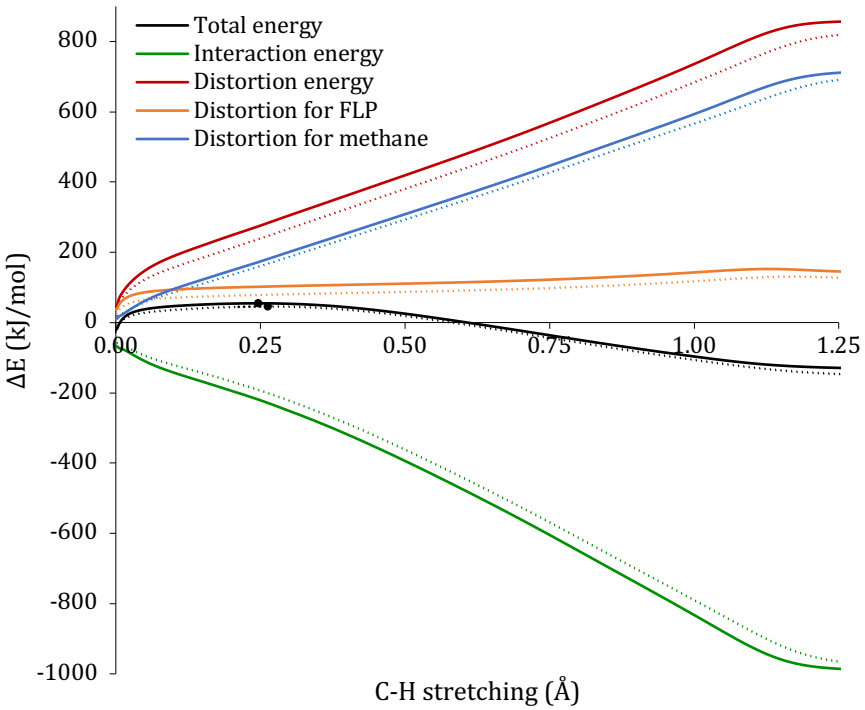

*Figure 36. Activation strain diagrams of system **VI.10** (full lines) and system **VI.3** (dashed lines) over the stretching distance of the C-H bond that is breaking in the first reaction pathway of methane activation (P1/TS1). The dots indicate the position of the transition states.*

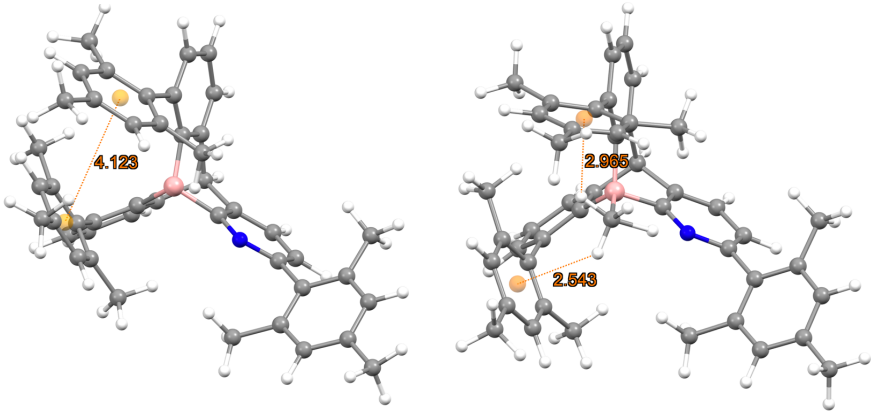

10 **10**-TS1

*Figure 37. Optimized structures of FLP **VI.10** and **VI.10**-TS1. The yellow dots indicate the positions of the centroids of the planes. The structures suggest the presence of π-π stacking in **VI.10** and C-H/π interactions in **VI.10**-TS1 allowed by the addition of mesityl groups. Distances indicated in Ångström.*

7. Conclusions and outlooks

In summary, DFT [M06-2X/6-311G(d)] calculations have demonstrated that the new 1-aza-9-boratriptycene **VI.3** is a conceptually simple FLP system capable of activating methane. This molecule was confronted to a representative selection of FLP systems reported previously in the literature and all now computed with the same DFT method, demonstrating its better performance. Systematic comparisons of the thermodynamics and kinetics (global reaction energies and activation barriers) of methane activation, natural charges and distortion/interaction or activation strain analysis along the reaction pathway enabled to detect patterns in their reactivity toward the methane moiety. In particular, the selectivity of the reaction toward methane (both possible products) depends on the nature of the Lewis base, nitrogen or phosphorus. Due mainly to electrostatic interactions between the system and methane, N Lewis bases favor the deprotonation mechanism via formal methyl anion formation while P Lewis bases favor hydride abstraction *via* formal methyl cation formation. In addition, the high performance of FLP system **VI.3** for methane activation is due to a) the non-planar character of the boron center that increases its Lewis acidity without the need for electron-withdrawing groups, b) the N Lewis base that allows stabilizing electrostatic interactions with methane, c) the side-on attack of the FLP due to its intramolecular nature, enabling better orbital overlaps, and d) the proximity in space between the N and the B in **VI.3** that increases the stability of the product by inductive effects. Finally, a screening of *ortho*-substituents was undertaken to prevent self-quenching of **VI.3** by dimerization, the determined ideal system being the mesityl-substituted one, completely preventing dimerization while almost unaffecting the methane activation.

From an applied perspective, the 1-aza-9-boratriptycene is an interesting system because 9-boratriptycene derivatives were recently synthesized by us.[43-44] The parent 9-boratriptycene was developed by a synthetic strategy based on the formation of halogenated triarylmethanes, the crucial step being Friedel-Crafts reactions that are in principle compatible with pyridines, yielding potential precursors to **VI.3**.[44] We thus consider **VI.3** as a synthetically attainable compound.

On a more fundamental level, this work is a proof-of-concept that high reactivities needed to activate inert molecules such as methane, traditionally

restricted to the domain of metals, is already reachable with only the most fundamental elements H, B, C, and N and conceptually simple structures, without needing further electron-withdrawing groups. In this case, such a reactivity can be obtained by combining multiple factors including distortion, electronic, electrostatic and the synergistic effect of neighboring Lewis acid and base that is unique to frustrated Lewis pair chemistry.

With these results in hand, we are currently devoting efforts to develop a viable synthesis of 1-aza-9-boratriptycene and *ortho*-substituted derivatives for the experimental activation of methane.

8. References

[1] G. N. Lewis, *Valence and the structure of atoms and molecules*, American Chemical Society, **1923**.

[2] F. A. Carey, R. J. Sundberg, *Advanced organic chemistry - Part A: Structure and mechanisms*, 5th ed., Springer, New-York, **2007**.

[3] A. Corma, H. Garcia, "Lewis acids: from conventional homogeneous to green homogeneous and heterogeneous catalysis", *Chem. Rev.* **2003**, *103*, 4307-4365.

[4] S. E. Denmark, G. L. Beutner, "Lewis base catalysis in organic synthesis", *Angew. Chem. Int. Ed.* **2008**, *47*, 1560-1638.

[5] G. C. Welch, R. R. San Juan, J. D. Masuda, D. W. Stephan, "Reversible, metal-free hydrogen activation", *Science* **2006**, *314*, 1124-1126.

[6] P. A. Chase, G. C. Welch, T. Jurca, D. W. Stephan, "Metal-free catalytic hydrogenation", *Angew. Chem. Int. Ed.* **2007**, *46*, 8050-8053.

[7] G. C. Welch, D. W. Stephan, "Facile heterolytic cleavage of dihydrogen by phosphines and boranes", *J. Am. Chem. Soc.* **2007**, *129*, 1880-1881.

[8] D. W. Stephan, ""frustrated Lewis pairs": A concept for new reactivity and catalysis", *Org. Biomol. Chem.* **2008**, *6*, 1535-1539.

[9] D. W. Stephan, "The broadening reach of frustrated Lewis pair chemistry", *Science* **2016**, *354*, 1248-1256.

[10] C. M. Mömming, E. Otten, G. Kehr, R. Fröhlich, S. Grimme, D. W. Stephan, G. Erker, "Reversible metal-free carbon dioxide binding by frustrated Lewis pairs", *Angew. Chem. Int. Ed.* **2009**, *48*, 6643-6646.

[11] E. Otten, R. C. Neu, D. W. Stephan, "Complexation of nitrous oxide by frustrated Lewis pairs", *J. Am. Chem. Soc.* **2009**, *131*, 9918-9919.

[12] A. J. P. Cardenas, B. J. Culotta, T. H. Warren, S. Grimme, A. Stute, R. Fröhlich, G. Kehr, G. Erker, "Capture of NO by a frustrated Lewis pair: a new type of persistent N-oxyl radical", *Angew. Chem. Int. Ed.* **2011**, *50*, 7567-7571.

[13] M. Sajid, A. Klose, B. Birkmann, L. Liang, B. Schirmer, T. Wiegand, H. Eckert, A. J. Lough, R. Fröhlich, C. G. Daniliuc, S. Grimme, D. W. Stephan, G. Kehr, G. Erker,

"Reactions of phosphorus/boron frustrated Lewis pairs with SO_2", *Chem. Sci.* **2013**, *4*, 213-219.

[14] D. W. Stephan, G. Erker, "Frustrated Lewis pair chemistry of carbon, nitrogen and sulfur oxides", *Chem. Sci.* **2014**, *5*, 2625-2641.

[15] T. A. Rokob, A. Hamza, A. Stirling, T. Soós, I. Pápai, "Turning frustration into bond activation: A theoretical mechanistic study on heterolytic hydrogen splitting by frustrated Lewis pairs", *Angew. Chem. Int. Ed.* **2008**, *47*, 2435-2438.

[16] T. A. Rokob, A. Hamza, I. Pápai, "Rationalizing the reactivity of frustrated Lewis pairs: Thermodynamics of H_2 activation and the role of acid–base properties", *J. Am. Chem. Soc.* **2009**, *131*, 10701-10710.

[17] T. Wiegand, H. Eckert, O. Ekkert, R. Fröhlich, G. Kehr, G. Erker, S. Grimme, "New insights into frustrated Lewis pairs: Structural investigations of intramolecular phosphane–borane adducts by using modern solid-state NMR techniques and DFT calculations", *J. Am. Chem. Soc.* **2012**, *134*, 4236-4249.

[18] L. Greb, P. Oña-Burgos, B. Schirmer, S. Grimme, D. W. Stephan, J. Paradies, "Metal-free catalytic olefin hydrogenation: Low-temperature H_2 activation by frustrated Lewis pairs", *Angew. Chem. Int. Ed.* **2012**, *51*, 10164-10168.

[19] G. Erös, K. Nagy, H. Mehdi, I. Pápai, P. Nagy, P. Király, G. Tárkányi, T. Soõs, "Catalytic hydrogenation with frustrated Lewis pairs: Selectivity achieved by size-exclusion design of Lewis acids", *Chem. Eur. J.* **2012**, *18*, 574-585.

[20] T. A. Rokob, I. Papai, "Hydrogen activation by frustrated Lewis pairs: insights from computational studies", *Top. Curr. Chem.* **2013**, *332*, 157-212.

[21] L. L. Zeonjuk, N. Vankova, A. Mavrandonakis, T. Heine, G.-V. Röschenthaler, J. Eicher, "On the mechanism of hydrogen activation by frustrated Lewis pairs", *Chem. Eur. J.* **2013**, *19*, 17413-17424.

[22] L. Greb, S. Tussing, B. Schirmer, P. Oña-Burgos, K. Kaupmees, M. Lõkov, I. Leito, S. Grimme, J. Paradies, "Electronic effects of triarylphosphines in metal-free hydrogen activation: a kinetic and computational study", *Chem. Sci.* **2013**, *4*, 2788.

[23] É. Dorkó, B. Kótai, T. Földes, Á. Gyömöre, I. Pápai, T. Soós, "Correlating electronic and catalytic properties of frustrated Lewis pairs for imine hydrogenation", *J. Organomet. Chem.* **2017**, *847*, 258-262.

[24] J. J. Cabrera-Trujillo, I. Fernandez, "Influence of the Lewis acid/base pairs on the reactivity of geminal E-CH_2-E' frustrated Lewis pairs", *Chemistry* **2018**, *24*, 17823-17831.

[25] N. A. Sitte, M. Bursch, S. Grimme, J. Paradies, "Frustrated Lewis pair catalyzed hydrogenation of amides: halides as active Lewis base in the metal-free hydrogen activation", *J. Am. Chem. Soc.* **2019**, *141*, 159-162.

[26] G. Sharma, P. D. Newman, J. A. Platts, "A review of quantum chemical studies of frustrated Lewis pairs", *J. Mol. Graphics Modell.* **2021**, *105*, 107846.

[27] J. Lam, K. M. Szkop, E. Mosaferi, D. W. Stephan, "FLP catalysis: main group hydrogenations of organic unsaturated substrates", *Chem. Soc. Rev.* **2019**, *48*, 3592-3612.

[28] B. Conley, W. J. I. Tenn, K. J. H. Young, S. Ganesh, S. Meier, J. Oxgaard, J. Gonzales, W. A. I. Goddard, R. A. Periana, "Methane functionalization" in *Activation of Small*

Molecules: Organometallic and Bioinorganic Perspectives (Ed.: W. B. Tolman), Wiley-VCH, Weiheim, **2006**, 382.

[29] P. Smith, D. Reay, A. Van Amstel, *Methane and climate change*, Earthscan, London, **2010**.

[30] E. McFarland, "Chemistry. Unconventional chemistry for unconventional natural gas", *Science* **2012**, *338*, 340-342.

[31] P. Tang, Q. Zhu, Z. Wu, D. Ma, "Methane activation: the past and future", *Energy Environ. Sci.* **2014**, *7*, 2580-2591.

[32] N. J. Gunsalus, A. Koppaka, S. H. Park, S. M. Bischof, B. G. Hashiguchi, R. A. Periana, "Homogeneous functionalization of methane", *Chem. Rev.* **2017**, *117*, 8521-8573.

[33] R. A. Periana, D. J. Taube, S. Gamble, H. Taube, T. Satoh, H. Fujii, "Platinum catalysts for the high-yield oxidation of methane to a methanol derivative", *Science* **1998**, *280*, 560-564.

[34] A. K. Cook, S. D. Schimler, A. J. Matzger, M. S. Sanford, "Catalyst-controlled selectivity in the C-H borylation of methane and ethane", *Science* **2016**, *351*, 1421-1424.

[35] K. T. Smith, S. Berritt, M. González-Moreiras, S. Ahn, M. R. Smith, M. H. Baik, D. J. Mindiola, "Catalytic borylation of methane", *Science* **2016**, *351*, 1424-1427.

[36] S. Ahn, D. Sorsche, S. Berritt, M. R. Gau, D. J. Mindiola, M.-H. Baik, "Rational Design of a Catalyst for the Selective Monoborylation of Methane", *ACS Catal.* **2018**, *8*, 10021-10031.

[37] H. Li, L. Zhao, G. Lu, Y. Mo, Z. X. Wang, "Insight into the relative reactivity of "frustrated Lewis pairs" and stable carbenes in activating H_2 and CH_4: a comparative computational study", *Phys. Chem. Chem. Phys.* **2010**, *12*, 5268-5275.

[38] G. Lu, L. Zhao, H. Li, F. Huango, Z. X. Wang, "Reversible heterolytic methane activation of metal-free closed-shell molecules: A computational proof-of-principle study", *Eur. J. Inorg. Chem.* **2010**, *15*, 2254-2260.

[39] G. Ma, Z. H. Li, "Methane activation by metal-free Lewis acid centers only - A computational design and mechanism study", *Phys. Chem. Chem. Phys* **2016**, *18*, 11539-11549.

[40] S. Frömel, C. G. Daniliuc, C. Bannwarth, S. Grimme, K. Bussmann, G. Kehr, G. Erker, "Indirect synthesis of a pair of formal methane activation products at a phosphane/borane frustrated Lewis pair", *Dalton Trans.* **2016**, *45*, 19230-19233.

[41] N. Villegas-Escobar, A. Toro-Labbé, M. Becerra, M. Real-Enriquez, J. R. Mora, L. Rincon, "A DFT study of hydrogen and methane activation by $B(C_6F_5)_3$/P(t-Bu)$_3$ and $Al(C_6F_5)_3$/P(t-Bu)$_3$ frustrated Lewis pairs", *J. Mol. Model.* **2017**, *23*.

[42] I. Migliaro, T. R. Cundari, "Density functional study of methane activation by frustrated Lewis pairs with group 13 trihalides and group 15 pentahalides and a machine learning analysis of their barrier heights", *J. Chem. Inf. Model.* **2020**, *60*, 4958-4966.

[43] A. Ben Saida, A. Chardon, A. Osi, N. Tumanov, J. Wouters, A. I. Adjieufack, B. Champagne, G. Berionni, "Pushing the Lewis acidity boundaries of boron compounds with non-planar triarylboranes derived from triptycenes", *Angew. Chem. Int. Ed.* **2019**, *58*, 16889-16893.

[44] A. Chardon, A. Osi, D. Mahaut, T. H. Doan, N. Tumanov, J. Wouters, L. Fusaro, B. Champagne, G. Berionni, "Controlled generation of 9-boratriptycene by Lewis adduct dissociation: Accessing a non-planar triarylborane", *Angew. Chem. Int. Ed.* **2020**, *59*, 12402-12406.

[45] W. J. van Zeist, F. M. Bickelhaupt, "The activation strain model of chemical reactivity", *Org. Biomol. Chem.* **2010**, *8*, 3118-3127.

[46] Y. X. Ma, C. F. Chen, *Iptycenes chemistry: from synthesis to applications*, Springer-Verlag, Berlin, **2013**.

[47] M. J. Frisch, G. W. Trucks, H. B. Schlegel, G. E. Scuseria, M. A. Robb, J. R. Cheeseman, G. Scalmani, V. Barone, G. A. Petersson, H. Nakatsuji, X. Li, M. Caricato, A. V. Marenich, J. Bloino, B. G. Janesko, R. Gomperts, B. Mennucci, H. P. Hratchian, J. V. Ortiz, A. F. Izmaylov, J. L. Sonnenberg, D. Williams-Young, F. Ding, F. Lipparini, F. Egidi, J. Goings, B. Peng, A. Petrone, T. Henderson, D. Ranasinghe, V. G. Zakrzewski, J. Gao, N. Rega, G. Zheng, W. Liang, M. Hada, M. Ehara, K. Toyota, R. Fukuda, J. Hasegawa, M. Ishida, T. Nakajima, Y. Honda, O. Kitao, H. Nakai, T. Vreven, K. Throssell, J. A. Montgomery, Jr., J. E. Peralta, F. Ogliaro, M. J. Bearpark, J. J. Heyd, E. N. Brothers, K. N. Kudin, V. N. Staroverov, T. A. Keith, R. Kobayashi, J. Normand, K. Raghavachari, A. P. Rendell, J. C. Burant, S. S. Iyengar, J. Tomasi, M. Cossi, J. M. Millam, M. Klene, C. Adamo, R. Cammi, J. W. Ochterski, R. L. Martin, K. Morokuma, O. Farkas, J. B. Foresman, D. J. Fox, *Gaussian 16, Revision A.03*, Gaussian Inc., Wallingford CT, **2016**.

[48] Y. Zhao, D. G. Truhlar, "The M06 suite of density functionals for main group thermochemistry, thermochemical kinetics, noncovalent interactions, excited states, and transition elements: Two new functionals and systematic testing of four M06-class functionals and 12 other functionals", *Theor. Chem. Acc.* **2008**, *120*, 215-241.

[49] C. Peng, P. Y. Ayala, H. B. Schlegel, M. J. Frisch, "Using redundant internal coordinates to optimize equilibrium geometries and transition states", *J. Comput. Chem.* **1996**, *17*, 49-56.

[50] P. Pulay, G. Fogarasi, "Geometry optimization in redundant internal coordinates", *J. Chem. Phys.* **1992**, *96*, 2856-2860.

[51] P. Pulay, G. Fogarasi, F. Pang, J. E. Boggs, "Systematic *ab initio* gradient calculation of molecular geometries, force constants, and dipole moment derivatives", *J. Am. Chem. Soc.* **1979**, *101*, 2550-2560.

[52] X. Li, M. J. Frisch, "Energy-represented direct inversion in the iterative subspace within a hybrid geometry optimization method", *J. Chem. Theory Comput.* **2006**, *2*, 835-839.

[53] J. Tomasi, B. Mennucci, R. Cammi, "Quantum mechanical continuum solvation models", *Chem. Rev.* **2005**, *105*, 2999-3094.

[54] C. P. Kelly, C. J. Cramer, D. G. Truhlar, "SM6: A Density Functional Theory Continuum Solvation Model for Calculating Aqueous Solvation Free Energies of Neutrals, Ions, and Solute-Water Clusters", *J. Chem. Theory Comput.* **2005**, *1*, 1133-1152.

[55] E. D. Glendening, A. E. Reed, J. E. Carpenter, F. Weinhold, *NBO Version 3.1*, Gaussian Inc., Pittsburgh, **2003**.

[56] D. Svatunek, K. N. Houk, "autoDIAS: a python tool for an automated distortion/interaction activation strain analysis", *J. Comput. Chem.* **2019**, *40*, 2509-2515.

[57] F. M. Bickelhaupt, K. N. Houk, "Analyzing reaction rates with the distortion/interaction-activation strain model", *Angew. Chem. Int. Ed.* **2017**, *56*, 10070-10086.

[58] I. Fernandez, F. M. Bickelhaupt, "The activation strain model and molecular orbital theory: understanding and designing chemical reactions", *Chem. Soc. Rev.* **2014**, *43*, 4953-4967.

[59] D. Yepes, P. Jaque, I. Fernandez, "Deeper insight into the factors controlling H_2 activation by geminal aminoborane-based frustrated Lewis pairs", *Chem. Eur. J.* **2016**, *22*, 18801-18809.

[60] D. Yepes, P. Jaque, I. Fernandez, "Hydrogenation of multiple bonds by geminal aminoborane-based frustrated Lewis pairs", *Chem. Eur. J.* **2018**, *24*, 8833-8840.

[61] P. Vermeeren, M. T. Doppert, F. M. Bickelhaupt, T. A. Hamlin, "How metallylenes activate small molecules", *Chem. Sci.* **2021**, *12*, 4526-4535.

[62] G. Hammond, "A correlation of reaction rates", *J. Am. Chem. Soc.* **1955**, *77*, 334-338.

[63] F. Weinhold, C. R. Landis, "Resonance delocalization corrections" in *Discovering chemistry with natural bond orbitals*, Wiley, Hoboken, NJ, **2012**.

[64] F. Weinhold, C. R. Landis, "Natural resonance structures and weightings" in *Valency and Bonding - A Natural Bond Orbital Donor-Acceptor Perspective*, Cambridge University Press, New-York, **2005**.

[65] A. Chardon, A. Osi, D. Mahaut, A. Ben Saida, G. Berionni, "Non-planar boron Lewis acids taking the next step: Development of tunable Lewis acids, Lewis superacids and bifunctional catalysts", *Synlett* **2020**, *31*, 1639-1648.

Summary, conclusions, and perspectives

Frustrated Lewis pair (FLP) chemistry has provided new prospects in the investigation and the application of main group elements in transition-metal-free catalysis. The aim of this PhD was to develop and study the properties and applications in FLP chemistry of a promising class of phosphines, the weakly basic 9-phosphatriptycenes. To this end, experimental and computational chemistry [in the form of density functional theory (DFT) calculations] were combined, giving a deeper understanding of the studied processes and allowing to establish new structure-reactivity relationships. In addition, quantum chemical investigations on the reactivity of "non-classical" triarylboranes were undertaken, as support to the work of experimental chemists in our research group. This study focused mainly on the 9-boratriptycene derivatives, aiming at explaining the unique reactivity observed experimentally of these compounds and probe their potential application in FLP chemistry.

The backbone of this thesis is the publication of several scientific papers in peer-reviewed journals, constituting the chapters of the manuscript, with one exception for the fourth chapter, on fluorophosphonium ions, paving the way to future research on 9-phosphatriptycene chemistry.

The first chapter of this manuscript describes the development of a new synthesis of *ortho*-functionalized 9-phosphatriptycenes. Expanding from a previous report in our group on the parent unsubstituted 9-phosphatriptycene,[1] a collaborative work with Dr. Lei Hu led to the report of a five-step approach to the first examples of *ortho*-substituted 9-phosphatriptycenes. The new compounds are featuring one or two functional groups, with either electron-withdrawing or -donating ability. This synthetic strategy is based on pre-functionalized triarylmethane precursors (*i.e.* bearing the final *ortho*-substituents from the first step of the synthesis), only introducing the phosphorus bridgehead atom in the last step. This convenient synthesis solved the problem that had long been hampering research on 9-phosphatriptycenes, which is the difficulty to produce them. It was thus a prerequisite for any further research on this topic. The general character of this method even allows to easily expand the scope of substituents or heteroelements beyond the ones reported, if one wishes so, since the reaction conditions are suitable for both electron-withdrawing and donating substituents and tolerates bulky groups.

The second chapter reports a fundamental investigation of the reactivity of 9-phosphatriptycenes, shedding light on the origins of their weak basicity. The triptycene scaffold forces the phosphorus atom into a more pyramidalized

geometry, increasing the *3s* character of its lone pair and, consequently, decreasing its energy and reactivity. The lowering of basicity was evidenced with the prediction of their pK_a. The Brønsted acidity of their conjugate phosphonium cation is an appropriate parameter to consider in the context of FLP-catalyzed hydrogenations, since it is that species that reacts with unsaturated substrates. An accurate predictive tool of phosphine pK_a's was developed, combining DFT calculations with experimental data from the literature and it showed that 9-phosphatriptycenes are significantly more deactivated phosphines than their classical triarylphosphine analogues only due to their cage-shaped structure. Their low pK_a's make these compounds ideal candidates for the FLP-catalyzed hydrogenation of challenging substrates, which is the topic of the following chapter. Beyond its application to this work, the development of this predictive method for pK_a's was built from a training set of experimentally known phosphines and was shown to be accurate over a large range of pK_a values, both in water and acetonitrile. It is thus also suitable for any phosphine outside of the 9-phosphatriptycene family and could prove a handy tool for researchers beyond the scope of this work.

Then, in the third chapter, we investigated the application of 9-phosphatriptycenes to the FLP-catalyzed hydrogenation of unactivated alkenes. Their low basicity and high thermal stability were taken advantage of for the hydrogenation of these challenging olefinic substrates, which constituted a limitation in the current scope of FLP-catalyzed reactions. *Ortho*-substituted 9-phosphatriptycenes featuring an electron-withdrawing substituent like the chlorine atom are ideal Lewis bases in this context, their steric hindrance preventing adduct formation with the $B(C_6F_5)_3$ Lewis acid while the high reactivity of their conjugate phosphonium allows reacting with the stable carbon-carbon double bond. Optimization of the reaction conditions led to hydrogenations of unactivated olefins in moderate to good yields with hydrogen pressures up to 40 bar and at 150°C. Finding alternatives to transition-metal catalysts is a major societal issue, mainly because of their depleting resources, increasing cost, and toxicity. The development of new reactions by exploiting the reactivity induced by original scaffolds such as the triptycene also contributes to expanding the scope of main group chemistry, both at the fundamental (structure-property relationships) and applied (new hydrogenation reactions) levels.

The chemistry of 9-phosphatriptycenes, as investigated in this PhD thesis, ends with the fourth chapter, that probes the reactivity of a new family of compounds, the difluoro-9-phosphoranetriptycenes and the fluoro-9-phosphonium-triptycenes cations. The chapter aims at opening a new avenue for future research on 9-phosphatriptycenes. This study started with a question: can the triptycene scaffold prevent a Lewis acidic behavior of fluorophosphonium cations derived from 9-phosphatriptycene and, consequently, allow their use as electrophilic fluorinating agents? Using an adapted reported procedure,[2] the first 9-phosphatriptycene-based difluorophosphoranes and fluorophosphonium cations were prepared and their structure discussed. While further research is needed to state on the actual Lewis character of the fluorophosphonium salt, strong evidence of their fluorinating ability on electron-rich arylphosphines was given when the Lewis adduct formation and side reactions are prevented. It is a first proof of concept that P-F derivatives can be used as fluorinating agents, when this reactivity typically belonged to N-F compounds. More experimentation on this topic will be undertaken in our research group in the future.

The last two chapters of the manuscript describe quantum chemical investigations on "non-classical" boranes, carried out in collaboration with other group members who focus on experimental chemistry. In line with the 9-phosphatriptycene chemistry described in the first four chapters, the goal on these investigations was always to extend our understanding of chemical reactivity and the unique electronic properties of these compounds induced by their scaffold.

The fifth chapter focuses on the 9-boratriptycene family of compounds and the "semi-planar" boranes. Forcing the boron atom outside of its classical trigonal planar structure significantly affects its reactivity. Notably, 9-boratriptycene derivatives mainly owe their reactivity to a decrease of their reorganization energy upon binding with Lewis bases. As a result, their Lewis acidity can be comparable or higher than that of strongly acidic boranes such as $B(C_6F_5)_3$. Other factors partially account for their reactivity as well, including the lack of conjugation between the formally empty $2p_B$ orbital and the neighboring π-system of the aryl rings and the insertion of an electron-withdrawing sulfonium cation in bridgehead position. In addition to rationalize the reactivity observed experimentally with these compounds, this fundamental research broadens our global understanding of chemical reactivity and the steric and electronic factors

that account for it, even outside the family of 9-bora-(or 9-phospha-)triptycenes, and is useful for the whole research community.

The final chapter dives into the potential application of a 9-boratriptycene-derived bifunctional system for the activation of methane. The activation and conversion of the latter into value-added products is another major goal of modern research worldwide and a great challenge of main group chemistry. Studied by DFT, the 1-aza-9-boratriptycene was predicted to be capable of activating methane and to outperform other FLP systems reported in the literature. The reactivity with methane was investigated in detail, with a systematic comparison of the thermodynamics and kinetics of reaction with the other systems. Interestingly, it was shown that the selectivity of the reaction toward methane is dictated by the nature of the Lewis base used (*e.g.* N or P), which constitutes a major point for the development of future catalytic systems outside of this work. The performance of the 1-aza-9-boratriptycene was due mainly to its non-planar character, as it is a member of the 9-boratriptycene family, but also to stabilizing electrostatic interactions due to the presence of the nitrogen atom and the side-on attack on methane made possible by the intramolecular character of this FLP. Finally, a screening of *ortho*-substituents on the 1-aza-9-boratriptycene was undertaken to guide future synthetic work toward a fully functional methane-activating system. By combining the increased reactivity due to the scaffold and the other favorable effects inherent to the 1-aza-9-boratriptycene molecule, this report constitutes a proof-of-concept that the high reactivity needed to activate inert molecules like methane (traditionally restricted to transition-metal complexes) can be reached with conceptually simple molecules bearing abundant elements (C, H, N and B) without the need for numerous electron-withdrawing groups.

In essence, the work presented in this PhD thesis allowed to expand our understanding of the steric and electronic factors affecting the reactivity of main group phosphorus and boron compounds, particularly in triptycene-based structures. This fundamental advancement, specific to our research topic, has also an echo outside of our domain of chemistry as it may inspire other researchers to investigate new strategies for the reactivity fine-tuning of main group molecules, outside of FLP chemistry or metal-free catalysis. On a more applied note, this thesis has also contributed to bringing new solutions to long-lasting challenges in main group chemistry and in our society, namely

developing alternatives to transition-metal catalysts and investigating solutions for the activation of methane.

Finally, the tools and methods developed to carry out this research, such as the synthesis of halogenated triarylmethane precursors, the optimization of a hydrogenation setup with a reactor, but also the DFT methods and studies, can find applications far outside of this work. For example, the pK_a prediction method was shown to be able to accurately predict the pK_a of any type of phosphines, not only phosphatriptycenes. Similarly, the DFT method employing the M06-2X functional with the Pople 6-311G(d) basis set was optimized to best describe Lewis acid-base interactions, and thermochemistry in general, and can be employed in future investigations.

A first perspective of this work is the investigation of difluorophosphoranes and fluorophosphonium cations of 9-phosphatriptycenes. The preliminary study of these compounds reported in the fourth chapter has proven that this chemistry should be further explored in the future. The effect of the triptycene core on the trigonal bipyramid of difluorophosphoranes was unknown so far and results in a high instability of these compounds. It is still unclear if the related fluorophosphonium can act as classical Lewis acids, or if this reactivity is prevented. The binding with large Lewis bases was shown to be prevented, but their behavior with small Lewis bases (such as ammonia, other small amines, the fluoride or hydride anions) should be tested. If large Lewis bases like triarylphosphines can undergo electrophilic fluorination with the fluorophosphonium cation, is it also the case with small bases? A plausible outcome is that small bases can bind to the phosphorus (after all, the difluoro-9-phosphoranetriptycene exists) while large ones undergo fluorination. Another possibility is that only the fluoride anion can bind to the phosphorus, the trigonal bipyramid formed with less electron-withdrawing elements being too unstable. A reactivity based on size-exclusion with these molecules could be developed.

Regarding FLP hydrogenations with 9-phosphatriptycenes, other “high-value” substrates could be targeted. These include for example amides or carbon dioxide that are long-lasting challenges in FLP chemistry and are of high interest in main group chemistry. The hydrogenation of amides on the one hand is one of the main ways of producing amines, a new metal-free method would thus be appealing. The carbon dioxide on the other hand is one of the main greenhouse gases and, like methane, its hydrogenation into formic acid derivatives or methanol, value-added product, is a great societal issue. Both substrates are

weakly reactive, and their hydrogenation would be facilitated using a weak base that generates a strong Brønsted acid.

Another important feature described in the third chapter of the manuscript is the recovery and recycling of the 9-phosphatriptycene catalyst, allowed by its high stability. An improvement of the recycling method would be possible if the 9-phosphatriptycene was grafted on the surface of a silica-based material. A derivative of the 9-phosphatriptycene, bearing an alcohol linked to the bridgehead carbon was already reported by our group, and could provide a suitable starting molecule to be grafted on a silanol surface *via* condensation.[1] Although 9-phosphatriptycenes grafted on silica-based materials are already reported (for Pd-catalyzed cross coupling reactions) and "Surface Frustrated Lewis pair" chemistry is also known, these two chemistry fields were never applied together.[3-5]

Interestingly, recent experimental work in our laboratory allowed to isolate derivatives of the 1-aza-9-boratriptycene. While the actual reaction with methane would require additional steric hindrance on the bifunctional system, as discussed in Chapter VI, an indirect synthesis of the product of methane activation could be attempted instead, in a similar fashion to Erker's work.[6] This allows experimenting the feasibility of using of methane as a C1-building block, for example in methyl transfer reactions, carboboration or hydrocarbation.[7-8]

Finally, to conclude on a fundamental note, a larger investigation of the effect of the triptycene scaffold on the reactivity of main group elements could be undertaken. Adventuring beyond 9-phosphatriptycene and 9-boratriptycene chemistry, a systematic comparison of the effect of the scaffold on the elements of group 3 and 5 (*e.g.* B, Al, Ga and N, P, As) would inevitably lead to a broader understanding of the phenomena already discussed in the present manuscript. As more elements (or other scaffolds) are included in the study, more general conclusions and trends could be drawn, further expanding the reach of main group chemistry.

References

[1] L. Hu, D. Mahaut, N. Tumanov, J. Wouters, R. Robiette, G. Berionni, "Complementary synthetic approaches toward 9-phosphatriptycene and structure–reactivity investigations of its association with sterically hindered Lewis acids", *J. Org. Chem.* **2019**, *84*, 11268-11274.

[2] C. B. Caputo, D. Winkelhaus, R. Dobrovetsky, L. J. Hounjet, D. W. Stephan, "Synthesis and Lewis acidity of fluorophosphonium cations", *Dalton Trans.* **2015**, *44*, 12256-12264.

[3] T. Iwai, S. Konishi, T. Miyazaki, S. Kawamorita, N. Yokokawa, H. Ohmiya, M. Sawamura, "Silica-supported triptycene-type phosphine. Synthesis, characterization, and application to Pd-catalyzed suzuki–miyaura cross-coupling of chloroarenes", *ACS Catal.* **2015**, *5*, 7254-7264.

[4] L. Wang, T. Yan, R. Song, W. Sun, Y. Dong, J. Guo, Z. Zhang, X. Wang, G. A. Ozin, "Room temperature activation of H_2 by a surface frustrated Lewis pair", *Angew. Chem. Int. Ed.* **2019**, *58*, 9501-9505.

[5] Y. Zhang, P. C. Lan, K. Martin, S. Ma, "Porous frustrated Lewis pair catalysts: advances and perspective", *Chem Catalysis* **2022**, *2*, 439-457.

[6] S. Frömel, C. G. Daniliuc, C. Bannwarth, S. Grimme, K. Bussmann, G. Kehr, G. Erker, "Indirect synthesis of a pair of formal methane activation products at a phosphane/borane frustrated Lewis pair", *Dalton Trans.* **2016**, *45*, 19230-19233.

[7] Y. Liu, W. Dong, Z. H. Li, H. Wang, "Methane activation by a borenium complex", *Chem* **2021**, *7*, 1843-1851.

[8] V. Fasano, L. D. Curless, J. E. Radcliffe, M. J. Ingleson, "Frustrated Lewis pair mediated 1,2-hydrocarbation of alkynes", *Angew. Chem. Int. Ed.* **2017**, 9202-9206.

Annex I
Supplementary information of the chapters

Material and methods of the experimental procedures

Commercial reagents were purchased from Sigma Aldrich, ABCR, TCI, FluoroChem, and used without further purification. Tris(pentafluorophenyl)-borane was purchased from TCI (98%) and used without further purification. Cyclohexene, cyclopentene, *n*-hexene and olefins with purity <97% were distilled and stored in a glovebox over preactivated 4Å molecular sieves, other olefins were purchased and used without further purification. Dihydrogen was bought from NipponGases with a purity grade 6.0 (99.9999%) for the reactions described in chapter II and a purity grade 5.0 (99.999%) for the reactions described in chapter III, with no difference noticed between the two. $CDCl_3$ was degassed and stored in a glovebox over preactivated 4Å molecular sieves. Hydrogenation reactions were performed in a stainless-steel autoclave (SS316/316L Asynt 100mL high pressure reactor with screwed closure). Air and moisture sensitive reactions were carried out using purified and dried solvents in a Schlenk flask or in a high-performance glovebox under an inert atmosphere (Argon or Nitrogen). Dichloromethane (DCM), diethyl ether (Et_2O), tetrahydrofuran (THF), and toluene were dried over a Pure Solv™ solvent purification system. Thin layer chromatographies were performed using Merck aluminum roll silica gel 60-F254 monitored by UV light at 254 nm. Flash chromatographies were performed using silica gel Silica Flash® 40-63 micron (230-400 mesh). TLC detection was done by irradiation with a UV lamp at 265 or 313 nm. ^{1}H Nuclear Magnetic Resonance (NMR) spectra were obtained on a JEOL ECX 400 or 500 MHz spectrometer. ^{31}P (202 MHz), ^{11}B (160 MHz) and ^{19}F (471 MHz) spectra were recorded on the JEOL ECX 500 MHz spectrometer. The chemical shifts (δ) are reported in ppm and referenced indirectly to residual solvent signals. The signal splitting patterns were described as *s* = singlet, *d* = doublet, *t* = triplet, *q* = quartet, *dd* = doublet of doublet, *dt* = doublet of triplet, *td* = triplet of doublet, *tt* = triplet of triplet, *ddd* = doublet of doublet of doublet, *br* = broad, and *m* = multiplet, with coupling constants (*J*) in Hertz (Hz). The IR spectra were acquired on a Perkin-Elmer Spectrum II FT-IR System UATR mounted with a diamond crystal on neat compounds. Selected absorption bands are reported by wavenumber (cm^{-1}). The spectra were measured between wavenumbers of 4000-450 cm^{-1}. High resolution mass spectra (HRMS) were recorded on a *Thermo Orbitrap Exactive* device and performed by the Molecular

Structural Analysis (ASM) technological platform of the Université catholique de Louvain (UCLouvain).

1. Chapter I

Spectra, experimental procedures and computational data are available online on the publication link:

https://pubs.rsc.org/en/content/articlelanding/2021/dt/d1dt00816a

2. Chapter II

Cartesian coordinates, electronic energies, enthalpies and free energies of optimized structures are available online on the publication link:

https://pubs.acs.org/doi/10.1021/acs.jpca.2c01339

2.1 Boltzmann population of rotamers

The calculation of the pK_a values of the phosphines has been performed by taking into account their different rotamers. This occurs for the phosphines with one fluorine atom in *ortho*-position of one or several phenyl substituents relative to the phosphorus. The different rotamers having different properties, including different pK_a values, the reported quantities are averages calculated by considering their Maxwell-Boltzmann populations. This is briefly illustrated below, for P(2-F-C_6H_4)$_3$. As shown in Figure S38, several positions are possible for its *ortho*-F atoms: including 3 “up” and 3 “down” positions shown respectively in dark and light green. Then, Figure S39 lists the rotamers of P(2-F-C_6H_4)$_3$ while the relative energies, populations, and pK_a values of the three phosphines with 2-F-C_6H_4 substituents are given in Table S21.

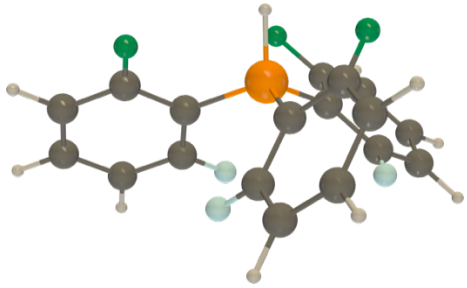

Figure S38. (2-F-C_6H_4)$_3$P$^+$-H highlighting the possible three "up" positions (dark green, pointing outward) and three "down" positions (light green, pointing inward) of the F atoms with respect to the direction of its P$^+$-H bond (or its P lone pair for phosphines).

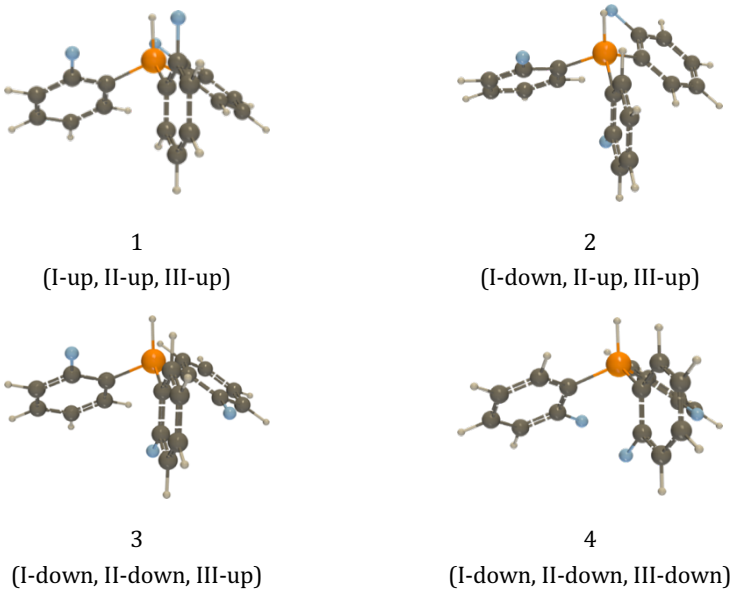

1
(I-up, II-up, III-up)

2
(I-down, II-up, III-up)

3
(I-down, II-down, III-up)

4
(I-down, II-down, III-down)

Figure S39. Optimized structures of the different rotamers taken into account, only the structures of the phosphonium are shown.

Table S21. Relative stability (ΔG^0, in kJ.mol^{-1}) and population (Pop., in %) of rotamers for several reference ortho-fluorinated phosphines.

Phosphine	Rotamer	Phosphine		Phosphonium		pK_a
		ΔG^0	Pop.	ΔG^0	Pop.	
P(2-F- C_6H_4)$_3$	1 (up-up-up)	0.0	91.1	0.0	95.4	3.9
	2 (up-up-down)	5.9	8.6	7.8	4.1	3.5
	3 (up-down-down)	14.0	0.3	12.9	0.5	4.0
	4 (down-down-down)	28.2	0.0	21.7	0.0	5.0
P(2-F- C_6H_4)$_2$(Ph)	1 (up-up)	0.0	89.7	0.0	87.2	4.8
	2 (up-down)	5.4	10.2	5.1	11.3	4.8
	3 (down-down)	16.0	0.1	10.1	1.5	5.8
P(2-F- C_6H_4)(Ph)$_2$	1 (up)	0.0	95.1	0.0	82.9	6.1
	2 (down)	7.4	4.9	3.9	17.1	6.7

2.2 Additional discussion on structure-property relationships in 9-phosphatriptycenes

As shown in Table 7 of Chapter II, the phosphorus lone pair energy is reduced when going from "classical" (*i.e.* non-strained, caged-shaped) triarylphosphines (representative example of **II.1**, PPh_3) to 9-phosphatriptycene derivatives **II.2-11** (-11.66 eV for **II.1** *vs* -12.65 to -13.05 eV for 9-phosphatriptycenes), this stabilization goes with an increase of the pyramidalization parameter (0.452 *vs* 0.532 to 0.540) and *s* character of the phosphorus lone pair (45.4% *vs* 49.9 to 51.6%).

Drawing a direct trend between ε_{LP} and the predicted pK_a values is not straightforward however (Figure S40). While the general tendency is, as expected, that lower pK_a's are attributed to phosphines with lower lone pair energies, several points come out of trend. Namely, the two phosphines bearing alkyl groups [Me_3P (pK_a 15.1; -11.79 eV) and $Me_2(Ph)P$ (pK_a 12.4; -11.80 eV)] and the highly sterically crowded $(2,6\text{-}Cl_2C_6H_4)_3P$ (pK_a 0.7; -11.54 eV).

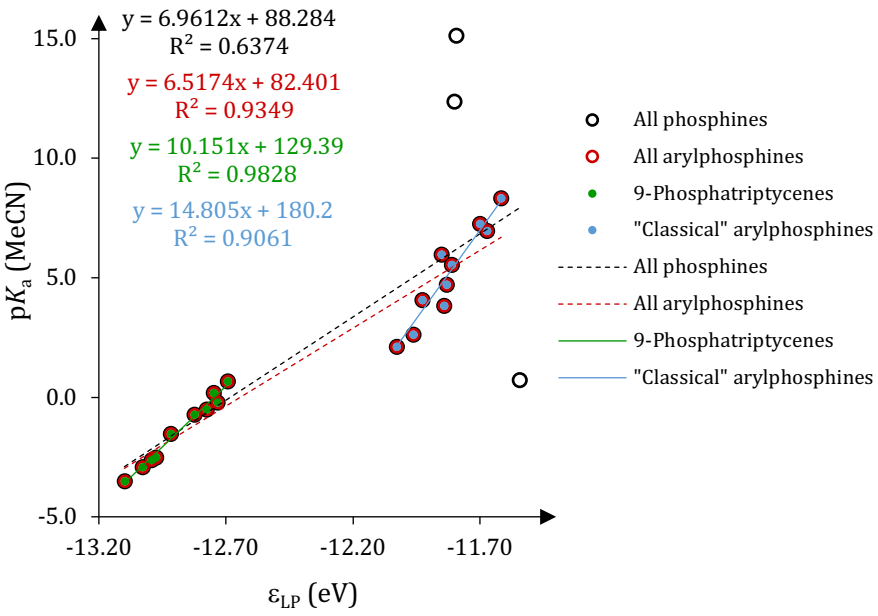

Figure S40. Predicted pK_a's in acetonitrile as a function of the NBO phosphorus lone pair energy (in eV) in acetonitrile. $(2,6\text{-}Cl_2C_6H_4)_3P$ is not included in the classical arylphosphines group.

Considering only a local descriptor such as lone pair energies is insufficient to accurately predict a global Brønsted acidity descriptor like pK_a values. Other

parameters, not taken into account in the LP energy, also affect the global reactivity, such as, for examples, the steric hindrance around the phosphorus atom, the position of the substituents and the reorganization energy of the phosphine upon protonation. Keeping this in mind, considering only phosphines with similar geometries, such as 9-phosphatriptycenes alone, or triarylphosphines alone, improves the correlation between ε_{LP} and pK_a values because phosphines displaying similar structures and steric hindrance should, in good approximation, display similar reorganization energies upon protonation. But when mixing 9-phosphatriptycenes, "classical" triaryl-phosphines, alkyl phosphines and phosphines with high steric hindrance, lone pair energies fail to reproduce pK_a trends.

The electron occupancy of **II.1**, 1.917 e^-, is lower than that of 9-phosphatriptycenes **II.2**-**11** (from 1.957 to 1.962 e^-). A similar trend is observed for the phosphorus natural charge (0.82*e*), slightly more positive in PPh_3 than 9-phosphatripycene **II.2** (0.79*e*) even though other 9-phosphatriptycene derivatives bearing electron-withdrawing substituents reach similar values to PPh_3 (**II.7**-**11**). The difference between **II.1** and 9-phosphatriptycene derivatives **II.2**-**11** for these two parameters is attributed to conjugation with the neighboring π-systems. The phosphorus lone pair in **II.1** is slightly delocalized in the π-system of the three aryl rings, while delocalization is prevented in the case of 9-phosphatriptycenes due to the almost perpendicular orientation of its lone pair relative to the π-systems. It results in lower LP occupancy and higher P charge in PPh_3 because more electrons are delocalized in the aromatic rings. Comparison of the lone pair occupancy and phosphorus charge in triarylphosphine and 9-phosphatriptycenes displaying increasing numbers of mesomeric attractive *para*-NO_2 groups (enhancing delocalization of the phosphorus lone pair) highlights this phenomenon (Table S22).

Table S22. NBO (CH_2Cl_2) phosphorus lone pair electronic occupancy and natural phosphorus charge (expressed as multiple of the fundamental charge, e).

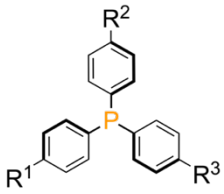

II.1, $R_{1,2,3}$ = H
II.1-NO_2, R_1 = NO_2, $R_{2,3}$ = H
II.1-N_2O_4, $R_{1,2}$ = NO_2, R_3 = H
II.1-N_3O_6, $R_{1,2,3}$ = NO_2

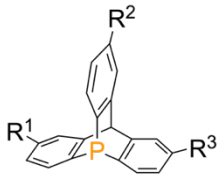

II.2, $R_{1,2,3}$ = H
II.2-NO_2, R_1 = NO_2, $R_{2,3}$ = H
II.2-N_2O_4, $R_{1,2}$ = NO_2, R_3 = H
II.2-N_3O_6, $R_{1,2,3}$ = NO_2

Compounds	$Occ._{LP}$ (e^-)	Q_P (e)
II.1	1.917	0.82
II.1-NO_2	1.909	0.84
II.1-N_2O_4	1.906	0.85
II.1-N_3O_6	1.905	0.86
II.2	1.961	0.79
II.2-NO_2	1.961	0.81
II.2-N_2O_4	1.961	0.82
II.2-N_3O_6	1.960	0.83

Structurally, 9-phosphatriptycenes display elongated P-C bond lengths and smaller C-P-C angles compared to their triphenylphosphine analogues (Table S23). In agreement with Bent's rule, this structural effect also translates in their atomic orbital mixing, with increased *3s* character in the phosphorus lone pair of 9-phosphatriptycenes compared to triarylphosphines.[1]

*Table S23. Mean P-C bond lengths (in Å) and mean C-P-C angles (in °) and phosphorus lone pair 3s character (in %) for triphenylphosphine (**II.1**) and 9-phosphatriptycene (**II.2**).*

Phosphine	$\bar{d}_{P-C}$(Å)	$\bar{\alpha}_{CPC}$(°)	*3s* (%)
II.1	1.844	116.9	45.4
II.2	1.852	94.0	49.9

2.3 Experimental hydrogenation of 1,1-diphenylethylene

Hydrogenation reactions were performed as follow: in a glovebox, 9-phosphatriptycene derivatives, tris(pentafluorophenyl)borane, 1,1-diphenyl-ethylene **II.12** (0.10 mL, 0.57 mmol) and the appropriate solvent were placed in a PTFE container equipped with a magnetic stirrer inside a stainless-steel autoclave (SS316/316L Asynt reactor). The reaction mixture is then exposed to dihydrogen pressure while stirring. After reaction, the autoclave is opened to air, solvents are removed *in vacuo* and an NMR analysis of the crude mixture is performed.

The hydrogenation of 1,1-diphenylethylene was performed with a FLP catalyst consisting of 1-chloro-9-phosphatriptycene **II.7** and tris(pentafluorophenyl)-borane. The optimization of reaction conditions is shown in Table S24. The product of hydrogenation, 1,1-diphenylethane **II.13**, was obtained with up to 88% yield (Table S24, entry 3). The ideal reaction conditions were 20 mol% of the FLP catalyst in toluene, 40 bar of H_2 pressure and overnight. Because the reaction proceeds cleanly, the results are determined by ^{1}H NMR of the crude mixture without purification. Milder reaction conditions than entry 3 can be used instead, such as lower pressures or less catalyst loading, but either the reaction time or the amount of dimer by-product **II.14** increased (entries 5-9). Heating at 50°C expectedly accelerated the reaction but favored the dimerization (entry 8). Using a FLP as catalyst is crucial for the reaction to work since phosphine **II.2**, which forms a Lewis adduct with $B(C_6F_5)_3$ **II.9**,[2] only led to traces of the hydrogenation product **II.13**.

A typical ^{1}H NMR spectrum (entry 2 in Table S24) of the crude reaction mixture containing the product **II.13**, the starting material **II.12**, the catalyst **II.7**, and the competing dimer **II.14** is shown in Figure S41, while the ^{1}H spectrum of the reaction with the optimal conditions is shown in Figure S42 (entry 3 in Table S24).

Table S24. Optimization of the reaction conditions for the hydrogenation of 1,1'-diphenylethylene. Conv. = Conversion. Catalyst loading in mol%.

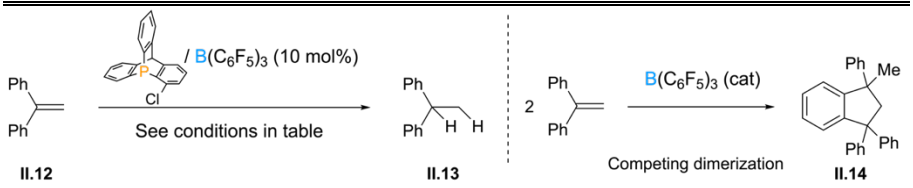

Entry	Catalyst		Conditions					Results		Proportions	
	LB	Cat. loading	Solvent	$V_{solvent}$ (mL)	T (°C)	Time	P_{H_2} (bar)	Conv. (%)[a]	^{1}H NMR yield (%)[a]	Product **II.13** (%)	Dimer **II.14** (%)
1	PTrpCl **II.7**	10		1.60	r.t.	3 d	40	95	78	83	17
2		10		1.60	r.t.	16h	40	86	52	61	39
3		20		1.60	r.t.	16h	40	98	88	90	10
4		10		1.60	r.t.	6 d	20	94	77	82	18
5		10	Toluene	0.16	r.t.	3 d	20	98	52	53	47
6		10		1.60	r.t.	16h	20	62	19	30	70
7		10		1.60	r.t.	6 d	10	99	73	74	26
8		10		1.60	50°C	16h	10	92	31	34	66
9		10		1.60	r.t.	16h	10	85	16	18	82
11	PTrp **II.2**	10	Toluene	1.60	r.t.	6 d	20	1	0	0	100
12		10	DCM	1.60	r.t.	6 d	10	1	0	0	100
13		10	Br-benzene	1.60	r.t.	6 d	10	1	0	0	100
14		10	Br-benzene	1.60	50°C	16h	10	1	0	25	75

[a] Conversions and ^{1}H NMR yields are evaluated without ^{1}H NMR internal standard as the ratio between the integrations, normalized to 1 proton, of the starting material (for conversion) or the product (for ^{1}H NMR yields) and the sum of the integration of the starting material, the product and the competing dimer (all normalized to 1 proton, the methyl groups of the product and the dimer are selected for integration).

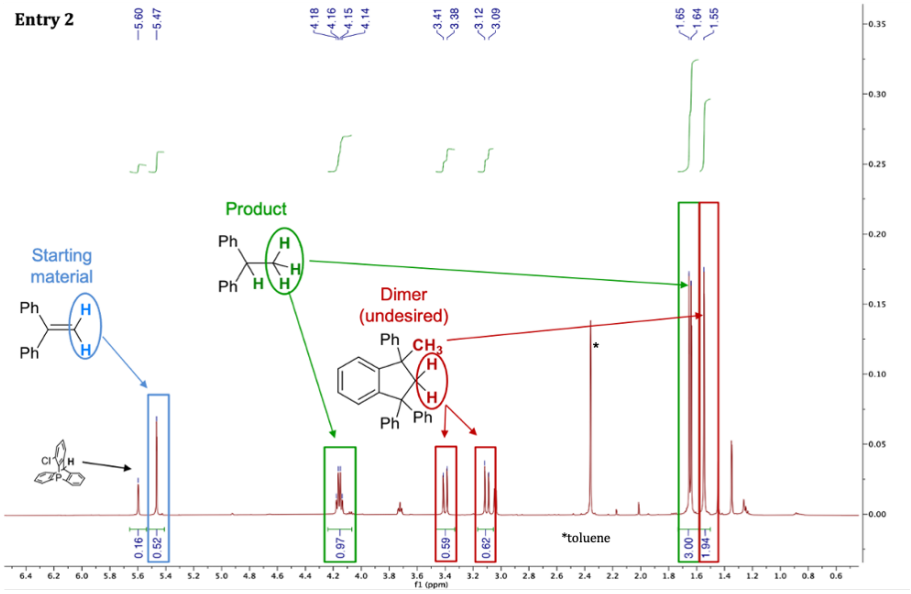

Figure S41. Typical example of a ^{1}H NMR spectrum of the crude reaction mixture after 1,1-diphenylethylene hydrogenation under experimental conditions described in entry 2.

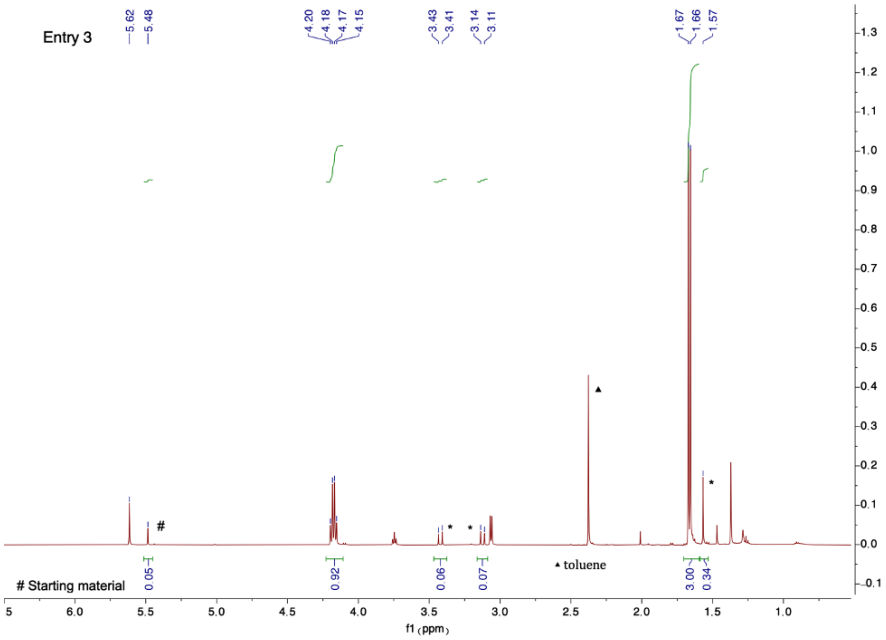

Figure S42. ^{1}H NMR spectrum for the hydrogenation of 1,1-diphenylethylene with the optimal conditions (entry 3). Asterix denotes traces of dimer.

3. Chapter III

The NMR spectra of the reactions described in tables 9, 10 and 11 of chapter III, the cartesian coordinates, electronic energies, enthalpies and free energies of optimized structures are available online on the publication link:

https://chemistry-europe.onlinelibrary.wiley.com/doi/10.1002/cctc.202200294

General procedure for the hydrogenation of alkenes (representative example of cyclohexene):

In a glovebox, 1-chloro-9-phosphatriptycene **III.3** (30.3 mg, 0.099 mmol), tris(pentafluorophenyl)borane (50.5 mg, 0.099 mmol), cyclohexene (0.10 mL, 0.99 mmol) or the appropriate alkene and $CDCl_3$ (5.6 mL) were added in a PTFE container equipped with a magnetic stir bar which was then placed inside a stainless-steel autoclave. Temperature and pressure are gradually increased until reaching the appropriate values listed in tables 9, 10 and 11 of chapter III. All reactions are performed under stirring (500 rpm). After reaction, the autoclave is opened to air, 2,3,5-trimethoxybenzene or triphenylmethane is added as ^{1}H NMR internal standard (166 mg or 241 mg respectively, 0.99 mmol) and an aliquot of the solution is taken for analysis, yield and conversion determination. The same procedure is applied for other substrates or catalysts.

3.1 Quantum chemical calculations

All calculations were performed using the Gaussian16 package.[3] Full geometry optimizations followed by vibrational frequency calculations were done at the M06-2X/6-311G(d) level of theory,[4] at a temperatures and a pressure of 298.15 K and 1 atm. Tight convergence thresholds were used for geometry optimizations, *e.g.* for the residual forces on the atoms, 1.5×10^{-5} Hartree/Bohr or Hartree/radian. Previous reports demonstrated that this method give satisfying results in thermochemistry when compared to higher-level methods such as double-hybrid DFT with an expanded basis set.[5] For ground state equilibrium structures, all vibrational frequencies of the optimized stationary points are real, demonstrating that the structures are minima on the potential energy surface. All transition state geometries were obtained by optimization to a saddle point using the Berny algorithm[6-9] and are characterized by a single imaginary frequency. Solvent effects (dichloromethane) were taken into account using the IEFPCM implicit solvation scheme.[10]

3.1.1 Hydrogenation reaction energy profiles

Two mechanisms were considered (Figure S43 and Figure S44) and computed for the hydrogenation reaction of cyclohexene catalyzed by **III.3**/BCF.

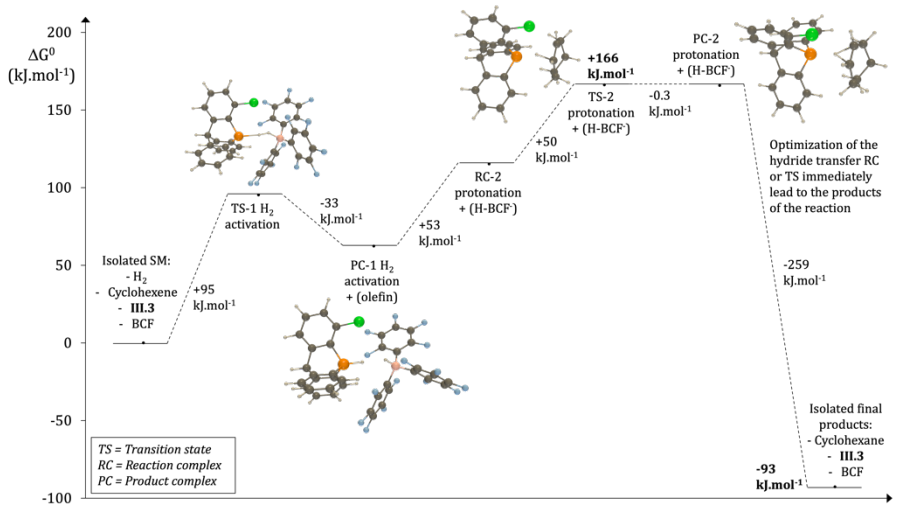

*Figure S43. Gibbs free energy profile of the hydrogenation of cyclohexene by the **III.3**/BCF FLP catalyst with according to the mechanism involving the direct hydride transfer after the protonation step.*

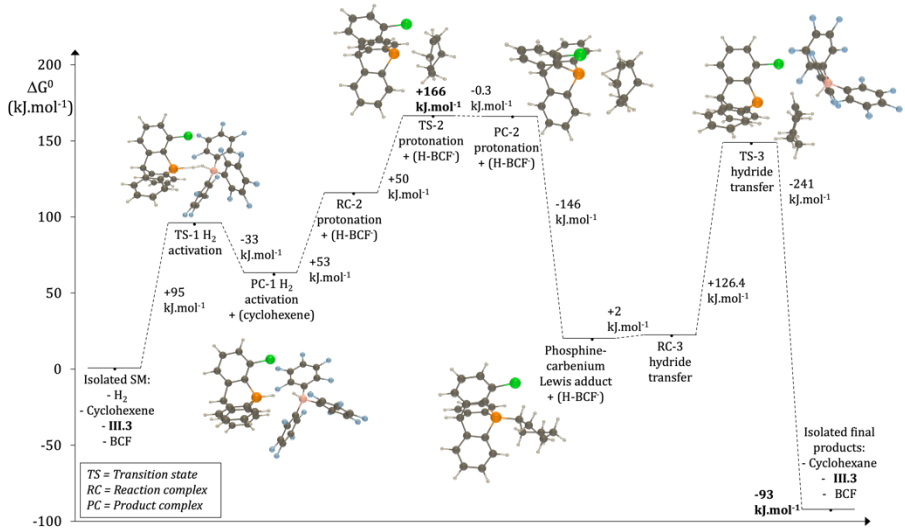

*Figure S44. Gibbs free energy profile of the hydrogenation of cyclohexene by the **III.3**/BCF FLP catalyst according to the mechanism involving the formation of the hydrophosphination product between **III.3** and the carbenium intermediate.*

3.1.2 Comment on the activation barrier

The reaction barrier of 166 kJ.mol^{-1} should be considered as an upper limit to the actual energy barrier of the reaction. Explicit solvent effects could have a stabilizing effect on it. Other approximations could also explain this high value: the transition state shown in the proposed mechanism has a global charge of +1 and could also be stabilized by the explicit presence of its counter anion. To check this assumption, we optimized the transition state of the protonation step this time in the presence of its counter anion $HB(C_6F_5)_3^-$. An IRC calculation on this new transition state confirmed that it is the one of the protonation reaction, generating the carbocation in the presence of the borohydride (Figure S45). The barrier is then reduced to +159 kJ.mol^{-1}. In addition, the Gibbs free energies of all computed structures refer to a standard gas phase pressure of 1 atm, a correction of +7.90 kJ.mol^{-1} [corresponding to *R.T.*ln(24.46)] to these values can be applied to refer to a standard concentration of 1 mol.L^{-1} instead of the initial reference. Taking into account both corrections, the barrier is now reduced to a value of +135 kJ.mol^{-1}. Since the exact position of the counter anion is uncertain and many similar structures with similar energies could be obtained,[11] the value without counter anion is shown in the main manuscript.

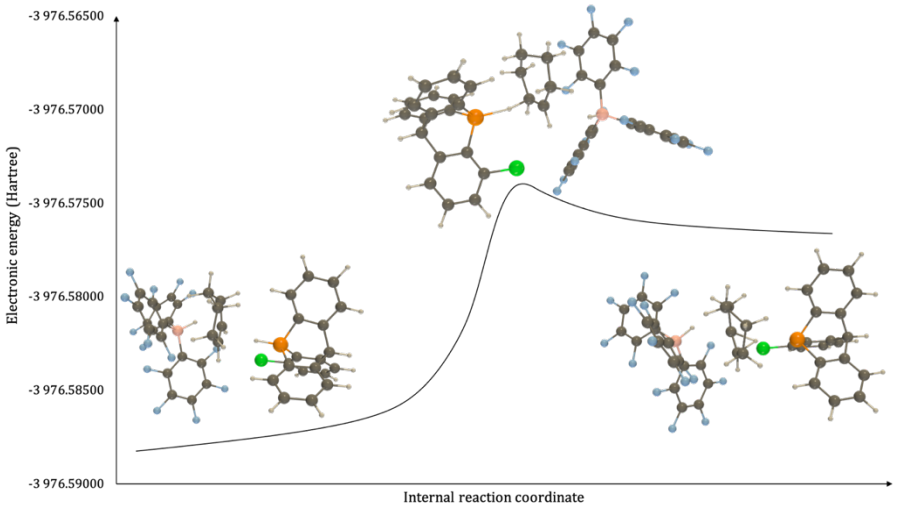

Figure S45. IRC profile of the cyclohexene protonation reaction in the presence of the counter-anion, showing the reaction complex (left), the transition state (center) and the product complex of the reaction (right).

4. Chapter IV

Materials and methods are given at the beginning of the section.

4.1 Experimental procedures and NMR data

Synthesis of difluoro-9-phosphoranetriptycene **IV.2**

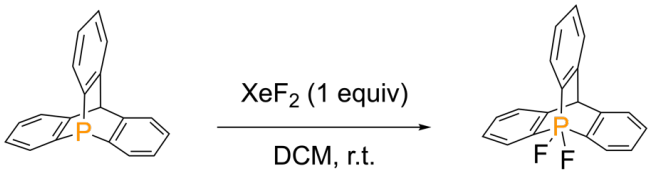

IV.1 **IV.2**

In a glovebox, under argon atmosphere, XeF_2 (12.4 mg, 0.074 mmol) is weighted in a glass vial, and then dissolved in 2.0 mL of dichloromethane. Next the 9-phosphatriptycene (20.0 mg, 0.074 mmol) is added to the colorless mixture, effervescence appears. The solution is stirred manually for a few minutes. The solvent is then removed *in vacuo* to yield the product **IV.2** as a white solid (21.9 mg, 95% yield). Crystals suitable for X-ray crystallography are obtained by slow evaporation of a saturated solution of **IV.2** in a 1:1 mixture DCM/*n*-hexane.

^{1}H NMR (500 MHz, $CDCl_3$) δ: 7.94 – 7.89 (m, 3H), 7.48 – 7.41 (m, 3H), 7.22 - 7.16 (m, 6H), 5.27 (s, 1H).

^{31}P NMR (202 MHz, $CDCl_3$) δ: -44.41 (t, J = 865.2 Hz).

^{19}F NMR (471 MHz, $CDCl_3$) δ: -57.33 (d, J = 865.2 Hz)

^{13}C NMR (126 MHz, $CDcl_3$) δ: 146.60 (d, J = 13.3 Hz), 140.29 (d, J = 116.5 Hz), 129.61, 128.89 (d, J = 3.0 Hz), 126.22 (d, J = 12.1 Hz), 125.15 (d, J = 12.1 Hz), 53.44 (d, J = 21.0 Hz).

^{1}H NMR spectrum of **IV.2** in $CDCl_3$:

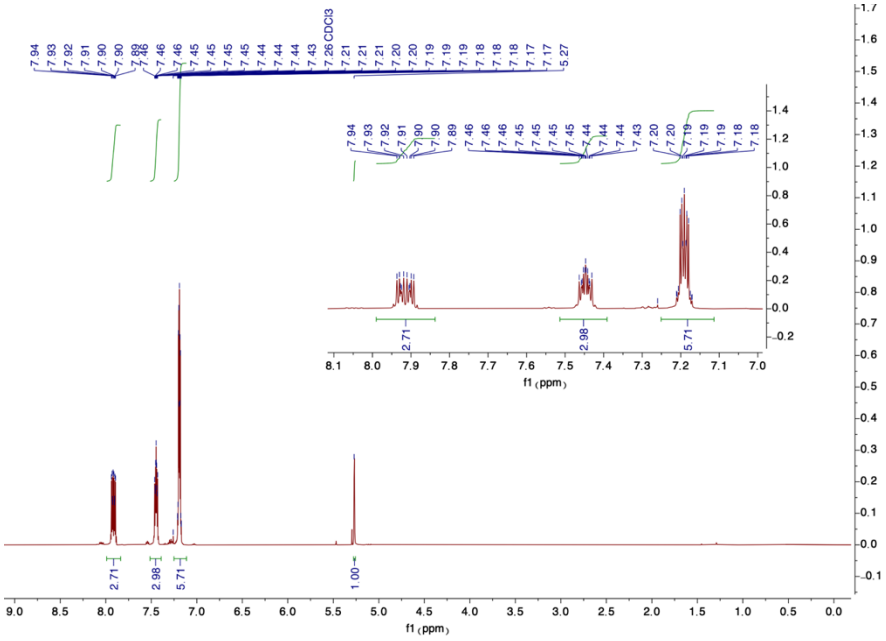

^{31}P NMR spectrum of **IV.2** in $CDCl_3$:

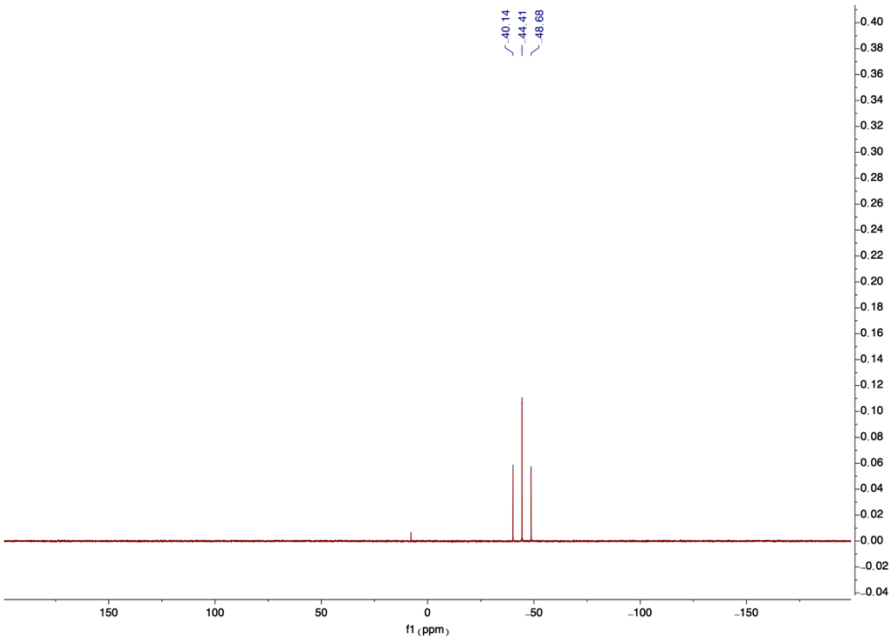

^{19}F NMR spectrum of **IV.2** in $CDCl_3$:

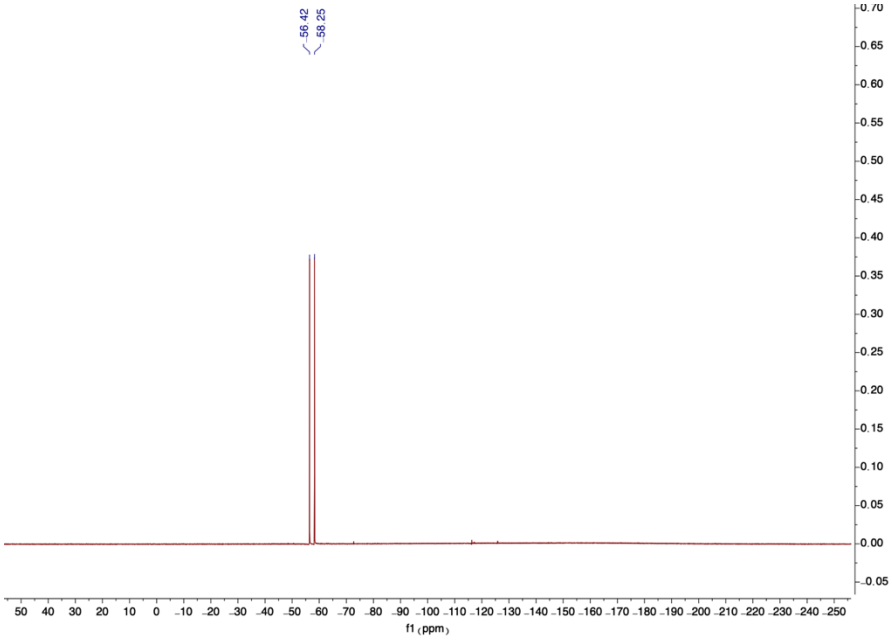

^{13}C NMR spectrum of **IV.2** in $CDCl_3$:

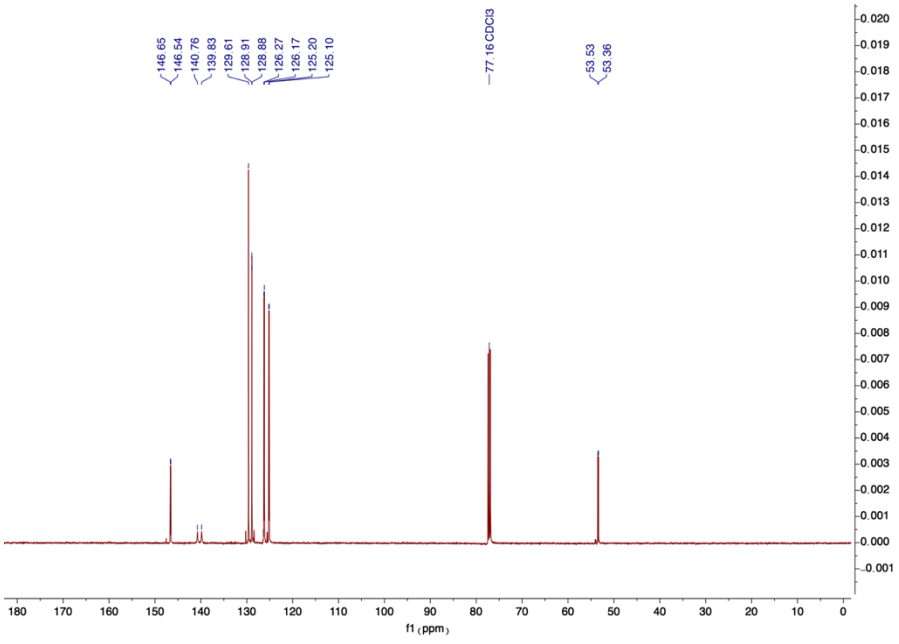

Synthesis of 9-fluorophosphoniumtriptycene tetrakis(2,3-bis(trifluoromethyl)-phenyl)borate **IV.5**

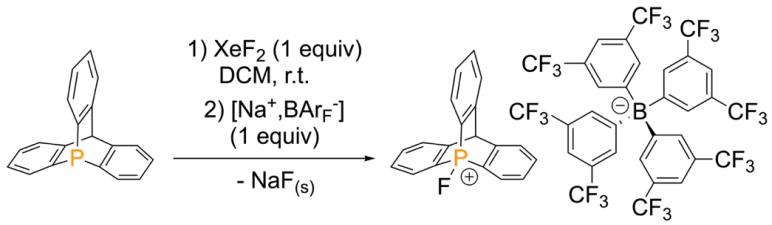

IV.1 **IV.5**

In a glovebox, under argon atmosphere, XeF_2 (24.9 mg, 0.147 mmol) is weighted in a glass vial, and then dissolved in 5.0 mL of dichloromethane. Next the 9-phosphatriptycene (40.0 mg, 0.147 mmol) is added to the colorless mixture, effervescence appears. The solution is stirred manually for a few minutes. $NaBAr_F$ is then added (130.2 mg, 0.147 mmol), a precipitate appears (NaF), the solution is then stirred again manually for a few minutes. Slow filtration through a Pasteur pipette with cotton followed by removal *in vacuo* of the solvent yielded the product **IV.5** as a white solid (157 mg, 92% yield). Crystals suitable for X-ray crystallography are obtained by slow evaporation of a saturated solution of **IV.5** in a 1:1 mixture DCM/*n*-hexane.

^{1}H NMR (500 MHz, $CDCl_3$) δ: 7.91 (ddd, J = 14.7, 7.5, 1.2 Hz, 3H), 7.76 (td, J = 7.8, 3.1 Hz, 3H), 7.72 (m, 8H), 7.53 (tt, J = 7.7, 1.2 Hz, 3H), 7.47 (s, 4H), 7.38 (tdd, J = 7.7, 4.4, 0.9 Hz, 3H), 5.89 (s, 1H).

^{31}P NMR (202 MHz, $CDCl_3$) δ: 83.75 (d, *J* = 1142.5 Hz).

^{19}F NMR (471 MHz, $CDCl_3$) δ: -62.28, -189.50 (d, *J* = 1141.6 Hz).

^{11}B NMR (160 MHz, $CDCl_3$) δ: -7.55.

^{13}C NMR (126 MHz, $CDcl_3$) δ: 161.86 (dd, *J* = 99.7, 50.0 Hz), 145.86 (dd, *J* = 10.7, 5.1 Hz), 135.09 (d, *J* = 2.9 Hz), 134.90, 129.54 – 128.64 (m), 128.33 (d, *J* = 14.3 Hz), 127.88, 127.62 – 127.50 (m), 127.45 (d, *J* = 3.0 Hz), 125.71, 123.55, 121.38, 119.67 (dd, *J* = 99.2, 5.8 Hz), 117.80 – 117.51 (m), 53.55 (d, *J* = 25.0 Hz).

^{1}H NMR spectrum of **IV.5** in $CDCl_3$:

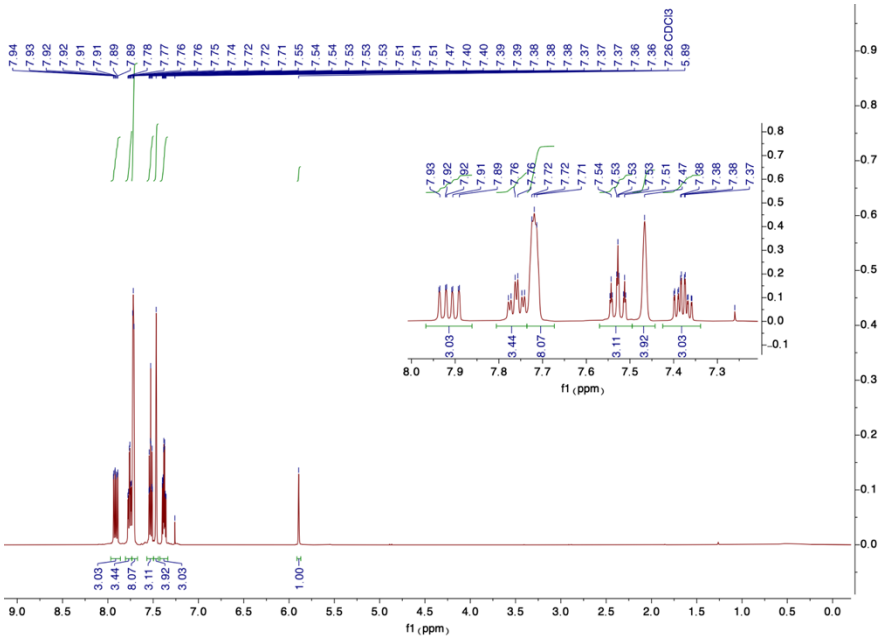

^{31}P NMR spectrum of **IV.5** in $CDCl_3$:

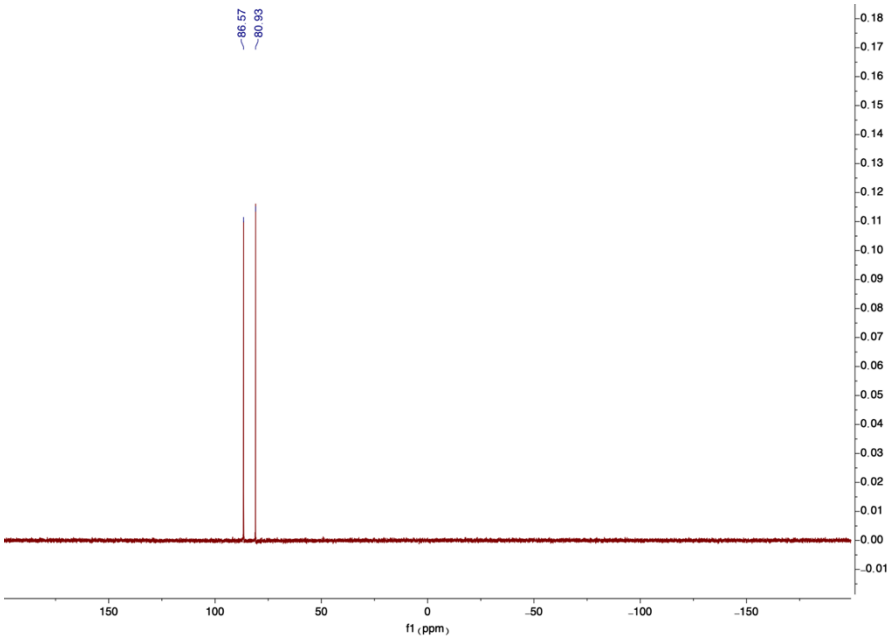

^{19}F NMR spectrum of **IV.5** in $CDCl_3$:

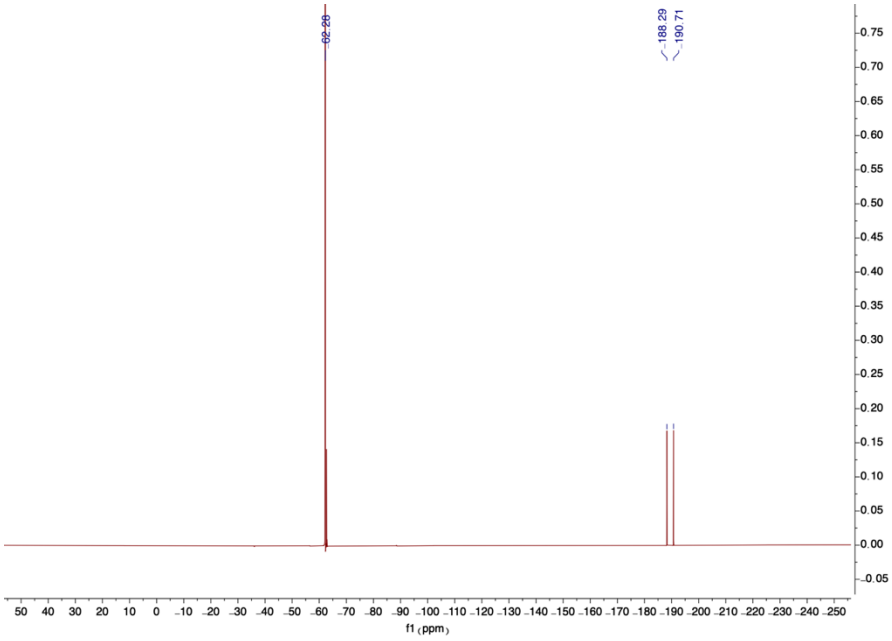

^{11}B NMR spectrum of **IV.5** in $CDCl_3$:

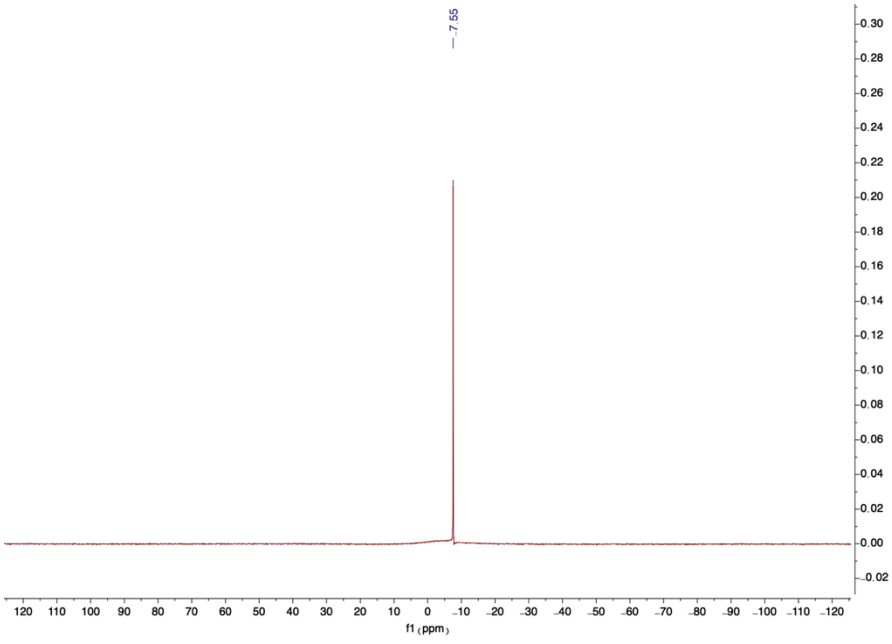

^{13}C NMR spectrum of **IV.5** in $CDCl_3$:

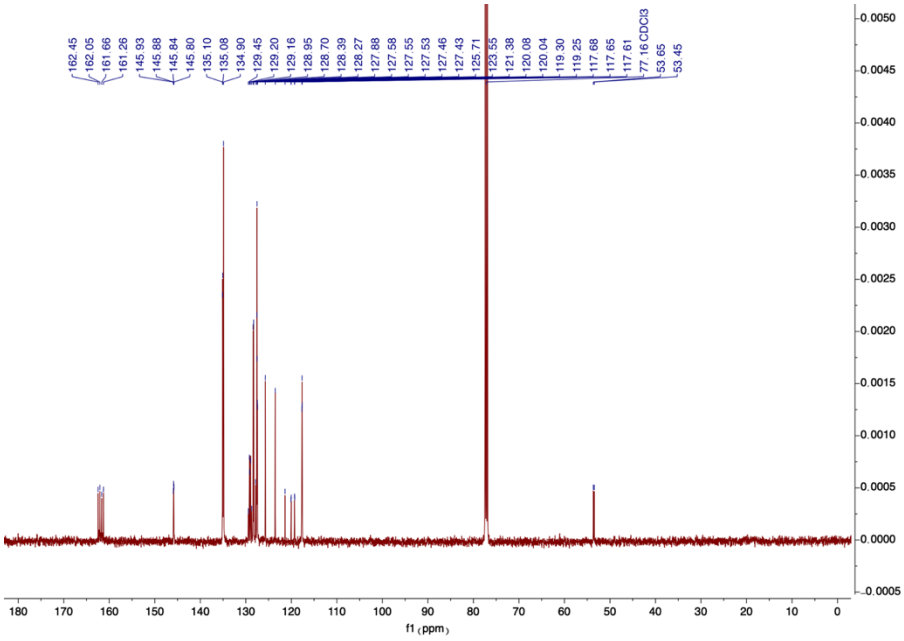

Synthesis of 1-chloro-9-difluorophosphoranetriptycene **IV.7**

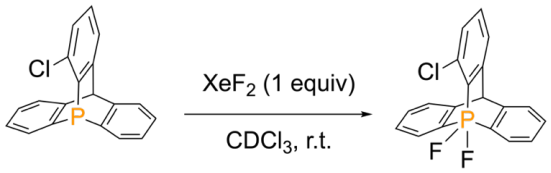

IV.6 **IV.7**

In a glovebox, under argon atmosphere, XeF_2 (5.5 mg, 0.033 mmol) is weighted in a glass vial, and then dissolved in 1.0 mL of deuterated chloroform ($CDCl_3$). Next the 1-chloro-9-phosphatriptycene (10.0 mg, 0.033 mmol) is added to the colorless mixture, effervescence appears. The solution is stirred manually for a few minutes. NMR analysis of the solution showed completed conversion of the starting material to the product.

^{1}H NMR (500 MHz, $CDCl_3$) δ: 7.93 – 7.84 (m, 2H), 7.51 – 7.38 (m, 2H), 7.36 (t, *J* = 7.2 Hz, 1H), 7.22 – 7.13 (m, 6H), 5.23 (s, 1H).

^{31}P NMR (202 MHz, $CDCl_3$) δ: -44.67 (t, *J* = 878.0 Hz).

^{19}F NMR (471 MHz, $CDCl_3$) δ: -52.84 (d, *J* = 877.9 Hz).

^{13}C NMR (126 MHz, $CDcl_3$) δ: 150.48 (d, *J* = 6.0 Hz), 146.94 (d, *J* = 6.9 Hz), 136.76, 132.50 (d, *J* = 100.0 Hz), 131.25, 130.52, 129.09 – 128.85(m), 127.95 (d, *J* = 129.8 Hz), 126.51 (d, *J* = 12.2 Hz), 125.48 (d, *J* = 8.0 Hz), 124.13 (d, *J* = 7.7 Hz), 53.88 (d, *J* = 18.9 Hz).

^{1}H NMR spectrum of **IV.7** in $CDCl_3$:

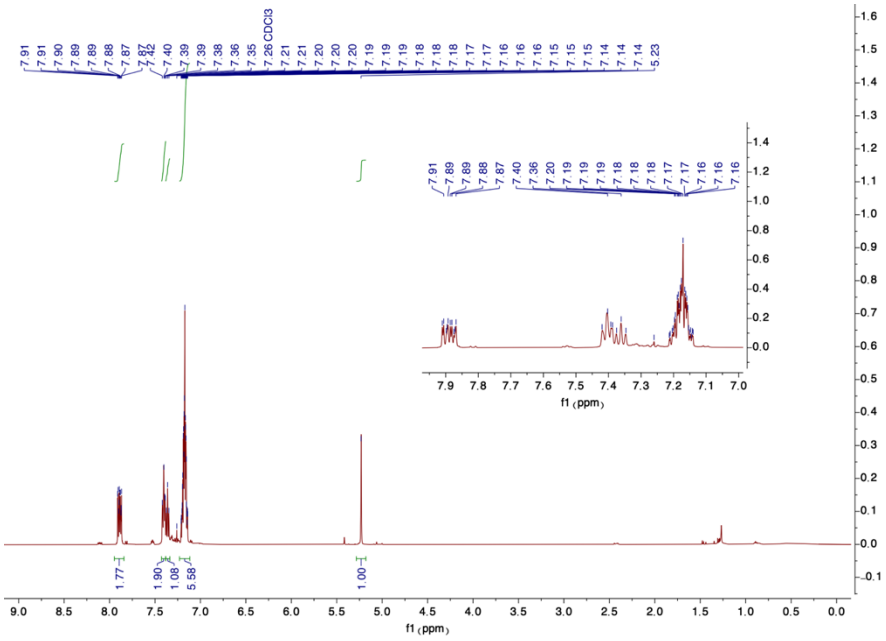

^{31}P NMR spectrum of **IV.7** in $CDCl_3$:

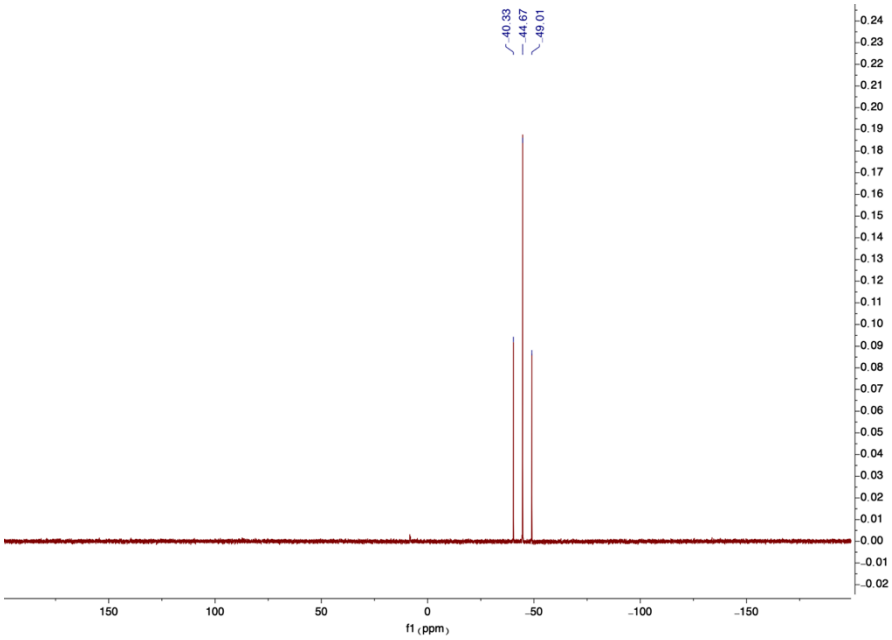

^{19}F NMR spectrum of **IV.7** in $CDCl_3$:

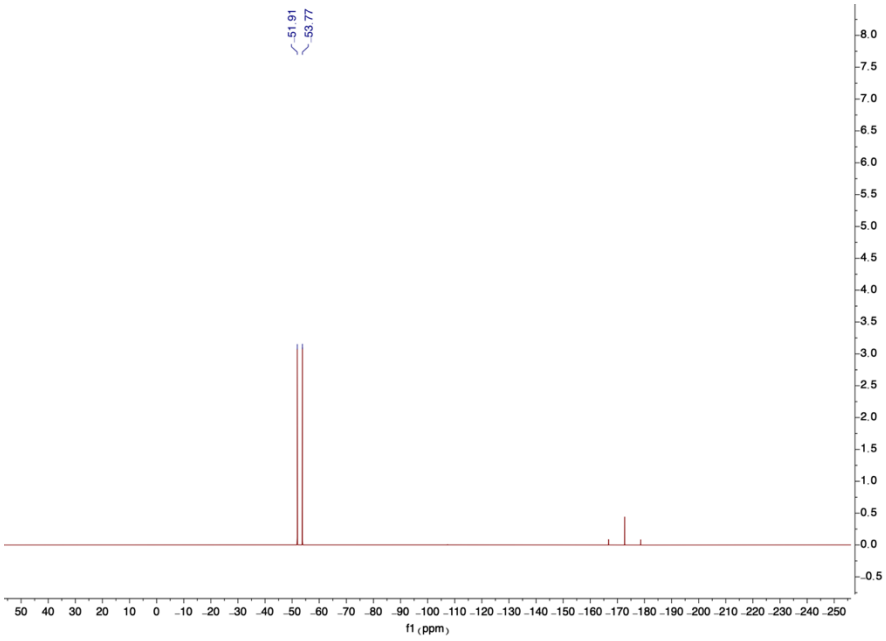

^{13}C NMR spectrum of **IV.7** in $CDCl_3$:

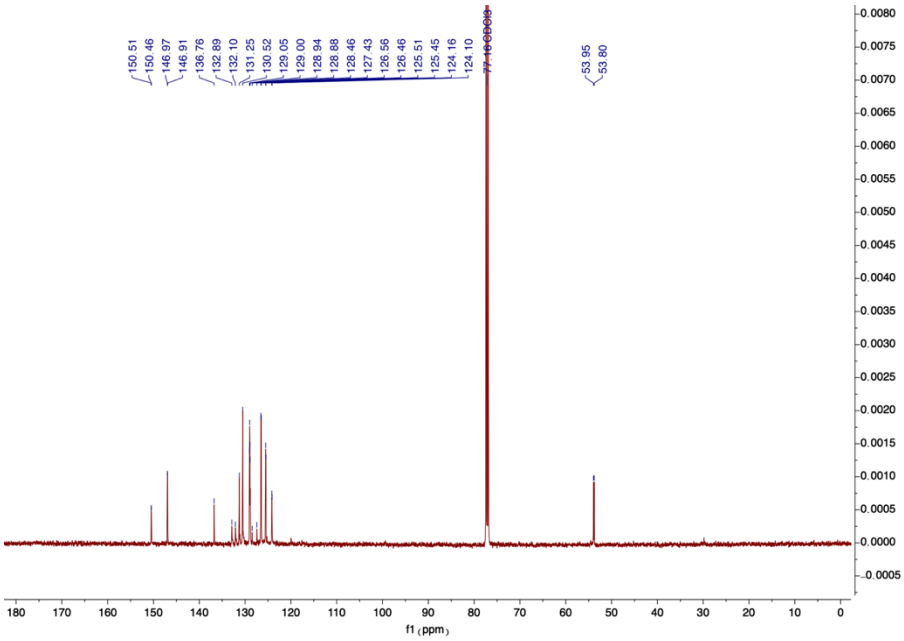

Synthesis of 1-chloro-9-fluorophosphoniumtriptycene tetrakis-(2,3-bis(trifluoromethyl)phenyl)borate **IV.8**

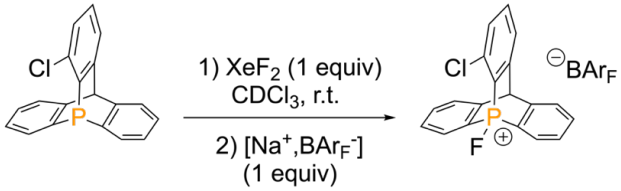

IV.6 **IV.8**

In a glovebox, under argon atmosphere, XeF_2 (5.5 mg, 0.033 mmol) is weighted in a glass vial, and then dissolved in 1.0 mL of deuterated chloroform ($CDCl_3$). Next the 1-chloro-9-phosphatriptycene (10.0 mg, 0.033 mmol) is added to the colorless mixture, effervescence appears. The solution is stirred manually for a few minutes. $NaBAr_F$ is then added (28.9 mg, 0.033 mmol), a precipitate appears (NaF), the solution is then stirred again manually for a few minutes. Slow filtration through a Pasteur pipette with cotton followed by NMR analysis of the resulting clear solution showed completed conversion of the starting material to the product.

^{1}H NMR (500 MHz, $CDCl_3$) δ: 8.00 (ddd, *J* = 14.8, 7.6, 1.3 Hz, 2H), 7.77 – 7.69 (m, 10H), 7.60 (td, *J* = 7.1, 3.1 Hz, 1H), 7.54 (tt, *J* = 7.6, 1.1 Hz, 2H), 7.47 (s, 4H), 7.44 – 7.38 (m, 3H), 7.32 (dd, *J* = 8.2, 5.5 Hz, 1H), 5.86 (s, 1H).

^{31}P NMR (202 MHz, $CDCl_3$) δ: 82.90 (d, *J* = 1157.5 Hz).

^{19}F NMR (471 MHz, $CDCl_3$) δ: -62.29, -183.17 (dd, *J* = 1157.3, 3.3 Hz).

^{11}B NMR (160 MHz, $CDCl_3$) δ: -7.55.

^{13}C NMR (126 MHz, $CDcl_3$) δ: 161.87 (dd, *J* = 99.7, 49.7 Hz), 149.39 – 147.71 (m), 145.43 (dd, *J* = 10.6, 5.3 Hz), 136.19, 135.65, 135.48 (d, *J* = 3.0 Hz), 134.92, 130.15 (d, *J* = 9.1 Hz), 129.61 – 128.78 (m), 128.59 (d, *J* = 14.3 Hz), 128.00 (d, *J* = 5.0 Hz), 127.59 (dd, *J* = 11.6, 3.0 Hz), 125.73, 125.57 (d, *J* = 11.6 Hz), 123.57, 121.40, 117.77 – 117.53 (m), 53.31 (d, *J* = 25.1 Hz).

^{1}H NMR spectrum of **IV.8** in $CDCl_3$:

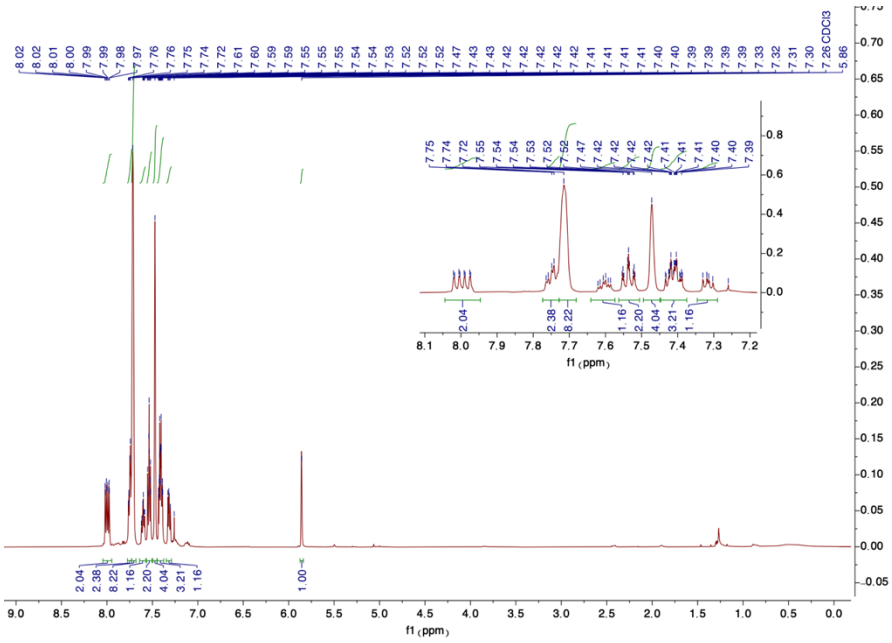

^{31}P NMR spectrum of **IV.8** in $CDCl_3$:

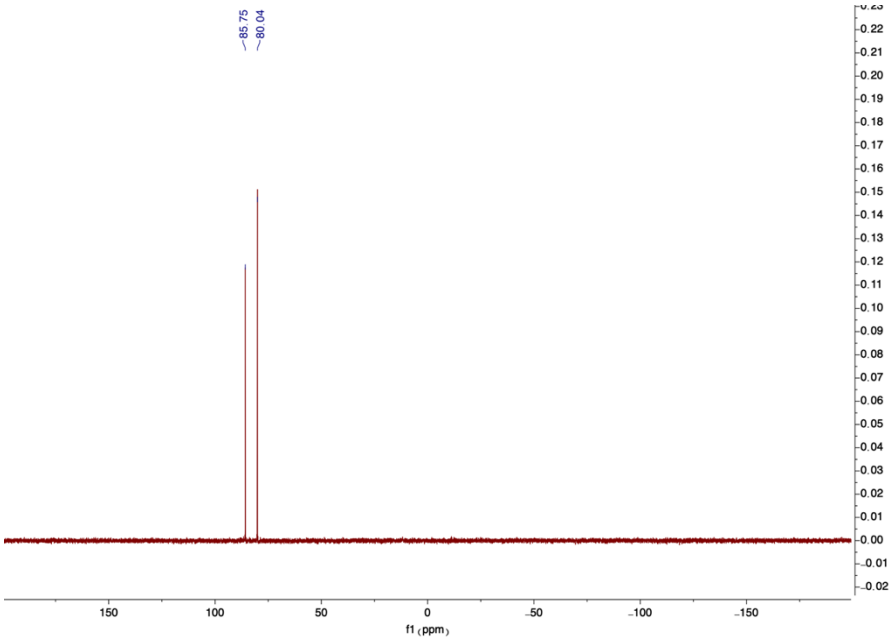

^{19}F NMR spectrum of **IV.8** in $CDCl_3$:

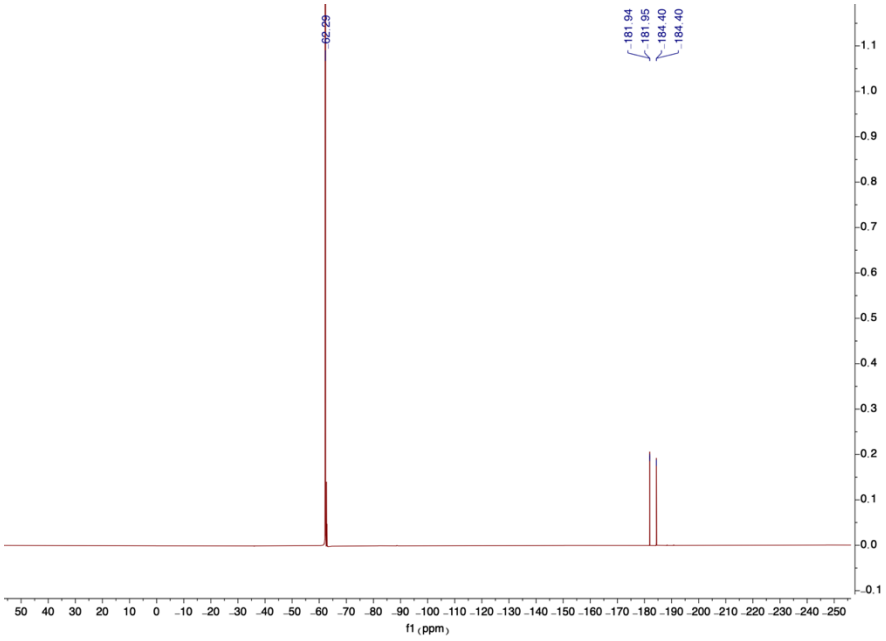

^{11}B NMR spectrum of **IV.8** in $CDCl_3$:

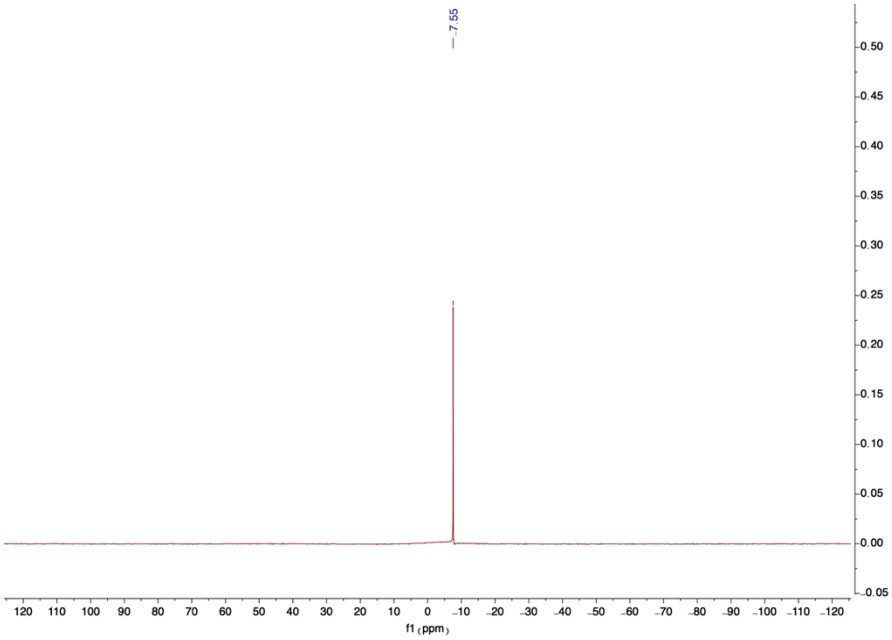

^{13}C NMR spectrum of **IV.8** in $CDCl_3$:

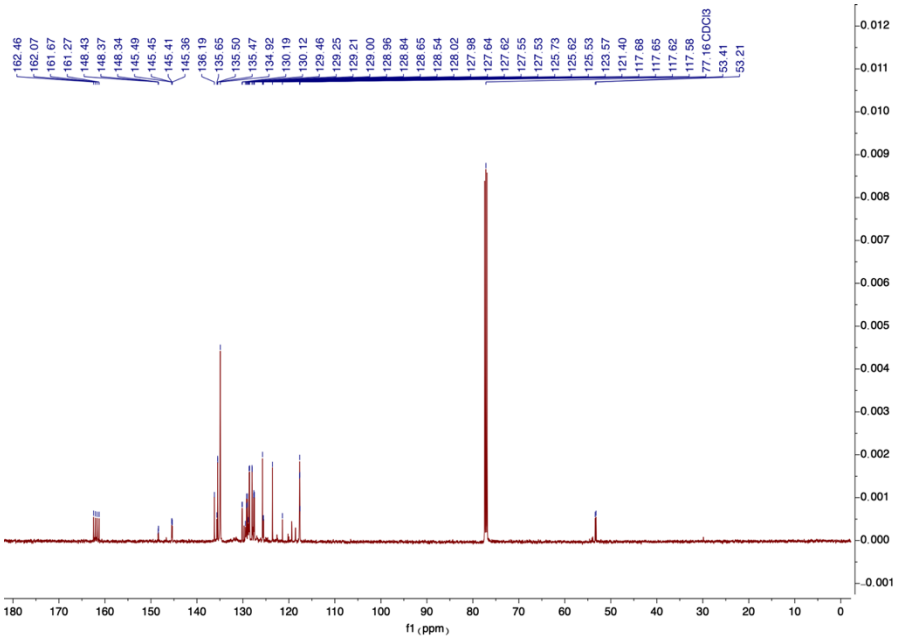

Fluoride abstraction of **IV.2** (generated from **IV.1**) by $B(C_6F_5)_3$

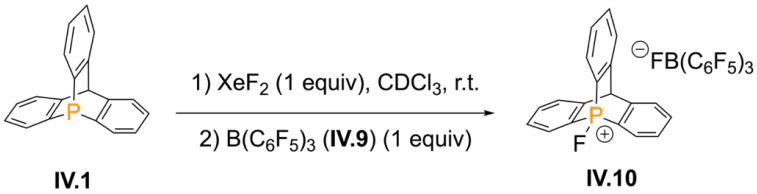

IV.1 **IV.10**

In a glovebox, under argon atmosphere, XeF_2 (12.4 mg, 0.073 mmol) is weighted in a glass vial, and then dissolved in 3.0 mL of deuterated chloroform ($CDCl_3$). Next the 9-phosphatriptycene (**IV.1**) (20.0 mg, 0.073 mmol) is added. The solution is stirred manually for a few minutes. $B(C_6F_5)_3$ is then added (37.6 mg, 0.074 mmol) the solution is then stirred again manually for a few minutes, a sample (0.5 mL) for NMR analysis while the rest of the solution is left to slowly evaporate.

Formation of the product is observed by ^{31}P (d, 83 ppm, J = 1148 Hz) and ^{19}F NMR (d, -189 ppm, J = 148 Hz). Still, significant amount of degradation product and impurities are found with ^{19}F, ^{11}B and ^{1}H NMR.

^{31}P NMR spectrum of the fluoride abstraction of **IV.2** (generated from **IV.1**) by $B(C_6F_5)_3$

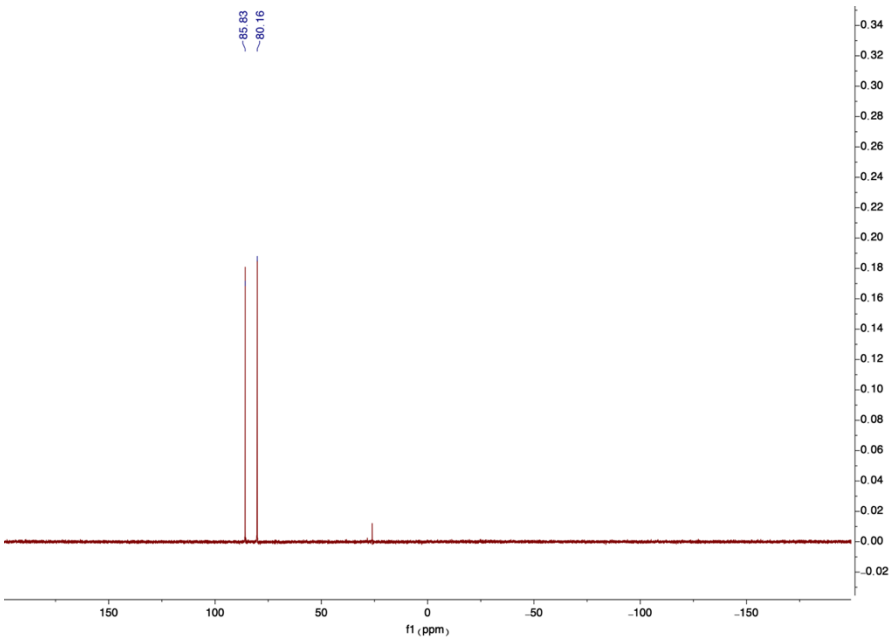

^{19}F NMR spectrum of the fluoride abstraction of **IV.2** (generated from **IV.1**) by $B(C_6F_5)_3$

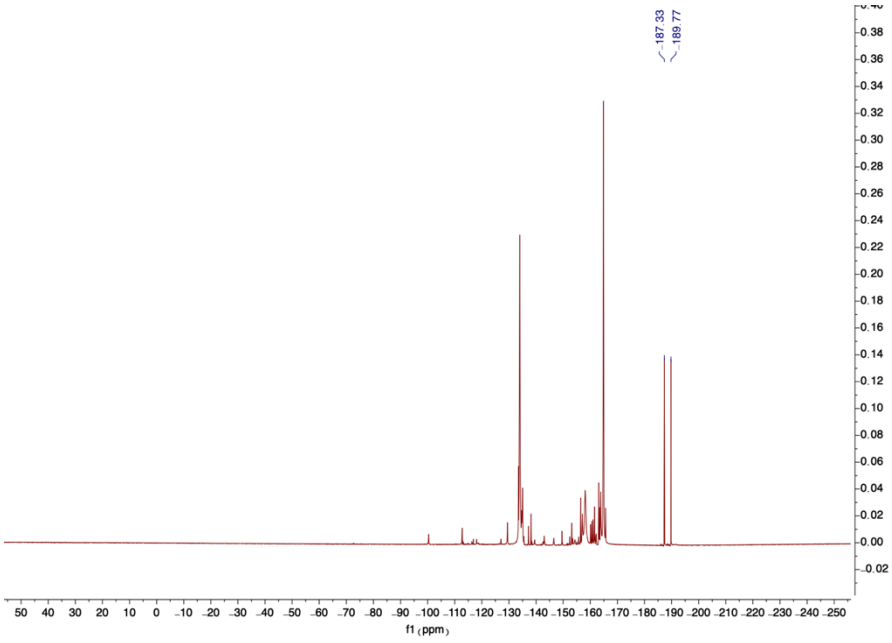

^{11}B NMR spectrum of the fluoride abstraction of **IV.2** (generated from **IV.1**) by $B(C_6F_5)_3$

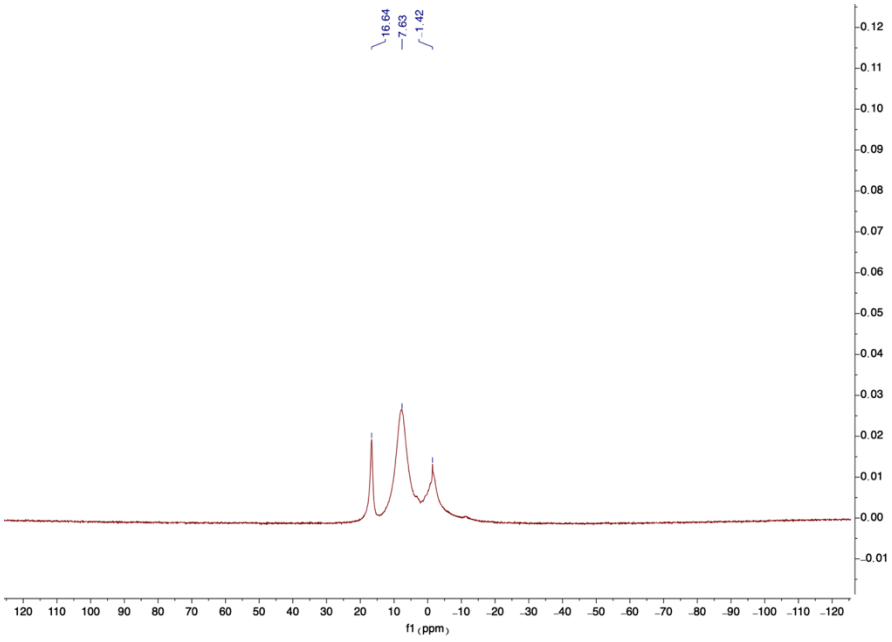

^{1}H NMR spectrum of the fluoride abstraction of **IV.2** (generated from **IV.1**) by $B(C_6F_5)_3$

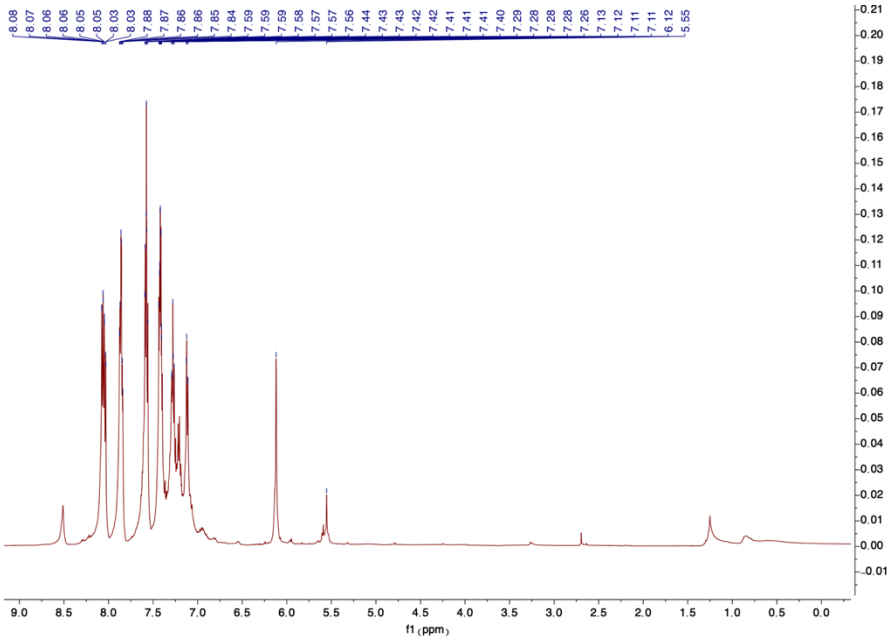

General procedure of fluoride transfer reactions of 9-fluorophosphoniumtriptycene tetrakis(2,3-bis(trifluoromethyl)-phenyl)borate **IV.5** to a triaryl phosphine PAr_3 [PAr_3 = PPh_3, P(4-Tol)$_3$ and P(4-$MeOC_6H_4$)$_3$]

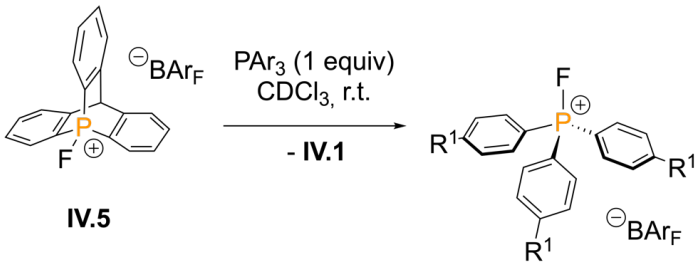

IV.5

IV.10, R^1 = H
IV.11, R^1 = Me
IV.12, R^1 = OMe

Representative example of tris(*p*-tolyl)phosphine [P(4-Tol)$_3$]: In a glovebox, under argon atmosphere, 9-fluorophosphoniumtriptycene tetrakis(2,3-bis(trifluoromethyl)phenyl)borate **IV.5** (10.0 mg, 0.0087 mmol) is weighted in a glass vial, then P(4-Tol)$_3$ (98%, 2.7 mg, 0.0087 mmol) and 0.5 mL of deuterated chloroform ($CDCl_3$). The outcome of the reaction is followed by ^{31}P NMR, which shows the conversion of P(4-Tol)$_3$ to **IV.11** and the appearance of **IV.1** in solution (s, -64.4 ppm), with a small amount of degradation of **IV.5** to a phosphine oxide.

The ^{31}P chemical shift of **IV.11** (d, 95.3 ppm, J = 991 Hz) and **IV.12** (d, 92.8 ppm, J = 987 Hz) are consistent with reported values.[12]

^{31}P NMR spectrum of the fluoride transfer of **IV.5** to P(4-Tol)$_3$:

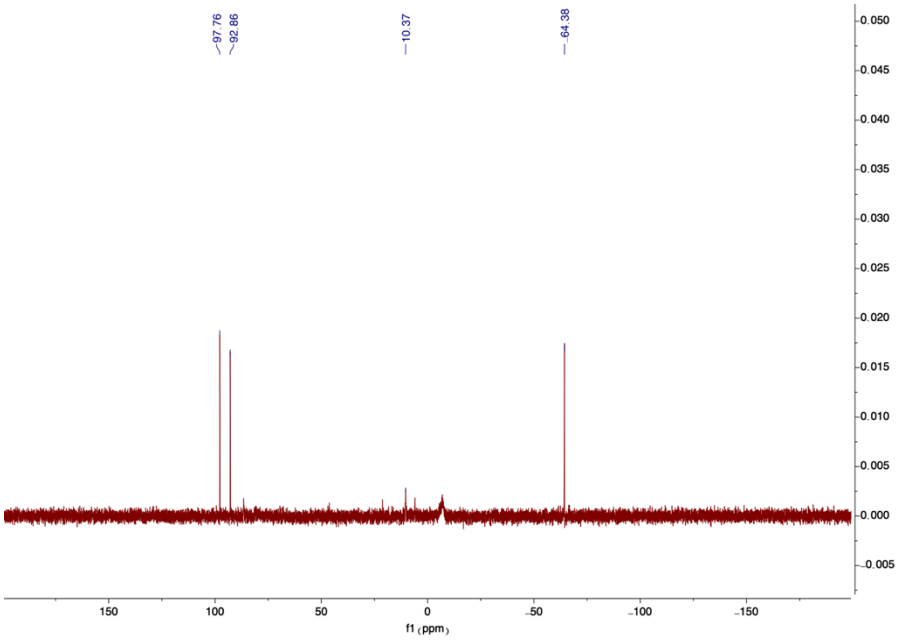

^{31}P NMR spectrum of the fluoride transfer of **IV.5** to P(4-MeOC$_6$H$_4$)$_3$:

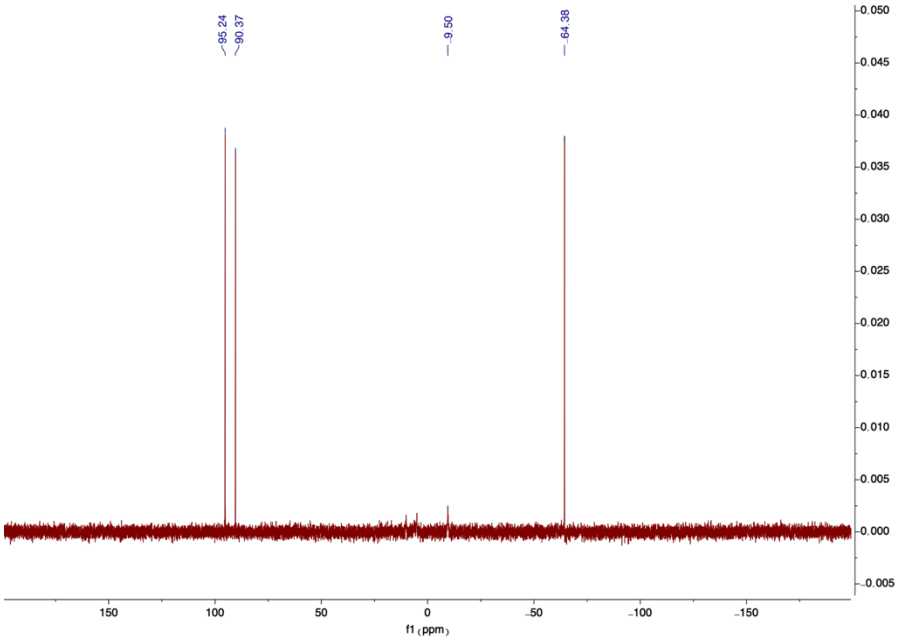

^{31}P NMR spectrum showing no reaction between PPh_3 and **IV.5**:

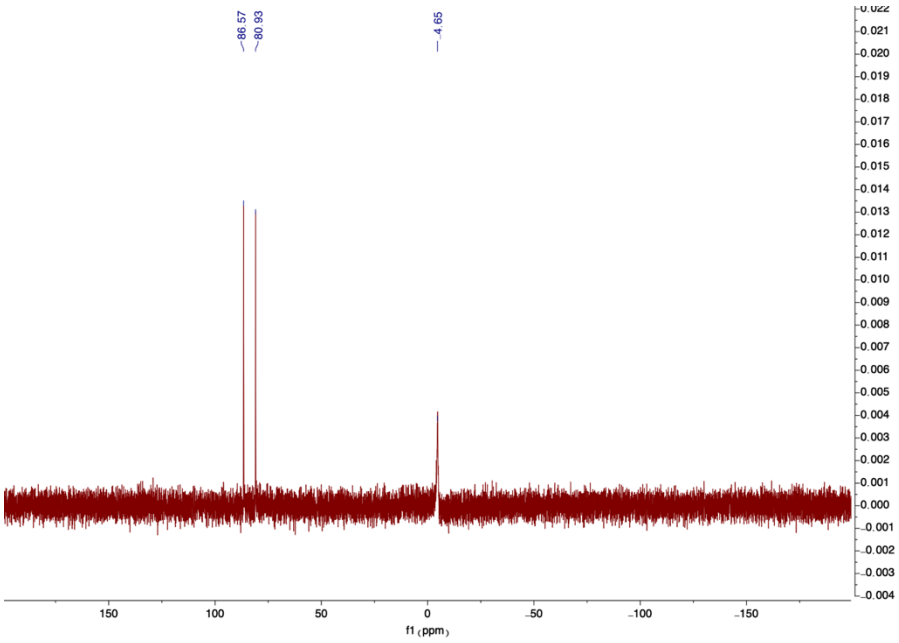

4.2 Crystallographic data

The crystal structures of **IV.2** (preliminary refinement of modulated 3D+1 crystal in 3D space) and **IV.5** were determined from single-crystal X-ray diffraction data collected using an Oxford Diffraction Gemini Ultra R diffractometer (Cu Kα radiation with multilayer mirror or Mo Kα radiation with graphite monochromator). The data were integrated using the CrysAlis^{Pro} software.[13] The structures were solved by the dual-space algorithm implemented in SHELXT,[14] and refined by full-matrix least squares on $|F|^2$ using SHELXL-2018/3,[15] the shelXLe,[16] and Olex2 software.[17] Non-hydrogen atoms were refined anisotropically. In case of **IV.5** hydrogen atoms were located from the difference Fourier map, but were placed on calculated positions in riding mode with equivalent isotropic temperature factors fixed at 1.2 times Ueq of the parent atoms for both structures.

*Table S25. Crystal data for compounds **IV.2**, **IV.5**. Ellipsoids shown at 50% probability.*

Compounds	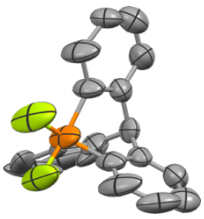 **IV.2**	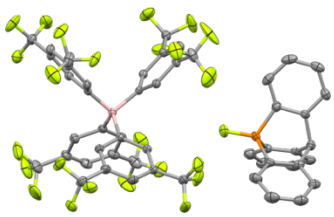 **IV.5**
Formula	$C_{19}H_{13}F_2P$	$C_{32}H_{12}BF_{24}^-$,$C_{19}H_{13}FP^+$
Crystal system	Monoclinic*	Monoclinic
Space group	I 2/a*	P 2_1/n
a (Å)	18.0631(6)*	10.0690(2)
b (Å)	10.1395(3)*	16.0535(3)
c (Å)	15.8905(5)*	30.1354(8)
α (°)	90*	90
β (°)	96.616(3)*	91.657(2)
γ (°)	90*	90
Volume (Å^3)	2890.98*	4869.13
Z, Z'	Z: 8; Z': 1*	Z: 4 Z': 1
R factor (%)	20.26*	5
T (K)	100	100

* values for preliminary refinement of modulated 3D+1 crystal in 3D space

4.3 Details on the quantum chemical calculations, cartesian coordinates, electronic energies, enthalpies and free energies of optimized structures

The calculations were performed using the Gaussian16 package.[3] Full geometry optimizations followed by vibrational frequency calculations were done at the M06-2X/6-311G(d) level of theory,[4] at a temperatures and a pressure of 298.15 K and 1 atm. Tight convergence thresholds were used for geometry optimizations, *e.g.* for the residual forces on the atoms, 1.5×10^{-5} Hartree/Bohr or Hartree/radian. All vibrational frequencies are real, demonstrating that the structures are minima on the potential energy surface. Implicit solvation effects for dichloromethane were taken into account using the IEFPCM scheme.[10]

IV.1

E (a.u.)	H (a.u.)	G (a.u.)
-1073.061592	-1072.784496	-1072.839781

P	0.0001130000	-0.0001570000	-1.6891540000
C	1.5256550000	-0.3450950000	-0.6966100000
C	1.3871270000	-0.3136820000	0.6968990000
C	2.4860180000	-0.5618260000	1.5076330000
H	2.3806510000	-0.5379200000	2.5875640000
C	3.7250910000	-0.8417730000	0.9294000000
H	4.5823460000	-1.0351810000	1.5643200000
C	3.8639120000	-0.8733660000	-0.4528900000
H	4.8280560000	-1.0913310000	-0.8977360000
C	2.7603630000	-0.6241790000	-1.2700070000
H	2.8654480000	-0.6480250000	-2.3498220000
C	-0.4639410000	1.4934960000	-0.6968020000
C	-0.4217230000	1.3577300000	0.6967140000
C	-0.7562150000	2.4334770000	1.5075230000
H	-0.7239760000	2.3301990000	2.5874520000
C	-1.1333020000	3.6465450000	0.9294980000
H	-1.3938580000	4.4857580000	1.5645030000
C	-1.1757000000	3.7826180000	-0.4528300000
H	-1.4689520000	4.7266210000	-0.8976000000
C	-0.8398850000	2.7022910000	-1.2700400000
H	-0.8718760000	2.8052620000	-2.3498710000
C	-1.0613880000	-1.1487290000	-0.6965710000
C	-0.9648940000	-1.0444410000	0.6969000000
C	0.0001490000	0.0000000000	1.2390930000
C	-1.7297030000	-1.8716350000	1.5076470000
H	-1.6562510000	-1.7922340000	2.5875760000
C	-2.5921050000	-2.8043150000	0.9294910000

H	-3.1886870000	-3.4494730000	1.5645270000
C	-2.6887900000	-2.9088360000	-0.4528270000
H	-3.3598960000	-3.6345820000	-0.8976680000
C	-1.9207870000	-2.0781200000	-1.2699200000
H	-1.9940020000	-2.1572620000	-2.3497410000
H	0.0000000000	0.0000000000	2.3300180000

IV.2

E (a.u.)	H (a.u.)	G (a.u.)
-1272.77403	-1272.48824	-1272.54909

P	0.0000000000	-0.1819660000	1.3065160000
C	-1.4165660000	-0.7682140000	0.3337230000
C	-1.2540870000	-0.5881310000	-1.0464700000
C	-2.2377210000	-1.0550640000	-1.9088400000
H	-2.1172650000	-0.9318720000	-2.9799400000
C	-3.3760550000	-1.6751310000	-1.3970900000
H	-4.1441390000	-2.0284870000	-2.0753220000
C	-3.5280390000	-1.8505390000	-0.0256540000
H	-4.4113740000	-2.3409830000	0.3657720000
C	-2.5354490000	-1.4119430000	0.8469160000
H	-2.6282800000	-1.5760080000	1.9139570000
C	-0.0001300000	1.5250590000	0.5098830000
C	-0.0001290000	1.5081660000	-0.8889980000
C	-0.0001220000	2.6887460000	-1.6165030000
H	-0.0001180000	2.6586660000	-2.7013230000
C	-0.0001800000	3.9101450000	-0.9435260000
H	-0.0002200000	4.8364500000	-1.5067200000
C	-0.0001840000	3.9381380000	0.4453180000
H	-0.0002290000	4.8875420000	0.9686320000
C	-0.0001330000	2.7477390000	1.1738840000
H	-0.0002370000	2.7809310000	2.2557000000
C	1.4166380000	-0.7680730000	0.3337330000
C	1.2541500000	-0.5880070000	-1.0464620000
C	0.0000000000	0.1302200000	-1.5299000000
C	2.2378360000	-1.0548410000	-1.9088260000
H	2.1173730000	-0.9316630000	-2.9799270000
C	3.3762280000	-1.6747960000	-1.3970690000
H	4.1443510000	-2.0280750000	-2.0752960000
C	3.5282210000	-1.8501890000	-0.0256320000
H	4.4116040000	-2.3405430000	0.3657990000
C	2.5355830000	-1.4116900000	0.8469320000
H	2.6284230000	-1.5757470000	1.9139730000
H	0.0000000000	0.2011250000	-2.6177940000
F	0.0000000000	0.5422670000	2.7599820000
F	0.0001350000	-1.5857580000	2.2424880000

IV.3

E (a.u.)	H (a.u.)	G (a.u.)
-1036.143946	-1035.851485	-1035.914334

P	-0.0001470000	-0.0012710000	-1.2893020000
C	1.3487710000	-0.9404390000	-0.4543860000
C	1.6736360000	-2.1928870000	-0.9866010000
C	2.0425230000	-0.4840910000	0.6693010000
C	2.6580160000	-2.9804540000	-0.4005340000
H	1.1507370000	-2.5550000000	-1.8667680000
C	3.0374110000	-1.2674750000	1.2487880000
H	1.8080630000	0.4840030000	1.0985230000
C	3.3447710000	-2.5164740000	0.7183710000
H	2.8965730000	-3.9501900000	-0.8226500000
H	3.5688020000	-0.9019100000	2.1202200000
H	4.1196160000	-3.1241930000	1.1715340000
C	0.1373160000	1.6377500000	-0.4564760000
C	-0.6056310000	2.0127220000	0.6650280000
C	1.0642280000	2.5415910000	-0.9882850000
C	-0.4213780000	3.2649090000	1.2456680000
H	-1.3299280000	1.3255680000	1.0898140000
C	1.2578840000	3.7864180000	-0.4001890000
H	1.6405730000	2.2677890000	-1.8671180000
C	0.5119300000	4.1517050000	0.7179720000
H	-1.0047280000	3.5438770000	2.1156830000
H	1.9822150000	4.4754750000	-0.8193460000
H	0.6548390000	5.1250380000	1.1728780000
C	-1.4892990000	-0.6978520000	-0.4545900000
C	-2.7349780000	-0.3570930000	-0.9919020000
C	-1.4426590000	-1.5212030000	0.6730210000
C	-3.9103470000	-0.8123460000	-0.4036650000
H	-2.7868430000	0.2737880000	-1.8746650000
C	-2.6188690000	-1.9898760000	1.2524460000
H	-0.4866250000	-1.7977370000	1.1046720000
C	-3.8539720000	-1.6325360000	0.7197880000
H	-4.8697960000	-0.5341460000	-0.8251590000
H	-2.5688180000	-2.6321210000	2.1246350000
H	-4.7685870000	-1.9953930000	1.1747480000

IV.4 (isomer I)

E (a.u.)	H (a.u.)	G (a.u.)
-1235.88055	-1235.57870	-1235.64656

P	0.0082960000	-0.0007970000	0.0015000000
C	-1.8150360000	-0.1825980000	0.0000000000
C	-2.4992000000	-0.5049600000	-1.1791040000
C	-2.5512640000	-0.0011950000	1.1781100000

C	-3.8819340000	-0.6476270000	-1.1751590000
H	-1.9559930000	-0.6391460000	-2.1025810000
C	-3.9351390000	-0.1319560000	1.1714530000
H	-2.0462440000	0.2356230000	2.1027620000
C	-4.6044590000	-0.4584210000	-0.0026080000
H	-4.3934410000	-0.9033570000	-2.0957700000
H	-4.4886610000	0.0179520000	2.0910660000
H	-5.6832640000	-0.5649070000	-0.0036820000
C	0.7505330000	1.6617800000	-0.0915070000
C	1.6909070000	1.9561890000	-1.0804880000
C	0.3769370000	2.6470410000	0.8249780000
C	2.2657910000	3.2209270000	-1.1383100000
H	1.9722390000	1.1999670000	-1.8019280000
C	0.9305750000	3.9193370000	0.7420510000
H	-0.3441720000	2.4222290000	1.6007540000
C	1.8808950000	4.2052560000	-0.2335930000
H	3.0075580000	3.4387770000	-1.8978280000
H	0.6248910000	4.6846840000	1.4458570000
H	2.3208590000	5.1944880000	-0.2885290000
C	1.0689740000	-1.4810610000	0.0942560000
C	2.0403990000	-1.5888330000	1.0915190000
C	0.9110680000	-2.5135670000	-0.8330070000
C	2.8581510000	-2.7121060000	1.1468400000
H	2.1566970000	-0.7979210000	1.8211100000
C	1.7091580000	-3.6486540000	-0.7526530000
H	0.1680160000	-2.4319620000	-1.6161410000
C	2.6884710000	-3.7457760000	0.2312250000
H	3.6217360000	-2.7823970000	1.9127190000
H	1.5709130000	-4.4533910000	-1.4652570000
H	3.3186020000	-4.6262890000	0.2841090000
F	0.0285120000	0.1071560000	1.7005430000
F	0.0511380000	-0.1010500000	-1.6975990000

IV.4 (Isomer II)

E (a.u.)	H (a.u.)	G (a.u.)
-1235.85187	-1235.55055	-1235.61676

P	-0.0575820000	-0.3270040000	0.8852290000
C	0.0938190000	1.4599220000	0.3049720000
C	1.0016330000	2.3041660000	0.9561750000
C	-0.5606760000	1.9480110000	-0.8295010000
C	1.2346360000	3.5961860000	0.5004910000
H	1.5337750000	1.9518060000	1.8326960000
C	-0.3264320000	3.2417510000	-1.2916150000
H	-1.2589420000	1.3219170000	-1.3734340000
C	0.5684000000	4.0705510000	-0.6262450000
H	1.9376970000	4.2331790000	1.0253930000

H	-0.8483190000	3.5983760000	-2.1725040000
H	0.7483850000	5.0782540000	-0.9831890000
C	-1.6787350000	-0.6854760000	0.1518050000
C	-1.8348330000	-1.7988500000	-0.6744250000
C	-2.7697110000	0.1342660000	0.4391780000
C	-3.0766480000	-2.0715420000	-1.2364560000
H	-0.9892340000	-2.4462690000	-0.8804420000
C	-4.0180070000	-0.1648220000	-0.0959600000
H	-2.6469400000	1.0054730000	1.0741500000
C	-4.1685070000	-1.2591450000	-0.9424140000
H	-3.1943110000	-2.9248960000	-1.8939550000
H	-4.8687340000	0.4637650000	0.1392660000
H	-5.1386910000	-1.4808870000	-1.3718910000
C	1.4593760000	-0.9100060000	0.0448250000
C	1.7787130000	-0.4539090000	-1.2379440000
C	2.3253760000	-1.7983650000	0.6908740000
C	2.9313960000	-0.9005050000	-1.8729840000
H	1.1298320000	0.2442610000	-1.7522300000
C	3.5006100000	-2.2045130000	0.0690660000
H	2.0790070000	-2.1720090000	1.6751220000
C	3.8009240000	-1.7652350000	-1.2159000000
H	3.1559850000	-0.5587680000	-2.8764700000
H	4.1746910000	-2.8767850000	0.5868670000
H	4.7100030000	-2.0961420000	-1.7048290000
F	0.0219970000	0.2091050000	2.4137120000
F	-0.1584940000	-1.8636760000	1.6522180000

IV.5 (counter anion ignored)

E (a.u.)	H (a.u.)	G (a.u.)
-1172.73289	-1172.45028	-1172.50809

P	0.0005330000	0.0000000000	1.2781150000
C	-1.2216930000	-1.0509900000	0.5345940000
C	-1.0898500000	-0.9367220000	-0.8600400000
C	-1.9463120000	-1.6706290000	-1.6645390000
H	-1.8682260000	-1.6022580000	-2.7434750000
C	-2.9062110000	-2.4953780000	-1.0767270000
H	-3.5730470000	-3.0673020000	-1.7106740000
C	-3.0204030000	-2.5951670000	0.3058330000
H	-3.7712840000	-3.2406430000	0.7436740000
C	-2.1707780000	-1.8664660000	1.1337760000
H	-2.2492060000	-1.9347450000	2.2117760000
C	-0.2987350000	1.5836100000	0.5346300000
C	-0.2663490000	1.4115060000	-0.8599420000
C	-0.4757890000	2.5195850000	-1.6645840000
H	-0.4577060000	2.4168630000	-2.7434550000
C	-0.7101910000	3.7634450000	-1.0772290000

H	-0.8732230000	4.6264070000	-1.7115310000
C	-0.7378090000	3.9130310000	0.3053240000
H	-0.9210270000	4.8861900000	0.7429650000
C	-0.5301840000	2.8133770000	1.1334730000
H	-0.5492570000	2.9156150000	2.2115080000
C	1.5218820000	-0.5328150000	0.5347530000
C	1.3559740000	-0.4758880000	-0.8598820000
C	0.0000000000	-0.0004910000	-1.3941090000
C	2.4199090000	-0.8494370000	-1.6647900000
H	2.3214300000	-0.8154920000	-2.7436610000
C	3.6147210000	-1.2675970000	-1.0777990000
H	4.4432030000	-1.5585840000	-1.7123020000
C	3.7590770000	-1.3165470000	0.3046740000
H	4.6940010000	-1.6433620000	0.7420140000
C	2.7033490000	-0.9458810000	1.1332580000
H	2.8020480000	-0.9791680000	2.2114170000
H	-0.0001190000	-0.0002450000	-2.4827180000
F	-0.0010050000	-0.0007030000	2.8320760000

5. Chapter V

The cartesian coordinates, electronic energies, enthalpies and free energies of optimized structures are available online on the publication link:

9-boratriptycene:

https://onlinelibrary.wiley.com/doi/full/10.1002/anie.202003119

9-sulfonium-10-boratriptycene:

https://onlinelibrary.wiley.com/doi/full/10.1002/ange.202112342

Semi-planar boranes:

https://chemistry-europe.onlinelibrary.wiley.com/doi/full/10.1002/chem.202003319

Table S26. Global (ω) and local (ω_B, on the boron atom) electrophilicity indexes for several Lewis acids. Structures are optimized at the M06-2X/6-311G(d) level of theory. The natural charges of the boron Q_B (N) and Q_B (N+1) are obtained after NBO analysis (respectively with charge=0, spin multiplicity=1 and charge=-1, spin multiplicity=2) on the same geometrical structures and at the same level of theory.

Compounds	Global Electrophilicity Index			Local (boron) electrophilicity index			
	ε_{HOMO} (eV)	ε_{LUMO} (eV)	**ω (eV)**	Q_B (N+1)	Q_B (N)	ΔQ_B	**ω_B (eV)**
1-boraadamantane **V.1**	-8.65	0.60	**0.88**	0.41	1.06	-0.65	**-0.57**
9-boratriptycene **V.3**	-7.43	-0.64	**1.20**	-0.25	1.00	-1.25	**-1.50**
1-borabarrelene **V.2**	-7.38	-0.24	**1.02**	-0.33	0.88	-1.21	**-1.23**
BPh_3 **V.10**	-8.17	-1.12	**1.53**	0.50	0.93	-0.42	**-0.65**
$B(C_6F_5)_3$ **V.11**	-9.00	-2.78	**2.79**	0.44	0.88	-0.44	**-1.23**
BEt_3	-9.13	0.49	**0.97**	0.43	1.12	-0.69	**-0.67**

6. Chapter VI

6.1 Validation study

In order to validate the results obtained with our standard DFT scheme (M06-2X/6-311G[d]), the same two reaction pathways were investigated with other calculation methods (Table S27). First, the exchange-correlation functional (XCF) was changed to ωB97X-D to assess the impact of using a range-separated hybrid XC functional, including a *a posteriori* London dispersion correction. Then, diffuse and supplementary polarization functions were added to the basis set (6-311+G[2d,p]), keeping the M06-2X XCF, to check the impact of a more flexible basis set. Finally, a higher level method was also employed as reference, using the double-hybrid B2PLYP-D3 XCF and the 6-311+G(2d,p) basis set. In all cases, solvent (cyclohexane) effects were taken into account by using the IEFPCM scheme.

Table S27. Thermodynamic state functions of the methane heterolytic splitting at several levels of theory in cyclohexane (IEFPCM). All energies are given in kJ.mol^{-1} except entropies, given in J.mol^{-1}.K^{-1}. Vibrational frequencies ω are given in cm^{-1}. In bold are highlighted the results obtained with the standard method of this work.

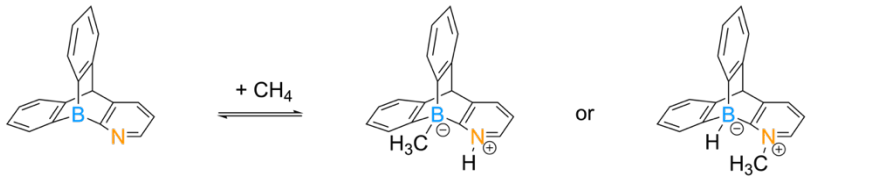

VI.3 **VI.3**-P1 (through transition state TS1) **VI.3**-P2 (through transition state TS2)

Product /TS	Method	ΔE	ΔH⁰	ΔS⁰	ΔG⁰	ΔE≠	ΔG≠	ωi
P1/TS1	**M06-2X/6-311G(d)**	**-156**	**-145**	**-152**	**-108**	**46**	**76**	**1430*i***
	ωB97X-D/6-311G(d)	-158	-146	-153	-108	47	78	1504*i*
	M06-2X/6-311+G(2d,p)	-153	-142	-160	-103	42	75	1393*i*
	B2PLYP-D3/ 6-311+G(2d,p)	-149	-138	-160	-98	47	79	1479*i*
P2/TS2	**M06-2X/6-311G(d)**	**-113**	**-102**	**-153**	**-64**	**227**	**258**	**1036*i***
	ωB97X-D/6-311G(d)	-112	-101	-151	-63	224	254	1007*i*
	M06-2X/6-311+G(2d,p)	-106	-95	-162	-55	232	265	1029*i*
	B2PLYP-D3/ 6-311+G(2d,p)	-101	-91	-160	-51	212	243	920*i*

No matter which calculation method is employed, the reaction leading to the formation of product P1 going through TS1 is always preferred to its competing pathway. Changing the functional to ωB97X-D had virtually no impact on the thermochemistry of both reactions. Increasing the size of the basis set leads to a small increase in both reactions ΔG^0, up to -103 kJ.mol^{-1} for P1 [*versus* -108 kJ.mol^{-1} with M06-2X/6-311G(d)] and -55 kJ.mol^{-1} for P2 [*versus* -64 kJ.mol^{-1} with M06-2X/6-311G(d)]. The difference is even smaller when the transition states are considered. A slightly larger impact was observed when the double-hybrid B2PLYP-D3 functional was used with the 6-311+G(2d,p) basis set. ΔE(P1) increases to -149 kJ.mol^{-1} [*versus* -156 kJ.mol^{-1} with M06-2X/6-311G(d)]. The differences are smaller for the other state functions, with positive shifts by 5 kJ.mol^{-1} or less for ΔG^0, ΔH^0, $\Delta E^{\neq}$ and $\Delta G^{\neq}$. Interestingly, the $\Delta E^{\neq}$ and $\Delta G^{\neq}$ are roughly the same [difference of only +1.2 and +3.5 kJ.mol^{-1} respectively going from M06-2X/6-311G(d) to B2PLYP-D3/6-311+G(2d,p)]. These comparisons with other methods, ωB97X-D/6-311G(d), M06-2X/6-311+G(2d,p), including the higher-level B2PLYP-D3/6-311+G(2d,p) validate the thermodynamic results obtained at the standard M06-2X/6-311G(d) level of theory.

On a structural point of view, there is in general no major difference in any structure (Table S28). Still, the parameters that are the most affected by changing the method are the interatomic distances in the transition states. In the structures of the products, all methods give very close results (with generally ±0.01-0.02 Å in interatomic distances, a maximum difference of 0.06 Å and maximum angle deviation of 0.1°). The standard M06-2X/6-311G(d) method can thus also be validated for its prediction of molecular structures.

Table S28(A). Comparison of a selection of structural parameters in P1/TS1 and P2/TS2 at several levels of calculation. The structures of both TS are shown to indicate the location of the C_3 and C_{Me} atoms. Distances (d) are given in Å, angles (α) and dihedral angles (β) are given in °. The dihedral angles $\beta_{NC_3BC_{Me}}$ and $\beta_{BC_3NC_{Me}}$ of the products P1 and P2 are equal to 0.0° for all methods.

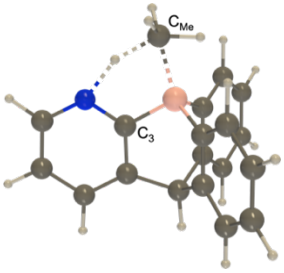

VI.3-TS1

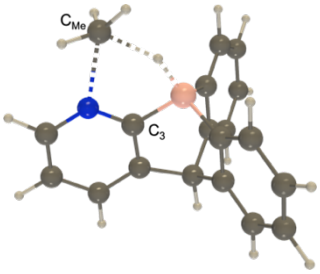

VI.3-TS2

Method	Structure of the transition state (TS1)					
	$d_{BC_{Me}}$	d_{NH}	$d_{C_{Me}H}$	α_{C_3NH}	$\alpha_{C_3BC_{Me}}$	$\beta_{NC_3BC_{Me}}$
M06-2X/6-311G(d)	1.799	1.400	1.354	87.3	105.3	0.0
ωB97X-D/6-311G(d)	1.798	1.388	1.353	87.3	105.1	0.0
M06-2X/6-311+G(2d,p)	1.800	1.398	1.350	86.6	105.3	0.0
B2PLYP-D3/6-311+G(2d,p)	1.810	1.388	1.358	87.0	105.2	0.0
Method	Structure of the transition state (TS2)					
	d_{BH}	$d_{NC_{Me}}$	$d_{C_{Me}H}$	$\alpha_{C_3NC_{Me}}$	α_{C_3BH}	$\beta_{BC_3NC_{Me}}$
M06-2X/6-311G(d)	1.318	2.171	1.658	107.0	91.2	3.4
ωB97X-D/6-311G(d)	1.310	2.202	1.693	106.9	92.4	2.9
M06-2X/6-311+G(2d,p)	1.312	2.185	1.661	106.6	91.7	3.4
B2PLYP-D3/6-311+G(2d,p)	1.305	2.229	1.701	106.2	92.0	2.8

Table S28(B). Comparison of a selection of structural parameters in P1/TS1 and P2/TS2 at several levels of calculation. The structures of both TS are shown to indicate the location of the C_3 and C_{Me} atoms. Distances (d) are given in Å, angles (α) and dihedral angles (β) are given in °. The dihedral angles $\beta_{NC_3BC_{Me}}$ and $\beta_{BC_3NC_{Me}}$ of the products P1 and P2 are equal to 0.0° for all methods.

Method	Structure of the product (P1)			
	$d_{BC_{Me}}$	d_{NH}	α_{C_3NH}	$\alpha_{C_3BC_{Me}}$
M06-2X/6-311G(d)	1.610	1.015	116.7	115.0
ωB97X-D/6-311G(d)	1.613	1.012	116.8	115.1
M06-2X/6-311+G(2d,p)	1.610	1.016	116.6	114.9
B2PLYP-D3/6-311+G(2d,p)	1.611	1.015	116.8	115.1
Method	Structure of the product (P2)			
	d_{BH}	$d_{NC_{Me}}$	$\alpha_{C_3NC_{Me}}$	α_{C_3BH}
M06-2X/6-311G(d)	1.207	1.473	118.7	116.1
ωB97X-D/6-311G(d)	1.213	1.470	119.0	116.0
M06-2X/6-311+G(2d,p)	1.204	1.472	118.8	116.1
B2PLYP-D3/6-311+G(2d,p)	1.205	1.474	119.0	116.3

6.2 Comparison with the literature ΔG^0 and $\Delta G^{\neq}$ results and formation of Lewis adducts for representative examples of FLPs

Using our DFT method the energetics of methane activation with system **VI.4a** (Table 17) shows similar results to the reported ones.[18] The reaction is slightly exergonic, ΔG^0 of -24 kJ.mol^{-1} while -22 kJ.mol^{-1} was reported previously, with comparable barriers of activation (87 kJ.mol^{-1} *versus* 85 kJ.mol^{-1} in ref. [18]). The second reaction pathway was not reported but Table 17 shows it is highly unfavorable. In general, the activation barriers and ΔG^0 reported above are higher than reported in the literature, which in some cases translates in an inversion of the sign of ΔG^0 but the same trends are drawn nonetheless: systems **VI.5**, **VI.6** and **VI.7** predict P2/TS2 to be thermodynamically favored but P1/TS1 to be kinetically favored and among them, system **VI.6** has the most favorable ΔG^0 and **VI.7** the most favorable $\Delta G^{\neq}$.

*Table S29. Thermodynamic state functions of Lewis acid-base adduct formation for systems **VI.5**, **VI.6** and **VI.7** at the M06-2X/6-311G(d) level of theory in cyclohexane (IEFPCM). All energies are given in kJ.mol^{-1} except entropies, given in J.mol^{-1}.K^{-1}. The Lewis adduct considered is intramolecular in the case of **VI.5**.*

FLP system	ΔE	ΔH^0	ΔS^0	ΔG^0
VI.5	-58	-56	-47	-42
VI.6	-37	-30	-197	21
VI.7	-116	-106	-213	-50

6.3 Characterization of the Lewis acidity

Table S30. Pyramidalization of the B atom, α (°), gas phase affinities, –ΔH^0 (kJ.mol^{-1}), of the complexation of selected B Lewis acids with typical Lewis bases (hydride, fluoride, ammonia, triphenylphosphine, and pyridine), as well as global (GEI) and local ($\omega_{B/Al}$) electrophilicity indices of the B or Al atom (eV) of the Lewis acids. Enthalpies for HIA and FIA are corrected via isodesmic reactions. "-H$^+$" suffixes to the molecule number indicate protonated Lewis base (P or N) centers. Btrp= boratriptycene.

Lewis acids	Affinities with Lewis bases and global/ local electrophilicities							
	α	HIA	FIA	NH_3	PPh_3	C_6H_5N	GEI (ω)	$\omega_{B/Al}$
9-phospha-10-Btrp. **VI.1**[19]	12.4	489	476	195	168	180	1.21	0.00[b]
9-phosphonium-10-Btrp. **VI.1**-H$^+$[19]	12.4	871	845	262	264	266	5.07	-4.03
9-Btrp. **VI.2**[20]	15.5	494	476	206	194	200	1.20	-1.50
1-aza-9-Btrp **VI.3**	16.0	498	476	239	215	239	1.25	-0.97
1-ammonium-9-Btrp **VI.3**-H$^+$	16.1	887	861	251	287	268	5.49	-0.04[b]
VI.4a	12.0	438	412	210	34[a]	118	0.97	-0.78
VI.4a-H$^+$	10.3	786	774	152	79[a]	135	3.77	-2.83
$B(C_6F_5)_3$[20]	0.0	514	466	159	133	144	2.79	-1.23
$Al(C_6F_5)_3$	0.0	504	505	194	184	185	2.38	-1.35
BPh_3[20]	0.0	350	333	88	72	79	1.53	-0.65
BEt_3[20]	0.9	290	285	92	38	86	0.97	-0.67

[a] The optimization did not lead to a Lewis adduct but a van der Waals complex (d_{B-P} = 4.840Å for **VI.4a** and 3.592Å for **VI.4a**-H$^+$). [b] The unpaired electron in these (N+1)-electron systems was not located on the boron but on the aromatic cycles and explains the almost 0 values of ω_B. All other unpaired electrons are located on the Lewis acid center.

The pyramidalization angle α is defined as the mean of three angles between, on the one hand, the line joining the Lewis acid center and a neighboring carbon and, on the other hand, the plane defined by the three neighboring carbons (Figure S46):

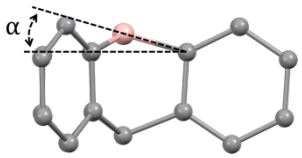

Figure S46. Pyramidalization angle α.

For fluoride (FIA) and hydride (HIA) affinities, isodesmic reactions were employed, using respectively $FSiMe_3 \rightarrow SiMe_3^+ + F^-$ (ΔH^0 = 958 kJ.mol^{-1}) and $HSiMe_3 \rightarrow SiMe_3^+ + H^-$ (ΔH^0 = 959 kJ.mol^{-1}) evaluated at the G3 level as anchor points, according to the scheme of Krossing.[21] The initial DFT values were therefore corrected by -119.1 kJ.mol^{-1} and -32.3 kJ.mol^{-1} for FIA and HIA, respectively.

The global electrophilicity index (ω, in eV) is defined as:[22]

$$\omega\ (eV) = {\chi^2}/{2\eta} \text{ with } \chi\ (eV) = {-1}/{2}\ (\varepsilon_{HOMO} + \varepsilon_{LUMO}) \text{ and } \eta\ (eV) = \varepsilon_{LUMO} - \varepsilon_{HOMO}$$

where χ is the electronegativity of Mulliken and η the chemical hardness.

The local electrophilicity index ω_k is defined as the product of the global electrophilicity ω with a local Fukui function f_k^+ (on the atomic site k):[23-25]

$$\omega_k(eV) = \omega\ f_k^+$$

the latter can itself be conveniently expressed from the electron population of atom k in the system of N and N+1 electrons:[26]

$$f_k^+ = Q_k(N+1) - Q_k(N) = \Delta Q_k$$

6.4 DIAS model diagrams

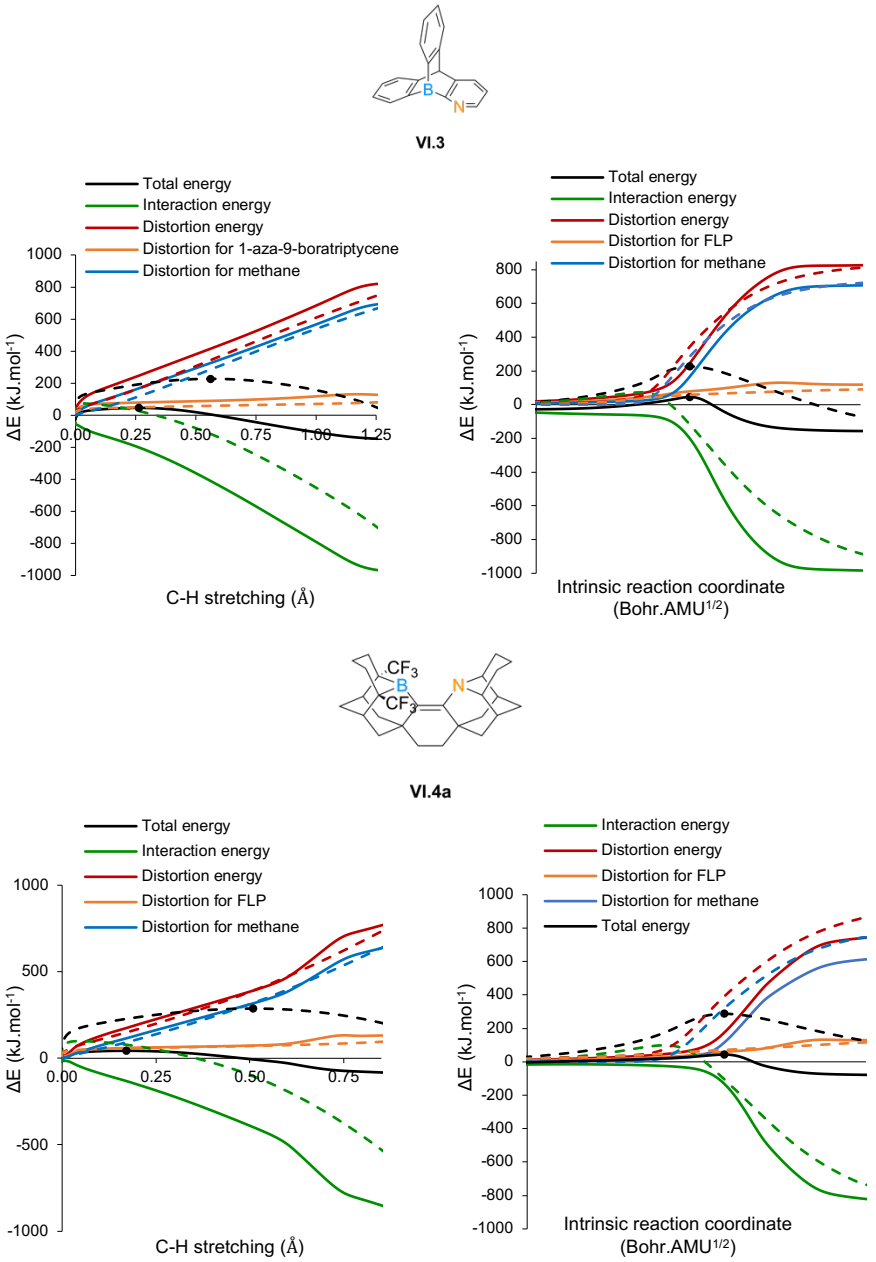

*Figure S47(A). Activation strain diagrams of FLP systems **VI.3** and **VI.4a** over the stretching distance of the C-H bond that is breaking (left) or the intrinsic reaction coordinate (right) in the methane activation for the first (P1/TS1, full line) and the second reaction pathway(P2/TS2, dashed). The dots indicate the position of the transition states.*

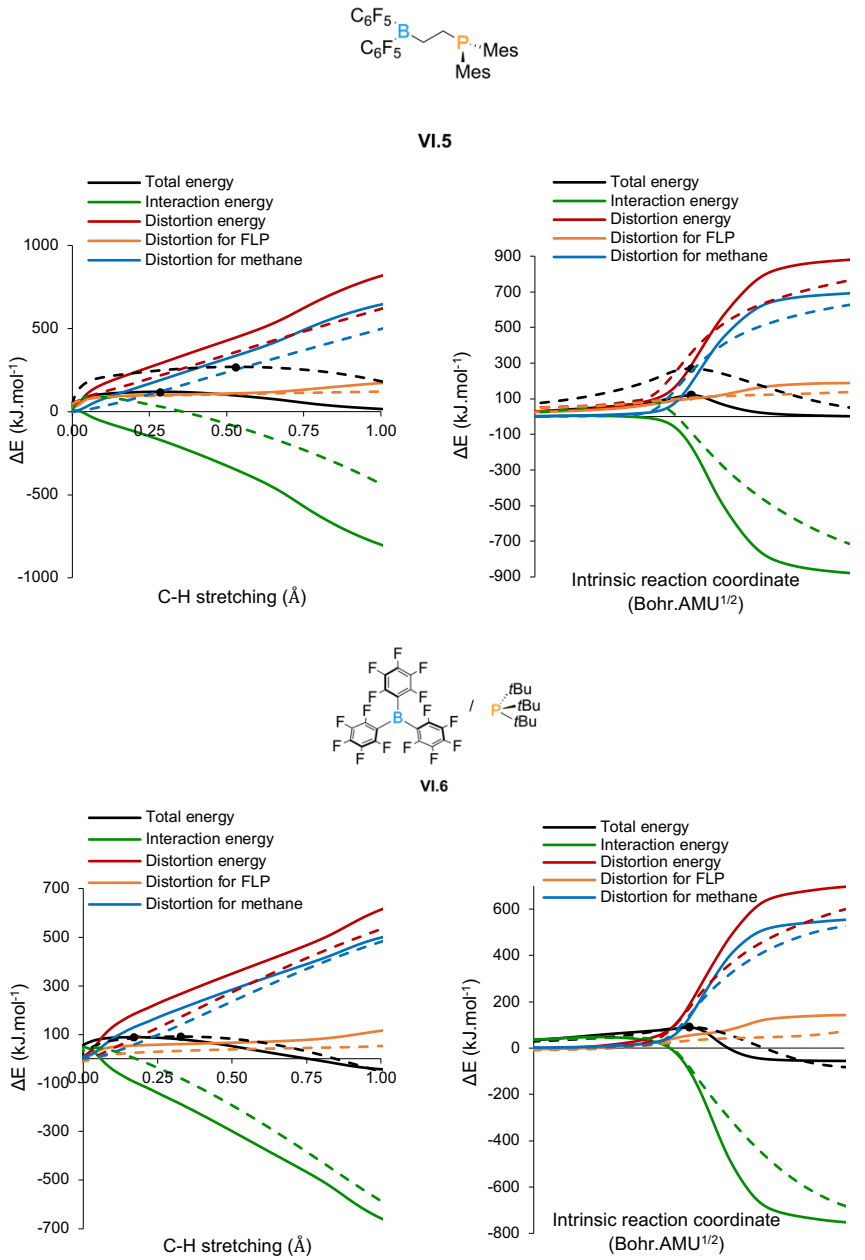

*Figure S47(B). Activation strain diagrams of FLP systems **VI.5** and **VI.6** over the stretching distance of the C-H bond that is breaking (left) or the intrinsic reaction coordinate (right) in the methane activation for the first (P1/TS1, full line) and the second reaction pathway(P2/TS2, dashed). The dots indicate the position of the transition states.*

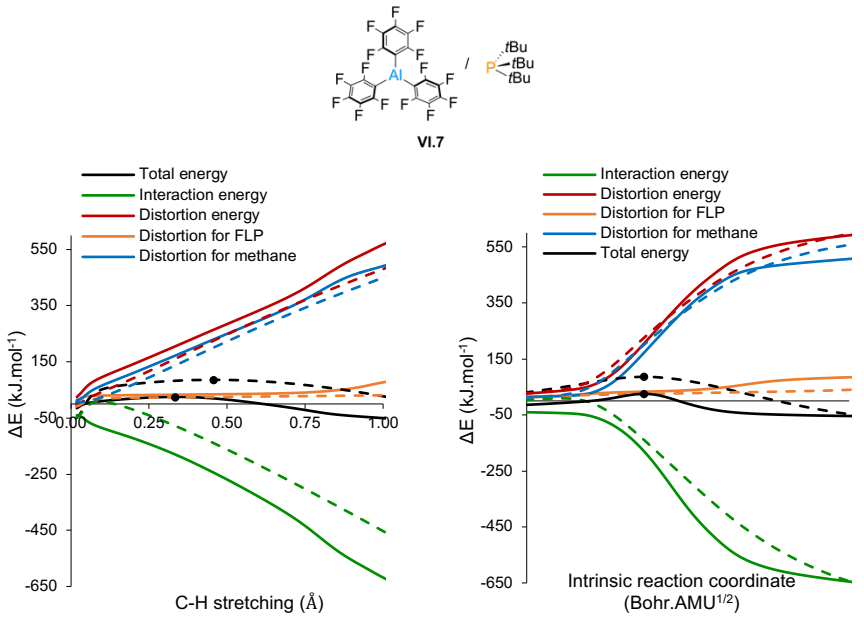

*Figure S47(C). Activation strain diagrams of FLP system **VI.7** over the stretching distance of the C-H bond that is breaking (left) or the intrinsic reaction coordinate (right) in the methane activation for the first (P1/TS1, full line) and the second reaction pathway(P2/TS2, dashed). The dots indicate the position of the transition states.*

6.5 Natural Bond Orbital analysis at the transition states and second-order perturbation theory model

Within the NBO scheme, the donor-acceptor or resonance interactions were evaluated within the second-order perturbative analysis of Weinhold and Landis.[27-28] These stabilization interactions occur between Lewis (L, formally doubly-occupied) and non-Lewis (NL, formally empty) orbitals. In that scheme, the interaction energy for the *i*(L), *j*(NL) pair of NBOs is determined using the following expression:

$$\Delta E_{ij}^{(2)} = \frac{-q_i \left|F_{ij}\right|^2}{\varepsilon_j^{(NL)} - \varepsilon_i^{(L)}}$$

where ε_j^{NL} and ε_i^{L} are the energies of the NL and L NBOs, q_i is the electron population of the Lewis-type NBO and F_{ij} is the element of the Kohn-Sham interaction matrix. To a good approximation, this interaction term is proportional to the overlap between the corresponding NBOs. The NBOs involved in the main orbital interactions at the transition states, the second-

order stabilization energies, and a visual sketch of the related NBOs overlaps are shown in Figure S48 and Figure S49 for system **VI.3**.

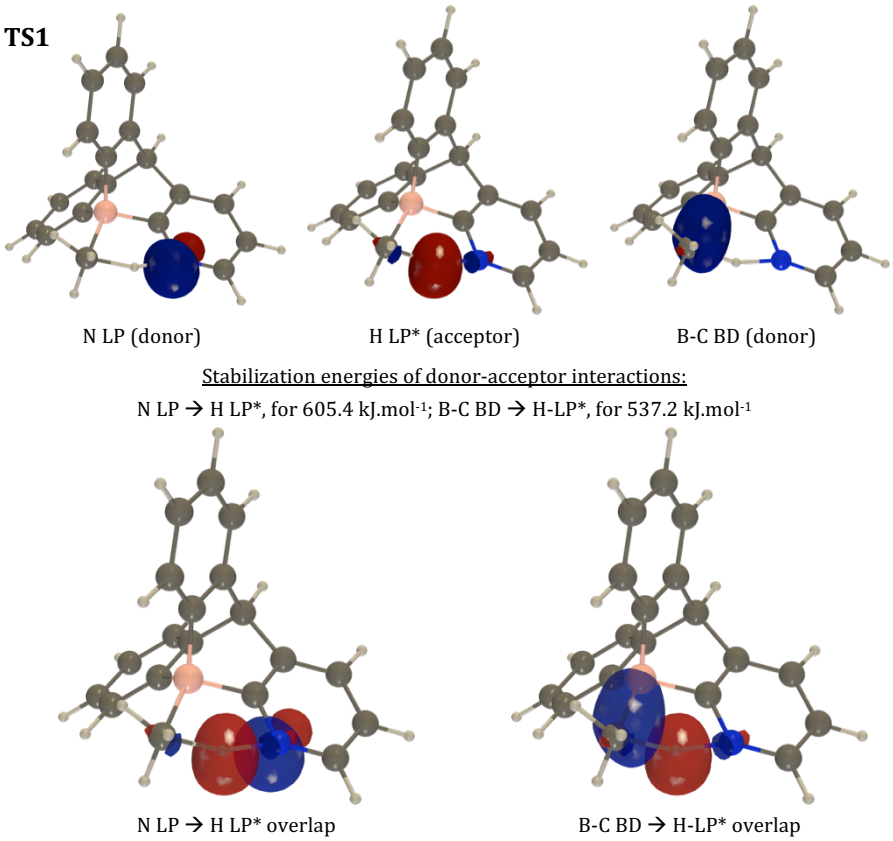

*Figure S48. Natural bond orbitals and orbital overlaps involved in the main donor-acceptor interactions of **VI.3**-TS1 and their interaction energies (kJ.mol-1). The LP label stands for Lone Pair and corresponds to one-center valence NBO, BD stands for Bond and corresponds to two-center valence NBO (σ-bonds), the * suffix indicates non-Lewis type (formally vacant) orbitals. Isosurface value of 0.10 a.u.*

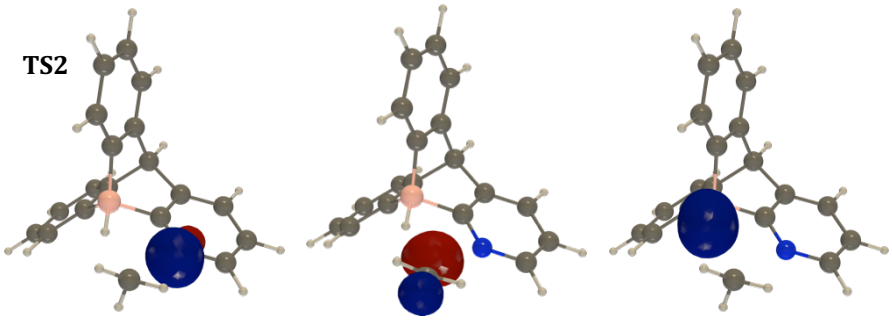

N LP (donor) C LP* (acceptor) B-H BD (donor)

Stabilization energies of donor-acceptor interactions:

N LP → C LP*, for 385.3 kJ.mol^{-1}; B-H BD → C-LP*, for 484.9 kJ.mol^{-1}

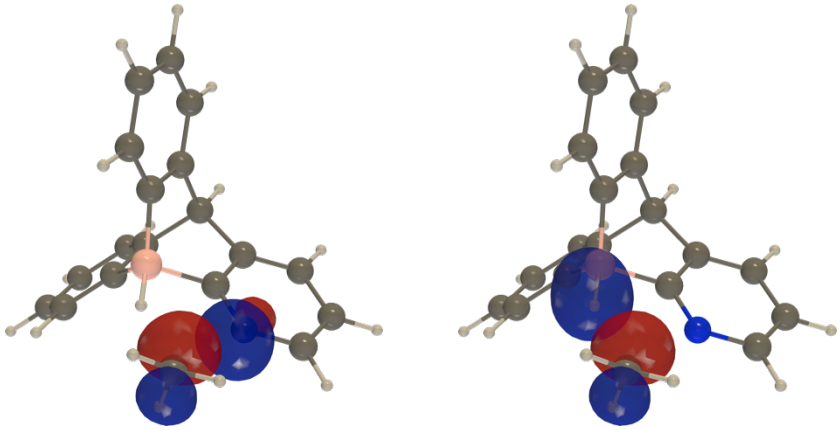

N LP → C LP* overlap B-H BD → C-LP* overlap

*Figure S49. Natural bond orbitals and orbital overlaps involved in the main donor-acceptor interactions of **VI.3**-TS2 and their interaction energies (kJ.mol^{-1}). The LP label stands for Lone Pair and corresponds to one-center valence NBO, BD stands for Bond and corresponds to two-center valence NBO (σ-bonds), the * suffix indicates non-Lewis type (formally vacant) orbitals. Isosurface value of 0.10 a.u.*

6.6 Dimerization

Table S31. Gibbs free energy of dimerization ($\Delta G^{0}_{dimer.}$, in kJ.mol^{-1}) for 1-aza-9-boratriptycene derivatives at the M06-2X/6-311G(d) IEFPCM (cyclohexane) level of theory in comparison to the corresponding Gibbs free energies of reaction ($\Delta G^{0}_{methane}$, in kJ.mol^{-1}) and activation ($\Delta G^{\neq}_{methane}$, in kJ.mol^{-1}).

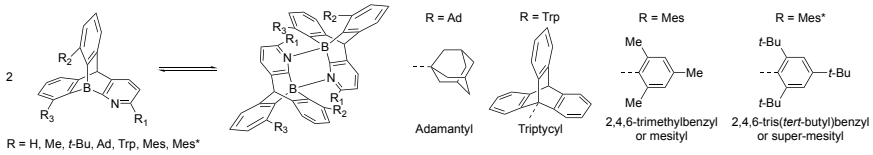

Entry	R_1	R_2	R_3	$\Delta G^{0}_{dimer.}$	$\Delta G^{0}_{methane}$	$\Delta G^{\neq}_{methane}$
SI-1 (**VI.3**)	H	H	H	-472	-108	76
SI-2	Mes	H	H	-319	-112	72
SI-3	*t*Bu	H	H	-295	-105	76
SI-4	Ad	H	H	-279	-	-
SI-5	Trp	H	H	-213	-	-
SI-6	Mes*	H	H	-199	-108	75
[a] SI-7	H	Mes	H	-487	-102	74
[a] SI-8	H	*t*Bu	H	-310	-68	134
[a] SI-9	Mes	Mes	H	-226	-108	69
[a] SI-10	Mes	*t*Bu	H	-129	-42	133
[a] SI-11	*t*Bu	tBu	H	-116	-37	131
[a] SI-12	Mes*	Mes	H	53	-106	75
[a] SI-13	Mes*	*t*Bu	H	145	-21	133
SI-14	H	Mes	Mes	-399	-85	79
SI-15	H	*t*Bu	*t*Bu	-123	48	207
SI-16	*t*Bu	Me	Me	-241	-	-
SI-17	*t*Bu	*t*Bu	*t*Bu	203	46	204
SI-18	Mes	Mes	Mes	110	-97	77
SI-19	Mes*	Mes	Mes	575	-87	86

[a] With different R_2 and R_3 substituents on the triptycene scaffold, it becomes chiral, with two enantiomers A and B, leading to two possible dimers (AA or AB, BB), both were computed and the most stable is reported here, BB was ignored.

The significant difference in the effects of *t*Bu and Mes groups is due to their respective shape: the *t*Bu group is directly shielding the front environment of the B atom (Figure S50, left), while the planar geometry of the Mes group leaves the front environment of the B almost vacant and the insertion of methane can proceed unaltered (Figure S50, right). In addition, C-H/π interactions between the methane and mesityl groups are also possible.

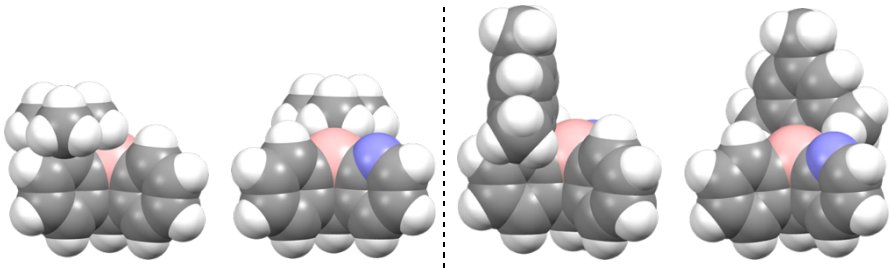

Figure S50. Compound SI-7 (left) and SI-8 (right) as visualized with van der Waals representation.

The penalty associated with the addition of tBu groups is thus attributed to the resulting large structural deformation (increase in B-$C_{Methane}$ bond length and dihedral NCB-$C_{Methane}$ angle) on both the transition state and the product of reaction (Figure S51).

Transition states

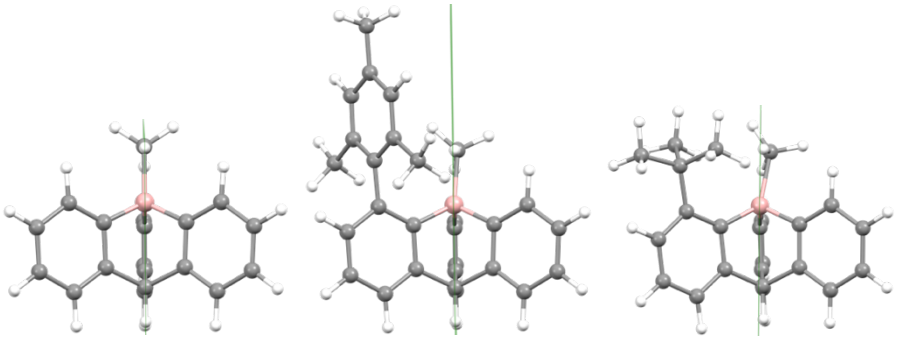

SI-1 – TS1 (R_1 = H, R_2 = H) SI-7 – TS1 (R_1 = H, R_2 = Mes) SI-8 – TS1 (R_1 = H, R_2 = *t*Bu)

Products

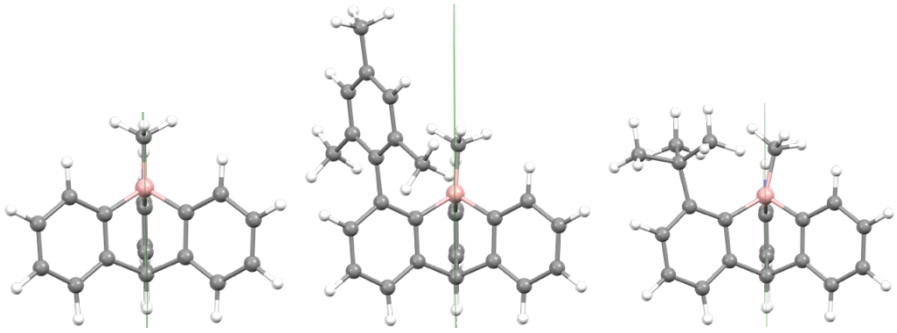

SI-1 – P1 (R_1 = H, R_2 = H) SI-7 – P1 (R_1 = H, R_2 = Mes) SI-8 – P1 (R_1 = H, R_2 = *t*Bu)

Figure S51. Structural impact on the TS and product by Mes and tBu groups. In green is shown the N-C_{sp2}-B plane of the 1-aza-9-boratriptycene scaffold. The methane moiety is increasingly tilted with larger substituents.

7. References

[1] H. A. Bent, "An appraisal of valence-bond structures and hybridization in compounds of the first-row elements", *Chem. Rev.* **1961**, *61*, 275-311.

[2] L. Hu, D. Mahaut, N. Tumanov, J. Wouters, R. Robiette, G. Berionni, "Complementary synthetic approaches toward 9-phosphatriptycene and structure–reactivity investigations of its association with sterically hindered Lewis acids", *J. Org. Chem.* **2019**, *84*, 11268-11274.

[3] M. J. Frisch, G. W. Trucks, H. B. Schlegel, G. E. Scuseria, M. A. Robb, J. R. Cheeseman, G. Scalmani, V. Barone, G. A. Petersson, H. Nakatsuji, X. Li, M. Caricato, A. V. Marenich, J. Bloino, B. G. Janesko, R. Gomperts, B. Mennucci, H. P. Hratchian, J. V. Ortiz, A. F. Izmaylov, J. L. Sonnenberg, D. Williams-Young, F. Ding, F. Lipparini, F. Egidi, J. Goings, B. Peng, A. Petrone, T. Henderson, D. Ranasinghe, V. G. Zakrzewski, J. Gao, N. Rega, G. Zheng, W. Liang, M. Hada, M. Ehara, K. Toyota, R. Fukuda, J. Hasegawa, M. Ishida, T. Nakajima, Y. Honda, O. Kitao, H. Nakai, T. Vreven, K. Throssell, J. A. Montgomery, Jr., J. E. Peralta, F. Ogliaro, M. J. Bearpark, J. J. Heyd, E.

N. Brothers, K. N. Kudin, V. N. Staroverov, T. A. Keith, R. Kobayashi, J. Normand, K. Raghavachari, A. P. Rendell, J. C. Burant, S. S. Iyengar, J. Tomasi, M. Cossi, J. M. Millam, M. Klene, C. Adamo, R. Cammi, J. W. Ochterski, R. L. Martin, K. Morokuma, O. Farkas, J. B. Foresman, D. J. Fox, *Gaussian 16, Revision A.03*, Gaussian Inc., Wallingford CT, **2016**.

[4] Y. Zhao, D. G. Truhlar, "The M06 suite of density functionals for main group thermochemistry, thermochemical kinetics, noncovalent interactions, excited states, and transition elements: Two new functionals and systematic testing of four M06-class functionals and 12 other functionals", *Theor. Chem. Acc.* **2008**, *120*, 215-241.

[5] D. Mahaut, A. Chardon, L. Mineur, G. Berionni, B. Champagne, "Rational development of a metal-free bifunctional system for the C-H activation of methane: a density functional theory investigation", *ChemPhysChem* **2021**, *22*, 1958-1966.

[6] C. Peng, P. Y. Ayala, H. B. Schlegel, M. J. Frisch, "Using redundant internal coordinates to optimize equilibrium geometries and transition states", *J. Comput. Chem.* **1996**, *17*, 49-56.

[7] P. Pulay, G. Fogarasi, "Geometry optimization in redundant internal coordinates", *J. Chem. Phys.* **1992**, *96*, 2856-2860.

[8] P. Pulay, G. Fogarasi, F. Pang, J. E. Boggs, "Systematic *ab initio* gradient calculation of molecular geometries, force constants, and dipole moment derivatives", *J. Am. Chem. Soc.* **1979**, *101*, 2550-2560.

[9] X. Li, M. J. Frisch, "Energy-represented direct inversion in the iterative subspace within a hybrid geometry optimization method", *J. Chem. Theory Comput.* **2006**, *2*, 835-839.

[10] J. Tomasi, B. Mennucci, R. Cammi, "Quantum mechanical continuum solvation models", *Chem. Rev.* **2005**, *105*, 2999-3094.

[11] T. N. Ramos, S. Canuto, B. Champagne, "Unraveling the electric field-induced second harmonic generation responses of stilbazolium ion pairs complexes in solution using a multiscale simulation method", *J. Chem. Inf. Model.* **2020**, *60*, 4817-4826.

[12] C. B. Caputo, D. Winkelhaus, R. Dobrovetsky, L. J. Hounjet, D. W. Stephan, "Synthesis and Lewis acidity of fluorophosphonium cations", *Dalton Trans.* **2015**, *44*, 12256-12264.

[13] *CrysAlis*^{Pro}, Rigaku Oxford Diffraction, Rigaku Corporation, Wrocklaw, Poland, **2020**.

[14] G. M. Sheldrick, "SHELXT - integrated space-group and crystal-structure determination", *Acta Crystallogr. A* **2015**, *71*, 3-8.

[15] G. M. Sheldrick, "Crystal structure refinement with SHELXL", *Acta Crystallogr. C* **2015**, *71*, 3-8.

[16] C. B. Hübschle, G. M. Sheldrick, B. Dittrich, "ShelXle: a Qt graphical user interface for SHELXL", *J. Appl. Crystallogr.* **2011**, *44*, 1281-1284.

[17] O. V. Dolomanov, L. J. Bourhis, R. J. Gildea, J. A. K. Howard, H. Puschmann, "OLEX2: a complete structure solution, refinement and analysis program", *J. Appl. Crystallogr.* **2009**, *42*, 339-341.

[18] G. Lu, L. Zhao, H. Li, F. Huango, Z. X. Wang, "Reversible heterolytic methane activation of metal-free closed-shell molecules: A computational proof-of-principle study", *Eur. J. Inorg. Chem.* **2010**, *15*, 2254-2260.

[19] A. Ben Saida, A. Chardon, A. Osi, N. Tumanov, J. Wouters, A. I. Adjieufack, B. Champagne, G. Berionni, "Pushing the Lewis acidity boundaries of boron compounds with non-planar triarylboranes derived from triptycenes", *Angew. Chem. Int. Ed.* **2019**, *58*, 16889-16893.

[20] A. Chardon, A. Osi, D. Mahaut, T. H. Doan, N. Tumanov, J. Wouters, L. Fusaro, B. Champagne, G. Berionni, "Controlled generation of 9-boratriptycene by Lewis adduct dissociation: Accessing a non-planar triarylborane", *Angew. Chem. Int. Ed.* **2020**, *59*, 12402-12406.

[21] H. Böhrer, N. Trapp, D. Himmel, M. Schleep, I. Krossing, "From unsuccessful H_2-activation with FLPs containing $B(Ohfip)_3$ to a systematic evaluation of the Lewis acidity of 33 Lewis acids based on fluoride, chloride, hydride and methyl ion affinities", *Dalton Trans.* **2015**, *44*, 7489-7499.

[22] R. G. Parr, L. V. Szentpály, S. Liu, "Electrophilicity index", *J. Am. Chem. Soc.* **1999**, *121*, 1922-1924.

[23] P. Pérez, A. Toro-Labbé, A. Aizman, R. Contreras, "Comparison between experimental and theoretical scales of electrophilicity in benzhydryl cations", *J. Org. Chem.* **2002**, *67*, 4747-4752.

[24] E. Chamorro, P. K. Chattaraj, P. Fuentealba, "Variation of the electrophilicity index along the reaction path", *J. Phys. Chem. A* **2003**, *107*, 7068-7072.

[25] P. K. Chattaraj, U. Sarkar, D. R. Roy, "Electrophilicity index", *Chem. Rev.* **2006**, *106*, 2065-2091.

[26] W. Yang, W. J. Mortier, "The use of global and local molecular parameters for the analysis of the gas-phase basicity of amines", *J. Am. Chem. Soc.* **1986**, *108*, 5708-5711.

[27] F. Weinhold, C. R. Landis, *Valency and bonding - a natural bond orbital donor-acceptor perspective*, Cambridge University Press, New-York, **2005**.

[28] F. Weinhold, C. R. Landis, *Discovering chemistry with natural bond orbitals*, Wiley, Hoboken, NJ, **2012**.

Annex II
Quantum chemistry aspects

1. Density functional theory

1.1 Introduction

This section introduces quantum chemistry and the density functional theory (DFT).[1-3] This method was employed for all quantum chemical calculations undertaken in the present thesis.

The fundamental goal of quantum chemistry is to solve the Schrödinger equation (13), allowing to access all information of a given system.

$$\hat{H}\Psi_i(\vec{x}_1, \vec{x}_2, \dots, \vec{x}_N, \vec{X}_1, \vec{X}_2, \dots, \vec{X}_M) = E_i\Psi_i(\vec{x}_1, \vec{x}_2, \dots, \vec{x}_N, \vec{X}_1, \vec{X}_2, \dots, \vec{X}_M) \qquad (13)$$

where $\hat{H}$ is the Hamilton operator (or Hamiltonian) of the system containing N electrons and M nuclei, $\vec{x}_i$ contain the spatial coordinates of the electrons $\vec{r}_i$ and the spin coordinate ω_i, $\vec{X}_i$ contain the spatial and spin coordinates of the nuclei, and Ψ_i is the wavefunction of the i^{th} state of the system, of energy E_i. This equation can be simplified by the Born-Oppenheimer approximation, which considers electrons moving in a field of fixed nuclei, allowing to set the kinetic energy of the latter to zero and establishing the nuclei-nuclei repulsions as a parameterizable constant. The resulting *electronic* Hamiltonian is expressed as:

$$\hat{H}^{elec} = -\frac{1}{2}\sum_{i=1}^{N}\nabla_i^2 - \sum_{i=1}^{N}\sum_{A=1}^{M}\frac{Z_A}{r_{iA}} + \sum_{i=1}^{N}\sum_{j>i}^{N}\frac{1}{r_{ij}} = \hat{T} + \hat{V}_{Ne} + \hat{V}_{ee} \qquad (14)$$

where Z_A is the charge of the nucleus A and r the distance between two particles. The first term describes the kinetic energy ($\hat{T}$) of the electrons in the form of the Laplacian operator [sum of three differential operators (15)] while the two remaining ones are the potential part of the Hamiltonian, consisting first in the electron-nuclei electrostatic attractions term $\hat{V}_{Ne}$ (refered to in DFT as the external potential) and the electron-electron repulsion term $\hat{V}_{ee}$.

$$\nabla_i^2 = \frac{\partial^2}{\partial x_i^2} + \frac{\partial^2}{\partial y_i^2} + \frac{\partial^2}{\partial z_i^2} \qquad (15)$$

This equation is expressed in the atomic unit system, in which physical constants, such as the mass of the electron m_e, the modulus of its charge $|e|$, the reduced Planck constants $\hbar$,or the permittivity of the vacuum $4\pi\varepsilon_0$ are set to one.

The solutions of this Schrödinger equation are the wavefunctions of the system and their electronic energies (Ψ_i and E_i). The former, in the ground state, is not an observable physical quantity, but its square value is, and defines the probability of finding the electrons 1, 2, … N simultaneously in volume elements $d\vec{x}_1, d\vec{x}_2 \ldots d\vec{x}_N$ around $\vec{x}_1, \vec{x}_2 \ldots \vec{x}_N$:

$$|\Psi(\vec{x}_1, \vec{x}_2, \ldots, \vec{x}_N)|^2 d\vec{x}_1, d\vec{x}_2 \ldots d\vec{x}_N \qquad (16)$$

To account for the indistinguishable character of electrons, this probability must remain unchanged if the coordinates of two given electrons are permuted. In the case of fermions, particles of half-integral spin and including electrons of spin ½, this translates in antisymmetric wave functions with respect to interchange of spatial and spin coordinates of any pair of electrons:

$$\Psi(\vec{x}_1, \vec{x}_2, \ldots, \vec{x}_i, \vec{x}_j, \ldots, \vec{x}_N) = -\Psi(\vec{x}_1, \vec{x}_2, \ldots, \vec{x}_j, \vec{x}_i, \ldots, \vec{x}_N) \qquad (17)$$

Solving the Schrödinger equation provides the wave function. However, this equation can only be solved for very simple systems. Approximations are thus necessary. The Hartree-Fock (HF) approximation is the most straightforward and represents the basis for all wave-function-based methods. In Hartree-Fock, the N-electron wavefunction is approximated as a Slater determinant, an anti-symmetrized product of N one-electron wavefunctions, the spinorbitals $\theta_i(\vec{x}_i)$:

$$\Psi^{HF}(\vec{x}_1, \vec{x}_2, \ldots, \vec{x}_N) = \frac{1}{\sqrt{N!}} \begin{vmatrix} \theta_1(\vec{x}_1) & \cdots & \theta_N(\vec{x}_1) \\ \vdots & \ddots & \vdots \\ \theta_1(\vec{x}_N) & \cdots & \theta_N(\vec{x}_N) \end{vmatrix} \qquad (18)$$

or more conveniently expressed only with the diagonal elements:

$$\Psi^{HF}(\vec{x}_1, \vec{x}_2, \ldots, \vec{x}_N) = \frac{1}{\sqrt{N!}} det|\theta_1(\vec{x}_1), \theta_2(\vec{x}_2), \ldots, \theta_N(\vec{x}_N)| \qquad (19)$$

Spinorbitals are defined as the products of a spatial orbital $\varphi(\vec{r})$ and one of the two spin functions α or β:

$$\theta(\vec{x}) = \varphi(\vec{r})\sigma(\omega) \quad \text{with} \quad \sigma(\omega) = \alpha, \beta \qquad (20)$$

ω being the spin variable. In the Slater determinant, spin functions, and consequently the spinorbitals themselves, are orthonormal. The $1/\sqrt{N!}$ factor

ensures the normalization of the wavefunction, so that the probability to find all N electrons in the whole space is exactly one.

Density functional theory uses another conceptual approach to solve the Schrödinger equation. It is a quantum mechanical method that replaces the Schrödinger equation and the N-electron wave function dependent on the spin-space coordinates $\Psi(\vec{x}_1, \vec{x}_2, \dots, \vec{x}_N)$ by the electron density dependent on the space coordinate $\rho(\vec{r})$, which is conceptually much simpler, and the equations to find it. Indeed, it has been shown that all properties of the system can be expressed using only the electron density as variable.

1.2 The Hohenberg-Kohn theorems

Reported in 1964, the Hohenberg and Kohn theorems represent the theoretical basis upon which is founded density functional theory.[4] The aforementioned affirmation that all the properties of the system can be expressed using only electron density as variable arises from the first of these theorems. It states that the external potential $V_{ext}(\vec{r})$ is determined (within a constant) by the electron density. Indeed, Hohenberg and Kohn proved by *reductio ad absurdum* that there cannot be two external potentials [$V_{ext}(\vec{r})$ and $V'_{ext}(\vec{r})$, differing by more than a constant], part of two Hamiltonians $\hat{H}$ and $\hat{H}'$, themselves differing only by the external potential, and associated to two different wavefunctions Ψ and Ψ', but ultimately yielding the same electron density. Reversely, it means that the ground state electron density uniquely determines the external potential. Furthermore, since the electron density, when integrated over the space, gives the number of electrons of the system [$N = \int \rho(\vec{r})\, d\vec{r}$], it therefore also determines the kinetic energy operator $\hat{T}$ and the electron repulsion operator $\hat{V}_{ee}$, given that both only depend on the number of electrons. With all the individual contributions to the Hamiltonian defined by the electron density, it also defines the Hamiltonian of the system and, subsequently, to all its properties through solving the Schrödinger equation:

$$\hat{H} = \hat{T} + \hat{V} \quad \Rightarrow \quad \hat{H}\Psi = E\Psi \tag{21}$$

The expression of the energy can thus be written as a functional of $\rho(\vec{r})$:

$$E_v[\rho(\vec{r})] = T[\rho(\vec{r})] + V_{ne}[\rho(\vec{r})] + V_{ee}[\rho(\vec{r})] \tag{22}$$

where V_{ne} is the electron-nuclei attraction term, which corresponds most of the time to the external potential when it does not include effects from magnetic or

electric fields. The above equation can be recast to split the V_{ee} terms into a coulomb $J[\rho(\vec{r})]$ and a non-classical electron-electron interaction term (of unknown exact analytical form) and further manipulation of the equation introduces the Hohenberg and Kohn functional ($F_{HK}[\rho(\vec{r})]$), a universal functional of which the form is independent of the given system.

$$E_v[\rho(\vec{r})] = T[\rho(\vec{r})] + V_{ne}[\rho(\vec{r})] + J[\rho(\vec{r})] + nonclassical\ term$$
$$E_v[\rho(\vec{r})] = \int \rho(\vec{r})v(\vec{r})d\vec{r} + F_{HK}[\rho(\vec{r})] \quad (23)$$

$F_{HK}[\rho(\vec{r})]$ thus contains the functional for the kinetic energy of the electrons and the electron-electron interactions, of which only the expression of the classical electrostatic interactions is known. One should note at this point that no approximation was introduced and that if the exact Hohenberg-Kohn functional was known, the ground state energy would be exact as well and, in effect, the Schrödinger equation would be solved. Unfortunately, the formulation of these functionals is not known, and the major challenge of DFT is to propose explicit expressions for the kinetic energy and electron-electron potential functionals.

The second Hohenberg-Kohn theorem is a variational principle that gives insight into how to actually calculate the electron density of a system. It states that the electron density of the ground state is the one that minimizes the total energy of the system. On the other hand, using approximate densities, this energy will always remain higher than the *real* energy of this ground state, as is the concept of the variation principle. Solutions can thus be obtained by minimizing the energy, using a Lagrange multiplier with the constraint that the integration of the electron density over space gives the number of electrons of the system, *N*:

$$\delta\left\{E_v[\rho(\vec{r})] - \mu\left[\int \rho(\vec{r})dr - N\right]\right\} = 0 \quad (24)$$

or,

$$\mu = \frac{\delta E_v[\rho(\vec{r})]}{\delta\rho(\vec{r})} = v(r) + \frac{\delta F_{HK}[\rho(\vec{r})]}{\delta\rho(\vec{r})} \quad (25)$$

where μ is the Lagrange multiplier.

Again, the resolution of this equation would provide the exact ground state energy, but F_{HK} contains a non-classical part, called the exchange-correlation that is not known. In order to solve this equation, approximate Hohenberg-Kohn functionals must be employed.

1.3 The Kohn-Sham method

Reported a year after the Hohenberg-Kohn theorems by Kohn and Sham, this method offers a practical approach to solving the problem of the universal functional mentioned above.[5] Understanding that a major part of the problem was to compute the kinetic energy of the system, and in order to simplify this challenge, their method consists in substituting the real system of interacting electrons by a fictitious one. In the latter, the electrons are independent but have the overall same density as the real system and are described by as set of spinorbitals, the Kohn-Sham spinorbitals $[\theta_i(\vec{x})]$. This way, the major part of the kinetic energy can be determined with good accuracy, as explained below, and the remaining part is merged with the non-classical part of the electron-electron repulsion. As much as possible of the energy is computed exactly, and the small remaining part is left approximated by the exchange-correlation functional.

The squares of the norm of the Kohn-Sham spinorbitals sum up to give the aforementioned Kohn-Sham density:

$$\rho(\vec{r}) = \sum_{i}^{N} \int |\theta_i(\vec{x})|^2 d\omega \qquad (26)$$

The global wavefunction of the system is described by a Slater determinant, the anti-symmetrized product of the N-lowest energy spinorbitals:

$$\Psi = \frac{1}{\sqrt{N!}} det|\theta_1(\vec{x}_1), \theta_2(\vec{x}_2), \dots, \theta_N(\vec{x}_N)| \qquad (27)$$

While in Hartree-Fock the Slater determinant approximates the exact wave-function of the system, it is in fact the exact wave-function of a fictitious system of non-interacting electrons. The formulation of the exact kinetic energy operator of this system is known:

$$\hat{T}_S[\rho(\vec{r})] = \sum_{i=1}^{N} \langle \theta_i \left| \frac{-1}{2} \nabla^2 \right| \theta_i \rangle \qquad (28)$$

The Hamiltonian of this fictitious system is said to be independent because it does not possess any two-electron term:

$$\widehat{H}_S = \sum_i^N \frac{-1}{2}\nabla_i^2 + \sum_i^N v_{eff}(\vec{r}_i) \qquad (29)$$

It describes electrons with a given kinetic energy evolving in an effective potential v_{eff}. The connection between the fictitious, non-interacting, system and the real, interacting, one is achieved by defining the effective potential v_{eff} so that the electron density defined in equation (26) equals the ground state electron density of the real system. In order to define this parameter, several steps are needed. Starting from the Kohn-Sham expression of the global energy and using the variational principle, the "new" Hohenberg-Kohn functional can be defined:

$$F[\rho(\vec{r})] = T_S[\rho(\vec{r})] + J[\rho(\vec{r})] + E_{XC}[\rho(\vec{r})] \qquad (30)$$

which leads to the exchange-correlation (XC) energy functional $E_{XC}[\rho(\vec{r})]$:

$$E_{XC}[\rho(\vec{r})] = T[\rho(\vec{r})] - T_S[\rho(\vec{r})] + V_{ee}[\rho(\vec{r})] - J[\rho(\vec{r})] \qquad (31)$$

It contains two terms, a positive (T-T_S, kinetic energy), the remaining part of the kinetic energy of the system (taking interacting electrons into account) and a negative one, containing the two-electron exchange energy, the correlation energy and the self-interaction correction. This functional is the one that must be selected at the beginning of each DFT calculation.

The differential of the energy functional $E_v[\rho(\vec{r})]$ with respect to the electron density defines the effective potential:

$$v_{eff}(\vec{r}) = v(\vec{r}) + \int \frac{\rho(\vec{r}')}{|\vec{r} - \vec{r}'|} d\vec{r}' + v_{xc}(\vec{r})$$
$$\text{with } v_{xc}(\vec{r}) = \frac{\delta E_{XC}[\rho(\vec{r})]}{\delta\rho(\vec{r})} \qquad (32)$$

where $v_{xc}(\vec{r})$ is the exchange-correlation potential. The effective potential corresponds to the potential that acts on all the electrons. It is a key part of the Kohn-Sham equation (shown below in its canonical form), which, in analogy to HF, applies to the spinorbitals through the one-electron Kohn-Sham operator (defined in brackets):

$$f^{KS}(\vec{r})\Theta_n(\vec{x}) = \left[\frac{-1}{2}\nabla^2 + v_{eff}(\vec{r})\right]\Theta_n(\vec{x}) = \varepsilon_n\Theta_n(\vec{x}) \quad (33)$$

The total energy of the system then reads:

$$\begin{aligned} E[\rho(\vec{r})] &= \int \rho(\vec{r})v(\vec{r})d\vec{r} + F[\rho(\vec{r})] \\ &= T_S[\rho(\vec{r})] + J[\rho(\vec{r})] + \int \rho(\vec{r})v(\vec{r})dr + E_{XC}[\rho(\vec{r})] \\ &= \sum_{i=1}^{N}\varepsilon_i - \frac{1}{2}\iint \frac{\rho(\vec{r})\rho(\vec{r}')}{|\vec{r}-\vec{r}'|}d\vec{r}d\vec{r}' + E_{XC}[\rho(\vec{r})] \\ &- \int \rho(\vec{r})v_{xc}(\vec{r})d\vec{r} \end{aligned} \quad (34)$$

$$where \quad \varepsilon_i = \langle\theta_i\left|\frac{-1}{2}\nabla^2 + v_{eff}(\vec{r})\right|\theta_i\rangle \quad and \quad \sum_{i=1}^{N}\varepsilon_i = T_S[\rho(\vec{r})] + \int \rho(\vec{r})v_{eff}(\vec{r})d\vec{r}$$

Introducing the LCAO formalism (35) within the Kohn-Sham equation (33) leads to the corresponding matrix Kohn-Sham equation (36):

$$\varphi_i(\vec{r}) = \sum_{p=1}^{K} C_{pi}\chi_p(\vec{r}) \quad (35)$$

$$FC = SCE \quad (36)$$

where the Kohn-Sham molecular orbitals $\varphi_i(\vec{r})$ are defined as a set of K basis functions $\chi_p(\vec{r})$ and their coefficients C_{pi}, F is the resulting Kohn-Sham matrix, S the overlap matrix, C the LCAO coefficients matrix and E the diagonal matrix of the orbital energies.

Solving the Kohn-Sham equation provides the electron density of the system. Since the effective potential depends on the electron density, the resolution starts from a guess density, and proceeds self-consistently. It is an iterative process, a SCF (Self-Consistent Field) cycle is carried out as follows: from a guess density, the effective potential is evaluated (32) and inserted in the Kohn-Sham equation (33) which is solved, (the energy and spinorbitals $\Theta_n(\vec{x})$ can be evaluated), a new density is proposed and the cycle starts again until convergence towards the minimum energy (variational principle).

1.4 Exchange-correlation functionals

In the effective potential, the exact expression of the exchange-correlation functional is not known. It is thus approximated, leading to approximate densities and energies. This term accounts for electron correlation and exchange effects. Many exchange-correlation functionals have been developed with several levels of approximation. Hereafter are cited several of these categories of approximate exchange-correlation functionals and their characteristic.

The Local (Spin)-Density Approximation [L(S)DA] is the bedrock of all functionals in the current state of the art. The starting point for these functionals and the subsequent ones is to express the exchange-correlation energy functional as:

$$E_{XC}[\rho(\vec{r})] = \int \rho(\vec{r})\, \varepsilon_{XC}[\rho(\vec{r})] d\vec{r} = \int \rho(\vec{r})\, \varepsilon_{XC}\left[\rho_\alpha(\vec{r}), \rho_\beta(\vec{r})\right] d\vec{r} \qquad (37)$$

where $\varepsilon_{XC}[\rho(\vec{r})]$ is the exchange-correlation energy per electron. Functionals can also be written in their unrestricted version, distinguishing the two spin densities $\rho_\alpha(\vec{r})$ and $\rho_\beta(\vec{r})$ so that $\rho(\vec{r}) = \rho_\alpha(\vec{r}) + \rho_\beta(\vec{r})$ (hence Local *Spin*-density Approximation, LSD). $\varepsilon_{XC}[\rho(\vec{r})]$ is described in two terms, the exchange term and the correlation term:

$$\varepsilon_{XC}[\rho(\vec{r})] = \varepsilon_X[\rho(\vec{r})] + \varepsilon_C[\rho(\vec{r})] \qquad (38)$$

These functionals within the local density approximation consider that the constitutive infinitesimal parts of the globally non-uniform system are described as a uniform electron gas. In other words, a given point of space is only associated with a density $\rho(\vec{r})$ (or two spin densities). To the density at this point are thus associated exchange and correlation energies $E_{XC}[\rho(\vec{r})]$ [obtained using expression (37)] that a uniform electron gas of same density has. The global inhomogeneity of the system arises from the summation of the individual contributions of each point in the system.

One example is the SVWN functional that uses the expression derived by Bloch and Dirac for the exchange part (called the Slater exchange, *S*) and the correlation functional reported by Vosko, Wilk and Nusair, *VWN*.[6] Another notable example of LDA correlation functional was reported by Perdew and Wang in 1992.[7] The LDA approximation would actually be an exact formulation of XC functional if the system was an uniform electron gas. It is of course not the

case since the nature of a system is in fact defined by its inhomogeneity. To compensate this problem, the Generalized Gradient Approximation (GGA) includes a dependence on the gradient of the electron density to the local density approximation. It allows to describe inhomogeneities in the real electron density:

$$E_{XC}[\rho(\vec{r})] = \int \rho(\vec{r})\, \varepsilon_{XC}\left[\rho(\vec{r}), \vec{\nabla}\rho(\vec{r})\right] d\vec{r} \qquad (39)$$

Among the first reported examples, one can note the exchange energy functionals of Becke[8] and Perdew[9] and correlation energy functionals of Lee, Yang and Parr[10] and Perdew.[11] XC functionals acronyms usually reflect their content or the place where it was developed (*e.g.* the BLYP XC functional consists in the Becke exchange, B, and the Lee, Yang, Parr, LYP, correlation energy functionals).

The *meta*-GGA functionals further add a dependence on the kinetic energy density $\tau_\sigma(\vec{r})$.

$$E_{XC}[\rho(\vec{r})] = \int \rho(\vec{r})\, \varepsilon_{XC}\left[\rho(\vec{r}), \vec{\nabla}\rho(\vec{r}), \tau_\sigma(\vec{r})\right] dr \quad where \quad \tau_\sigma(\vec{r}) = \sum_{i=1}^{occ} \frac{1}{2} \left|\vec{\nabla}\theta_{i,\sigma}(\vec{r})\right|^2 \qquad (40)$$

In exchange and correlation energies, the exchange contribution is significantly larger than the correlation one. A better description of the exchange part of the XC functional is thus necessary to significantly improve the efficiency of the DFT method. Hybrid functionals are obtained by adding a given percentage (depending on the functional) of HF exchange. The exchange potential displays this way the correct *-1/r* asymptotic behavior, compensating the Coulomb part. The most popular hybrid functional, B3LYP, proposed by the group of Stephens,[12] is based on a hybrid exchange functional introduced by Becke:[13]

$$E_{XC}^{B3LYP} = (1-a)E_X^{LSD} + aE_X^{HF} + bE_X^{B88} + E_C^{LSD} + cE_C^{LYP} \qquad (41)$$

where the parameters *a*, *b* and *c* are optimized to best fit reference atomization and ionization energies, proton affinities and total energies. In this work, NMR calculations were performed with the B3LYP functional since it is known to consistently display NMR chemical shifts with satisfying accuracy.[14-15]

The M06-2X functional, broadly used in this work, is part of the set of Minnesota functionals developed by the group of Truhlar. It is a hybrid (with respectively 27 and 54% of exact HF exchange) *meta*-GGA functional best suited, according to their developers, to describe main-group thermochemistry, kinetics and noncovalent interactions.[16] Although not including explicit empirical corrections for dispersion forces as introduced by Grimme,[17] the Minnesota functionals are highly parameterized to effectively take these into account: to cite Grimme, "The M06-2X functional is probably the most accurate dispersion-uncorrected functional that gives good results for the S22 set as well as stacked aromatic structures".[18]

The long-range corrected or range-separated hybrid functionals split the exchange potential into short- and long-range terms with different HF exchange percentages. This allows to better describe charge-transfer effects due to a correct *-1/r* asymptotic dependence of the exchange potential as in global hybrid XCFs while retaining more DFT exchange at short range to avoid results similar to a "classical" HF method. The Ewald split of the exchange potential takes the following form:[19-21]

$$\frac{1}{r} = \frac{1 - [\alpha + \beta erf(\omega r)]}{r} + \frac{\alpha + \beta erf(\omega r)}{r} \qquad (42)$$

where the first term describes the short-range part retaining more DFT exchange and the second term the HF exchange at long range. The HF exchange at short range (for $r = 0$) is given by α, while the longe-range (for $r \to \infty$) percentage of HF exchange is given by $\alpha + \beta$. The HF exchange percentage increases smoothly over r, its evolution is dictated by the standard error function $erf(\omega r)$, with the range-separating parameter ω. Each range-separated hybrid functional has its specific α, β and ω parameters. Among these, the B97 family of functionals, including ωB97, ωB97X and ωB97X-D, are notable examples.[22]

In double hybrids functionals, the correlation functional is partially described by second order perturbation theory while HF exchange is still added to the exchange functional. These functionals significantly improve the results but their computational cost is far higher than that of the other functionals. Empirical dispersion corrections can also be included to better describe the London dispersion forces. These include B2PLYP-D3 or ωB97X-2.[23-24]

Note that increasing the complexity of the functional does not necessarily ensure better results. Simpler functionals can be more suited for a given system or target property.

2. Solvent effects and the polarizable continuum model

Since our compounds under investigation are in solution, an adequate description of the solvent effects is also crucial. The solvent molecules and their interactions with the solute affect the later at all levels: structure, reactivity, responses to perturbation, *etc*. They are divided in several contributions. The electrostatic interactions between the solute and the solvent molecules, the cavitation energy which is the amount of energy needed to form the cavity in solution that will contain the solute before considering solute-solvent interactions, the dispersion forces (induced dipole/induced dipole interactions), and finally the changes in the bulk solvent structure.

Solvents effects can be described using two types of models: the explicit and implicit models. The former simulate the solvent molecules, give better, more precise results, but require much higher computational costs while the latter do not simulate the solvent molecules explicitly and are therefore less time-and energy consuming.

The Polarizable Continuum Model (PCM) is an implicit solvation method.[25] In this model a cavity that contains the solvated molecule is drawn by circulating a probe sphere around the solute molecule. This sphere has a radius equal to the van der Waals radius of the solvent molecule. It defines two surfaces, the outer one is the solvent accessible surface, and the inner is the solvent exclusion surface (Figure S52).

In this method, the explicit solvent molecules are replaced by a continuum characterized by a dielectric constant ε, which determines the polarization of the surroundings due to a solute (and its inhomogeneous charge distribution), that will act in return on the solute, thus simulating the solvent effects. The mathematical development of the PCM model is put in the form of an integral equation (IEF, in the IEFPCM approach). The subtlety in the PCM approach is that the charge distribution of the solute induces a polarization of the dielectric continuum which in turn polarizes the solute charge distribution. It is thus a self-consistent model that must be solved in an iterative manner.

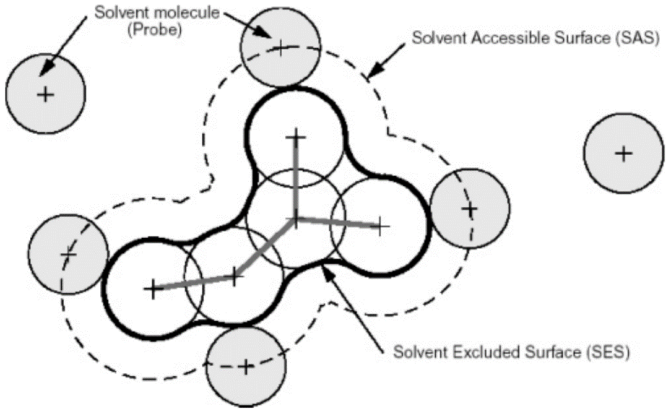

Figure S52. Cavity formed by circulating a probe solvent molecule around the studied compound. Picture reprinted with permission from reference 25. Copyright 2005 American Chemical Society.

3. Responses to an external magnetic field and NMR chemical shifts

The response of the system to an external magnetic field is the principle of the NMR analysis. As a function of their electronic environment, nuclei having a non-zero magnetic moment will react differently to that perturbation so that their response will serve as an indication of their chemical environment. The magnetic shielding tensor of a nucleus ($\overleftrightarrow{\sigma}$) is the measure of the relative change is the local magnetic field $\vec{B}$ at this nucleus with respect to the external magnetic field $\vec{B}^{ext}$. It is formally defined as the mixed second-order derivative of the energy relative to the magnetic moment of the nucleus, $\vec{m}$ and the external magnetic field. Any component of the magnetic shielding tensor reads:[14]

$$\sigma_{\zeta\eta} = \frac{\partial^2 E}{\partial m_\zeta \partial B_\eta^{ext}} = -\frac{\partial B_\zeta}{\partial B_\eta^{ext}} \quad where \quad \partial B_\zeta = -\frac{\partial E}{\partial m_\zeta} \qquad (43)$$

where ζ and η are cartesian coordinates. The NMR chemical shift of a nucleus A is defined as the variation of the isotropic nuclear magnetic shielding with respect to that of a given reference:

$$\delta_A = \sigma_{ref} - \sigma_A \quad where \quad \sigma = \frac{1}{3}(\sigma_{xx} + \sigma_{yy} + \sigma_{zz}) \qquad (44)$$

In order to determine these quantities, the response of the system to the external magnetic field must be evaluated. The Hamiltonian of the system is thus modified

to include the contributions from the interactions with the external magnetic field. A direct modification of the Hamiltonian is however problematic as its perturbed expression depends on the choice of the origin of the system. It does not have any consequences when exact wavefunctions and complete atomic basis sets are used but it is no longer the case for approximate situations. An indirect approach that solves this problem is the use of London atomic orbitals χ^{London}, that are themselves dependent on the origin and on the magnetic field, the expression for an atomic orbital *p* is:

$$\chi_p{}^{London}(\vec{r}, \vec{G}, \vec{B}) = \chi_p(\vec{r}) e^{\frac{-i}{2}(\vec{B}\times\vec{G}).\vec{r}} \qquad (45)$$

where $\vec{G}$ is the center of the atomic orbital. The resulting $\overleftrightarrow{\sigma}$ values become thereafter independent of the choice of the origin. It is the GIAO (Gauge Including Atomic Orbitals) scheme. It was employed for the determination of NMR chemical shifts in this thesis, using Coupled-Perturbed Kohn-Sham method.[2]

4. Atomic basis sets

Within the LCAO approximation (35), any calculation requires choosing an atomic orbital basis set.[26] These basis set functions are contractions of gaussian functions. The basis sets have been built to best simulate the wavefunctions and electron densities of any system. They have been divided in several categories with respect to their composition. The minimal basis sets or simple ζ comprise a single basis function for each atomic orbital of a shell or sub-shell, which is at least partially occupied in the isolated atom. One of these basis sets is STO-3G (Slater Type Orbital) where each basis function is a contraction of three gaussian primitive functions. Double or Triple ζ include two or three basis functions, respectively, for each occupied atomic orbital of a given atom. The split valence basis sets split the number of basis functions between the core orbitals (usually described with simple ζ) and the valence orbitals (with double or triple ζ). This method comes from the understanding that most of the chemistry of an atom is determined by the valence orbitals, so they should be more flexible than the core ones. Basis sets with two or three valence atomic orbitals are called valence double- and triple ζ basis sets, respectively. The addition of polarization functions to these basis sets can account for environment effects on the atom. *p* functions can be implemented on hydrogen atoms or *d* and *f* functions can be added on atoms from the second and third period. For example, a hydrogen atom

involved in a covalent bond will no longer possess a perfectly spherical 1*s* orbital. The addition of a set of *p* functions can correct this approximation. Furthermore, diffuse functions can also be added to the basis sets. They allow a better description of the outer part of the orbitals and the electron density. Diffuse *s* and *p* functions are added on atoms from the second and third period while only diffuse *s* functions are applied on hydrogen atoms.

Pople developed a series of basis sets such as STO-3G, 6-31G, 6-311G(d,p), 6-311++G(3df,3pd), *etc.*, mainly valence double or triple ζ.[27] In this thesis, the 6-311G(d) basis sets was mainly used. It is a Pople valence triple ζ basis set with a set of *d* polarization functions. It possesses a single basis function, contraction of six gaussians for the core orbitals while the valence orbitals are described by three basis functions, one is a contraction of 3 gaussians and the two other of a single gaussian function. A set of polarization functions are added: *d* orbitals for the atoms of the second and third period. NMR calculations will be performed using the 6-311+G(2d,p) basis set. It contains as set of diffuse functions *s* and *p* on second and third period atoms and one set of s functions on hydrogens. Two sets of *d* polarization functions on second and third period atoms and a set of diffuse *s* functions on hydrogens.

5. Thermochemistry and equilibrium constants

Thermochemistry is the study of the thermodynamic functions of a given chemical system.[28] Those are macroscopic values, resulting from the state and the energy of matter at the microscopic level. Statistical thermodynamics makes the bridge between the microscopic (molecular) and macroscopic levels. The partition function (Ω) is of paramount importance in this field as it contains all the information of the system. It is defined as the following summation over the L energy levels of the system:

$$\Omega = \sum_{i}^{L} g_i e^{\frac{-\varepsilon_i}{kT}} \qquad (46)$$

$$\Omega = \Omega_{trans}\, \Omega_{vib}\, \Omega_{rot}\, \Omega_{el} \qquad (47)$$

where g_i is the degeneracy of the i^{th} level of energy, ε_i, k, is the Boltzmann constant and T, the temperature. Equation (47) highlights that the partition function is the product of several contributions (*trans* = translation; *vib* =

vibrations; *rot* = rotation; *el* = electronic). Each state function of the system (internal energy, Gibbs free enthalpy, entropy, enthalpy, …) can be expressed as a function of the partition function.

For the thermochemical studies of the present work, vibrational frequency calculations were then performed. From these calculations, in addition to the mass and the rotation constants, one determines the partition function and subsequently the various state functions of the system.

Equilibrium constants are also determined in this work. The calculated values are K_C: equilibrium constant expressed as a function of the concentrations in solution reported to the standard 1 M concentration $C^\ominus$. K_C and K_P (K_P: equilibrium constant in terms of the pressure of the constituents of the system, reported to the standard 1 atm pressure $P^\ominus$) are related in our case by the following expression:

$$K_P = K_C \left(\frac{C^\ominus RT}{P^\ominus}\right)^{\Delta\nu} \qquad (48)$$

where $C^\ominus$ is the standard concentration of 1M and $P^\ominus$ is the standard 1 atm pressure and $\Delta\nu$ the variation of the sum of stoichiometric coefficient between products and reagents.

6. The distortion-interaction/activation strain model

The distortion-interaction/activation strain (DIAS) model of reactivity is a tool to analyze activation barriers, it consists in decomposing the total reaction energy into two contributions, the distortion energy and the interaction energy.[29] Developed in parallel by the groups of Bickelhaupt ("activation strain" model[30]) and Houk ("distortion-interaction" model[31]), it came from the understanding that existing reactivity models, such as the frontier molecular orbital (FMO) theory or Valence bond theory (VB) were insufficient to fully understand reaction barriers. While they explain the chemical transformations, the electronic mechanisms and interactions happening at the transition state (TS), they fail at actually describing why an activation barrier has a given height. For instance, some reactions predicted to be *symmetry allowed*, in the sense that molecular orbitals in the reactants should easily overlap according to the FMO theory, do not proceed readily. Indeed, for a given reaction between A and B, the

activation barrier is not only dictated by their ability to interact in the transition state, but also by how distorted they are from their original geometry. According to Bickelhaupt and Houk, the missing factor is the activation strain, or distortion energy, defined as the "energy penalty associated with the deformation of the reactants as the reaction progresses".[32] They thus proposed to split the energy over the reaction profile as follows:

$$\Delta E(\zeta) = \Delta E_{int}(\zeta) + \Delta E_{strain}(\zeta) \tag{49}$$

where ζ is the intrinsic reaction coordinate or a selected critical geometry parameter. On the one hand, the interaction energy is usually stabilizing (negative values), it depends on the electronic structure of the reactants and their orientation, and it is composed, over the reaction coordinate, of the mutual interactions between the increasingly deformed reactants. On the other hand, the distortion energy is always positive, it depends on the strength of the bonds that are breaking or the rigidity of bond angles that are distorted. It can be pictured by the two curves of Figure S53 summing up to the total reaction energy. In this model, the TS is defined as the point where the interaction energy overcomes the distortion penalty [equations (50) and (51)]:

$$\frac{d\Delta E_{strain}(\zeta = TS)}{d\zeta} = -\frac{d\Delta E_{int}(\zeta = TS)}{d\zeta} \tag{50}$$

$$\Delta E^{\neq}(\zeta = TS) = \Delta E^{\neq}_{int}(\zeta = TS) + \Delta E^{\neq}_{strain}(\zeta = TS) \tag{51}$$

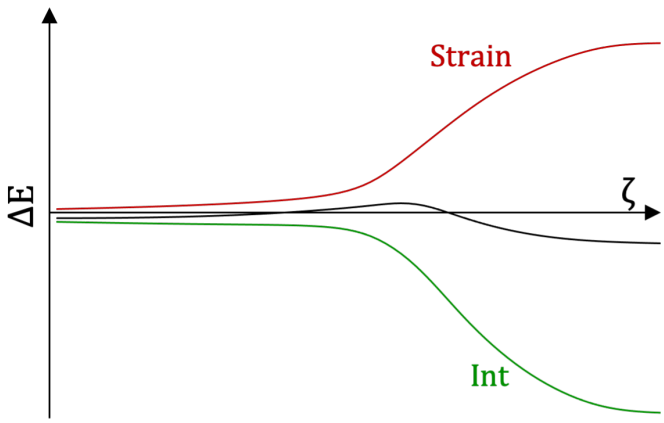

Figure S53. Typical DIAS diagram showing the strain and interactions curves summing up to yield the total energy of the reaction over the reaction coordinate or a selected critical geometry parameter.

However, when using the DIAS model, it is important to note that analyzing interaction and distortion energies at the transition state alone is not enough to get a proper overview of the reaction barrier. Indeed, evaluation of the behavior of both curves over the whole reaction profile and not only at the TS is necessary to avoid misleading conclusions. The height of the reaction barrier must be put in perspective with the stage at which the TS happens. The classical example put forward to illustrate this point, is the S_N2 reaction, comparing the effect of using a strong nucleophile (X^-) or a poor leaving group (Y) (Figure S54). In the first case (Figure S54a), a stronger nucleophile means better interactions at the TS, resulting in a lower interaction curve compared with the moderate nucleophile, and an earlier TS on the reaction profile. In the second case (Figure S54b), a poorer leaving group means a stronger bond to break, resulting in a higher distortion curve and, on the reaction profile, a later transition state. Note that both situations are in agreement with Hammond's postulate, stating that a more exergonic reaction has an earlier-stage transition state and a less exergonic or endergonic reaction has a later-stage transition state.[33] For the first situation for example, if one were to only compute the values at the TS, one would find similar interaction energy at the TS and a lower strain value at the TS and would erroneously conclude that lower distortions are responsible for the lower barrier while it is actually the opposite, but happening earlier along the reaction coordinate. This demonstrates that the behavior of the whole curves must be considered along the reaction pathway.

Finally, additional insight can be gained by splitting the global distortion and interaction values into individual contributions. For example, between individual reactants [A and B] for the distortion [equation (52)] or by partitioning the interaction energy, using for example the energy decomposition analysis (EDA), introduced by Frenking [equation (53)].[34]

$$\Delta E_{strain} = \Delta E_{strain-A} + \Delta E_{strain-B} \quad (52)$$

$$\Delta E_{int} = \Delta E_{elec.} + \Delta E_{Pauli} + \Delta E_{orb.} \quad (53)$$

where the $\Delta E_{elec.}$ term describes electrostatic interactions, ΔE_{Pauli} the electronic repulsions between filled orbitals and $\Delta E_{orb.}$ the stabilizing orbitals interactions.

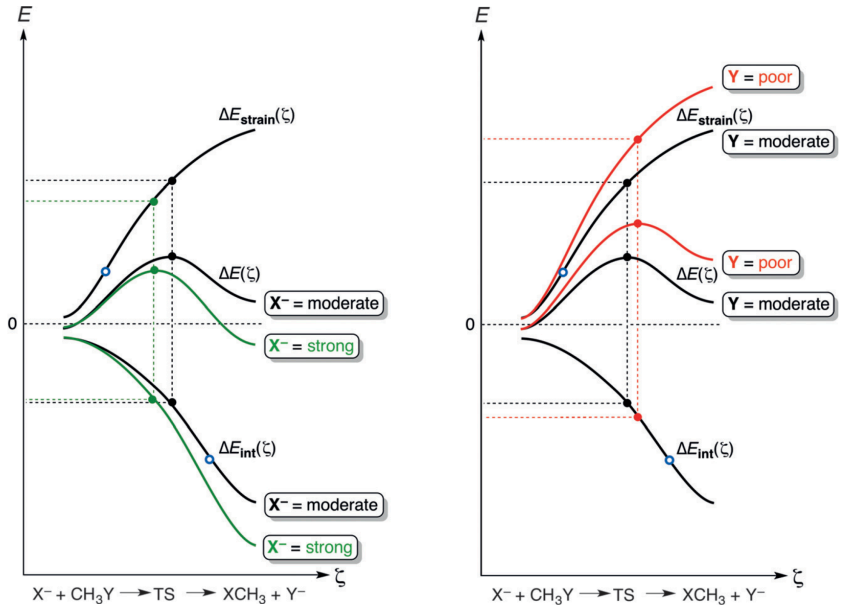

Figure S54. Comparison of two DIAS diagrams for S_N2 reactions using either a) a stronger nucleophile (X-) or b) a weaker leaving group (Y). Figure extracted from reference 32 with permission from John Wiley and Sons.

7. The Natural Bond Orbital analysis

Natural Bond Orbitals (NBOs) are a concept put forward by Weinhold and Landis to describe valency and bonding, aiming at translating solutions to Schrödinger's equation available to computational chemistry, including Kohn-Sham DFT, into the Lewis picture of atoms and molecules, familiar to the chemists, based on the transformation of a given electronic structure in a *localized* form.[35-37] It is achieved by employing localized electronic units, in the form of one-center units ("lone pairs") and two-center units (bonds).

The NBO program works in parallel with the initial calculation, be it DFT or other forms of calculation, and requires only the first reduced density matrix. Because the latter can be generated by any form of calculation (variational or perturbative, correlated or not) the resulting orbitals and properties displayed are called intrinsic or *natural*.

The NBO analysis is performed by an algorithmic sequence of generations of sets of orbitals, each arising from variations of the previous one. Starting from the set of atomic orbitals defined by the host calculation, a set of "natural" atomic

orbitals (NAOs) are defined, these are then combined as natural hybrid orbitals (NHOs, linear combinations of valence natural atomic orbitals), then again combined to generate a set of natural bond orbitals (NBOs, linear combinations of hybrid orbitals) as schematized in Figure S55.

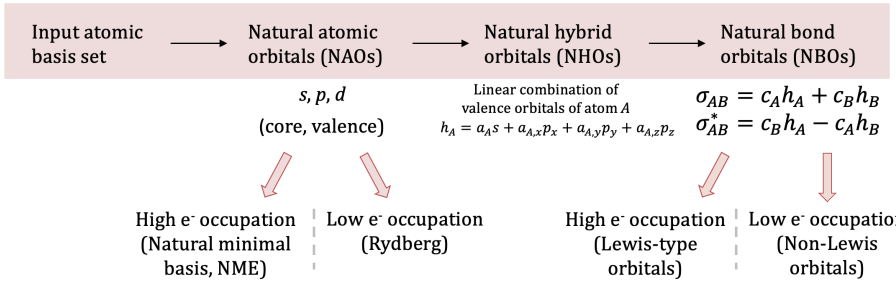

Figure S55. Sequence of generation of sets of natural orbitals.

The optimization of electronic occupancy in natural orbitals leads to the distinction between orbitals of high and low occupancy. The (small) set of the most occupied NAOs is called the natural minimal basis (NMB) and it consists in all core and valence atomic orbitals. They are distinguished from the Rydberg orbitals, beyond the valence shell, that complete the space of NAOs but have only a limited contribution to molecular properties. Similarly, the set of high occupation NBOs ("Lewis-type" orbitals, occupied or donor orbitals) that form the Natural Lewis Structure are distinguished from non-Lewis orbitals (vacant, acceptor or anti-bonding orbitals) that complete the space of NBOs. Each pair of valence hybrid h_A and h_B (for atoms A and B) in the space of NHOs gives rise to a bonding (σ_{AB}) and an antibonding (σ^*_{AB}) orbital in the space of NBOs:

$$\sigma_{AB} = c_A h_A + c_B h_B \rightarrow Lewis\ orbital \quad (54)$$

$$\sigma^*_{AB} = c_B h_A - c_A h_B \rightarrow Non - Lewis\ orbital \quad (55)$$

where c_A and c_B are bonding coefficients.

The ideal Lewis structure where all electrons are located in valence/bonding orbital is not physical however. In "real" systems, there is resonance: stabilizing donor-acceptor interactions between Lewis-type and non-Lewis type NBOs. However, since the Lewis structure is the major contribution to the energy of the system, it is a good starting point for a perturbation approach.

$$E = E^{(L)} + E^{(L-NL)} \quad (56)$$

$E^{(NL)}$ is thus a correction to the energy of the Lewis structure due to resonance between filled/empty NBOs. This "second order perturbation" stabilization

energy serves as an estimation of the stabilization due to L-NL NBO interactions and can be written as:[38]

$$\Delta E_{ij}^{(2)} = \frac{-q_i \left|F_{ij}\right|^2}{\left(\varepsilon_j^{(NL)} - \varepsilon_i^{(L)}\right)} \qquad (57)$$

where q_i is the occupancy of the donor orbital, $\varepsilon_i^{(L)}$ and $\varepsilon_j^{(NL)}$ are respectively the donor and acceptor orbital energies and F_{ij} the interaction element derived from the Kohn-Sham matrix in DFT, a measure of the overlap between the two orbitals.

In the NBO analysis scheme, the NLS representation is optimized for a maximum electron occupancy in the Lewis structure $[\rho(L)]$. The remaining electron occupancy, found in the non-Lewis-type orbitals $[\rho(NL)]$ is a measure of the deviation from the idealized Lewis structure and is indicated at the end of any NBO calculation.

NBO is most useful for its natural population analysis (NPA), a listing of all NAOs and their electron occupation. The summation of the electronic populations of the NAOs of a given atom gives its natural charge. The sum of all natural partial charges gives exactly the total charge of the molecule. Reportedly, NPA is a significant improvement compared to the classical Mulliken population analysis, mostly due to the orthogonal nature of all NAOs.[39-40] It avoids mixing of electron population between neighboring atoms, that can lead to some aberrant partial charges and that do not sum up to the total charge of the molecule, as is the case of Mulliken.

8. References

[1] R. G. Parr, W. Yang, *Density-functional theory of atoms and molecules*, Oxford University Press, New-York, **1995**.

[2] W. Koch, M. C. Holtausen, *A chemist's guide to density functional theory*, 2nd ed., Wiley-VCH, Weinheim, **2001**.

[3] P. Geerlings, F. De Proft, W. Langenaeker, "Conceptual density functional theory", *Chem. Rev.* **2003**, *103*, 1793-1873.

[4] P. Hohenberg, W. Kohn, "Inhomogeneous electron gas", *Physical Review* **1964**, *136*, B864-B871.

[5] W. Kohn, L. J. Sham, "Self-consistent equations including exchange and correlation effects", *Physical Review* **1965**, *140*, A1133-A1138.

[6] S. H. Vosko, L. Wilk, M. Nusair, "Accurate spin-dependent electron liquid correlation energies for local spin density calculations: a critical analysis", *Can. J. Phys.* **1980**, *58*, 1200-1211.

[7] J. P. Perdew, Y. Wang, "Accurate and simple analytic representation of the electron-gas correlation energy", *Phys. Rev. B* **1992**, *45*, 13244-13249.

[8] A. D. Becke, "Density-functional exchange-energy approximation with correct asymptotic behavior", *Phys. Rev. A* **1988**, *38*, 3098-3100.

[9] J. P. Perdew, Y. Wang, "Accurate and simple density functional for the electronic exchange energy: Generalized gradient approximation", *Phys. Rev. B* **1986**, *33*, 8800-8802.

[10] C. Lee, W. Yang, R. G. Parr, "Development of the Colle-Salvetti correlation-energy formula into a functional of the electron density", *Phys. Rev. B* **1988**, *37*, 785-789.

[11] J. P. Perdew, "Density-functional approximation for the correlation energy of the inhomogeneous electron gas", *Phys. Rev. B* **1986**, *33*, 8822-8824.

[12] P. J. Stephens, F. J. Devlin, C. F. Chabalowski, M. J. Frisch, "*Ab initio* calculation of vibrational absorption and circular dichroism spectra using density functional force fields", *The Journal of Physical Chemistry* **1994**, *98*, 11623-11627.

[13] A. D. Becke, "A new mixing of Hartree–Fock and local density-functional theories", *J. Chem. Phys.* **1993**, *98*, 1372-1377.

[14] J. R. Cheeseman, G. W. Trucks, T. A. Keith, M. J. Frisch, "A comparison of models for calculating nuclear magnetic resonance shielding tensors", *J. Chem. Phys.* **1996**, *104*, 5497-5509.

[15] P. R. Rablen, S. A. Pearlman, J. Finkbiner, "A comparison of density functional methods for the estimation of proton chemical shifts with chemical accuracy", *The Journal of Physical Chemistry A* **1999**, *103*, 7357-7363.

[16] Y. Zhao, D. G. Truhlar, "The M06 suite of density functionals for main group thermochemistry, thermochemical kinetics, noncovalent interactions, excited states, and transition elements: Two new functionals and systematic testing of four M06-class functionals and 12 other functionals", *Theor. Chem. Acc.* **2008**, *120*, 215-241.

[17] S. Grimme, "Accurate description of van der Waals complexes by density functional theory including empirical corrections", *J. Comput. Chem.* **2004**, *25*, 1463-1473.

[18] S. Grimme, "Density functional theory with London dispersion corrections", *WIREs Comput. Chem. Sci.* **2011**, *1*, 211-228.

[19] H. Iikura, T. Tsuneda, T. Yanai, K. Hirao, "A long-range correction scheme for generalized-gradient-approximation exchange functionals", *J. Chem. Phys.* **2001**, *115*, 3540-3544.

[20] Y. Tawada, T. Tsuneda, S. Yanagisawa, T. Yanai, K. Hirao, "A long-range-corrected time-dependent density functional theory", *J. Chem. Phys.* **2004**, *120*, 8425-8433.

[21] T. Yanai, D. P. Tew, N. C. Handy, "A new hybrid exchange–correlation functional using the Coulomb-attenuating method (CAM-B3LYP)", *Chem. Phys. Lett.* **2004**, *393*, 51-57.

[22] J. D. Chai, M. Head-Gordon, "Long-range corrected hybrid density functionals with damped atom-atom dispersion corrections", *Phys. Chem. Chem. Phys* **2008**, *10*, 6615-6620.

[23] L. Goerigk, S. Grimme, "Efficient and accurate double-hybrid-*meta*-GGA density functionals - Evaluation with the extended GMTKN30 database for general main group thermochemistry, kinetics, and noncovalent interactions", *J. Chem. Theory Comput.* **2011**, *7*, 291-309.

[24] J. D. Chai, M. Head-Gordon, "Long-range corrected double-hybrid density functionals", *J. Phys. Chem.* **2009**, *131*, 174105.

[25] J. Tomasi, B. Mennucci, R. Cammi, "Quantum mechanical continuum solvation models", *Chem. Rev.* **2005**, *105*, 2999-3094.

[26] A. Szabo, N. S. Ostlund, *Modern quantum chemistry: Introduction to advanced electronic structure theory*, Dover Publictions, New-York, **1996**.

[27] R. Ditchfield, W. J. Hehre, J. A. Pople, "Self-consistent molecular-orbital methods. IX. An extended gaussian-type basis for molecular-orbital studies of organic molecules", *J. Chem. Phys.* **1971**, *54*, 724-728.

[28] P. Atkins, J. De Paula, *Atkins' physical chemistry*, 10th ed., Oxford University Press, Oxford, **2014**.

[29] I. Fernandez, F. M. Bickelhaupt, "The activation strain model and molecular orbital theory: understanding and designing chemical reactions", *Chem. Soc. Rev.* **2014**, *43*, 4953-4967.

[30] F. M. Bickelhaupt, "Understanding reactivity with Kohn-Sham molecular orbital theory: E2-S_N2 mechanistic spectrum and other concepts", *J. Comput. Chem.* **1999**, *20*, 114-128.

[31] D. H. Ess, K. N. Houk, "Distortion/interaction energy control of 1,3-dipolar cycloaddition reactivity", *J. Am. Chem. Soc.* **2007**, *129*, 10646-10647.

[32] F. M. Bickelhaupt, K. N. Houk, "Analyzing reaction rates with the distortion/interaction-activation strain model", *Angew. Chem. Int. Ed.* **2017**, *56*, 10070-10086.

[33] G. Hammond, "A correlation of reaction rates", *J. Am. Chem. Soc.* **1955**, *77*, 334-338.

[34] L. Zhao, M. von Hopffgarten, D. M. Andrada, G. Frenking, "Energy decomposition analysis", *WIREs Comput. Chem. Sci.* **2017**, *8*, 1-37.

[35] F. Weinhold, C. R. Landis, *Valency and bonding - a natural bond orbital donor-acceptor perspective*, Cambridge University Press, New-York, **2005**.

[36] F. Weinhold, C. R. Landis, *Discovering chemistry with natural bond orbitals*, Wiley, Hoboken, NJ, **2012**.

[37] F. Weinhold, C. R. Landis, E. D. Glendening, "What is NBO analysis and how is it useful?", *Int. Rev. Phys. Chem.* **2016**, *35*, 399-440.

[38] F. Weinhold, C. R. Landis, "Resonance delocalization corrections" in *Discovering chemistry with natural bond orbitals*, Wiley, Hoboken, NJ, **2012**.

[39] A. E. Reed, R. B. Weinstock, F. Weinhold, "Natural population analysis", *J. Chem. Phys.* **1985**, *83*, 735-746.

[40] K. C. Gross, P. G. Seybold, "Substituent effects on the physical properties and pK_a of aniline", *Int. J. Quantum Chem* **2000**, *80*, 1107-1115.

Annex III
Benchmark study: choice of the exchange-correlation functional

This comparative DFT study was undertaken before the start of the PhD, to select the density functional to be used for the following calculations.

1. Introduction

The concept of Lewis acids and bases was first introduced by G. Lewis in 1923, these compounds and the complexes they form have now a major role in chemistry and more particularly in catalysis.[1] It is therefore crucial to comprehend their structure and properties. Hereafter is reported a Density Functional Theory (DFT) study of three reactions between a Lewis acid (LA) and a Lewis base (LB) to form a Lewis adduct. The studied reactions are the following:

$$NMe_3 + AlMe_3 \rightleftharpoons [Me_3N - AlMe_3] \quad (A)$$

$$PMe_3 + BMe_3 \rightleftharpoons [Me_3P - BMe_3] \quad (B)$$

$$NMe_3 + BMe_3 \rightleftharpoons [Me_3N - BMe_3] \quad (C)$$

A comparison of fourteen exchange-correlation functionals picked from different rungs of Jacob's Ladder was undertaken for these three reactions.[2] Calculations were performed to determine the geometric parameters of the adduct and reagents as well as the thermodynamic state functions of these equilibria. The results obtained were compared to reference values calculated using wavefunction methods, namely MP2 and CCSD(T). Eventually, a selection of the functionals best-suited for describing Lewis acids-bases interactions is provided.

2. Computational methods

All calculations were performed with the *Gaussian16* program and the atomic basis set used was 6-311+G(d,p) in gas phase.[3] The studied exchange-correlation functionals (XCF) are given in Table S32. For each one, geometry optimization and vibrational frequency calculations were performed on all compounds. Reference results were obtained a) at the MP2/6-311+G(d,p) level of theory, and b) with the CCSD(T)' method, defined hereafter: CCSD(T)/6-311+G(d,p) single point calculations were performed upon all MP2-optimized structures, with MP2 thermal corrections added to the CCSD(T)/6-311+G(d,p) electronic energies for the determination of temperature-dependent state functions.

3. Exchange-correlation functionals

The Kohn-Sham method in DFT is an exact method, assuming the exact exchange-correlation (XC) functional is known.[4] Since it is not the case, approximate functionals are used. Over the years, many functionals have been designed and are sorted in different categories (Table S32).

Table S32. Exchange-correlation functionals and their type.

Functional types	% HF exchange		Range-separating parameter (ω, in a_0^{-1})	Functionals
LDA	0			SVWN
GGA	0			BLYP
meta-GGA	0			TPSS
Hybrid GGA	20			B3LYP
	21.98			B98
	25			PBE0
Hybrid *m*-GGA	10			TPSSh
	27			M06
	54			M06-2X
Hybrid long range corrected	0 (α)	100 ($\alpha + \beta$)	0.4	ωB97
	16	100	0.3	ωB97X
	22	100	0.2	ωB97X-D
	0	100	0.47	LC-BLYP
	19	65	0.33	CAM-B3LYP

As mentioned in the previous section, in the Local Density Approximation (LDA), a uniform electron gas is applied on infinitesimal parts of the globally non-uniform system. The Generalized Gradient Approximation (GGA) adds a dependence on the gradient of the electron density to the local density approximation. The *meta*-GGA adds a dependence on the kinetic energy density. Hybrid functionals are obtained when a certain percentage (depending on the functional) of exact Hartree-Fock (HF) exchange is added. The long-range corrected or range-separated hybrid functionals split the exchange potential in a short- and a long-range term with different HF exchange percentages. As

explained in the previous section, the HF exchange fraction varies between its short range (α) and its long-range value ($\alpha + \beta$), following a standard error function $erf(\omega r)$, with the partitioning parameter ω characteristic of each functional and detailed in Table S32. Empirical London dispersion corrections can be included to better describe the London dispersion forces, as in ωB97X-D.[5]

4. Results and discussion

4.1 Structural aspects

The main geometrical parameters of the equilibrium structures were retrieved on all compounds of the three reactions. It was observed that the most difficult parameter to accurately describe is the bond length between the LA and the LB in the complex (*i.e.* Al-N, B-P, B-N). This bond length is given for all adducts in Table S33.

Table S33. Bond lengths in Å of the LA-LB bond for the adduct of all three reactions (A, B and C). Colors indicate deviations from the reference values. Green: between 0 and 0.5%; yellow: between 0.5 and 1%.

Adduct		A	B	C
Functional types	Functionals	$d_{Al\text{-}N}$	$d_{B\text{-}P}$	$d_{B\text{-}N}$
LDA	SVWN	2.068	1.932	1.683
GGA	BLYP	2.190	2.050	1.840
meta-GGA	TPSS	2.131	2.018	1.764
Hybrid GGA	B3LYP	2.153	2.027	1.793
	B98	2.143	2.028	1.767
	PBE0	2.120	1.987	1.739
Hybrid *m*-GGA	TPSSh	2.122	2.012	1.754
	M06	2.118	1.991	1.768
	M06-2X	2.091	1.990	1.727
Hybrid long range corrected	ωB97	2.131	1.977	1.760
	ωB97X	2.129	1.988	1.758
	ωB97X-D	2.125	1.991	1.751
	LC-BLYP	2.087	1.968	1.716
	CAM-B3LYP	2.122	2.002	1.755
REF	MP2	2.105	1.969	1.710

The bond lengths gradually decrease with the size of the LA and LB from reaction A to C. LDA, GGA and *meta*-GGA functionals have difficulties to describe these bonds. SVWN systematically underestimates the bond length, as was already reported,[6] while BLYP and TPSS overestimate them. Hybrid functionals are necessary to accurately describe these bonds. Among those, the long-range corrected and *m*-GGA, especially LC-BLYP and M06-2X, yield the best results.

4.2 Thermodynamics

The thermodynamics state functions of the reactions were also studied. The electronic energies, enthalpies, Gibbs free enthalpies and entropies of the reactions are reported in Table S34. The negative ΔS^0 indicates a disfavored entropic process, which was expected as two molecules assemble to form one. The reaction is however thermally favored with a negative ΔH^0, and the overall process is exergonic as the ΔG^0 is also negative.

Table S34. Thermodynamic state functions of reactions A, B and C. ΔE, ΔH^0, and ΔG^0 are given in kJ.mol^{-1}, ΔS^0 in J.mol^{-1}.K^{-1}. Colors indicate absolute deviations (in kJ.mol^{-1} for all energies except entropies in J.mol^{-1}.K^{-1}) from the reference values [CCSD(T)'] with the following color code: $\Delta < 5$; $5 \leq \Delta \leq 10$; $10 < \Delta \leq 15$; $15 < \Delta \leq 30$.

Reaction	A				B				C			
XCF	ΔE	ΔH^0	ΔS^0	ΔG^0	ΔE	ΔH^0	ΔS^0	ΔG^0	ΔE	ΔH^0	ΔS^0	ΔG^0
SVWN	-148	-133	-145	-90	-120	-113	89	-55	-130	-117	-228	-49
BLYP	-69	-53	-134	-14	-19	-10	-206	51	-15	-2	-223	64
TPSS	-96	-87	-206	-26	-48	-40	-205	21	-51	-38	-222	28
B3LYP	-81	-72	-199	-13	-30	-22	-213	42	-28	-14	-225	53
B98	-93	-78	-123	-41	-46	-37	-211	25	-43	-30	-228	38
PBE0	-102	-85	-134	-45	-66	-58	-198	2	-59	-46	-227	22
TPSSh	-99	-83	-132	-44	-51	-43	-196	16	-53	-40	-223	26
M06	-120	-112	-230	-43	-62	-55	-224	12	-73	-61	-244	12
M06-2X	-136	-127	-219	-62	-71	-64	-202	-4	-93	-80	-237	-9
ωB97	-122	-114	-219	-49	-74	-67	-197	-8	-76	-63	-231	6
ωB97X	-117	-108	-211	-45	-67	-59	-198	0	-69	-56	-228	12
ωB97X-D	-125	-113	-193	-56	-75	-67	-199	-7	-80	-66	-230	2
LC-BLYP	-124	-114	-172	-63	-67	-59	-199	0	-78	-64	-232	5
CAM-B3LYP	-99	-89	-172	-38	-44	-36	-200	24	-49	-35	-228	33
MP2	-132	-124	-204	-63	-94	-87	-211	-24	-107	-94	-224	-27
CCSD(T)'	-130	-122	-204	-61	-81	-74	-211	-11	-98	-86	-224	-19

The LDA, GGA and *m*-GGA functionals do not accurately describe the thermodynamics of the systems. The best results are again given by the hybrid *m*-GGA and the long-range corrected hybrids, except CAM-B3LYP. LC-BLYP and ωB97 give good results while the best are obtained by M06-2X and ωB97X-D.

For these two latter XCF, a scaling factor was applied on the vibrational frequencies as they are generally larger (~ 4%[7]) than the experimental one. This happens because anharmonicity effects are neglected in the calculations.[8] The scaling factors used are 0.957 for ωB97X-D [6-311G(d,p)],[9] 0.967 for M06-2X [6-31+G(d,p)][10] and 0.9523 [6-311+G(d,p)] for MP2.[8] The deviation is generally lower than 1 kJ/mol, which is insignificant compared to the much higher gap between the unscaled values and the reference ones. Therefore, no scaling of the vibrational frequencies will be undertaken for subsequent calculations.

Table S35. Results of the scaling of the vibrational frequencies for the M06-2X and ωB97X-D functionals and MP2 for all three reactions. The s subscript refers to scaled values, the u subscript refers to unscaled values. Energies in kJ.mol^{-1} except entropies in J.mol.K^{-1}. Abs. stands for absolute error. XCF = exchange correlation functional. R° = Reaction.

R°	XCF	ΔH_s^0	ΔH_u^0	Abs.	ΔS_s^0	ΔS_u^0	Abs.	ΔG_s^0	ΔG_u^0	Abs.
	M06-2X	-127.2	-127.1	0.2	-217.0	-218.5	1.5	-62.5	-61.9	0.6
A	ωB97X-D	-113.7	-113.5	0.2	-190.6	-193.0	2.4	-56.9	-55.9	0.9
	MP2	-123.9	-123.7	0.2	-201.7	-203.9	2.2	-63.8	-62.9	0.9
	M06-2X	-64.1	-64.0	0.2	-200.5	-201.9	1.4	-4.4	-3.8	0.6
B	ωB97X-D	-66.9	-66.6	0.3	-197.6	-199.4	1.8	-8.0	-7.2	0.8
	MP2	-87.0	-86.7	0.2	-200.1	-202.1	2.0	-27.3	-26.5	0.9
	M06-2X	-80.3	-79.9	0.4	-236.3	-237.4	1.2	-9.9	-9.1	0.8
C	ωB97X-D	-66.8	-66.3	0.6	-228.7	-230.3	1.6	1.4	2.4	1.0
	MP2	-94.6	-94.1	0.6	-222.6	-224.4	1.8	-28.3	-27.2	1.1

Finally, potential energy curves were then established for the three adducts. The distance was increased step by step but with no optimized at each step (fixed geometry). The profiles of adduct A are shown in Figure S56, the same trends are observed for the other reactions. The profiles are typical of a Morse-like potential, observed when new chemical bonds are formed. When the bond length increases, so does the energy, and its value should tend to reach the sum of both isolated LA and LB energies when the distance between them tends to infinity. SVWN systematically overestimates the electronic energy in all profiles, while

BLYP, B3LYP, B98 and TPSS underestimate it. Long-range corrected functionals give by far the best results, displaying similar potential energy curve and remaining closer in energy to the MP2 and CCSD(T) curves. M06-2X also displays consistently good profiles.

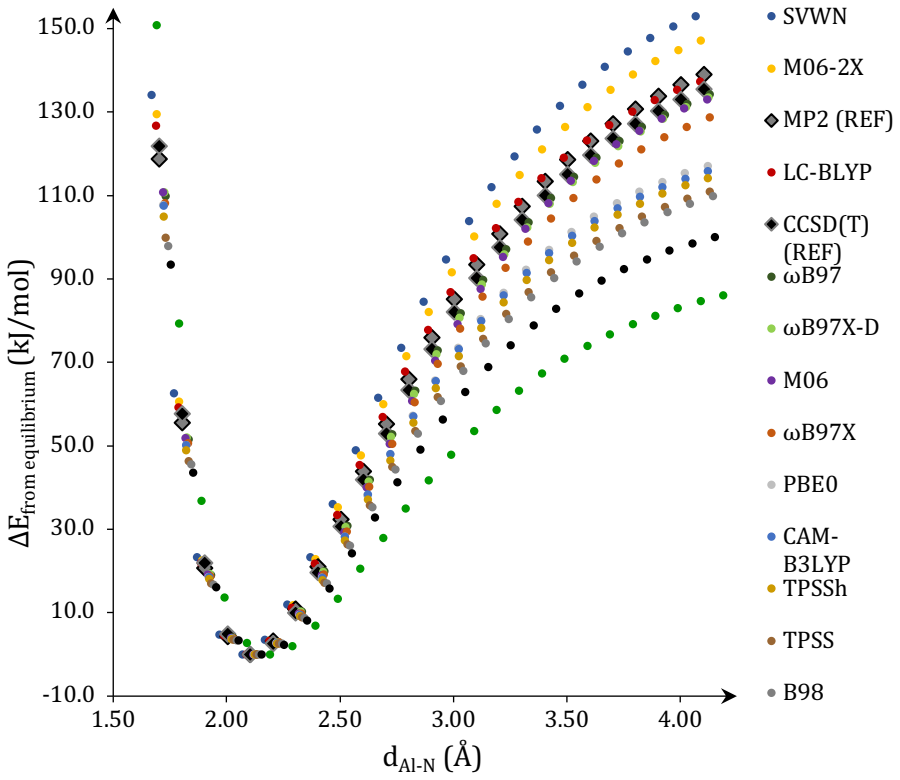

Figure S56. Energetic profiles of adduct A. The energy of the equilibrium geometry is set to 0. The legend order (on the right) reflects the top-bottom order of the profiles.

5. Conclusions

In conclusion, three reactions involving a LA and a LB to form a Lewis adduct were studied using DFT and fourteen exchange-correlation functionals were compared. It was found that the hybrid *m*-GGA and hybrid LR-corrected functionals covering different rungs of Jacob's ladder were the most suited to describe these systems both on the geometric level and on the energetic one. Among those functionals, LC-BLYP and M06-2X or ωB97X-D stand out, as they consistently yield accurate results. M06-2X was selected for further calculations since it describes satisfyingly both the thermodynamic state functions and the studied geometric parameters.

6. References

[1] G. N. Lewis, *Valence and the structure of atoms and molecules*, American Chemical Society, **1923**.

[2] J. P. Perdew, K. Schmidt, "Jacob's ladder of density functional approximations for the exchange-correlation energy", *AIP Conf. Proc.* **2001**, *577*, 1-20.

[3] M. J. Frisch, G. W. Trucks, H. B. Schlegel, G. E. Scuseria, M. A. Robb, J. R. Cheeseman, G. Scalmani, V. Barone, G. A. Petersson, H. Nakatsuji, X. Li, M. Caricato, A. V. Marenich, J. Bloino, B. G. Janesko, R. Gomperts, B. Mennucci, H. P. Hratchian, J. V. Ortiz, A. F. Izmaylov, J. L. Sonnenberg, D. Williams-Young, F. Ding, F. Lipparini, F. Egidi, J. Goings, B. Peng, A. Petrone, T. Henderson, D. Ranasinghe, V. G. Zakrzewski, J. Gao, N. Rega, G. Zheng, W. Liang, M. Hada, M. Ehara, K. Toyota, R. Fukuda, J. Hasegawa, M. Ishida, T. Nakajima, Y. Honda, O. Kitao, H. Nakai, T. Vreven, K. Throssell, J. A. Montgomery, Jr., J. E. Peralta, F. Ogliaro, M. J. Bearpark, J. J. Heyd, E. N. Brothers, K. N. Kudin, V. N. Staroverov, T. A. Keith, R. Kobayashi, J. Normand, K. Raghavachari, A. P. Rendell, J. C. Burant, S. S. Iyengar, J. Tomasi, M. Cossi, J. M. Millam, M. Klene, C. Adamo, R. Cammi, J. W. Ochterski, R. L. Martin, K. Morokuma, O. Farkas, J. B. Foresman, D. J. Fox, *Gaussian 16, Revision A.03*, Gaussian Inc., Wallingford CT, **2016**.

[4] W. Kohn, L. J. Sham, "Self-consistent equations including exchange and correlation effects", *Physical Review* **1965**, *140*, A1133-A1138.

[5] J. D. Chai, M. Head-Gordon, "Long-range corrected hybrid density functionals with damped atom-atom dispersion corrections", *Phys. Chem. Chem. Phys* **2008**, *10*, 6615-6620.

[6] W. Koch, M. C. Holtausen, *A chemist's guide to density functional theory*, 2nd ed., Wiley-VCH, Weinheim, **2001**.

[7] R. G. Parr, W. Yang, *Density-functional theory of atoms and molecules*, Oxford University Press, New-York, **1995**.

[8] J. P. Merrick, D. Moran, L. Radom, "An evaluation of harmonic vibrational frequency scale factors", *J. Phys. Chem. A* **2007**, *111*, 11683-11700.

[9] R. D. Johnson (**1999**), "Precomputed vibrational scaling factors" in *NIST 101. Computational chemistry comparison and benchmark database*, [online], http://cccbdb.nist.gov (Accessed on March 24, 2023).

[10] I. M. Alecu, J. Zheng, Y. Zhao, D. G. Truhlar, "Computational thermochemistry: Scale factor databases and scale factors for vibrational frequencies obtained from electronic model chemistries", *J. Chem. Theory Comput.* **2010**, *6*, 2872-2887.